UNIVERSITY OF COPENHAGEN

PhD Thesis

Gediminas Kiršanskas

Electron Transport in Quantum Dots and Heat Transport in Molecules

Tunneling renormalization
of cotunneling spectroscopy

Sub-gap states in superconductors
due to spinful quantum dots

Designing π-stacked molecules
as phonon insulators

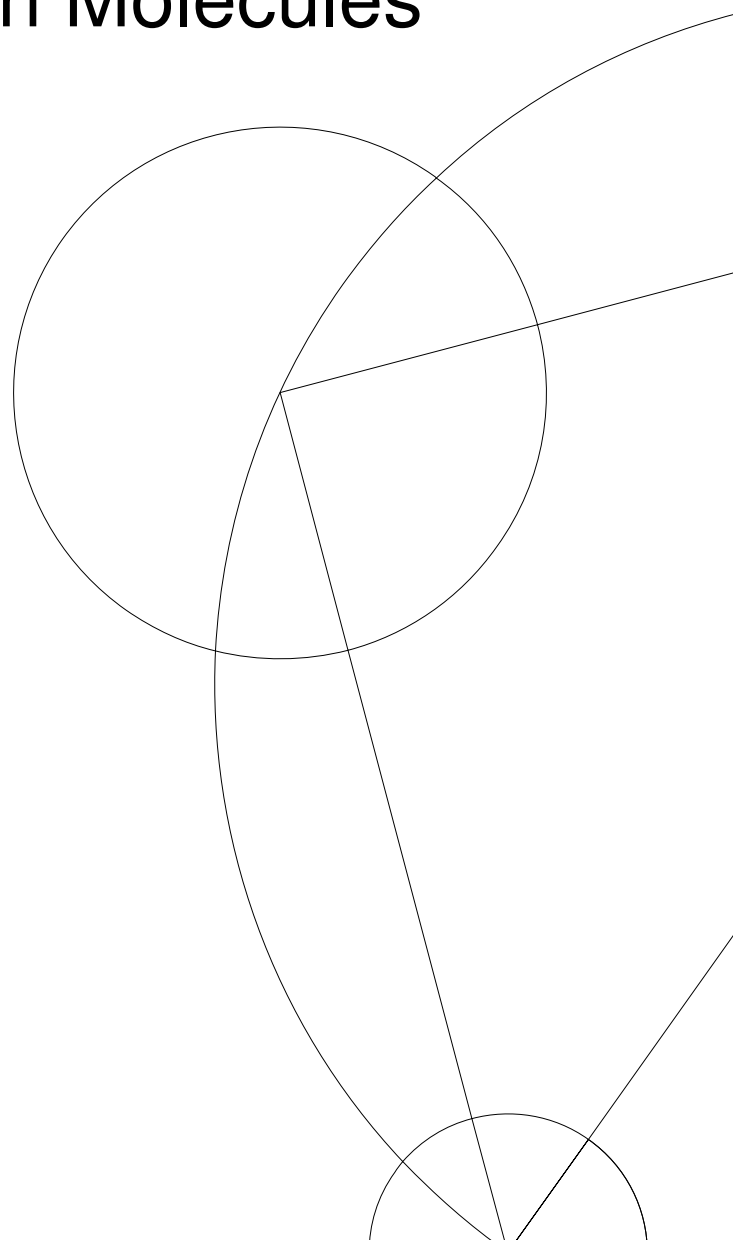

Prof. Jens Paaske, Prof. Karsten Flensberg

Friday 27th June, 2014

Contents

Acknowledgements

Doing the work, which is presented in this thesis, was a delightful experience. Quite a lot of people have helped and inspired me during the PhD studies.

I was lucky to have two supervisors, Jens Paaske and Karsten Flensberg, who I thank for admitting me as their PhD student and providing me the guidance and direction for my research during the last several years. Also I am thankful for all the amusing discussions we had, for teaching me the importance of communicating my research, and allowing me to go to various conferences.

My PhD would not have been so much fun without my office companions Kim Georg Lind Pedersen, Konrad Wölms, and Samuel Sánchez, who were always up for some physics (or not necessarily) discussion and would help me regarding various things. Additionally, I am grateful to Kim and Konrad for reading my thesis draft and giving me useful comments.

I am thankful to Martin Leijsne for supervising me on the thermoelectrics project, and I enjoyed a fruitful collaboration with Qian Li and Gemma C. Solomon on the same project. During my visit at the Yale University I learned a lot from Leonid Glazman and Moshe Goldstein, and I am grateful to them for sharing their experience with me. It was a pleasant stay in New Haven and for that I have to thank to Chad Sanada and the people in the Department of Physics of the Yale University: Ion Garate, Jukka Väyrynen, Claudia De Grandi, Simon Nigg, and Jérome Dubail.

I had very interesting and fruitful discussions regarding the transport experiments with Jonas Hauptman and Kasper Grove-Rasmussen. Also I have to thank Willy Chang for numerous discussions regarding his experiments and teaming up with me for the first joint experiment-theory QDev group meeting.

I would not have done any of this work unless someone made me interested in the theoretical physics to start with. For this I am thankful to Gediminas Gaigalas and Algirdas Matulis. I want to thank Erikas Gaidamauskas for being a colleague and a friend for a long time. I am indebted to Per Hedegård for helping me to resolve some administrative difficulties during my first few months of the PhD. I would also like to express my sincere thanks for the people (former and present) in the Center of Quantum Devices and the Condensed Matter Theory group at the Niels Bohr Institute: Sthephan Weiss, Verena Koerting, Brian M. Andersen, Heider Moradi, Chiara Stevanato, Maria N. Gastiasoro, Sven Albrecht, Mark Rudner, Jeroen Danon, Morten H. Christensen, Andrew Higginbotham, Ferdinand Kuemmeth, Johanness Beil, Vladimir Posvyanskij, Mathias Lunde, Shantanu Mukherjee, Astrid T. Rømer, Morten Kjaergaard, Michael Bjerngaard, Rasmus B. Christensen, Mingtang Deng, Charles M. Marcus, and probably many others which I forgot to mention.

Finally, I would like to thank my friends and family, in particular my parents, for their continuous support through all the years. Special thanks goes to my wife Gabija for simply being great.

Introduction

Since the invention of the transistor in 1947 and the development of integrated circuits in the late 1950's, there was a rapid progress in the development and miniaturization of the solid state devices and electronic circuit components. This miniaturization raises a question "How small do we have to make a device in order to get fundamentally new properties?" [1], or more concretely, when do the quantum effects become important. During the last 30 years, the innovations in fabrication and cooling techniques allowed to produce nanometer scale solid-state or single molecule-based devices and to perform electrical *transport* experiments at temperatures below one Kelvin (1 K), and thus to address such question. In this thesis we are concerned with the theoretical description of one kind of such devices called *quantum dots*.

As the name suggest a quantum dot is a system where particles are confined in all three directions, which makes it effectively zero dimensional and corresponds to discrete electronic orbitals (levels) and excitation spectrum. This is analogous to the situation in atoms, where confinement potential replaces the potential of the nucleus, thus quantum dots are often referred to as artificial atoms [2, 3]. Additionally, in order for the system to be truly quantum, the size of the dot has to be comparable to the de Broglie wavelength of the electrons in it. What we have mentioned so far is rather abstract conditions, which practically can be realized in various systems, such as, electrically confined electrons in semiconductor nanowires, two dimensional electron gases, carbon nanotubes, or just small metallic particles, nanoscale pieces of semiconductor.

One of the usual ways to make an electronic device with quantum dots is the transistor setup, where the dot is coupled by electron tunneling to the source and drain leads, which can maintain a voltage bias across it. This kind of setup can be referred to as *transport junction*. If the temperature and the tunnel couplings to the leads are low compared to the energy scale associated with charging of the dot, the electrons from the leads are either transferred one-by-one through the junction or the transport is blocked, which is known as the *Coulomb blockade* regime [4]. This depends on the positions of the levels and electrostatic environment of the dot, which can be tuned with an additional gate electrode. As a practical application, it was proposed that operating in such a regime the junction can be used as charge sensor [5], for sensitive temperature measurements [6], or as high efficiency thermoelectric device [7]. Also the current signal acts as a spectroscopic tool, and gives the information about quantum properties of the quantum dot, which is interesting for the studies of fundamental physics. For instance, if a quantum dot has an odd number of electrons, because of the one unpaired electron spin, it acts as a magnetic impurity, which can be screened by conduction electrons, which is known as the *Kondo effect*. This is an interesting phenomenon, which was first observed in 1930's experimentally in metals containing magnetic impurities [8], and only 30 years later the first theoretical explanation was given by Jun Kondo in 1964 [9]. The observation of the Kondo effect in quantum dots in late 1990's [10, 11], where it manifests itself through zero bias differential conductance due to so-called Abrikosov-Suhl resonance [12, 13], has revived the interest in this problem. Additionally, during the last decade it became possible to fabricate hybrid systems where quantum dots are contacted to *superconducting leads* [14]. These kind of systems allow to study the interplay between superconductivity and Coulomb blockade

with Kondo effect.

In this thesis we are investigating three problems, which deal with quantum dots in transistor type setup. Even though the setup is similar for all examined problems, the theoretical tools used to solve them are rather distinct. That is why the thesis is divided in three parts. In the following paragraphs we give a short technical description of the individual parts.

The first part is dedicated to the examination of the so-called *cotunneling spectroscopy* of the quantum dots, where in the Coulomb blockade regime simultaneous electron transport happens through the junction by virtual occupation of the excited states of the dot. More specifically, we address the renormalization effects of such spectroscopy due to higher order tunneling processes by considering energy level shifts using leading order quasi-degenerate perturbation theory. Then the renormalization of the cotunneling spectrum for particular carbon nanotube quantum dots connected either to normal metal or ferromagnetic leads is examined using the presented theory.

The second part is devoted to the study of the emergence of sub-gap states in a junction consisting of two superconducting leads coupled to a spinful quantum dot. The system is modelled by an effective Kondo model, where conduction electron spins are interacting with an impurity spin. If the impurity spin is treated as a classical quantity the problem can be solved exactly, which yields the so-called *Yu-Shiba-Rusinov* states inside the gap. For a quantum spin the bound states and their energy are found using the *Yosida's wavefunction ansatz* approach. Additionally, the relation between the supercurrent and the sub-gap states is studied.

In the last part we address the question "How the heat transport due to center of mass vibrational modes can be reduced in a *molecular junction*, while maintaining electrical conductivity?". As one of the possible suggestions we consider a molecular design consisting of two large masses coupled to each other and to the leads. By having a small spring constant between the masses, it is possible to reduce the heat transport due to vibrations. As one of the possible realization of this idea we examine *π-stacked* molecular structures. The resulting heat transport is compared with the situation when the molecule is modelled as a single mass.

Part I

Tunneling renormalization of cotunneling spectroscopy

Chapter 1

Sequential tunneling and cotunneling spectroscopy of quantum dots

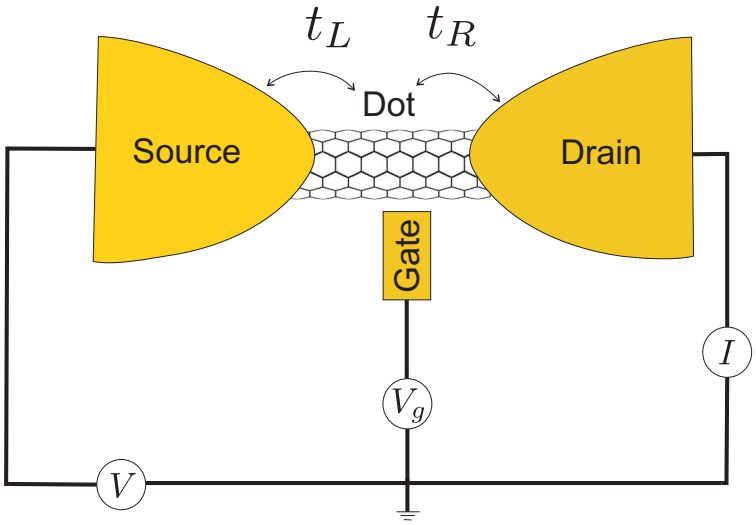

Figure 1.1: Quantum dot coupled to the source, drain, and gate electrodes. Here V denotes source-drain bias, V_g is the gate voltage, I is the current flowing through the device, and $t_{L,R}$ are tunnel couplings from the quantum dot to the source and drain.

Solid-state quantum dot devices are made of nanostructure tunnel coupled to source and drain electrodes. If the temperature is very low and the Coulomb interaction is sufficiently strong, the device is said to be in the Coulomb blockade regime [4]. The characteristic feature of such a system is the suppression of the single electron transport processes and the appearance of simultaneous few electron transport, called the cotunneling effect, in which energetically unfavorable states are populated by virtual transitions from the lead having higher chemical potential for the electrons, and then this population is relaxed to the lead having smaller chemical potential. The chemical potential difference across the junction can be obtained by voltage biasing it. The cotunneling processes are classified either as elastic, if the quantum dot energy state is unchanged, or inelastic, if the quantum dot is left in the excited state after charge transport [15]. Whether the device will be left in the excited state depends on the applied bias across the device. In such a way, by performing bias spectroscopy [16–18], one can obtain the energy level structure of the quantum dot, which is important for understanding and predicting the behavior of the device.

It is known that the coupling to the leads produces quantum dot energy level shifts [19, 20]

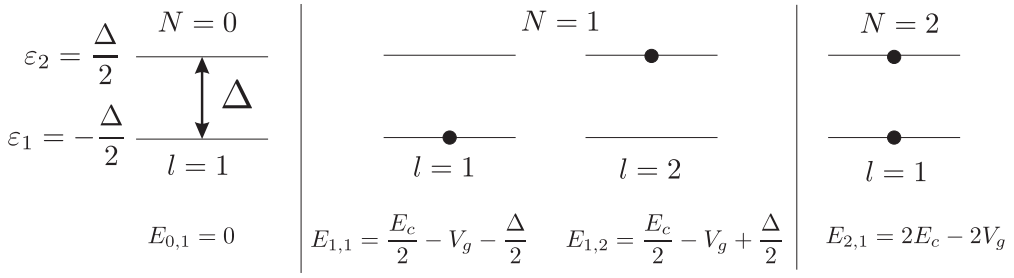

Figure 1.2: Different charge states N of a simple case of a quantum dot containing two single particle states $\varepsilon_1 = -\frac{\Delta}{2}$ and $\varepsilon_2 = \frac{\Delta}{2}$. Black dots denote occupied single particle states and Δ is energy difference between them. Here constant energy for all charge states $\frac{E_c N_g^2}{2}$ is neglected.

and broadening due to hybridization of the lead states with the quantum dot states. These kind of effects were already experimentally observed for carbon nanotube quantum dots with normal leads [21], where asymmetry between coupling to different orbitals causes a gate dependent cotunneling threshold, and with ferromagnetic leads [22–28], where spin-dependent tunneling creates an exchange field, which may depend on the gate voltage. A large number of theoretical works dealing with the case of ferromagnetic leads and exploiting different methods was already presented [29–44].

In this part of the thesis Iinvestigate the carbon nanotube quantum dot cotunneling thresholds and the effects of their renormalization due to the tunneling to the leads. Two different cases of normal (Chapter 4) and ferromagnetic (Chapter 5) leads are examined. Throughout this part, except in Chapter 3, we employ units in which the Planck constant, the Boltzmann constant, the elementary charge, and the Bohr magneton are equal to one, i.e. $\hbar = k_B = e = \mu_B = 1$.

The device under consideration is a quantum dot coupled to the source and drain electrodes, which have an applied bias V and maintain a current I through the device (Figure 1.1). There is also another gate electrode, capacitively coupled to the quantum dot, which is used to change the electrostatic environment on the dot by applying a voltage V_g to it. By sweeping the source-drain voltage V and the gate voltage V_g it is possible to acquire spectroscopic information about the quantum dot region. If the device is in the Coulomb blockade regime one gets diamond like differential conductance ($\mathrm{d}I/\mathrm{d}V$) dependence on the source-drain V and the gate V_g voltages, which is shown in schematic contour plot, called a *stability diagram*, in Figure 1.4.

1.1 Constant interaction model

The interpretation of the experimental data of transport through quantum dots operating in the Coulomb blockade regime can be based on a constant interaction model [4, 15]. In this model it is assumed that the Coulomb interactions on the dot can be parameterized by a charging energy E_c required when adding an additional electron to the quantum dot. It is also assumed that the single particle energy level spectrum ε_n of the quantum dot is independent of these interactions. So the total energy of the system having N electrons, and occupying particular single particle states ε_n is given by

$$E_{N,l} = \frac{E_c}{2}(N - N_g)^2 + \sum_{n \text{ corresponding to } l} \varepsilon_n, \tag{1.1}$$

where the label l denotes a particular occupation of single particle orbitals for a given number of electrons, and we will simply call it the orbital quantum number. Here $V_g = E_c N_g$ corresponds to the gate voltage.

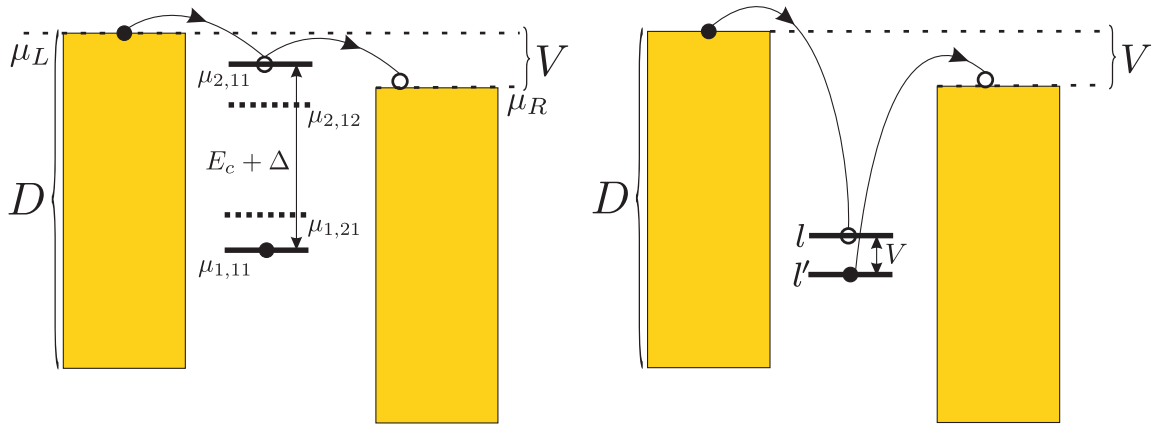

(a) Sequential tunneling (b) Cotunneling

Figure 1.3: Illustration of first order sequential tunneling and second order cotunneling processes. For sequential tunneling (a) the solid lines denote the transitions through the ground states and the dashed lines through the excited states. The yellow regions schematically denote filled continuum states of the leads. Here D denotes the bandwidth of the leads, V is symmetrically applied bias, with $\mu_L = -\mu_R = \frac{V}{2}$ being chemical potentials of the source (μ_L) and the drain (μ_R).

Let us consider some empirical rules used to determine the position of the differential conductance peaks in the stability diagram. A differential conductance peak appears, whenever the energy difference between two different charge states matches the chemical potential of the source (μ_L) or drain (μ_R) lead. For simplicity, we assume the bias to be applied symmetrically to the leads, i.e. $\mu_L = -\mu_R = V/2$. Such peaks result from first order processes called sequential tunneling, and are illustrated in Figure 1.3a, for a simple case of a quantum dot containing two single particle orbitals. So the bias threshold value for sequential tunneling is

$$\mu_{\mathrm{L,R}} = \pm\frac{V_{\mathrm{seq}}}{2} = E_{N,l} - E_{N-1,l'} \equiv \mu_{N,ll'}. \tag{1.2}$$

Sequential tunneling processes determine the Coulomb diamond structure of the stability diagram. There can also appear differential conductance peaks inside the diamonds, called "inelastic cotunneling lines", and they result from second order tunneling processes (Figure 1.3b). The bias threshold value for inelastic cotunneling is given by the energy difference between different orbitals l and l' in a given charge state:

$$|V_{\mathrm{cot}}| = E_{N,l} - E_{N,l'}. \tag{1.3}$$

More precisely this condition corresponds to a inflection point position of $\mathrm{d}I/\mathrm{d}dV$. Note that if the single particle level spacing does not contain any kind of gate voltage dependence, then the cotunneling threshold always corresponds to a horizontal line in the stability diagram. For a quantum dot containing two single particle orbitals the schematic stability diagram is shown in Figure 1.4.

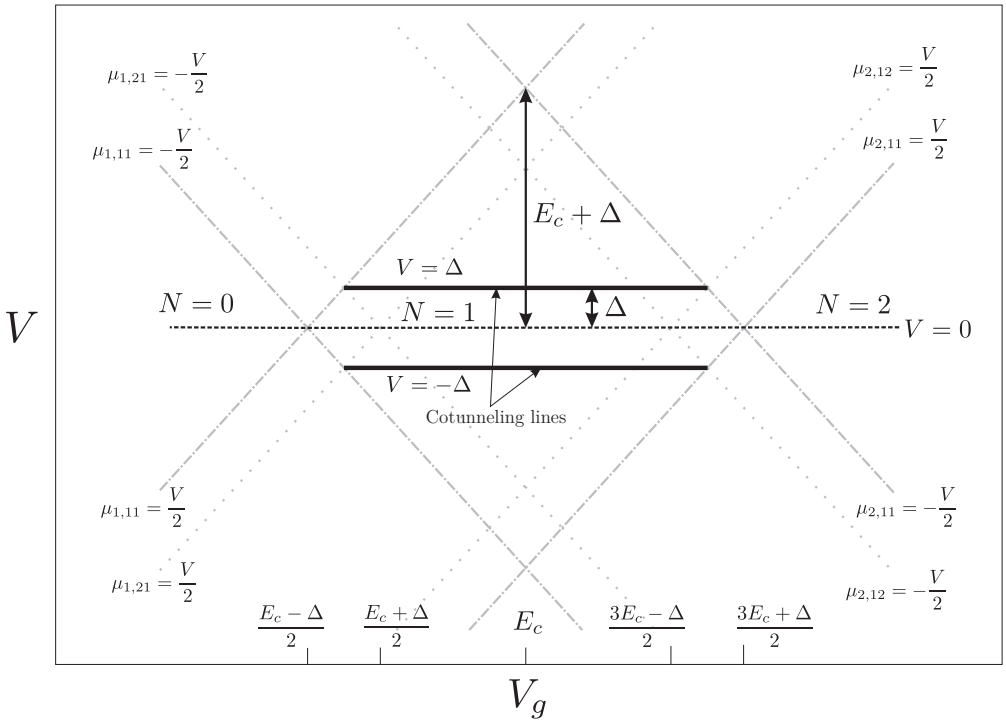

Figure 1.4: Schematic stability diagram for a quantum dot containing two single particle orbitals. In this case there is one Coulomb diamond and (black solid) cotunneling line due to transition from the single particle state ε_1 to the state ε_2 in a charge state $N = 1$. Gray dashed-dotted lines depict the threshold for the sequential tunneling through the ground state, and gray dotted lines depict the threshold for the sequential tunneling through the excited state. Black dashed line shows the position of the zero bias $V = 0$.

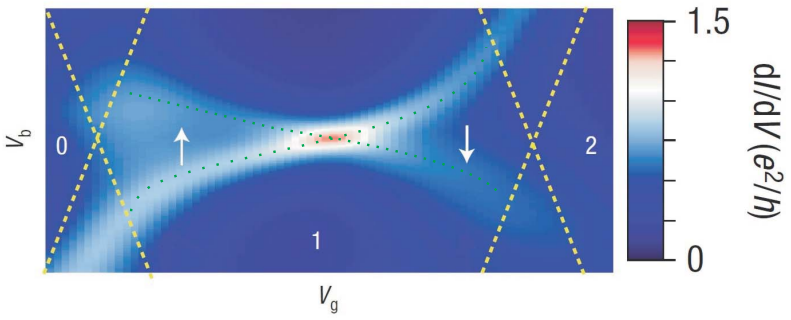

Figure 1.5: Bias spectroscopy performed for a carbon nanotube quantum dot attached to ferromagnetic leads with an applied perpendicular to the tube axis magnetic field of size $B = -1$ T. The gate dependent cotunneling thresholds are observed, which are accentuated by the green dotted curves. For a particular gate voltage the external magnetic field is compensated by an exchange field appearing due to tunneling renormalization. The white arrows denote the ground state of the quantum dot, i.e. either spin-up or spin-down depending on the gate voltage. The yellow dashed lines depict differential conductance peaks corresponding to the sequential tunneling threshold, and the numbers 0, 1, 2 mark the charge state of the quantum dot. The differential conductance $\mathrm{d}I/\mathrm{d}V_b$ is measured in terms of the conductance quanta $G_0 = e^2/h$.

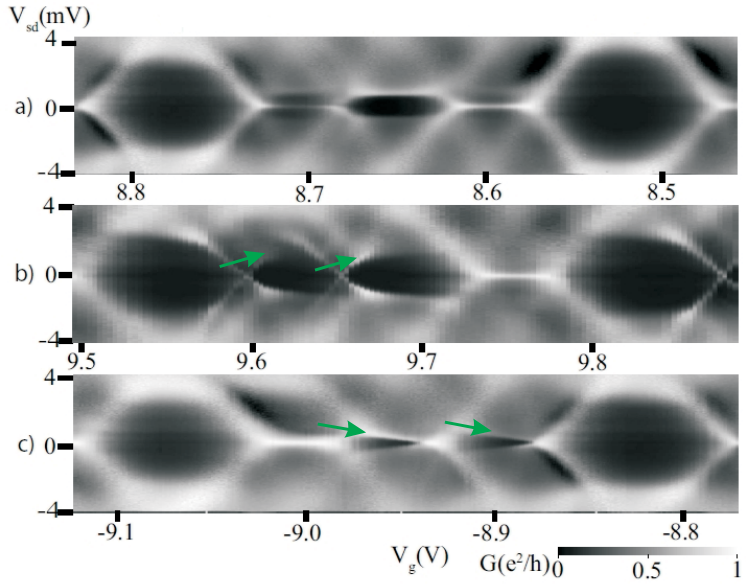

Figure 1.6: Bias spectroscopy performed for a carbon nanotube quantum dot attached to normal leads. The gate dependent cotunneling thresholds are observed for different Coulomb diamonds in b) and c). The green arrows denote the slopes of the positive bias cotunneling thresholds. The differential conductance $G = \mathrm{d}I/\mathrm{d}V_{\mathrm{sd}}$ is measured in terms of the conductance quanta $G_0 = e^2/h$.

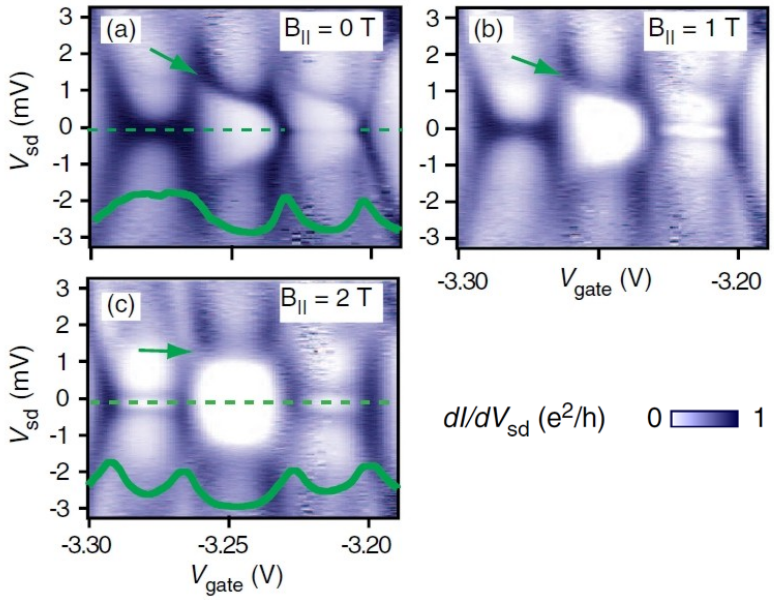

Figure 1.7: Bias spectroscopy performed for a carbon nanotube quantum dot attached to normal leads, with an applied magnetic field parallel to the tube axis. Here also the gate dependent cotunneling thresholds are observed. When the magnetic field is increased the gate dependence becomes diminished. The green arrows show the slopes of the positive bias cotunneling thresholds, and the green curves correspond to zero bias differential conductance. The differential conductance $\mathrm{d}I/\mathrm{d}V_{\mathrm{sd}}$ is measured in terms of the conductance quanta $G_0 = e^2/h$.

1.2 Experiments regarding the tunneling renormalization of cotunneling spectroscopy

From the analysis method presented in Section 1.1 we saw that when the single particle level spacing does not depend on the gate voltage, the cotunneling threshold is also independent of it. However, in several experiments the gate dependence of cotunneling thresholds was observed, which shows that the above analysis is oversimplified [21, 26, 45]. The reason is that a basic cotunneling process itself corresponds to a virtual charge fluctuation of the dot, and as such it also renormalizes the very spectrum which is being observed. Of course the strength of the renormalization effects depends on the relative size of the tunneling coupling and the single particle level spacing.

In this section we shortly review experimental data of Hauptmann *et al.* [26], Holm *et al.* [21], and Grove-Rasmussen *et al.* [45]. In the Hauptmann experiment a carbon nanotube quantum dot was attached to ferromagnetic leads and a magnetic field perpendicular to the tube axis was applied. They observed that tunneling renormalization exerts a gate dependent exchange field, which can compensate the external magnetic field for a particular gate voltage (Figure 1.5). In the Holm experiment the bias spectroscopy of a carbon nanotube quantum dot attached to normal leads was performed, and for some Coulomb diamonds a gate dependent cotunneling thresholds were observed, as it is shown in Figure 1.6. In the Grove-Rasmussen experiment again a the carbon nanotube quantum dot with normal leads was examined, but now a magnetic field parallel to the tube axis was applied. The observation was that for zero magnetic field a gate dependent cotunneling thresholds appeared. However, when the parallel magnetic field was increased this gate dependence was diminished (Figure 1.7).

Chapter 2

Tunneling induced level shifts

2.1 The model

A quantum dot connected to the source and drain electrodes and capacitively coupled to a gate electrode (Figure 1.1) can be modeled by the following constant interaction Hamiltonian

$$H = H_{\mathrm{LR}} + H_{\mathrm{D}} + H_{\mathrm{T}}, \tag{2.1}$$

where

$$H_{\mathrm{LR}} = \sum_{\alpha\nu s} \varepsilon_{\alpha\nu s} c^{\dagger}_{\alpha\nu s} c_{\alpha\nu s}, \tag{2.2}$$

describes the source and drain electrodes as two reservoirs of noninteracting electrons. Operator $c^{\dagger}_{\alpha\nu s}$ creates an electron with quantum number ν and spin $s \in \{\uparrow, \downarrow\}$ in a lead $\alpha \in \{\mathrm{L}, \mathrm{R}\}$, which has energy $\varepsilon_{\alpha\nu s}$. Here L or R stands for the left or right lead, and $\mu_{\mathrm{L,R}} = \pm V/2$ is the chemical potential of the leads, which depends on the applied bias voltage V.

The quantum dot region is described by H_{D} and it is modeled as N_s localized single particle states with the interaction between electrons assumed to be constant:

$$H_{\mathrm{D}} = \sum_{n=1}^{N_s} \varepsilon_n d^{\dagger}_n d_n + U(N - N_g)^2. \tag{2.3}$$

Here $d^{\dagger}_n$ creates an electron in the dot level n with energy ε_n, N_g corresponds to the gate voltage ($V_g = 2UN_g$), $N = \sum_{n=1}^{N} d^{\dagger}_n d_n$ is the total number of electrons on the dot and U denotes the total capacitive charging energy of the dot. The single particle spectrum ε_n for a carbon nanotube quantum dot single "shell", which we are interested in, will be defined in Section 3.3.

The coupling between the leads and the dot is described by the following tunneling Hamiltonian

$$H_{\mathrm{T}} = \sum_{\substack{\alpha\nu s \\ n}} \left(t^{n}_{\alpha\nu s} c^{\dagger}_{\alpha\nu s} d_n + (t^{n}_{\alpha\nu s})^{*} d^{\dagger}_n c_{\alpha\nu s} \right), \tag{2.4}$$

where $t^{n}_{\alpha\nu s}$ is the tunneling amplitude from the dot state n to the lead state $\alpha\nu s$. For a carbon nanotube quantum dot these tunneling amplitudes will be defined in Section 3.4. We will treat the tunneling Hamiltonian H_{T} as a perturbation to $H_{\mathrm{LR}} + H_{\mathrm{D}}$, when examining its influence on the spectrum of the dot.

We will denote the many body eigenstates of the lead Hamiltonian H_{LR} by

$$H_{\mathrm{LR}}|\mathrm{LR}\rangle = E_{\mathrm{LR}}|\mathrm{LR}\rangle, \tag{2.5}$$

where E_{LR} is the energy of the state $|\mathrm{LR}\rangle$, and of the quantum dot Hamiltonian H_{D} by

$$H_{\mathrm{D}}|Nl\rangle = E_{Nl}|Nl\rangle, \tag{2.6}$$

with E_{Nl} being the energy of the state $|Nl\rangle$, where N denotes the number of electrons in the state (which we will call a charge state N) and l is an orbital quantum number of the state. Note that when there are N_s single particle states, the number N_l of different orbitals l for a given charge state N is $N_l = \binom{N_s}{N} = \frac{N_s!}{N!(N_s-N)!}$. From Hamiltonian (2.3) we can read-off the energy of the state $|Nl\rangle$ as

$$E_{Nl} = U(N - N_g)^2 + \sum_{n\in|Nl\rangle} \varepsilon_n, \tag{2.7}$$

where by $\sum_{n\in|Nl\rangle}\ldots$ we mean sum over all occupied single particle states in a many body state $|Nl\rangle$. We will also denote the many body eigenstates of the dot by $|\mathcal{D}\rangle$, where $\mathcal{D}$ is labeled by integers, i.e.

$$|\mathcal{D}\rangle \in \{|1\rangle,\ldots,|2^{N_s}\rangle\}, \tag{2.8}$$

and all the states first are sorted by the number of charges in the state, and for the same charge by increasing energy.

2.2 Application of quasi-degenerate perturbation theory

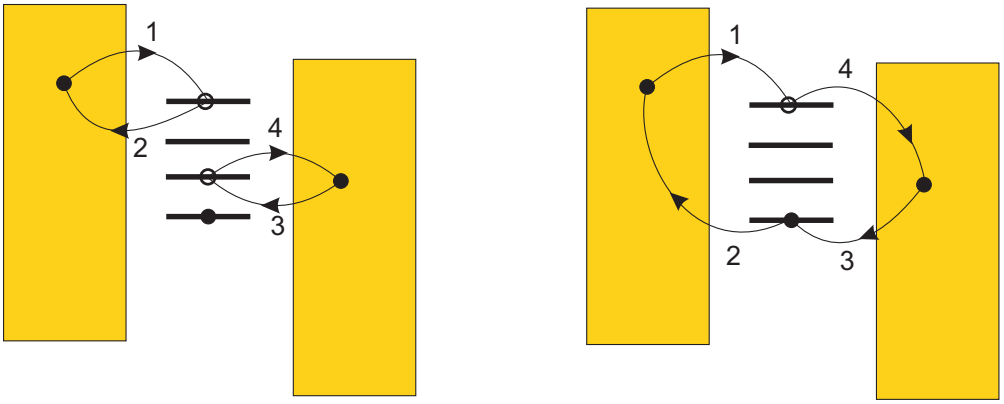

Figure 2.1: Examples of processes (which have the ground state of the leads $|\overline{\mathrm{LR}}\rangle$ as an intermediate state) responsible for appearance of the terms proportional to $\frac{\Gamma}{\Delta}$ in fourth order expansion of usual Rayleigh-Schrödinger perturbation theory. The numbers denote the order of processes.

We want to determine how the tunneling renormalizes the energy of the many-body states of Hamiltonian $H_{\mathrm{LR}} + H_{\mathrm{D}}$. For this purpose, we will use quasi-degenerate perturbation theory ("Löwdin partitioning") described in [46, 47] to determine this energy renormalization. More precisely, we want to derive an effective Hamiltonian and calculate the energy shifts of the states $|\mathcal{D}\rangle|\overline{\mathrm{LR}}\rangle$, where $|\mathcal{D}\rangle$ is any many body state of the dot Hamiltonian (2.3), and $|\overline{\mathrm{LR}}\rangle$ is one particular many body state of the leads (for example, zero temperature ground state of the leads). We are also interested in the regime, where gate voltage V_g is around the middle of a particular charge state diamond (see Figure 1.4), i.e. far from charge degeneracy points, and the tunneling rates Γ are comparable or larger than a single particle level spacing Δ.

The idea of quasi-degenerate perturbation theory is to divide the eigenstates of $H_0 = H_{\mathrm{LR}} + H_{\mathrm{D}}$ into two subsets $|m\rangle \in A$ and $|l\rangle \in B$, and perform a unitary transformation $\mathrm{e}^{\mathrm{i}S}$ to the full

Hamiltonian (2.1) in such a way that for the transformed Hamiltonian

$$\tilde{H} = \mathrm{e}^{-\mathrm{i}S} H \mathrm{e}^{\mathrm{i}S}, \tag{2.9}$$

the matrix elements $\tilde{H}_{ml} = \langle m|\tilde{H}|l\rangle$ between the states in different sets A and B vanish to desired order in the tunneling Hamiltonian H_T (2.4). The matrix elements of the effective Hamiltonian (2.9) for $|m\rangle$ states in a set A takes the following form

$$\tilde{H}_{mm'} = H^{(0)}_{mm'} + H^{(1)}_{mm'} + H^{(2)}_{mm'} + H^{(3)}_{mm'} + H^{(4)}_{mm'} + \ldots, \tag{2.10}$$

and up to second order we have the following expressions [47]

$$H^{(0)}_{mm'} = \left(H^{\mathrm{LR}}_{mm} + H^{\mathrm{D}}_{mm}\right)\delta_{mm'}, \tag{2.11a}$$

$$H^{(1)}_{mm'} = H^{\mathrm{T}}_{mm'}, \tag{2.11b}$$

$$H^{(2)}_{mm'} = \frac{1}{2}\sum_l H^{\mathrm{T}}_{ml} H^{\mathrm{T}}_{lm'} \left(\frac{1}{E_m - E_l} + \frac{1}{E_{m'} - E_l}\right), \tag{2.11c}$$

where E are energies of the states. Here the sum $\sum_l \ldots$ runs over all the states $|l\rangle$ in the set B. We also have changed the subscripts D, LR, T into superscripts for convenience. The expression of the fourth order effective Hamiltonian, to which we will perform our calculations, is specified in Appendix B.

Now we need to specify the states in the set A, which we will call *the model space*. Because we are interested in the energy shift of the many body state $|\mathcal{D}\rangle|\overline{\mathrm{LR}}\rangle$, we could make our model space consisting only of this state, and then we would recover the usual Rayleigh-Schrödinger perturbation theory. However, we are interested in a particular regime, when tunneling rates Γ are comparable or larger than the single particle level spacing Δ (note that the tunneling rates are defined in the beginning of the Chapter 4). In such a case the usual Rayleigh-Schrödinger perturbative expansion with only a single state in the model space breaks down due to the fourth order terms, which are proportional to $\frac{\Gamma}{\Delta}$. This situation occurs because it is possible to have intermediate states $|l\rangle$, containing the particular state of the leads $|\overline{\mathrm{LR}}\rangle$, as depicted in Figure 2.1. But, if it is projected to an extended model space, containing all many body states having $|\overline{\mathrm{LR}}\rangle$ particular state of the leads, this situation is resolved. The calculation of fourth order terms is more thoroughly discussed in Appendix B. So we choose our model space $|m\rangle \in A$ to consist of all the states containing any quantum dot state $|\mathcal{D}\rangle$ and the particular state of the leads $|\overline{\mathrm{LR}}\rangle$:

$$A = \{|1\rangle|\overline{\mathrm{LR}}\rangle, \ldots, |2^{N_s}\rangle|\overline{\mathrm{LR}}\rangle\}. \tag{2.12a}$$

The space of intermediate states $|l\rangle \in B$ contains

$$B = \{|1\rangle|\mathrm{LR}'\rangle, \ldots, |2^{N_s}\rangle|\mathrm{LR}'\rangle\}, \tag{2.12b}$$

where $|\mathrm{LR}'\rangle \neq |\overline{\mathrm{LR}}\rangle$. As can be seen from (2.11) such procedure introduces off-diagonal elements between different quantum dot states.

After having defined our model space A, we start calculating more explicit expressions for the effective Hamiltonian (2.10). Expression (2.11a) simply gives the energy of the state $|m\rangle$ if $m = m'$:

$$H^{(0)}_{\mathcal{D}\mathcal{D}',\overline{\mathrm{LR}}} = \left(E_{\overline{\mathrm{LR}}} + E_{\mathcal{D}}\right)\delta_{\mathcal{D}\mathcal{D}'}, \tag{2.13}$$

We see that the energy of a particular state of the leads $E_{\overline{\mathrm{LR}}}$ is a common constant term for all the dot states, so we neglect it. The first order contribution is equal to zero as is the case with all odd order contributions

$$\begin{aligned} H^{(1)}_{\mathcal{D}\mathcal{D}',\overline{\mathrm{LR}}} &= \sum_{\substack{\alpha\nu s\\ n}} \Big(t^n_{\alpha\nu s} \langle\overline{\mathrm{LR}}|\langle\mathcal{D}|c^\dagger_{\alpha\nu s} d_n|\mathcal{D}'\rangle|\overline{\mathrm{LR}}\rangle + (t^n_{\alpha\nu s})^* \langle\overline{\mathrm{LR}}|\langle\mathcal{D}|d^\dagger_n c_{\alpha\nu s}|\mathcal{D}'\rangle|\overline{\mathrm{LR}}\rangle \Big) \\ &= \sum_{\substack{\alpha\nu s\\ n}} \Big(t^n_{\alpha\nu s} (-1)^{N_{\mathcal{D}}} \langle\overline{\mathrm{LR}}|c^\dagger_{\alpha\nu s}|\overline{\mathrm{LR}}\rangle\langle\mathcal{D}|d_n|\mathcal{D}'\rangle \\ &\qquad + (t^n_{\alpha\nu s})^* (-1)^{N_{\mathcal{D}'}} \langle\overline{\mathrm{LR}}|c_{\alpha\nu s}|\overline{\mathrm{LR}}\rangle\langle\mathcal{D}|d^\dagger_n|\mathcal{D}'\rangle \Big) = 0, \end{aligned} \tag{2.14}$$

$$H^{(2n+1)}_{\mathcal{D}\mathcal{D}',\overline{\mathrm{LR}}} = 0, \quad n \in \mathbb{N}, \tag{2.15}$$

because we have chosen our model space to contain only one lead state $|\overline{\mathrm{LR}}\rangle$ and the odd powers of tunneling Hamiltonian does not conserve the number of particles in the leads. Here $N_{\mathcal{D}}$ denotes the number of electrons in the state $|\mathcal{D}\rangle$. Now we will work out the second order expression (2.11c):

$$\begin{aligned} H^{(2)}_{\mathcal{D}\mathcal{D}',\overline{\mathrm{LR}}} &= \frac{1}{2} \sum_{|\mathcal{D}''\rangle|\mathrm{LR}'\rangle\notin A} \left(\frac{1}{E_{\overline{\mathrm{LR}}} + E_{\mathcal{D}} - E_{\mathrm{LR}'} - E_{\mathcal{D}''}} + \frac{1}{E_{\overline{\mathrm{LR}}} + E_{\mathcal{D}'} - E_{\mathrm{LR}'} - E_{\mathcal{D}''}} \right) \\ &\qquad \times \langle\overline{\mathrm{LR}}|\langle\mathcal{D}|H_{\mathrm{T}}|\mathcal{D}''\rangle|\mathrm{LR}'\rangle\langle\mathrm{LR}'|\langle\mathcal{D}''|H_{\mathrm{T}}|\mathcal{D}'\rangle|\overline{\mathrm{LR}}\rangle \\ &= \frac{1}{2} \sum_{|\mathrm{LR}'\rangle,|\mathcal{D}''\rangle} \sum_{\substack{n\\ \alpha\nu s}} \sum_{\substack{n'\\ \alpha'\nu's'}} \left(\frac{1}{E_{\overline{\mathrm{LR}}} + E_{\mathcal{D}} - E_{\mathrm{LR}'} - E_{\mathcal{D}''}} + \frac{1}{E_{\overline{\mathrm{LR}}} + E_{\mathcal{D}'} - E_{\mathrm{LR}'} - E_{\mathcal{D}''}} \right) \\ &\qquad \times \langle\overline{\mathrm{LR}}|\langle\mathcal{D}|\Big(t^n_{\alpha\nu s} c^\dagger_{\alpha\nu s} d_n + (t^n_{\alpha\nu s})^* d^\dagger_n c_{\alpha\nu s}\Big)|\mathcal{D}''\rangle|\mathrm{LR}'\rangle \\ &\qquad \times \langle\mathrm{LR}'|\langle\mathcal{D}''|\Big(t^{n'}_{\alpha'\nu's'} c^\dagger_{\alpha'\nu's'} d_{n'} + (t^{n'}_{\alpha'\nu's'})^* d^\dagger_{n'} c_{\alpha'\nu's'}\Big)|\mathcal{D}'\rangle|\overline{\mathrm{LR}}\rangle \\ &= \frac{1}{2} \sum_{|\mathrm{LR}'\rangle,|\mathcal{D}''\rangle} \sum_{\substack{n\\ \alpha\nu s}} \sum_{\substack{n'\\ \alpha'\nu's'}} \left(\frac{1}{E_{\overline{\mathrm{LR}}} + E_{\mathcal{D}} - E_{\mathrm{LR}'} - E_{\mathcal{D}''}} + \frac{1}{E_{\overline{\mathrm{LR}}} + E_{\mathcal{D}'} - E_{\mathrm{LR}'} - E_{\mathcal{D}''}} \right) \\ &\qquad \times \Big\{ \langle\overline{\mathrm{LR}}|\langle\mathcal{D}|t^n_{\alpha\nu s} c^\dagger_{\alpha\nu s} d_n|\mathcal{D}''\rangle|\mathrm{LR}'\rangle\langle\mathrm{LR}'|\langle\mathcal{D}''|t^{n'}_{\alpha'\nu's'} c^\dagger_{\alpha'\nu's'} d_{n'}|\mathcal{D}'\rangle|\overline{\mathrm{LR}}\rangle \\ &\qquad + \langle\overline{\mathrm{LR}}|\langle\mathcal{D}|t^n_{\alpha\nu s} c^\dagger_{\alpha\nu s} d_n|\mathcal{D}''\rangle|\mathrm{LR}'\rangle\langle\mathrm{LR}'|\langle\mathcal{D}''|(t^{n'}_{\alpha'\nu's'})^* d^\dagger_{n'} c_{\alpha'\nu's'}|\mathcal{D}'\rangle|\overline{\mathrm{LR}}\rangle \\ &\qquad + \langle\overline{\mathrm{LR}}|\langle\mathcal{D}|(t^n_{\alpha\nu s})^* d^\dagger_n c_{\alpha\nu s}|\mathcal{D}''\rangle|\mathrm{LR}'\rangle\langle\mathrm{LR}'|\langle\mathcal{D}''|t^{n'}_{\alpha'\nu's'} c^\dagger_{\alpha'\nu's'} d_{n'}|\mathcal{D}'\rangle|\overline{\mathrm{LR}}\rangle \\ &\qquad + \langle\overline{\mathrm{LR}}|\langle\mathcal{D}|(t^n_{\alpha\nu s})^* d^\dagger_n c_{\alpha\nu s}|\mathcal{D}''\rangle|\mathrm{LR}'\rangle\langle\mathrm{LR}'|\langle\mathcal{D}''|(t^{n'}_{\alpha'\nu's'})^* d^\dagger_{n'} c_{\alpha'\nu's'}|\mathcal{D}'\rangle|\overline{\mathrm{LR}}\rangle \Big\} \\ &= \frac{1}{2} \sum_{\substack{\alpha\nu s\\ nn'\\ |\mathcal{D}''\rangle}} \Bigg\{ t^n_{\alpha\nu s} (t^{n'}_{\alpha\nu s})^* |\langle\overline{\mathrm{LR}}|c^\dagger_{\alpha\nu s} c_{\alpha\nu s}|\overline{\mathrm{LR}}\rangle|^2 \langle\mathcal{D}|d_n|\mathcal{D}''\rangle\langle\mathcal{D}''|d^\dagger_{n'}|\mathcal{D}'\rangle \left(\frac{1}{\varepsilon_{\alpha\nu s} + E_{\mathcal{D}} - E_{\mathcal{D}''}} + \frac{1}{\varepsilon_{\alpha\nu s} + E_{\mathcal{D}'} - E_{\mathcal{D}''}} \right) \\ &\qquad + (t^n_{\alpha\nu s})^* t^{n'}_{\alpha\nu s} |\langle\overline{\mathrm{LR}}|c_{\alpha\nu s} c^\dagger_{\alpha\nu s}|\overline{\mathrm{LR}}\rangle|^2 \langle\mathcal{D}|d^\dagger_n|\mathcal{D}''\rangle\langle\mathcal{D}''|d_{n'}|\mathcal{D}'\rangle \left(\frac{1}{-\varepsilon_{\alpha\nu s} + E_{\mathcal{D}} - E_{\mathcal{D}''}} + \frac{1}{-\varepsilon_{\alpha\nu s} + E_{\mathcal{D}'} - E_{\mathcal{D}''}} \right) \Bigg\}. \end{aligned} \tag{2.16}$$

After the second equality we extended the sum over all lead and dot states, because the matrix element $\langle\overline{\mathrm{LR}}|H_{\mathrm{T}}|\overline{\mathrm{LR}}\rangle$ is always equal to zero. After the third equality the first and fourth terms in curly brackets vanish, because we always have $\langle\overline{\mathrm{LR}}|c_{\alpha\nu s}|\mathrm{LR}'\rangle\langle\mathrm{LR}'|c_{\alpha'\nu's'}|\overline{\mathrm{LR}}\rangle = 0$, for any state $|\mathrm{LR}'\rangle$. For the second and the third term we get that the terms with $\alpha\nu s = \alpha'\nu's'$ give contribution, and the energy of the intermediate state $|\mathrm{LR}'\rangle$ for the second term is $E_{\mathrm{LR}'} = E_{\overline{\mathrm{LR}}} - \varepsilon_{\alpha\nu s}$ and for the third is $E_{\mathrm{LR}'} = E_{\overline{\mathrm{LR}}} + \varepsilon_{\alpha\nu s}$.

Now we make a thermal average over the particular lead state $|\overline{\mathrm{LR}}\rangle$ for $H^{(0)}_{\mathcal{D}\mathcal{D}',\overline{\mathrm{LR}}}$ and $H^{(2)}_{\mathcal{D}\mathcal{D}',\overline{\mathrm{LR}}}$ assuming grand-canonical ensemble with chemical potentials $\mu_{\mathrm{L,R}}$ and inverse temperatures $\beta_{\mathrm{L,R}} = 1/T_{\mathrm{L,R}}$ for the leads. This yields:

$$H^{(0)}_{\mathcal{D}\mathcal{D}'} = \sum_{|\overline{\mathrm{LR}}\rangle} W_{\overline{\mathrm{LR}}} H^{(0)}_{\mathcal{D}\mathcal{D}',\overline{\mathrm{LR}}} = \delta_{\mathcal{D}\mathcal{D}'}\left(E_{\mathcal{D}} + \sum_{\alpha\nu s}(\varepsilon_{\alpha\nu s} - \mu_\alpha) f_\alpha\right), \tag{2.17a}$$

$$\begin{aligned} H^{(2)}_{\mathcal{D}\mathcal{D}'} &= \sum_{|\overline{\mathrm{LR}}\rangle} W_{\overline{\mathrm{LR}}} H^{(2)}_{\mathcal{D}\mathcal{D}',\overline{\mathrm{LR}}} = \frac{1}{\mathcal{Z}} \sum_{|\overline{\mathrm{LR}}\rangle} \mathrm{e}^{-\beta_{\mathrm{L}}(E_{\mathrm{L}} - \mu_{\mathrm{L}} N_{\mathrm{L}})} \mathrm{e}^{-\beta_{\mathrm{R}}(E_{\mathrm{R}} - \mu_{\mathrm{R}} N_{\mathrm{R}})} H^{(2)}_{\mathcal{D}\mathcal{D}',\overline{\mathrm{LR}}} \\ &= \frac{1}{2} \sum_{\substack{\alpha\nu s \\ nn' \\ |\mathcal{D}''\rangle}} \Bigg\{ t^n_{\alpha\nu s} (t^{n'}_{\alpha\nu s})^* \langle \mathcal{D}|d_n|\mathcal{D}''\rangle\langle\mathcal{D}''|d^\dagger_{n'}|\mathcal{D}'\rangle \left(\frac{1}{\varepsilon_{\alpha\nu s} + E_{\mathcal{D}} - E_{\mathcal{D}''}} + \frac{1}{\varepsilon_{\alpha\nu s} + E_{\mathcal{D}'} - E_{\mathcal{D}''}}\right) f_\alpha \\ &\quad + (t^n_{\alpha\nu s})^* t^{n'}_{\alpha\nu s} \langle \mathcal{D}|d^\dagger_n|\mathcal{D}''\rangle\langle\mathcal{D}''|d_{n'}|\mathcal{D}'\rangle \left(\frac{1}{-\varepsilon_{\alpha\nu s} + E_{\mathcal{D}} - E_{\mathcal{D}''}} + \frac{1}{-\varepsilon_{\alpha\nu s} + E_{\mathcal{D}'} - E_{\mathcal{D}''}}\right)(1 - f_\alpha) \Bigg\}. \end{aligned} \tag{2.17b}$$

Here

$$W_{\overline{\mathrm{LR}}} = \frac{1}{\mathcal{Z}} \mathrm{e}^{-\beta_{\mathrm{L}}(E_{\mathrm{L}} - \mu_{\mathrm{L}} N_{\mathrm{L}})} \mathrm{e}^{-\beta_{\mathrm{R}}(E_{\mathrm{R}} - \mu_{\mathrm{R}} N_{\mathrm{R}})}, \tag{2.18}$$

$$\mathcal{Z} = \sum_{|\overline{\mathrm{LR}}\rangle} \mathrm{e}^{-\beta_{\mathrm{L}}(E_{\mathrm{L}} - \mu_{\mathrm{L}} N_{\mathrm{L}})} \mathrm{e}^{-\beta_{\mathrm{R}}(E_{\mathrm{R}} - \mu_{\mathrm{R}} N_{\mathrm{R}})}, \tag{2.19}$$

is probability to be in particular lead state $|\overline{\mathrm{LR}}\rangle$ and partition function, respectively, and

$$f_\alpha = f(\varepsilon_{\alpha\nu s} - \mu_\alpha) = \frac{1}{\mathrm{e}^{\beta_\alpha(\varepsilon_{\alpha\nu s} - \mu_\alpha)} + 1} \tag{2.20}$$

is Fermi-Dirac distribution. Also E_{L}, E_{R} denote the energy, and N_{L}, N_{R} denote the number of particles in the left and the right lead, respectively, for the state $|\overline{\mathrm{LR}}\rangle$. We see that in (2.17a) only the constant term (which we neglect) is affected when averaging. We note that in the calculations we will take the temperatures of the left and the right lead to be equal, i.e. $\beta_L = \beta_R = \beta$.

To derive the final expression for the effective Hamiltonian to second order in tunneling we need to perform the ν-sums. To do that we make a flat band approximation for the lead electrons, i.e. we assume constant density of states, which is of the form

$$\rho_{\alpha\nu s}(\xi) = \rho_{\alpha s}\theta(D_{a,\alpha s} + \xi_{\alpha\nu s})\,\theta(D_{b,\alpha s} - \xi_{\alpha\nu s}), \tag{2.21}$$

where

$$\xi_{\alpha\nu s} = \varepsilon_{\alpha\nu s} - \mu_\alpha, \tag{2.22}$$

and $\rho_{\alpha s}$, $D_{a,\alpha s}$, $D_{b,\alpha s} > 0$ denotes different constants for the lead index α and spin s, which are all positive. Also $\theta(x)$ denotes Heaviside step function. In a case of normal leads we set the following values of constants

$$D_{a,\alpha s} = D, \quad D_{b,\alpha s} = D, \quad \rho_{\alpha s} = \rho, \tag{2.23}$$

and for ferromagnetic leads we use

$$D_{a,\alpha s} = D + \frac{s\Delta_{\mathrm{st}}}{2}, \quad D_{b,\alpha s} = D - \frac{s\Delta_{\mathrm{st}}}{2}, \tag{2.24}$$

with arbitrary $\rho_{\alpha s}$, and $s = +1(-1)$ for spin up (down). Here $2D$ denotes the bandwidth of the leads, and $\Delta_{\rm st}$ is the Stoner splitting of the bands with different spins s [48]. Lastly, to be able to perform the ν-sums we also assume that tunneling amplitudes do not depend on quantum number ν

$$t^n_{\alpha\nu s} \quad \to \quad t^n_{\alpha s}, \tag{2.25}$$

and then we replace the ν-sums by an integral in the following way

$$\sum_\nu t^n_{\alpha\nu s}\ldots \quad \to \quad \rho_{\alpha s} t^n_{\alpha s}\int_{-D_{a,\alpha s}}^{D_{b,\alpha s}} {\rm d}\xi\ldots. \tag{2.26}$$

Using the above mentioned approximations the second order effective Hamiltonian becomes

$$\begin{aligned}
H^{(2)}_{\mathcal{D}\mathcal{D}'} \approx \lim_{\eta\to+0}\frac{1}{2}\sum_{\alpha s,nn',|\mathcal{D}''\rangle}\rho_{\alpha s}\,{\rm Re}\int_{-D_{a,\alpha s}}^{D_{b,\alpha s}}{\rm d}\xi\Bigg\{& f(\xi)t^n_{\alpha s}(t^{n'}_{\alpha s})^*\langle\mathcal{D}|d_n|\mathcal{D}''\rangle\langle\mathcal{D}''|d^\dagger_{n'}|\mathcal{D}'\rangle\\
&\times\left(\frac{1}{\xi+\mu_\alpha+E_{\mathcal{D}}-E_{\mathcal{D}''}+{\rm i}\eta}+\frac{1}{\xi+\mu_\alpha+E_{\mathcal{D}'}-E_{\mathcal{D}''}+{\rm i}\eta}\right)\\
&+\{1-f(\xi)\}(t^n_{\alpha s})^*t^{n'}_{\alpha s}\langle\mathcal{D}|d^\dagger_n|\mathcal{D}''\rangle\langle\mathcal{D}''|d_{n'}|\mathcal{D}'\rangle\\
&\times\left(\frac{1}{-\xi+\mu_\alpha+E_{\mathcal{D}}-E_{\mathcal{D}''}+{\rm i}\eta}+\frac{1}{-\xi+\mu_\alpha+E_{\mathcal{D}'}-E_{\mathcal{D}''}+{\rm i}\eta}\right)\Bigg\}\\
\overset{T\to0}{\approx}\frac{1}{2}\sum_{\alpha s,nn',|\mathcal{D}''\rangle}\rho_{\alpha s}\Bigg\{& t^n_{\alpha s}(t^{n'}_{\alpha s})^*\langle\mathcal{D}|d_n|\mathcal{D}''\rangle\langle\mathcal{D}''|d^\dagger_{n'}|\mathcal{D}'\rangle\\
&\times\left(\ln\left|\frac{E_{\mathcal{D}}-E_{\mathcal{D}''}+\mu_\alpha}{E_{\mathcal{D}}-E_{\mathcal{D}''}+\mu_\alpha-D_{a,\alpha s}}\right|+\ln\left|\frac{E_{\mathcal{D}'}-E_{\mathcal{D}''}+\mu_\alpha}{E_{\mathcal{D}'}-E_{\mathcal{D}''}+\mu_\alpha-D_{a,\alpha s}}\right|\right)\\
&+(t^n_{\alpha s})^*t^{n'}_{\alpha s}\langle\mathcal{D}|d^\dagger_n|\mathcal{D}''\rangle\langle\mathcal{D}''|d_{n'}|\mathcal{D}'\rangle\\
&\times\left(\ln\left|\frac{E_{\mathcal{D}}-E_{\mathcal{D}''}-\mu_\alpha}{E_{\mathcal{D}}-E_{\mathcal{D}''}-\mu_\alpha-D_{b,\alpha s}}\right|+\ln\left|\frac{E_{\mathcal{D}'}-E_{\mathcal{D}''}-\mu_\alpha}{E_{\mathcal{D}'}-E_{\mathcal{D}''}-\mu_\alpha-D_{b,\alpha s}}\right|\right)\Bigg\}.
\end{aligned} \tag{2.27}$$

After the first equality we have included infinitesimal imaginary part ${\rm i}\eta$ to regularize the integral, and then took only the real part of the integral. After the second equality we took the zero temperature limit in which Fermi-Dirac distribution becomes $f(x) = 1-\theta(x)$. For the finite temperature the logarithms should be replaced by digamma function, as it is discussed in Appendix A. Here we also used the following integrals

$$\lim_{\eta\to+0}\int_0^D\frac{{\rm d}x}{a-x+{\rm i}\eta}=\lim_{\eta\to+0}\int_{-D}^0\frac{{\rm d}x}{a+x+{\rm i}\eta}=\ln\left|\frac{a}{a-D}\right|-\frac{{\rm i}\pi}{2}\{{\rm sgn}(a)-{\rm sgn}(a-D)\}. \tag{2.28}$$

There is one additional approximation, which we make — we assume that the bandwidth of the leads is much larger than the charging energy $2U$, the single particle level spacing Δ, and the applied bias V, and using expressions (2.24) for ferromagnetic leads we obtain the final result for

the second order effective Hamiltonian ($D_{a,\alpha s}, D_{b,\alpha s} >> |E_{\mathcal{D}}|, |E_{\mathcal{D}'}|, |\mu_\alpha|$):

$$
\begin{aligned}
H^{(2)}_{\mathcal{D}\mathcal{D}'} \overset{T\to 0}{\approx} \frac{1}{2} \sum_{\alpha s, nn', |\mathcal{D}''\rangle} \rho_{\alpha s} \Bigg\{ & t^{n}_{\alpha s} (t^{n'}_{\alpha s})^{*} \langle \mathcal{D}|d_n|\mathcal{D}''\rangle\langle\mathcal{D}''|d^{\dagger}_{n'}|\mathcal{D}'\rangle \\
& \times \left(\ln\left|\frac{E_{\mathcal{D}} - E_{\mathcal{D}''} + \mu_\alpha}{D + s\Delta_{\mathrm{st}}/2}\right| + \ln\left|\frac{E_{\mathcal{D}'} - E_{\mathcal{D}''} + \mu_\alpha}{D + s\Delta_{\mathrm{st}}/2}\right| \right) \\
& + (t^{n}_{\alpha s})^{*} t^{n'}_{\alpha s} \langle \mathcal{D}|d^{\dagger}_{n}|\mathcal{D}''\rangle\langle\mathcal{D}''|d_{n'}|\mathcal{D}'\rangle \\
& \times \left(\ln\left|\frac{E_{\mathcal{D}} - E_{\mathcal{D}''} - \mu_\alpha}{D - s\Delta_{\mathrm{st}}/2}\right| + \ln\left|\frac{E_{\mathcal{D}'} - E_{\mathcal{D}''} - \mu_\alpha}{D - s\Delta_{\mathrm{st}}/2}\right| \right) \Bigg\}.
\end{aligned}
\tag{2.29}
$$

We see that the effective Hamiltonian $\tilde{H} \approx H^{(0)} + H^{(2)}$ has a block structure to second order in H_{T}, i.e. only the matrix elements between the same charge dot states $|\mathcal{D}\rangle = |Nl\rangle$ and $|\mathcal{D}'\rangle = |Nl'\rangle$ are non-zero, i.e. $H_{Nl,N'l'} = H_{Nl,Nl'}\delta_{NN'}$. After diagonalizing the effective Hamiltonian $\tilde{H}$, we find the new eigenspectrum $\tilde{E}$ to second order in H_{T}, which will be used to determine the tunneling renormalized cotunneling thresholds in Chapters 4 and 5.

Chapter 3

Carbon nanotube quantum dots

In this Chapterwe shortly review the long wavelength limit, which constitutes the low energy spectrum of carbon nanotubes. We start by reviewing the geometry, the lattice, and the reciprocal lattice of carbon nanotubes (for explanation of these properties one can also see Figure 1 of Ref. [49–51] or Chapter 3 in [52]). Then we introduce an effective low energy Hamiltonian derived by Izumida *et al.* [53]. This Hamiltonian is used to obtain the single particle energy spectrum of the carbon nanotube quantum dot.

3.1 The geometry, the lattice, and the reciprocal lattice of carbon nanotubes

Carbon nanotubes can be thought of as folded two dimensional graphene sheet into a tube (see Figure 3.1a). The lattice of graphene can be described by such a choice of primitive lattice vectors

$$\mathbf{a}_1 = a\{1,0,0\}, \quad \mathbf{a}_2 = a\left\{\frac{1}{2},\frac{\sqrt{3}}{2},0\right\}, \quad \mathbf{a}_3 = h\{0,0,1\}, \tag{3.1}$$

where a is the lattice constant, and $\mathbf{a}_3$ is an additional lattice vector, which is not necessary for describing the graphene lattice, but we will need it, when we calculate the reciprocal lattice. We note that graphene has two sublattices commonly denoted by A and B. The nearest neighbors of a particular carbon atom, denoted by empty circle in sublattice B, belong to different sublattice A, as shown in Figure 3.1a. Vectors connecting nearest neighbor carbon atoms from sublattice B to sublattice A are given by

$$\boldsymbol{\tau}_1 = a\left\{0,\frac{1}{\sqrt{3}},0\right\}, \quad \boldsymbol{\tau}_2 = a\left\{-\frac{1}{2},-\frac{1}{2\sqrt{3}},0\right\}, \quad \boldsymbol{\tau}_3 = a\left\{\frac{1}{2},-\frac{1}{2\sqrt{3}},0\right\}. \tag{3.2}$$

The folding of graphene into a cylinder shape carbon nanotube is described by a chiral vector $\mathbf{C}$ and a chiral angle θ,

$$\mathbf{C} = n\mathbf{a}_1 + m\mathbf{a}_2 \equiv (n,m), \quad n,m \in \mathbb{Z}, \tag{3.3}$$

$$\cos\theta = \frac{\mathbf{C}\cdot\mathbf{a}_1}{|\mathbf{C}||\mathbf{a}_1|} = \frac{2n+m}{2\sqrt{n^2+m^2+nm}}, \tag{3.4}$$

where n and m are integers, and it is enough to consider the following values of n and m

$$0 \le |m| \le n, \tag{3.5}$$

because of the hexagonal symmetry of the lattice. The chiral angle θ shows how much the hexagons of a graphene sheet are tilted with respect to the tube axis direction $\mathbf{T}$, defined by

$$\mathbf{C}\cdot\mathbf{T} = 0. \tag{3.6}$$

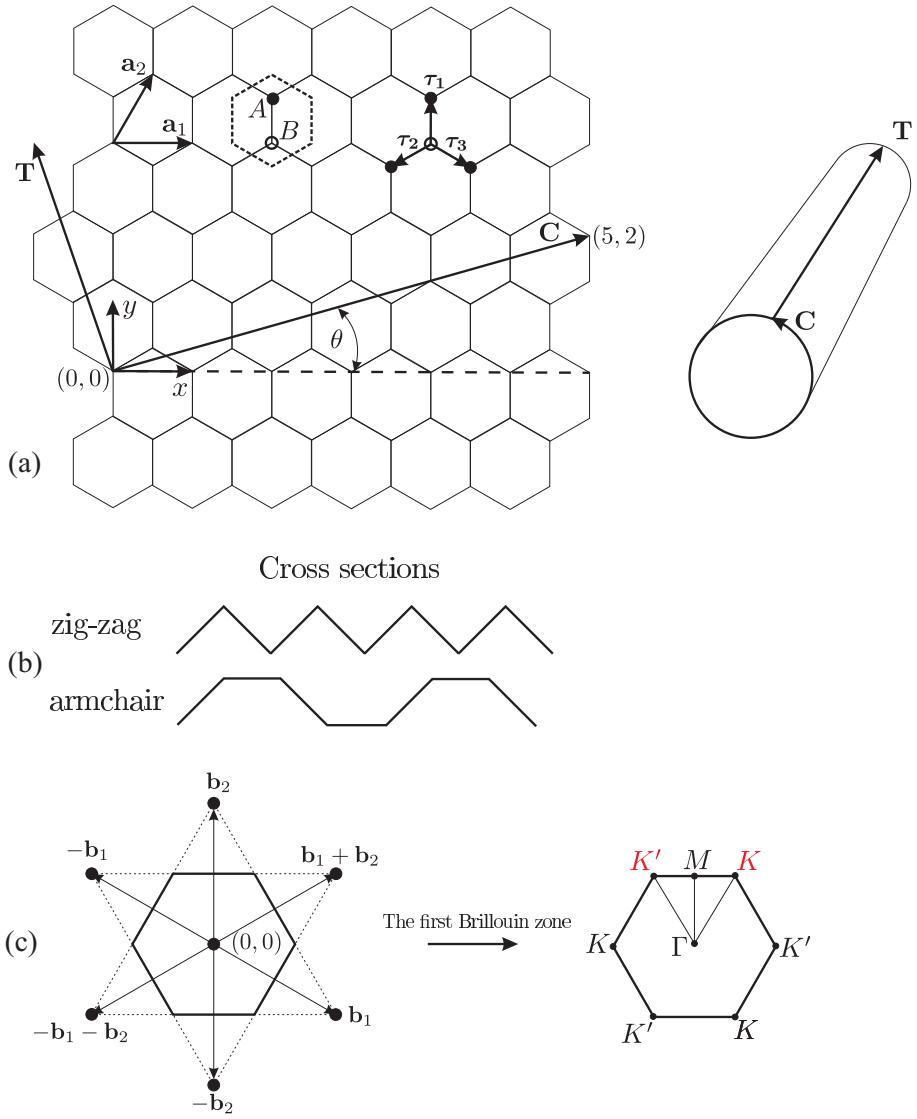

Figure 3.1: The geometry, lattice, and reciprocal lattice of carbon nanotubes.

Also because of the hexagonal symmetry of the graphene sheet it is enough to consider such angles

$$0 \leq \theta \leq \frac{\pi}{6}. \tag{3.7}$$

Tubes with chiral angle $\theta = 0$ are called *zig-zag* and are given by integers $(n, 0)$, and tubes with chiral angle $\theta = \pi/6$ are called *armchair* and are given by integers (n, n). The names *zig-zag* and *arm-chair* come from the appearance of the cross section of the tubes shown in Figure 3.1b. The length of a chiral vector $\mathbf{C}$ gives the circumference of the nanotube, which is

$$|\mathbf{C}| = \sqrt{\mathbf{C} \cdot \mathbf{C}} = \pi D = 2\pi R = a\sqrt{n^2 + m^2 + nm}. \tag{3.8}$$

Here D is the diameter of the tube and R is the radius of the tube. We also note that the lattice vectors are not orthogonal to each other, i.e.

$$\mathbf{a}_1 \cdot \mathbf{a}_2 = \frac{a^2}{2}. \tag{3.9}$$

Now we will construct the reciprocal lattice and the first Brillouin zone of the graphene sheet. The reciprocal lattice translation vectors are defined to satisfy the following orthogonality condition

$$\mathbf{a}_i \cdot \mathbf{b}_j = 2\pi\delta_{ij}. \tag{3.10}$$

We choose the following form of primitive translation vectors of the reciprocal lattice [54] (these relations can also be used as definitions of the reciprocal lattice)

$$\mathbf{b}_1 = 2\pi\frac{\mathbf{a}_2 \times \mathbf{a}_3}{\mathbf{a}_1 \cdot (\mathbf{a}_2 \times \mathbf{a}_3)} = \frac{2\pi}{a}\left\{1, -\frac{1}{\sqrt{3}}, 0\right\}, \tag{3.11a}$$

$$\mathbf{b}_2 = 2\pi\frac{\mathbf{a}_3 \times \mathbf{a}_1}{\mathbf{a}_1 \cdot (\mathbf{a}_2 \times \mathbf{a}_3)} = \frac{2\pi}{a}\left\{0, \frac{2}{\sqrt{3}}, 0\right\}, \tag{3.11b}$$

$$\mathbf{b}_3 = 2\pi\frac{\mathbf{a}_1 \times \mathbf{a}_2}{\mathbf{a}_1 \cdot (\mathbf{a}_2 \times \mathbf{a}_3)} = \frac{2\pi}{h}\{0, 0, 1\}. \tag{3.11c}$$

Here

$$V_a = \mathbf{a}_1 \cdot (\mathbf{a}_2 \times \mathbf{a}_3) = S_a h = \frac{\sqrt{3}}{2}a^2 h \tag{3.12}$$

correspond to the volume of the unit cell (also called the Wigner-Seitz primitive cell) with

$$S_a = \frac{\sqrt{3}}{2}a^2 \tag{3.13}$$

being the area of the unit cell of graphene.

The first Brillouin zone is defined as a primitive unit cell in the reciprocal lattice. We consider the two dimensional Brillouin zone of graphene. The zone boundary, which is defined by vectors $\mathbf{k}_{\mathrm{BZ}}$, can be constructed by satisfying the condition

$$\mathbf{k}_{\mathrm{BZ}} \cdot \left(\frac{1}{2}\mathbf{G}_0\right) = \left|\frac{1}{2}\mathbf{G}_0\right|^2, \tag{3.14}$$

where G_0 is any smallest reciprocal lattice vector satisfying

$$|\mathbf{G}_0| = |u\mathbf{b}_1 + v\mathbf{b}_2| = \frac{4\pi}{a\sqrt{3}}, \quad u, v \in \mathbb{Z}. \tag{3.15}$$

The geometrical construction of the first Brillouin zone is shown in Figure 3.1c. We see that it has hexagonal shape. The volume of the reciprocal lattice unit cell is defined as

$$V_a V_b = (2\pi)^3 \quad \rightarrow \quad V_b = 2\pi S_b h = \frac{2}{\sqrt{3}}\frac{(2\pi)^3}{a^2 h}, \tag{3.16}$$

with

$$S_b = \frac{2}{\sqrt{3}}\left(\frac{2\pi}{a}\right)^2 \tag{3.17}$$

being the area of the two dimensional first Brillouin zone. The corners of the hexagon are called K and K' points, and are given by the vectors

$$\mathbf{K}^\tau = \frac{2\pi}{a}\left\{\frac{\tau}{3}, \frac{1}{\sqrt{3}}\right\}, \tag{3.18}$$

where $\tau = +1$ for K and $\tau = -1$ for K' point. These points corresponds to the Fermi energy of the undoped graphene sheet. We are interested in the low energy excitations in the carbon nanotubes around these points.

3.2 Low energy single particle spectrum of carbon nanotubes

The effective low energy Hamiltonian for π electrons derived using $\mathbf{k}\cdot\mathbf{p}$ perturbation theory near the K and K' points in the first Brillouin zone of carbon nanotube is given by [53]

$$H = H_0 + H_{\mathrm{SO}} + H_{\mathrm{curv}}, \tag{3.19}$$

where H_0 is the effective Hamiltonian without spin-orbit coupling and curvature induced $\sigma-\pi$ band hybridization, and is given by

$$H_0 = \hbar v_F(\sigma_1\tau_0 s_0 k_c + \sigma_2\tau_3 s_0 k_t), \tag{3.20}$$

where k_c is the electron momentum along the circumference, and k_t is the momentum along the tube axis. Also s_i denote Pauli matrices in spin subspace, σ_i in $A-B$ sublattices subspace, τ_i corresponds to K and K' point subspace, and v_F is the Fermi velocity of graphene given by

$$v_F = -\frac{\sqrt{3}aH_\pi}{2\hbar}. \tag{3.21}$$

Here a is the lattice constant of graphene and H_π is the overlap (hopping) integral between π orbitals. We note that spin quantization axis is chosen along the tube axis $\mathbf{T}$. The hybridization of $\sigma-\pi$ bands induced by spin-orbit coupling is described by the effective Hamiltonian

$$H_{\mathrm{SO}} = \hbar v_F\left(-\sigma_1\tau_0 s_3 k_{\mathrm{SO}} + \sigma_0\tau_3 s_3 k_0\right), \tag{3.22}$$

where

$$k_{\mathrm{SO}} = \alpha_1\frac{\Delta_C}{2\hbar v_F R}, \tag{3.23a}$$

$$k_0 = \alpha_2\frac{\Delta_C}{2\hbar v_F R}\cos(3\theta), \tag{3.23b}$$

with Δ_C being the spin-orbit coupling energy in carbon atom, α_1, α_2 are parameters, which were calculated using tight binding approach in Ref. [53], θ is the chiral angle of the nanotube defined in the interval $\{0,\pi/6\}$, and R is the radius of the nanotube.

The hybridization of $\sigma-\pi$ bands induced by curvature effects is described by the effective Hamiltonian

$$H_{\mathrm{curv}} = -\hbar v_F(\sigma_1\tau_3 s_0 k_{c,\mathrm{cv}} + \sigma_2\tau_0 s_0 k_{t,\mathrm{cv}}), \tag{3.24}$$

where

$$k_{c,\mathrm{cv}} = \beta\frac{\cos(3\theta)}{4\hbar v_F R^2}, \tag{3.25a}$$

$$k_{t,\mathrm{cv}} = \zeta\frac{\sin(3\theta)}{4R^2}, \tag{3.25b}$$

with β and ζ being parameters again calculated using a tight binding approach. We again rewrite the effective Hamiltonian, but now explicitly specify the $A-B$ sublattices subspace:

$$H = \hbar v_F \begin{array}{c} \\ \tau s k_0 \\ (k_c - \tau k_{c,\mathrm{cv}} - s k_{\mathrm{SO}}) + \mathrm{i}(\tau k_t - k_{t,\mathrm{cv}}) \end{array} \begin{array}{c} \begin{array}{cc} A & \qquad B \end{array} \\ \begin{pmatrix} \tau s k_0 & (k_c - \tau k_{c,\mathrm{cv}} - s k_{\mathrm{SO}}) - \mathrm{i}(\tau k_t - k_{t,\mathrm{cv}}) \\ (k_c - \tau k_{c,\mathrm{cv}} - s k_{\mathrm{SO}}) + \mathrm{i}(\tau k_t - k_{t,\mathrm{cv}}) & \tau s k_0 \end{pmatrix} \end{array}. \tag{3.26}$$

Here $\tau = +1$ for K and $\tau = -1$ for K' point, and $s = +1$ for spin up $\uparrow$ and $s = -1$ for spin down $\downarrow$. We can write the above Hamiltonian in a different gauge used in Ref. [51, 55] by performing the following unitary transformation $H \to UHU^{-1}$,

$$U = \begin{pmatrix} \tau & 0 \\ 0 & 1 \end{pmatrix}. \tag{3.27}$$

Then the Hamiltonian (3.26) becomes

$$H = \hbar v_F \begin{array}{c} \\ A \\ B \end{array} \begin{array}{c} \begin{array}{cc} A & \quad B \end{array} \\ \begin{pmatrix} \tau s k_0 & (\tau k_c - k_{c,\mathrm{cv}} - \tau s k_{\mathrm{SO}}) - \mathrm{i}(k_t - \tau k_{t,\mathrm{cv}}) \\ (\tau k_c - k_{c,\mathrm{cv}} - \tau s k_{\mathrm{SO}}) + \mathrm{i}(k_t - \tau k_{t,\mathrm{cv}}) & \tau s k_0 \end{pmatrix} \end{array}. \tag{3.28}$$

After performing the $\mathbf{k}\cdot\mathbf{p}$ perturbative expansion near the K and K' points the wavefunction in a real space representation happens to be [49]

$$\Psi_{\tau,s,k_c,k_t}(c,t) = \mathrm{e}^{\mathrm{i}\mathbf{K}^\tau\cdot\mathbf{r}}\psi_{\tau,s,k_c,k_t}(c,t) = \mathrm{e}^{\mathrm{i}\mathbf{K}^\tau\cdot\mathbf{r}}\mathrm{e}^{\mathrm{i}(k_c c + k_t t)}\begin{pmatrix} z_{\tau,s,k_c,k_t} \\ 1 \end{pmatrix}, \tag{3.29}$$

where ψ_{τ,s,k_c,k_t} is the eigenfunction of Hamiltonian (3.26) expressed in either real space or momentum representations, with

$$\begin{aligned} &z_{\tau,s,k_c,k_t} = \pm\frac{\tilde{k}_c - \mathrm{i}\tilde{k}_t}{\sqrt{\tilde{k}_c^2 + \tilde{k}_t^2}}, \quad \tilde{k}_c = k_c - \tau k_{c,\mathrm{cv}} - s k_{\mathrm{SO}}, \quad \tilde{k}_t = \tau k_t - k_{t,\mathrm{cv}}, \\ &\text{or} \quad \tilde{k}_c = \tau k_c - k_{c,\mathrm{cv}} - \tau s k_{\mathrm{SO}}, \quad \tilde{k}_t = k_t - \tau k_{t,\mathrm{cv}}, \quad \text{for Hamiltonian (3.28)}, \end{aligned} \tag{3.30}$$

Here a minus sign in z_{τ,s,k_c,k_t} corresponds to the valence band, a plus sign corresponds to the conduction band, and the vector $\begin{pmatrix} z_{\tau,s,k_c,k_t} \\ 1 \end{pmatrix}$ is written in $A-B$ sublattices subspace. Here

$$\mathbf{r} = \{c\cos\theta - t\sin\theta, c\sin\theta + t\cos\theta\}, \tag{3.31}$$

is radius vector in coordinate system xy before folding the graphene sheet into a nanotube and (c,t) denote the coordinates along the circumference and tube axis, respectively. We also note that the wavefunctions are not normalized, but are orthogonal, because they have the forms

$$\begin{pmatrix} z_{+1,+1} \\ 1 \\ 0 \\ 0 \\ 0 \\ 0 \\ 0 \\ 0 \end{pmatrix}, \begin{pmatrix} 0 \\ 0 \\ z_{-1,+1} \\ 1 \\ 0 \\ 0 \\ 0 \\ 0 \end{pmatrix}, \begin{pmatrix} 0 \\ 0 \\ 0 \\ 0 \\ z_{+1,-1} \\ 1 \\ 0 \\ 0 \end{pmatrix}, \begin{pmatrix} 0 \\ 0 \\ 0 \\ 0 \\ 0 \\ 0 \\ z_{-1,-1} \\ 1 \end{pmatrix}, \tag{3.32}$$

and for the valence and conduction bands we have the following orthogonality condition:

$$\begin{pmatrix} -\frac{\tilde{k}_c + \mathrm{i}\tilde{k}_t}{\sqrt{\tilde{k}_c^2 + \tilde{k}_t^2}} & 1 \end{pmatrix} \cdot \begin{pmatrix} \frac{\tilde{k}_c - \mathrm{i}\tilde{k}_t}{\sqrt{\tilde{k}_c^2 + \tilde{k}_t^2}} \\ 1 \end{pmatrix} = 0. \tag{3.33}$$

The states can also be described by "backward going" waves in (3.29), i.e. $(k_c, k_t) \to (-k_c, -k_t)$. Using these "backward going" waves we can form pairs of wavefunctions, which are time-reversal partners, i.e.

$$k_c,\ k_t,\ \tau = +1,\ s = +1 \quad \text{with} \quad -k_c,\ -k_t,\ \tau = -1,\ s = -1, \tag{3.34}$$

and

$$k_c,\ k_t,\ \tau = +1,\ s = -1 \quad \text{with} \quad -k_c,\ -k_t,\ \tau = -1,\ s = +1, \tag{3.35}$$

are time-reversal pairs. Here c and v stands for conduction and valence bands respectively. Such pairs have the same energy, when there is no magnetic field, as can be seen from (3.54a). Also when the Hamiltonian is in (3.26) gauge the pairs are related to each other in the following way:

$$\Psi_{+1,+1,k_c,k_t} = -\sigma_3 \Psi^*_{-1,-1,-k_c,-k_t}, \quad \Psi_{+1,-1,k_c,k_t} = -\sigma_3 \Psi^*_{-1,+1,-k_c,-k_t}. \tag{3.36}$$

When the Hamiltonian is in (3.28) gauge they are related as

$$\Psi_{+1,+1,k_c,k_t} = \Psi^*_{-1,-1,-k_c,-k_t}, \quad \Psi_{+1,-1,k_c,k_t} = \Psi^*_{-1,+1,-k_c,-k_t}. \tag{3.37}$$

We note that when performing complex conjugation we need to pay attention to the symmetry of the first Brillouin zone (Figure 3.1c), for instance, these are two equivalent points

$$-\mathbf{K}^{'} \equiv \mathbf{K}. \tag{3.38}$$

We will denote states in (3.37) as

$$\Psi_{+1,+1,k_c,k_t} \quad \rightarrow \quad |K\ \uparrow\rangle, \tag{3.39a}$$
$$\Psi_{-1,-1,-k_c,-k_t} \quad \rightarrow \quad |K'\downarrow\rangle, \tag{3.39b}$$
$$\Psi_{+1,-1,k_c,k_t} \quad \rightarrow \quad |K\ \downarrow\rangle, \tag{3.39c}$$
$$\Psi_{-1,+1,-k_c,-k_t} \quad \rightarrow \quad |K'\uparrow\rangle, \tag{3.39d}$$

and will refer to it as the KK'-basis, which can be either for the conduction band or the valence band. Note that in the case when there is no spin-orbit coupling all of the KK'-basis states have the same energy, i.e. there is a fourfold degeneracy.

The wavefunction (3.29) also has to be periodic in the circumferential direction

$$\Psi_{\tau,s,k_c,k_t}(\mathbf{r}) = \Psi_{\tau,s,k_c,k_t}(\mathbf{r} + \mathbf{C}), \tag{3.40}$$

which requires that

$$e^{i(\mathbf{k}+\mathbf{K}^\tau)\cdot\mathbf{C}} = 1 \quad \rightarrow \quad (\mathbf{k} + \mathbf{K}^\tau)\cdot\mathbf{C} = 2\pi m, \quad m \in \mathbb{Z}, \tag{3.41}$$

where $\mathbf{k} = (k_c, k_t)$ is in ct coordinates. This condition quantizes values of circumferential momentum k_c. Firstly, we need to know the product

$$\mathbf{K}^\tau \cdot \mathbf{C} = \frac{2\pi}{3}\left\{\tau n + \left(\frac{\tau}{2} + \frac{3}{2}\right)m\right\}, \tag{3.42}$$

and when exponentiated it can be written as

$$e^{i\mathbf{K}^\tau\cdot\mathbf{C}} = e^{\frac{2\pi i}{3}(n-m)\tau} = e^{\frac{2\pi i}{3}\nu\tau}, \tag{3.43}$$

where

$$\nu = 0, \pm 1, \tag{3.44}$$

depending on n and m values. For $\nu = 0$ the nanotube is called metallic, and for $\nu = \pm 1$ it is called semiconducting. So the periodic boundary condition (3.41) can be written as

$$k_c R + \frac{\nu\tau}{3} = m, \tag{3.45}$$

which quantizes k_c as

$$k_c \to k_m = \left(m - \frac{\nu\tau}{3}\right)\frac{1}{R}. \tag{3.46}$$

When a magnetic field **B** is applied, it couples to the angular momentum and the spin of the electron. Now we examine the coupling to the angular momentum of the electron. If we choose Coulomb gauge for the vector potential

$$\mathbf{A} = \frac{1}{2}[\mathbf{B}\times\mathbf{r}], \tag{3.47}$$

because of the cylindrical geometry of the nanotube, only the component of the field $B_\parallel$ parallel with the tube axis **T**, couples to the electrons, through so-called minimal coupling

$$p_c = -\mathrm{i}\hbar\frac{\partial}{\partial c} \quad \to \quad p_c + \frac{\Phi_{AB}}{\Phi_0}\frac{1}{R}, \tag{3.48}$$

where

$$\Phi_{AB} = \pi R^2 B_\parallel \tag{3.49}$$

is the Aharonov-Bohm flux through the cross section of the tube, and

$$\Phi_0 = \frac{h}{e} \tag{3.50}$$

is a flux quantum. We denote the momentum associated with the Aharonov-Bohm flux as

$$k_\Phi = \frac{\Phi_{AB}}{\Phi_0}\frac{1}{R} = \frac{\pi e}{h}RB_\parallel. \tag{3.51}$$

The magnetic field coupling to the orbital degrees of freedom gives a shift in the $\tilde{k}_c \to \tilde{k}_c + k_\Phi$. Also note that the parallel and perpendicular components of the **B** field with respect to the tube axis are given by

$$B_\parallel = B\cos\zeta, \quad B_\perp = B\sin\zeta, \tag{3.52}$$

with ζ being the angle between tube axis direction **T** and **B**.

The coupling of the magnetic field to the spin is described by the Zeeman term

$$H_Z = -\sigma_0\tau_0\mathbf{B}\cdot\boldsymbol{\mu}_s = \frac{1}{2}g_s\mu_B\mathbf{B}\cdot\mathbf{s}, \tag{3.53}$$

where $\boldsymbol{\mu}_s = -g_s\mu_B\mathbf{s}$ is the spin magnetic moment, $g_s \approx 2$ is the electron's Landé factor, and $\mathbf{s} = \{s_1, s_2, s_3\}$ is a vector of the Pauli matrices in spin space. After the first equality we also specified that this term is diagonal in sublattice (σ_0) and K and K' point (τ_0) subspaces.

Comment: Here I replaced $(k_c, k_t) \to (\tilde{k}_c, \tilde{k}_t)$ in z_{τ,s,k_c,k_t}, because this diagonalizes the Hamiltonian (3.26), and left the plane wave factor $\mathrm{e}^{\mathrm{i}(k_c c + k_t t)}$ with bare (k_c, k_t), because in real space representation of the Hamiltonian (3.26) we replace $\hbar k_c \to p_c = -\mathrm{i}\hbar\frac{\partial}{\partial c}$ and $\hbar k_t \to p_t = -\mathrm{i}\hbar\frac{\partial}{\partial t}$, and all other terms are kept as they are. Also when the magnetic field is applied, the Aharonov-Bohm flux $\Phi = \pi R^2 B_\parallel$ through the tube circumference affects only $\tilde{k}_c \to \tilde{k}_c + k_\Phi$.

After diagonalizing the (3.26) (or 3.28) Hamiltonian we find the eigenspectrum, when the coupling of the magnetic field to orbital motion of electron is included:

$$\begin{aligned} &E_{\tau,s,k_c,k_t} = \hbar v_F\left(\pm\sqrt{\tilde{k}_c^2 + \tilde{k}_t^2} + \tau s k_0\right) \\ &\text{with} \quad \tilde{k}_c = k_c - \tau k_{c,\mathrm{cv}} - s k_{\mathrm{SO}} + k_\Phi, \\ &\text{and} \quad \tilde{k}_t = \tau k_t - k_{t,\mathrm{cv}}. \end{aligned} \tag{3.54a}$$

Here again plus is for the conduction band and minus for the valence band. By assuming that $|k_c - \tau k_{c,\mathrm{cv}}| >> |k_{\mathrm{SO}}|, |k_\Phi|$ we can expand the square root in the (3.54a) eigenenergies

$$\frac{E_{\tau,s,k_c,k_t}}{\hbar v_F} \approx \pm\sqrt{(k_c - \tau k_{c,\mathrm{cv}})^2 + \tilde{k}_t^2} + \left(\tau s k_0 \mp \frac{\mathrm{sgn}(k_c - \tau k_{c,\mathrm{cv}})}{\sqrt{1 + \left(\frac{\tilde{k}_t}{k_c - \tau k_{c,\mathrm{cv}}}\right)^2}} s k_{\mathrm{SO}} \right) \pm \frac{\mathrm{sgn}(k_c - \tau k_{c,\mathrm{cv}})}{\sqrt{1 + \left(\frac{\tilde{k}_t}{k_c - \tau k_{c,\mathrm{cv}}}\right)^2}} k_\Phi \tag{3.54b}$$

$$\downarrow$$

$$E_{\tau,s,k_c,k_t} \approx E_\tau^0 + s\tau \frac{\Delta_{\mathrm{SO}}}{2} \mp \tau \frac{g_{\mathrm{orb}} \mu_B B_\parallel}{2},$$

where

$$E_\tau^0 = \pm \hbar v_F \sqrt{(\tau k_c - k_{c,\mathrm{cv}})^2 + (\tau k_t - k_{t,\mathrm{cv}})^2}, \tag{3.54c}$$

$$\Delta_{\mathrm{SO}} = 2\hbar v_F \left(k_0 \pm \frac{\mathrm{sgn}(k_{c,\mathrm{cv}} - \tau k_c)}{\sqrt{1 + \left(\frac{\tau k_t - k_{t,\mathrm{cv}}}{\tau k_c - k_{c,\mathrm{cv}}}\right)^2}} k_{\mathrm{SO}} \right), \tag{3.54d}$$

$$g_{\mathrm{orb}} = 2 \frac{\mathrm{sgn}(k_{c,\mathrm{cv}} - \tau k_c)}{\sqrt{1 + \left(\frac{\tau k_t - k_{t,\mathrm{cv}}}{\tau k_c - k_{c,\mathrm{cv}}}\right)^2}} \frac{e v_F R}{2\mu_B}. \tag{3.54e}$$

We also note that $\mathrm{sgn}(k_{c,\mathrm{cv}} - \tau k_c)$ returns a dimensionless number ± 1. The above result coincides with the result (13) in Ref. [55], when we have the zeroth circumferential mode $m = 0$, and a metallic nanotube $\nu = 0$, noting that $\hbar v_F k_0 = \Delta_0$, $\hbar v_F k_{\mathrm{SO}} = -\Delta_1$, $\hbar v_F k_{c,\mathrm{cv}} = \Delta_g$, and $R = D/2$.

3.3 Single particle spectrum of a carbon nanotube quantum dot

If a carbon nanotube has a finite length L and is confined by a very sharp rectangular potential near the ends, which defines the quantum dot region, the wavevector k_t along the tube axis becomes discrete, and may be assumed to have values [51, 55]

$$k_t \approx \frac{N\pi}{L},\ N \in \mathbb{Z}. \tag{3.55}$$

In such a case we can write the normalized wavefunction as

$$\Psi_{\tau,s,k_c,k_t}(c,t) = \frac{1}{\sqrt{2\pi L}} \mathrm{e}^{\mathrm{i}\mathbf{K}^\tau \cdot \mathbf{r}} \mathrm{e}^{\mathrm{i}(k_c c + k_t t)} \begin{pmatrix} z_{\tau,s,k_c,k_t} \\ 1 \end{pmatrix}, \tag{3.56}$$

and we use this result to define the tunneling amplitudes.

In Section 3.2 we saw that carbon nanotubes have a nearly fourfold degenerate energy level structure, which is due to the intrinsic spin ($\uparrow$, $\downarrow$), and the so-called isospin or valley index (K, K') [18, 53, 55, 56]. In a lot of experimental cases such every four states described by particular k_t and k_c, "a shell", are separated by a large energy ΔE comparable or bigger than the charging energy $2U$ [55]. The fourfold degeneracy is broken by spin-orbit coupling and disorder. However, if there is no magnetic field, the system still has time-reversal symmetry and we are left with a pair of twofold degenerate states, called Kramers doublets. The time-reversal partners (Kramers doublets) in the KK'-basis (3.39) are the states

$$|K\uparrow\rangle = T|K'\downarrow\rangle, \tag{3.57a}$$

$$|K\downarrow\rangle = T|K'\uparrow\rangle, \tag{3.57b}$$

where T is the time-reversal operator.

Now we turn our interest to the single "shell" eigenspectrum. If a carbon nanotube contains disorder, i.e. defects in the lattice structure, tube is placed on the substrate and etc., this can induce mixing in KK'-basis states. However, such mixing should not break time-reversal symmetry. The single particle Hamiltonian with $\mathbf{B}$ field and KK' mixing for a single "shell" of a carbon nanotube quantum dot becomes:

$$\begin{aligned} H = & \begin{array}{c} \begin{matrix} |K\uparrow\rangle & |K'\downarrow\rangle & |K\downarrow\rangle & |K'\uparrow\rangle \end{matrix} \\ \begin{pmatrix} E_{+1,+1} & 0 & 0 & \frac{1}{2}\Delta_{KK'} \\ 0 & E_{-1,-1} & \frac{1}{2}\Delta^*_{KK'} & 0 \\ 0 & \frac{1}{2}\Delta_{KK'} & E_{+1,-1} & 0 \\ \frac{1}{2}\Delta^*_{KK'} & 0 & 0 & E_{-1,+1} \end{pmatrix} \end{array} \\ & + \frac{1}{2} g_s \mu_B B \begin{array}{c} \begin{matrix} |K\uparrow\rangle & |K'\downarrow\rangle & |K\downarrow\rangle & |K'\uparrow\rangle \end{matrix} \\ \begin{pmatrix} \cos\zeta & 0 & \sin\zeta & 0 \\ 0 & -\cos\zeta & 0 & \sin\zeta \\ \sin\zeta & 0 & -\cos\zeta & 0 \\ 0 & \sin\zeta & 0 & \cos\zeta \end{pmatrix} \end{array}, \end{aligned} \tag{3.58}$$

remembering, that the spin quantization axis is chosen along the tube axis $\mathbf{T}$, and $\mathbf{B}$ field lies in zx plane of spin-quantization coordinate system. We also note that in this KK'-basis for $\tau = -1$ we have $(k_c, k_t) \to -(k_c, k_t)$. Here $\Delta_{KK'}$ is the KK'-mixing due to disorder, $g_s \approx 2$ is the electron's Landé g-factor, ζ is the angle between the magnetic $\mathbf{B}$ field and the tube axis, and energies in the diagonal are given by

$$E_{\tau,s} = \tau s \frac{\Delta_{\mathrm{SO}}}{2} \mp \tau g_{\mathrm{orb}} \mu_B \frac{B \cos\zeta}{2}, \tag{3.59}$$

where $\tau = +1(-1)$ for $K(K')$, $s = +1(-1)$ for spin up (down), g_{orb} is the effective orbital Landé g-factor, and the upper (lower) sign corresponds to the conduction (valence) band. Note that a constant factor for particular "shell" E^0_τ in (3.54b) was neglected. After diagonalizing the Hamiltonian (3.58), we find the eigenspectrum ε_n, which defines the single particle orbitals of the quantum dot. In our discussion of tunneling induced energy shifts, we will use the energy spectrum for the conduction band and assume $\Delta_{\mathrm{SO}} > 0$.

3.4 Tunneling amplitudes

To define the tunneling amplitudes in KK'-basis, we need to specify the lead states. We assume that the lead states constitute Kramers doublets, when there is no magnetic field, which we will denote:

$$|\alpha\nu\uparrow\rangle = T|\alpha\tilde{\nu}\downarrow\rangle, \tag{3.60}$$

where $\alpha = \mathrm{L}, \mathrm{R}$ is a lead index. In general if there is spin-orbit coupling in the leads, the lead states in real space have the form

$$\langle \mathbf{r}|\alpha\nu\uparrow\rangle = \begin{pmatrix} a_{\alpha\nu}(\mathbf{r}) \\ b_{\alpha\nu}(\mathbf{r}) \end{pmatrix}, \quad \langle \mathbf{r}|\alpha\tilde{\nu}\downarrow\rangle = \begin{pmatrix} -b^*_{\alpha\nu}(\mathbf{r}) \\ a^*_{\alpha\nu}(\mathbf{r}) \end{pmatrix}, \tag{3.61}$$

where $a_{\alpha\nu}(\mathbf{r})$, $b_{\alpha\nu}(\mathbf{r})$ are complex functions of the coordinate. Now using KK'-basis states (3.39) and lead states (3.61), which are written in spin s space, we get the following tunneling amplitudes

$$t^{\tau s}_{\alpha\xi} = \langle \alpha\xi | H_{\text{tot}} | \tau s\rangle = (1 \pm \mathrm{e}^{\mathrm{i}\varphi_{\tau,s}}) \int \mathrm{d}\mathbf{r} A_{\xi s}(\mathbf{r}) H_{\text{tot}}(\mathbf{r}) \mathrm{e}^{\mathrm{i}\mathbf{K}\cdot\mathbf{r}} \mathrm{e}^{\mathrm{i}\tau(k_c c + k_t t)}, \tag{3.62a}$$

$$\varphi_{\tau,s} = \tau \operatorname{Arg}\left[k_c - k_{c,\text{cv}} - \mathrm{i}(k_t - k_{t,\text{cv}}) - \tau s k_{\text{SO}} + \tau k_\Phi\right], \tag{3.62b}$$

$$A_{\xi s} = \begin{pmatrix} A_{\nu\uparrow,\uparrow} & A_{\nu\uparrow,\downarrow} \\ A_{\tilde{\nu}\downarrow,\uparrow} & A_{\tilde{\nu}\downarrow,\downarrow} \end{pmatrix} = \frac{1}{\sqrt{2\pi L}} \begin{pmatrix} a^*_{\alpha\nu} & b^*_{\alpha\nu} \\ -b_{\alpha\nu} & a_{\alpha\nu} \end{pmatrix}. \tag{3.62c}$$

Here ξ denotes either $\nu\uparrow$ or $\tilde{\nu}\downarrow$, and H_{tot} is the total single particle Hamiltonian representing leads, dot region, and tunneling barriers. In general, the lead states can also depend on magnetic field $\mathbf{B}$, however, we do not consider a such situation. If $|k_c - k_{c,\text{cv}} - \mathrm{i}(k_t - k_{t,\text{cv}})| >> |sk_{\text{SO}} - k_\Phi|$, which covers most cases for carbon nanotubes, we can safely neglect the dependence of tunneling amplitudes on spin-orbit coupling (k_{SO}) and parallel magnetic field (k_Φ) to the tube axis.

We can simplify the above tunneling amplitudes (3.62a) by assuming that the Hamiltonian describing electrons in the leads is real and that we can choose arbitrary spin-quantization direction (for example, there is no spin-orbit coupling in the leads). In the case of no spin-orbit interaction the states (3.60) can be represented in real space as

$$\langle \mathbf{r}|\alpha\nu\uparrow\rangle = \begin{pmatrix} a_{\alpha\nu}(\mathbf{r}) \\ 0 \end{pmatrix}, \quad \langle \mathbf{r}|\alpha\tilde{\nu}\downarrow\rangle = \begin{pmatrix} 0 \\ a_{\alpha\nu}(\mathbf{r}) \end{pmatrix}, \tag{3.63}$$

where $a_{\alpha\nu}(\mathbf{r})$ is a real function of coordinates. Here the spin-quantization direction is chosen along the tube axis. When there is no magnetic field, we can define the following tunneling amplitudes

$$\begin{aligned} t^{K\uparrow}_{\alpha\nu\uparrow} &= \langle \alpha\nu\uparrow | H_{\text{tot}} | K\uparrow\rangle = t_{\alpha\nu,1}, \\ t^{K'\downarrow}_{\alpha\nu\downarrow} &= \langle \alpha\tilde{\nu}\downarrow | H_{\text{tot}} | K'\downarrow\rangle = t^*_{\alpha\nu,1}, \\ t^{K\downarrow}_{\alpha\nu\downarrow} &= \langle \alpha\tilde{\nu}\downarrow | H_{\text{tot}} | K\downarrow\rangle = t_{\alpha\nu,2}, \\ t^{K'\uparrow}_{\alpha\nu\uparrow} &= \langle \alpha\nu\uparrow | H_{\text{tot}} | K'\uparrow\rangle = t^*_{\alpha\nu,2}, \end{aligned} \tag{3.64}$$

where we also used the time-reversal symmetry of the states. As we can see from (3.62) the difference between tunneling amplitudes $t_{\alpha\nu,1}$ and $t_{\alpha\nu,2}$ appears due to spin-orbit coupling and that it can be neglected, when spin-orbit coupling is small compared to the curvature induced splitting in the carbon nanotube, i.e.

$$t_{\alpha\nu,1} \approx t_{\alpha\nu,2} \quad \rightarrow \quad t_{\alpha\nu}. \tag{3.65}$$

In general the tunneling amplitudes (3.64) also depend on the parallel magnetic field, however this effect is small, when magnetic field is small compared to the curvature induced splitting, and we do not consider it in our calculations. We also neglect ν dependence of the tunneling amplitudes $t_{\alpha\nu,1/2} \rightarrow t_{\alpha,1/2}$.

Note that if spin-orbit coupling in the leads is present, as can be seen from (3.62a), this may additionally introduce the following non-vanishing tunneling amplitudes

$$\begin{aligned} t^{K\uparrow}_{\alpha\tilde{\nu}\downarrow} &= \langle \alpha\tilde{\nu}\downarrow | H_{\text{tot}} | K\uparrow\rangle = t_{\alpha\nu,3}, \quad t^{K'\downarrow}_{\alpha\nu\uparrow} = \langle \alpha\nu\uparrow | H_{\text{tot}} | K'\downarrow\rangle = -t^*_{\alpha\nu,3}, \\ t^{K\downarrow}_{\alpha\nu\uparrow} &= \langle \alpha\nu\uparrow | H_{\text{tot}} | K\downarrow\rangle = t_{\alpha\nu,4}, \quad t^{K'\uparrow}_{\alpha\tilde{\nu}\downarrow} = \langle \alpha\tilde{\nu}\downarrow | H_{\text{tot}} | K'\uparrow\rangle = -t^*_{\alpha\nu,4}. \end{aligned} \tag{3.66}$$

The inclusion of such terms does not change the qualitative picture of the results presented in Chapters 4 and 5, so for simplicity we will neglect them.

Chapter 4

Tunneling renormalized cotunneling spectroscopy of carbon nanotube quantum dots with normal leads

The objective of this chapter is to examine how the tunneling renormalization affects the cotunneling spectroscopy of carbon nanotube quantum dots attached to normal leads. The quantum dot is assumed to have four single particle orbitals of single "shell" defined in Section 3.3. We are interested in how the cotunneling threshold is modified by the tunneling in the middle of the single charge $N = 1$ diamond. The following equation is solved for the cotunneling threshold $\tilde{V}_{\text{th}}$:

$$|\tilde{V}_{\text{th}}| = \Delta E(\mathbf{B}, V_g, \tilde{V}_{\text{th}}) = \tilde{E}_{Nl} - \tilde{E}_{Nl'}, \tag{4.1}$$

where $\tilde{E}$ is the tunneling renormalized eigenspectrum, which is determined by the method specified in Chapter 2.

We will be interested in the parameter regime where the charging energy $2U$ is much larger than the single particle spectrum energies ε_n, the bias V and the tunneling rates

$$\Gamma^n_{\alpha s} = \pi \rho_{\alpha s} |t^n_{\alpha s}|^2, \tag{4.2}$$

in order for our expansion in H_{T} to be valid. Also we need to be far away from the charge degeneracy points, so the gate voltage has to be not too far from the middle of the diamond, and because of this we can linearize the logarithms in (2.29) and be able to get some simple analytical results. However, in order not to overwhelm the physical interpretation presented in upcoming sections by cumbersome expressions, the derivation of analytical results is presented in Appendix C.

We note that cotunneling thresholds $\tilde{V}_{\text{th}}$ will be measured in units of

$$\Gamma = \sum_{\alpha j} \Gamma_{\alpha j} = \pi \rho \sum_{\alpha j} |t_{\alpha j}|^2 \tag{4.3}$$

for normal leads, where $t_{\alpha j}$ are the tunneling amplitudes defined by (3.64), and in units of

$$\Gamma_\Sigma = \pi \sum_{\alpha s j} \Gamma_{\alpha s j} = \pi \sum_{\alpha s j} \rho_{\alpha s} |t_{\alpha j}|^2 \tag{4.4}$$

for ferromagnetic leads.

4.1 Zero magnetic field $B = 0$ cotunneling thresholds

First we study the case when $B = 0$, all single particle orbitals are coupled symmetrically to the leads $\Gamma^n_{\alpha s} = \Gamma/4$, and the tunneling rate Γ is much larger than the disorder splitting $\Delta_{KK'} \approx 0$ and spin-orbit coupling $\Delta_{\text{SO}} \approx 0$, with the resulting tunneling renormalized threshold shown in

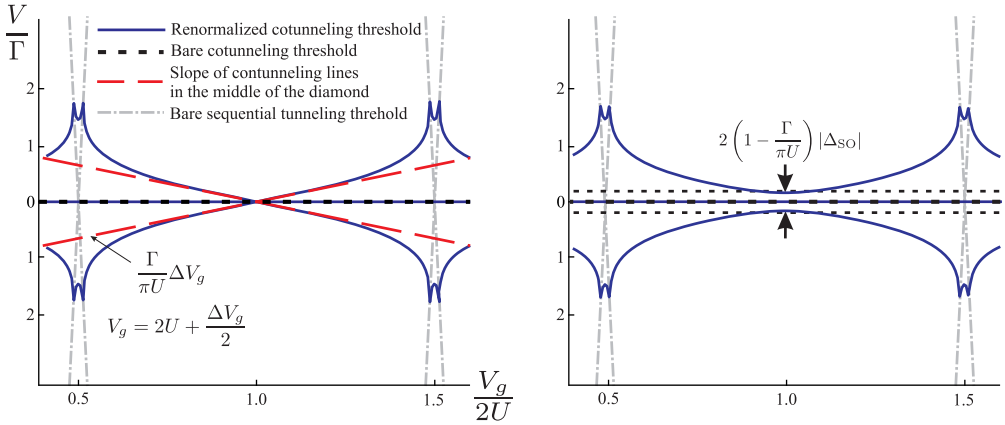

(a) $\Delta_{\mathrm{SO}} = 0$, $\Delta_{KK'} = 0$ (b) $\Delta_{\mathrm{SO}} = 0.16\Gamma$, $\Delta_{KK'} = 0$

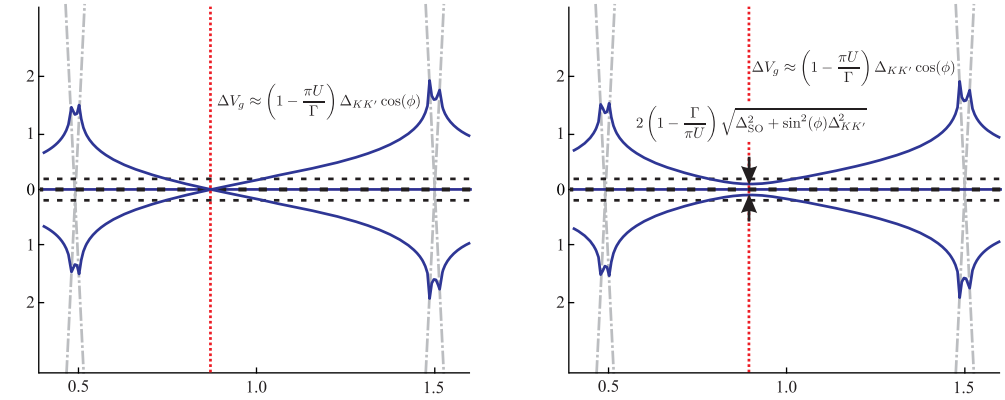

(c) $\Delta_{\mathrm{SO}} = 0$, $\Delta_{KK'} = 0.16\Gamma$ (d) $\Delta_{\mathrm{SO}} = 0.1\Gamma < \Delta_{KK'} = 0.13\Gamma$

Figure 4.1: Tunneling renormalized cotunneling thresholds shown as solid curves (blue) for different KK'-mixing and spin-orbit coupling values. The dashed lines (black) depict bare cotunneling thresholds and dashed-dotted lines (gray) show bare sequential tunneling thresholds. The long dashed lines (red) in (a) show linearized cotunneling threshold, when there is no KK'-mixing and spin-orbit coupling, and the dotted lines (red) in (c) and (d) depict, respectively, the position of zero bias crossing and minimum separation of the cotunneling threshold from zero bias. The values of the other parameters are $B = 0$, $U = 32\Gamma$, $D = 10^9\Gamma$, with all tunneling amplitudes $t_{L/R,1/2}$ being equal and $\mathrm{Arg}[t_{L/R,1/2}] = 0$.

Figure 4.1a. We see that the fourfold degenerate "shell" spectrum is split in a gate dependent way, and we get the 1st cotunneling line at zero bias (for $B \neq 0$ it is visible at finite bias, and for $T < T_K$ it evolves into a Kondo peak, which is not included in our approach, with T being the temperature and T_K the so-called Kondo temperature), and one twofold degenerate gate dependent line, which splits into 2nd and 3rd cotunneling line for $B \neq 0$. The slope of the 2nd, 3rd cotunneling lines is given by (dashed (red) line in Figure 4.1a)

$$S = \pm\frac{\Gamma}{\pi U}\Delta V_g. \tag{4.5}$$

There is also a crossing of cotunneling lines exactly in the middle of the diamond, i.e. the tunneling renormalization effects vanish.

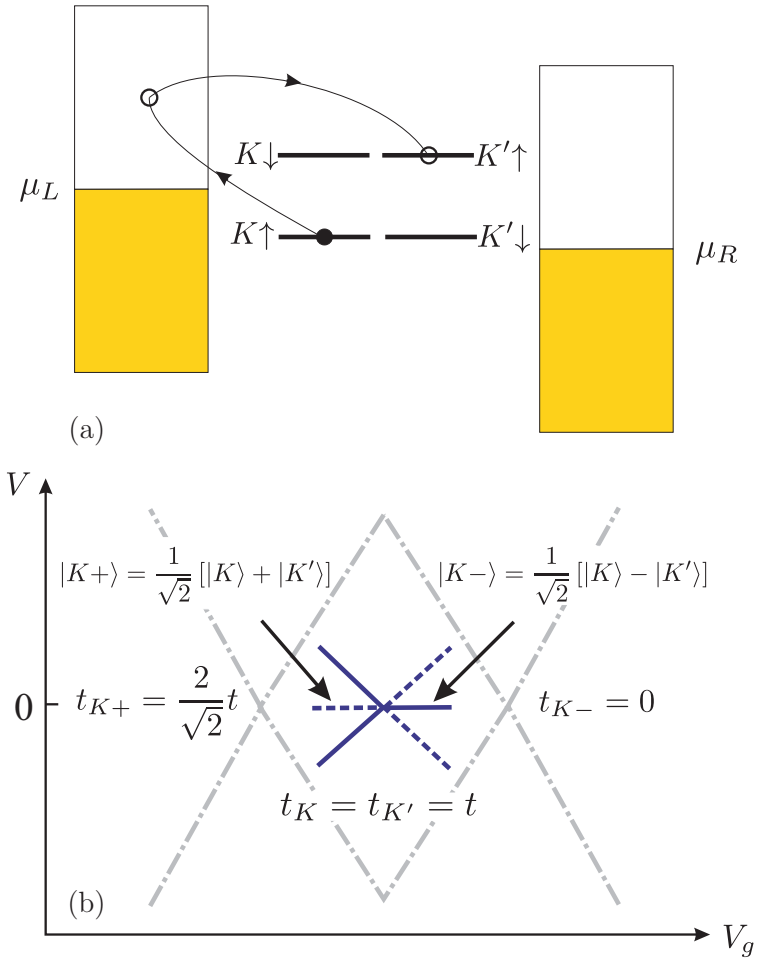

Figure 4.2: Qualitative picture of tunneling induced KK'-mixing for a carbon nanotube coupled to normal leads in zero magnetic $B = 0$ field. (a) Example of tunneling process, which introduces KK'-mixing with a single electron in a carbon nanotube "shell". Here $\mu_{L,R}$ denotes chemical potentials of the leads. (b) Schematic of cotunneling threshold (solid and dashed blue lines) for a single charge Coulomb diamond, in the absence of spin-orbit coupling and disorder induced KK'-mixing, and with real tunneling amplitudes t_K, $t_{K'}$. The effective tunneling renormalized ground state of the quantum dot is $|K+\rangle$ with larger tunneling rate $\Gamma_{K+} \sim |t_{K+}|^2$ (dashed blue line) at the left side of the diamond and $|K-\rangle$ with smaller tunneling rate $\Gamma_{K-} \sim |t_{K-}|^2$ (solid blue line) at the right side.

Even though formally it is possible to speak only about tunneling renormalization of the many-body eigenstates, however, effectively this splitting appears due to the mixing of single particle K and K' states because of the tunneling to the leads (Figure 4.2). This KK'-mixing appears because in the leads K and K' are no longer good quantum numbers. The resulting schematic cotunneling threshold without spin-orbit coupling and intrinsic KK'-mixing is depicted in Figure 4.2b, where the spin quantum number s and lead index α are disregarded for simplicity. Also the tunneling amplitudes to the states K and K' are taken to be real. In such a case the tunneling renormalization determines that the effective ground state of the quantum dot has a larger tunneling rate $\Gamma_{K+} \sim |t_{K+}|^2$ on the left side of the diamond and a smaller one $\Gamma_{K-} \sim |t_{K-}|^2$ on the right side. Also if tunnel couplings are complex and different for the left and right lead, then this

conclusion holds for tunneling rate summed over the lead index α. This situation occurs, because the charge fluctuations on the left side tends to empty the quantum dot and it is energetically favorable to have ground state with larger tunneling rate. On the right side of the diamond the situation is different, because charge fluctuations to doubly occupied dot states are preferable and it is energetically more favorable to have an excited state with the larger tunneling rate.

If the tunneling couplings are different for the left and the right lead, the positive and the negative slopes get corrections and instead of the above expression (4.5), we obtain for the slope

$$S_{\pm} = \pm\frac{\Gamma_L + \Gamma_R}{\pi U}\left(1 \pm \frac{\Gamma_L - \Gamma_R}{\pi U}\right)\Delta V_g, \tag{4.6}$$

where $\Gamma_\alpha = \Gamma_{\alpha 1} + \Gamma_{\alpha 2}$. We see that asymmetry between positive and negative bias appears, however, this corresponds only to a second order effect in Γ/U.

When spin-orbit coupling is included, instead of cotunneling lines crossing in the middle of the diamond, we get an anticrossing of size (Figure 4.1b)

$$A_1 = 2\left(1 - \frac{\Gamma}{\pi U}\right)|\Delta_{\mathrm{SO}}|. \tag{4.7}$$

It is not possible to restore a crossing if both Kramers doublets defined in Section 3.3 (Eq. 3.57) have the same tunneling couplings to the leads ($t_{\alpha,1} \approx t_{\alpha,2}$), even if mixing of K and K' due to disorder $\Delta_{KK'}$ is included (Figure 4.1d). In this case, for symmetric couplings to the left and right leads we can find the eigenspectrum around the middle of the diamond, which yields the following energy difference between ground and excited states

$$\begin{aligned}\Delta E = \Bigg\{ &\left[\left(1 - \frac{\Gamma}{\pi U}\right)\Delta_\Sigma + \frac{\Gamma}{\pi U}\cos(\phi)\frac{\Delta_{KK'}}{\Delta_\Sigma}\Delta V_g\right]^2 \\ &+ \left|\frac{\Gamma}{\pi U}\left(\frac{\Delta_{\mathrm{SO}}}{\Delta_\Sigma}\cos(\phi) + \mathrm{i}\sin(\phi)\right)\Delta V_g\right|^2 \Bigg\}^{1/2},\end{aligned} \tag{4.8}$$

where

$$\Delta_\Sigma = \sqrt{\Delta_{\mathrm{SO}}^2 + \Delta_{KK'}^2}, \tag{4.9}$$

and the phase ϕ is the sum of the KK'-mixing phase ($\Delta_{KK'} = |\Delta_{KK'}|\mathrm{e}^{\mathrm{i}\phi_{KK'}}$) and the tunneling amplitudes' phase ($t_{L/R,1/2} = |t|\mathrm{e}^{\mathrm{i}\phi_t}$):

$$\phi = \phi_{KK'} + 2\phi_t. \tag{4.10}$$

From the above expression (4.8) we find that an anticrossing appears near the point

$$\Delta V_g \approx \left(1 - \frac{\pi U}{\Gamma}\right)\Delta_{KK'}\cos(\phi), \tag{4.11}$$

and its size is

$$A_2 = 2\left(1 - \frac{\Gamma}{\pi U}\right)\sqrt{\Delta_{\mathrm{SO}}^2 + \sin^2(\phi)\Delta_{KK'}^2}. \tag{4.12}$$

We note that in this case the middle of the bare diamond is given by $\Delta V_g = -\Delta_\Sigma$. If spin-orbit coupling is neglected $\Delta_{\mathrm{SO}} = 0$, but there is KK'-mixing $\Delta_{KK'}$, and the total phase ϕ is equal to zero, a crossing instead of anticrossing appears near the point (4.11), as shown in Figure 4.1c.

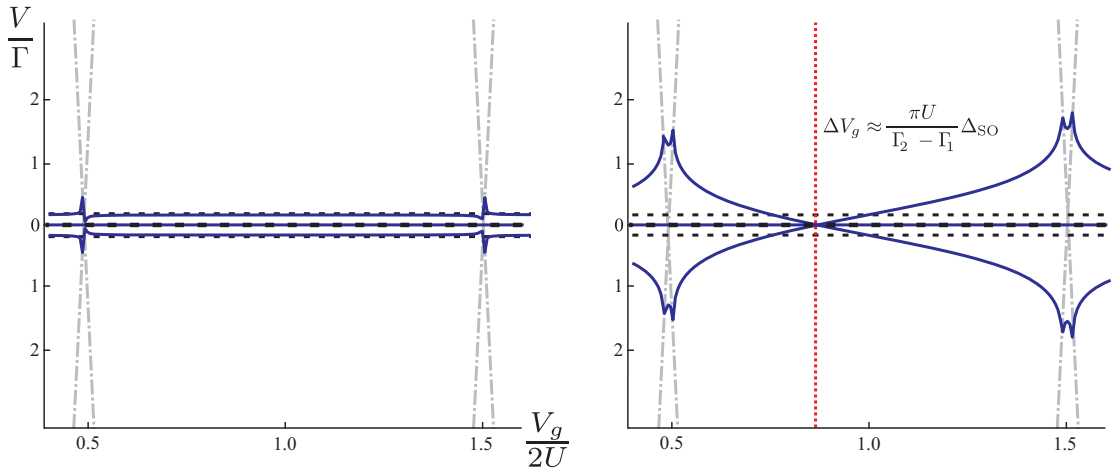

(a) $\Delta_{SO} = 0.1\Gamma$, $\Delta_{KK'} = 0.13\Gamma$ (b) $\Delta_{SO} = 0.16\Gamma$, $\Delta_{KK'} = 0$

Figure 4.3: (a) Illustration of tunneling renormalization reduction, when there is a phase difference between the left and right leads tunneling couplings, and the relations (4.13) are satisfied. The values of the parameters are $B = 0$, $U = 32\Gamma$, $D = 10^9\Gamma$, $\frac{t_{R,1/2}}{t_{L,1/2}} = e^{i\pi/2}$, $\text{Arg}[t_{L,1/2}] = 0$. (b) Illustration of a zero bias crossing, when there is only spin-orbit coupling, and the Kramers doublets have different tunneling couplings to the leads (only relation (4.13a) is satisfied). The values of the parameters are $B = 0$, $U = 32\Gamma$, $D = 10^9\Gamma$, $\left|\frac{t_{L/R,1}}{t_{L/R,2}}\right| = 7$, $\text{Arg}[t_{L,1/2}] = \text{Arg}[t_{R1}] = 0$, $\text{Arg}[t_{R2}] = \pi$. The legend is the same as in Figure 4.1.

By changing the relative phases between the left and right couplings, we can reduce the tunneling renormalization, as shown in Figure 4.3(a). The condition for complete reduction of the tunneling renormalization around the middle of the diamond is

$$t_{L1}t_{L2} + t_{R1}t_{R2} = 0, \tag{4.13a}$$
$$|t_{L1}|^2 + |t_{R1}|^2 = |t_{L2}|^2 + |t_{R2}|^2, \tag{4.13b}$$

which can be rewritten as

$$t_{R1} = e^{i\varphi}t_{L2}, \quad t_{R2} = -e^{-i\varphi}t_{L1}, \tag{4.14}$$

where $t_{L/R,1/2}$ are complex numbers, and φ is some arbitrary phase.

It is possible to get a crossing if the Kramers doublets are coupled differently, i.e. $t_{\alpha 1} \neq t_{\alpha 2}$, as shown in Figure 4.3(b), where we for simplicity consider the case with only spin-orbit coupling, but the statement is also true when KK'-mixing is included. In this case, the condition for crossing is given by relation (4.13a), when relation (4.13b) is not satisfied. Then the position of the crossing is given by

$$\Delta V_g \approx \frac{\pi U}{\Gamma_2 - \Gamma_1}\Delta_{SO}, \tag{4.15}$$

where $\Gamma_j = \Gamma_{Lj} + \Gamma_{Rj}$, and the middle of the diamond is in this case given by $\Delta V_g = -|\Delta_{SO}|$. To be able to observe it experimentally, the value of Eq. (4.15) has to be between $-2U$ and $2U$.

4.2 Finite magnetic field $B \neq 0$ cotunneling thresholds. Gate dependence of g-factors

Now we investigate how the tunneling induced level shifts effect the magnetic field dependence of the cotunneling threshold, i.e. we examine the gate dependence of the g-factors. As in the previous section, we restrict our examination to the single charge $N = 1$ diamond. We start by examining the case when the spin-orbit coupling and KK'-mixing are neglected, the magnetic field is parallel to the tube axis, and the couplings to the left and right leads are equal. When the gate voltage is exactly in the middle of the diamond the bare g-factors are almost unaffected and they are reduced only by a factor $(1 - \Gamma/\pi U)$

$$\tilde{g}_{s,\mathrm{orb}} \approx (1-\kappa)\, g_{s,\mathrm{orb}}, \quad \kappa = \frac{\Gamma}{\pi U}. \tag{4.16}$$

For very small Γ/U ratio, the renormalized threshold matches the bare one (dashed (black) curves in Figure 4.4a). For perpendicular magnetic field $B_\perp$ the renormalization of g-factors is also small and for 1st, 2nd, and 3rd cotunneling lines, respectively, are given by

$$\kappa g_s,\ (1-\kappa) g_s,\ g_s. \tag{4.17}$$

Going away from the middle of the diamond, we find that g-factors acquire gate dependence (solid (blue) curves in Figure 4.4a), which for the $\kappa \Delta V_g >> B > 0$ case is written in Table 4.1, for different transitions. The situation when spin-orbit coupling is included is depicted in Figure 4.4b. We see that the tunneling renormalization again acts as a gate dependent $\Delta_{KK'}$ splitting. The effective g-factors for small magnetic B fields ($\kappa \Delta V_g,\ \Delta_{\mathrm{SO}} >> B > 0$) are written in Table 4.1, where the following notation is introduced:

$$\tilde{\kappa} \approx \kappa \left[1 + \left(\frac{1-\kappa}{\kappa} \frac{\Delta_{\mathrm{SO}}}{\Delta V_g} \right)^2 \right]^{-1/2}, \tag{4.18a}$$

$$\tilde{g}_s \approx g_s (1-\kappa) \left[1 + \left(\frac{1-\kappa}{\kappa} \frac{\Delta_{\mathrm{SO}}}{\Delta V_g} \right)^2 \right]^{-1/2}, \tag{4.18b}$$

$$\tilde{g}_{\mathrm{orb}} \approx g_{\mathrm{orb}} (1-\kappa) \left[1 + \left(\frac{\kappa}{1-\kappa} \frac{\Delta V_g}{\Delta_{\mathrm{SO}}} \right)^2 \right]^{-1/2}. \tag{4.18c}$$

When there is only KK'-mixing, the magnetic field dependence of the cotunneling threshold does not change qualitatively, and the only difference at finite ΔV_g is an effective enhancement of the KK'-mixing due to tunneling-renormalization, as can be seen from Figure 4.4c. The situation when both spin-orbit coupling and KK'-mixing are included is depicted in Figure 4.4d.

In an experiment, the cotunneling threshold dependence on the magnetic field angle ζ (with respect to the tube axis) also could be measured. The angle dependence of the bare cotunneling threshold is shown in Figure 4.5a. Again, in the middle of the diamond there is almost no renormalization due to tunneling and it matches Figure 4.5a. The situation at finite ΔV_g is shown in Figure 4.5b. If the quantum dot is coupled to the leads asymmetrically, then the asymmetry between positive and negative bias thresholds acquires angle dependence, which can be seen by adding positive and negative bias thresholds in Figure 4.5b, and the result is shown in Figure 4.5c.

Cotunneling line	$\kappa\Delta V_g >> B > 0,\ \Delta_{SO} = 0$		$\kappa\Delta V_g > \Delta_{SO} >> B > 0$	
	Bare g-factor	Renormalized g	Bare g	Renormalized g
		Parallel field $B_\parallel$		
1st	g_s	$(1-\kappa)\,g_s$	$g_s + g_{orb}$	$(1-\kappa-\tilde{\kappa})g_s + \tilde{g}_{orb}$
2nd	g_{orb}	$\kappa g_s + \frac{g_{orb}^2 B}{2\kappa\Delta V_g}$	g_s	$(1-\kappa)g_s$
3rd	$g_s + g_{orb}$	$g_s + \frac{g_{orb}^2 B}{2\kappa\Delta V_g}$	g_{orb}	$-\tilde{\kappa}g_s + \tilde{g}_{orb}$
		Perpendicular field $B_\perp$		
1st	0	g_s	0	$\kappa g_s + \tilde{g}_s$
2nd	g_s	κg_s	$\frac{g_s B}{2\Delta_{SO}}$	κg_s
3rd	g_s	$(1-\kappa)g_s$	$\frac{g_s B}{2\Delta_{SO}}$	$\tilde{g}_s$

Table 4.1: Bare and renormalized g-factors for carbon nanotube quantum dot, when $g_{orb} > g_s$ and $\Delta_{KK'} = 0$.

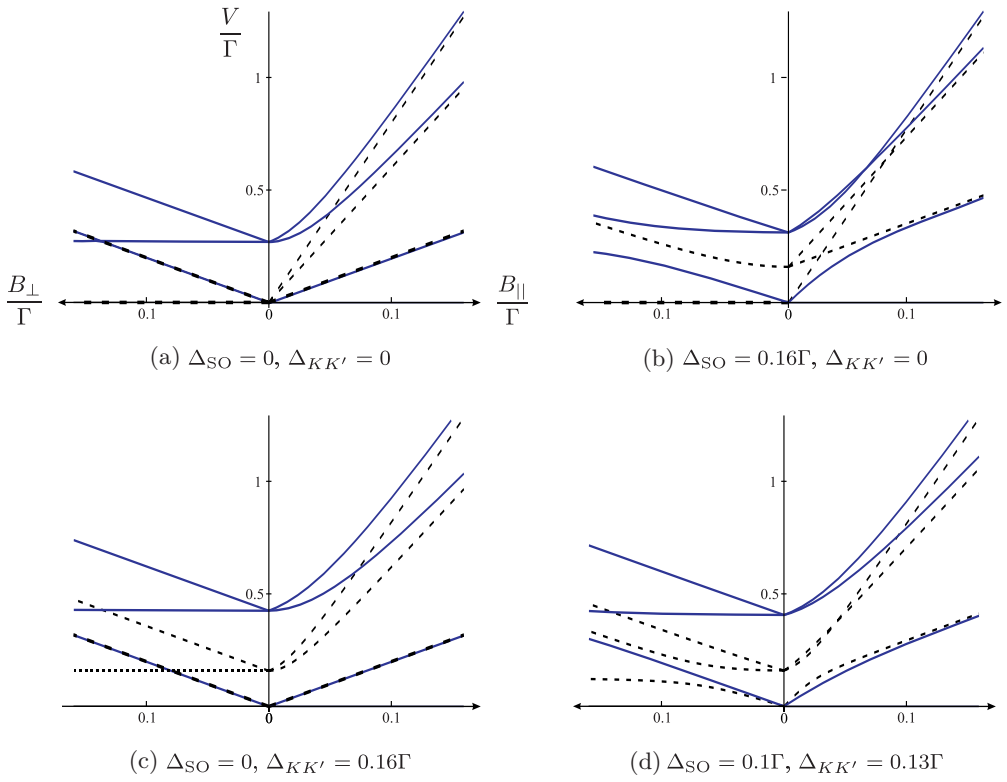

(a) $\Delta_{SO} = 0$, $\Delta_{KK'} = 0$

(b) $\Delta_{SO} = 0.16\Gamma$, $\Delta_{KK'} = 0$

(c) $\Delta_{SO} = 0$, $\Delta_{KK'} = 0.16\Gamma$

(d) $\Delta_{SO} = 0.1\Gamma$, $\Delta_{KK'} = 0.13\Gamma$

Figure 4.4: Comparison of the dependence on parallel $B_\parallel$ and perpendicular $B_\perp$ magnetic field of the bare (dashed curves (black)) and the tunneling renormalized (solid curves (blue)) cotunneling threshold for different values of KK'-mixing and spin-orbit coupling at a gate voltage $V_g = 1.2 \times 2U$ away from the middle of the diamond. The values of the other parameters are $U = 32\Gamma$, $D = 10^9\Gamma$, with all tunneling amplitudes $t_{L/R,1/2}$ being equal and $\mathrm{Arg}[t_{L/R,1/2}] = 0$.

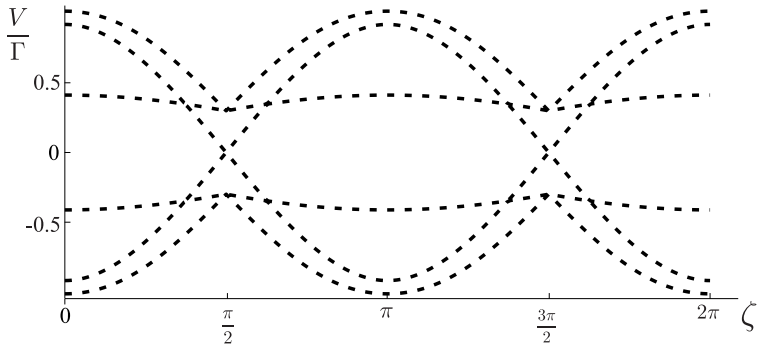

(a) Bare cotunneling threshold

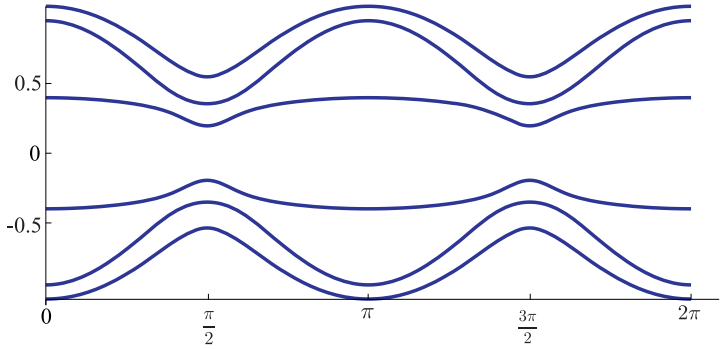

(b) Tunneling renormalized cotunneling threshold

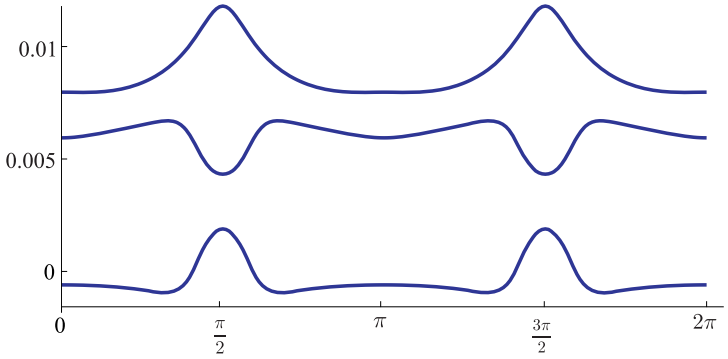

(c) Asymmetry between negative and positive bias tunneling renormalized cotunneling thresholds

Figure 4.5: Angle dependence of cotunneling threshold. The values of the parameters are $B = 0.13\Gamma$, $\Delta_{SO} = 0.16\Gamma$, $\Delta_{KK'} = 0$, $U = 32\Gamma$, $D = 10^9\Gamma$, $\frac{t_{L,1/2}}{t_{R,1/2}} = 7$, $\mathrm{Arg}[t_{L/R,1/2}] = 0$.

4.3 Comparison of second and fourth order corrections

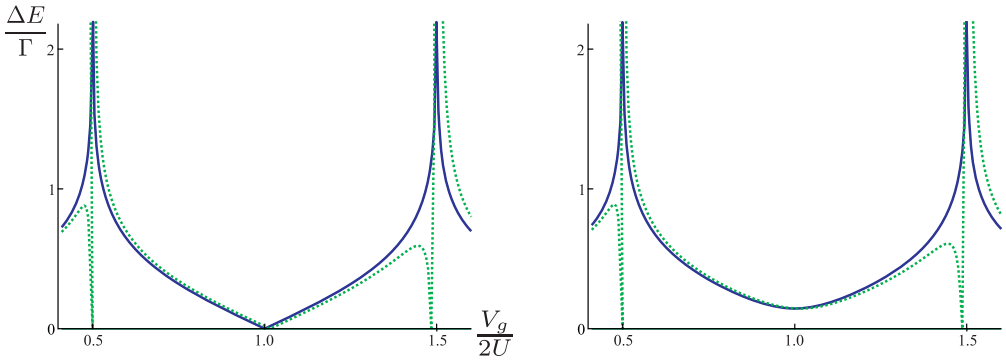

(a) $\Delta_{\mathrm{SO}} = 0$, $\Delta_{KK'} = 0$

(b) $\Delta_{\mathrm{SO}} = 0.16\Gamma$, $\Delta_{KK'} = 0$

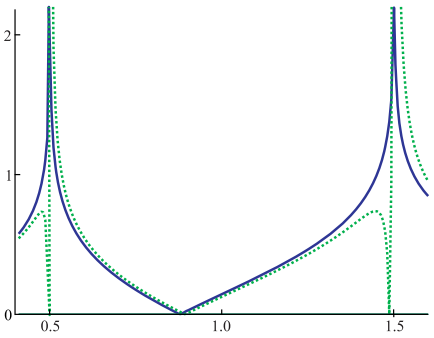

(c) $\Delta_{\mathrm{SO}} = 0$, $\Delta_{KK'} = 0.16\Gamma$

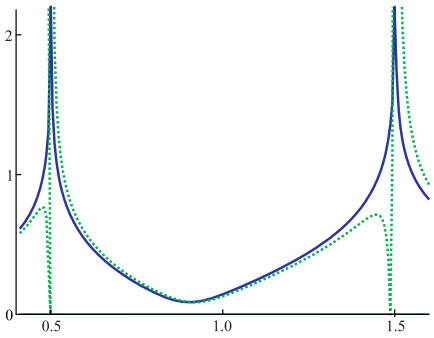

(d) $\Delta_{\mathrm{SO}} = 0.1\Gamma < \Delta_{KK'} = 0.13\Gamma$

Figure 4.6: The comparison of energy differences corresponding to cotunneling thresholds in Figure 4.1, where solid curves (blue) correspond to energy differences with corrections up to second order in H_{T}, and dotted (green) curves up to fourth order in H_{T}. The values of the other parameters for calculation are $B = 0$, $U = 32\Gamma$, $D = 10^9\Gamma$, with all tunneling amplitudes $t_{L/R,1/2}$ being equal and $\mathrm{Arg}[t_{L/R,1/2}] = 0$.

To show the region of validity of the perturbative expansion, we consider the energy shifts with fourth order corrections included, which are examined in Appendix B, for the cases discussed in Section 4.1. The comparison of the energy differences corresponding to cotunneling thresholds in Figure 4.1 is shown in Figure 4.6, where solid curves (blue) correspond to energy differences with corrections up to second order in H_{T}, and dotted (green) curves - up to fourth order in H_{T}. From this figure we see that for chosen parameters in our calculation we have wide range of gate voltage V_g for which second order perturbation theory in H_{T} is valid.

Chapter 5

Tunneling renormalized cotunneling spectroscopy of quantum dots with ferromagnetic leads

In this chapter we discuss the cotunneling thresholds in the presence of ferromagnetic leads, the effect of the exchange field, and its compensation by external magnetic field.

5.1 Tunneling amplitudes

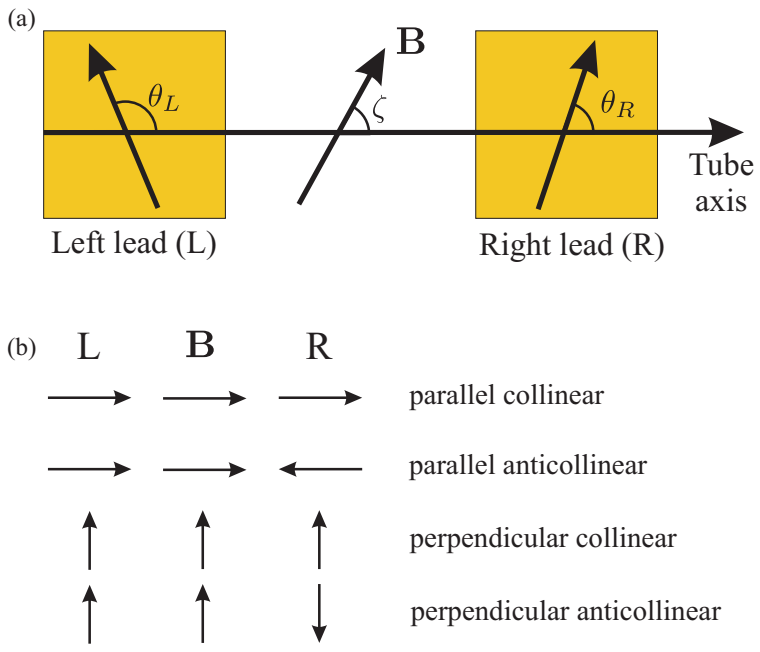

Figure 5.1: Orientation of the lead polarizations and magnetic field with respect to quantum dot spin quantization axis (or the carbon nanotube axis). (a) Arbitrary orientation of lead polarization when $\varphi_\alpha = 0$. (b) Orientations of polarizations discussed in the thesis.

If spin quantization axes of the leads are rotated with respect to the quantum dot spin quantization axis by angles θ_α and φ_α (Figure 5.1), then the new eigenstates of the leads, expressed in terms of the old ones (which have spin quantization axis the same as the quantum dot), are eigenstates of

$$(\boldsymbol{a}_\alpha \cdot \boldsymbol{\tau}) = \begin{pmatrix} \cos\theta_\alpha & \sin\theta_\alpha \cos\varphi_\alpha - \mathrm{i}\sin\theta_\alpha \sin\varphi_\alpha \\ \sin\theta_\alpha \cos\varphi_\alpha + \mathrm{i}\sin\theta_\alpha \sin\varphi_\alpha & -\cos\theta_\alpha \end{pmatrix}, \tag{5.1}$$

where $\boldsymbol{a}_\alpha$ denotes the spin quantization directions in the leads ($\alpha = \mathrm{L},\mathrm{R}$)

$$\boldsymbol{a}_\alpha = \{\sin\theta_\alpha\cos\varphi_\alpha, \sin\theta_\alpha\sin\varphi_\alpha, \cos\theta_\alpha\}, \tag{5.2}$$

and $\boldsymbol{\tau}$ is vector consisting of Pauli matrices. The eigenvectors of the above matrix written as columns of P_α are

$$P_\alpha = \begin{pmatrix} \cos(\theta_\alpha/2) & -\sin(\theta_\alpha/2)\mathrm{e}^{-\mathrm{i}\varphi_\alpha} \\ \sin(\theta_\alpha/2)\mathrm{e}^{\mathrm{i}\varphi_\alpha} & \cos(\theta_\alpha/2) \end{pmatrix}. \tag{5.3}$$

So the new eigenstates in the leads are expressed as

$$|\alpha\xi\tilde{\uparrow}\rangle = \cos(\theta_\alpha/2)|\alpha\nu\uparrow\rangle + \sin(\theta_\alpha/2)\mathrm{e}^{\mathrm{i}\varphi_\alpha}|\alpha\tilde{\nu}\downarrow\rangle, \tag{5.4a}$$
$$|\alpha\tilde{\xi}\tilde{\downarrow}\rangle = \cos(\theta_\alpha/2)|\alpha\tilde{\nu}\downarrow\rangle - \sin(\theta_\alpha/2)\mathrm{e}^{-\mathrm{i}\varphi_\alpha}|\alpha\nu\uparrow\rangle. \tag{5.4b}$$

and the tunneling amplitudes in the new basis become

$$t^n_{\alpha\xi\tilde{\uparrow}} = \cos(\theta_\alpha/2)t^n_{\alpha\nu\uparrow} + \sin(\theta_\alpha/2)\mathrm{e}^{-\mathrm{i}\varphi_\alpha}t^n_{\alpha\tilde{\nu}\downarrow}, \tag{5.5a}$$
$$t^n_{\alpha\tilde{\xi}\tilde{\downarrow}} = \cos(\theta_\alpha/2)t^n_{\alpha\tilde{\nu}\downarrow} - \sin(\theta_\alpha/2)\mathrm{e}^{\mathrm{i}\varphi_\alpha}t^n_{\alpha\nu\uparrow}. \tag{5.5b}$$

The new spins $\tilde{\uparrow}$ and $\tilde{\downarrow}$ have corresponding new constant tunneling density of states $\rho_{\tilde{\uparrow}}$ and $\rho_{\tilde{\downarrow}}$, because we are considering ferromagnetic leads.

5.2 Two orbital quantum dot

In this section we will look at the simple quantum dot containing only two single particle orbitals spin-up $|\uparrow\rangle$ and spin-down $|\downarrow\rangle$ (Figure 1.2, $E_c = 2U$). Uncoupled from the leads quantum dot has the following bare many-body eigenstates

$$|\psi_d\rangle \in \{|0\rangle,\ |1\uparrow\rangle,\ |1\downarrow\rangle,\ |2\rangle\}, \tag{5.6}$$

with corresponding bare eigenenergies

$$E^{(0)}_0 = 0, \tag{5.7a}$$
$$E^{(0)}_{1\uparrow} = \frac{\Delta}{2} + U - V_g, \tag{5.7b}$$
$$E^{(0)}_{1\downarrow} = -\frac{\Delta}{2} + U - V_g, \tag{5.7c}$$
$$E^{(0)}_2 = 4U - 2V_g, \tag{5.7d}$$

Here $\Delta = g_s B$ corresponds to applied external magnetic field, with g_s being the electron Landé factor. We assume that the tunneling amplitudes have the following form

$$t^{\uparrow}_{\alpha s} = t_\alpha\delta_{s,\uparrow}, \tag{5.8a}$$
$$t^{\downarrow}_{\alpha s} = t_\alpha\delta_{s,\downarrow}, \tag{5.8b}$$

i.e., that spin quantization-axes in the leads and in the quantum dot are in the same direction, which will be the case for large enough external magnetic field B, which polarizes the leads in

its direction. Having the above eigenenergies and tunneling amplitudes we can find tunneling induced level shifts, by using expression (2.29)

$$E_0^{(2)} = \frac{\Gamma_\uparrow}{\pi}\ln\left|\frac{U-\frac{\Delta}{2}+\frac{\Delta V_g}{2}}{D+\frac{\Delta_{\rm st}}{2}}\right| + \frac{\Gamma_\downarrow}{\pi}\ln\left|\frac{U+\frac{\Delta}{2}+\frac{\Delta V_g}{2}}{D-\frac{\Delta_{\rm st}}{2}}\right|, \tag{5.9a}$$

$$E_{1\uparrow}^{(2)} = \frac{\Gamma_\downarrow}{\pi}\ln\left|\frac{U-\frac{\Delta}{2}-\frac{\Delta V_g}{2}}{D-\frac{\Delta_{\rm st}}{2}}\right| + \frac{\Gamma_\uparrow}{\pi}\ln\left|\frac{U-\frac{\Delta}{2}+\frac{\Delta V_g}{2}}{D-\frac{\Delta_{\rm st}}{2}}\right|, \tag{5.9b}$$

$$E_{1\downarrow}^{(2)} = \frac{\Gamma_\uparrow}{\pi}\ln\left|\frac{U+\frac{\Delta}{2}-\frac{\Delta V_g}{2}}{D+\frac{\Delta_{\rm st}}{2}}\right| + \frac{\Gamma_\downarrow}{\pi}\ln\left|\frac{U+\frac{\Delta}{2}+\frac{\Delta V_g}{2}}{D+\frac{\Delta_{\rm st}}{2}}\right|, \tag{5.9c}$$

$$E_2^{(2)} = \frac{\Gamma_\uparrow}{\pi}\ln\left|\frac{U+\frac{\Delta}{2}-\frac{\Delta V_g}{2}}{D-\frac{\Delta_{\rm st}}{2}}\right| + \frac{\Gamma_\downarrow}{\pi}\ln\left|\frac{U-\frac{\Delta}{2}-\frac{\Delta V_g}{2}}{D+\frac{\Delta_{\rm st}}{2}}\right|, \tag{5.9d}$$

where the following notations were introduced

$$\Gamma_{\alpha\eta} = \pi\rho_{\alpha\eta}|t_\alpha|^2, \tag{5.10a}$$

$$\Gamma_\eta = \sum_\alpha \Gamma_{\alpha\eta} = \Gamma_{L\eta} + \Gamma_{R\eta}, \quad \eta \in \{\uparrow,\downarrow\} \tag{5.10b}$$

$$V_g = 2UN_g = 2U + \frac{\Delta V_g}{2}. \tag{5.10c}$$

Note that when calculating the energy corrections (5.9) we have set the voltage bias to zero $V = 0$ for simplicity.

With the above energy corrections (5.9) we find that the cotunneling threshold becomes

$$\begin{aligned} V_c = \left(E_{1\uparrow}^0 + E_{1\uparrow}^{(2)}\right) - \left(E_{1\downarrow}^{(0)} + E_{1\downarrow}^{(2)}\right) = \Delta + \frac{\Gamma_\uparrow}{\pi}\ln\left|\frac{1+\frac{\Delta V_g}{2U}-\frac{\Delta}{2U}}{1-\frac{\Delta V_g}{2U}+\frac{\Delta}{2U}}\right| + \frac{\Gamma_\downarrow}{\pi}\ln\left|\frac{1-\frac{\Delta V_g}{2U}-\frac{\Delta}{2U}}{1+\frac{\Delta V_g}{2U}+\frac{\Delta}{2U}}\right| \\ + \frac{\Gamma_\uparrow+\Gamma_\downarrow}{\pi}\ln\left|\frac{1+\frac{\Delta_{\rm st}}{2D}}{1-\frac{\Delta_{\rm st}}{2D}}\right|, \end{aligned} \tag{5.11}$$

and if the gate voltage is around the middle of the diamond ($\Delta V_g << 2U$), then the above threshold can be linearized to give

$$V_c \approx \left(1-\frac{\Gamma_\uparrow+\Gamma_\downarrow}{\pi U}\right)\Delta + \frac{\Gamma_\uparrow-\Gamma_\downarrow}{\pi U}\Delta V_g + \frac{\Gamma_\uparrow+\Gamma_\downarrow}{\pi D}\Delta_{\rm st}. \tag{5.12}$$

We see that the gate dependent splitting appears if the leads are ferromagnetic, i.e. $\Gamma_\uparrow \neq \Gamma_\downarrow$. That kind of splitting in the literature is called gate dependent exchange field [26]. Also there is a correction $\frac{\Gamma_\uparrow+\Gamma_\downarrow}{\pi D}\Delta_{\rm st}$ if the spin-up and spin-down bands of the leads are shifted with respect to one another by the Stoner splitting. And lastly there is a correction $\left(1-\frac{\Gamma_\uparrow+\Gamma_\downarrow}{\pi U}\right)\Delta$, which renormalizes the magnetic field by diminishing it. In a way it corresponds to the Lamb shift from atomic physics [57, 58], or the Knight shift from nuclear magnetic resonance physics [59].

Now let us examine zero-bias sequential tunneling thresholds and the possible motion of the middle of the diamond due to tunneling renormalization. The bare threshold for ground state

transitions between zero-to-single and single-to-two charge states is determined respectively by the conditions (here we assume that $\Delta < 0$, i.e. spin-up is the ground state):

$$E_{1\uparrow} - E_0 = U - V_g^{1\leftrightarrow 0} - \frac{|\Delta|}{2} = -U - \frac{\Delta V_g^{1\leftrightarrow 0} + |\Delta|}{2} = 0, \tag{5.13a}$$

$$E_2 - E_{1\uparrow} = 3U - V_g^{2\leftrightarrow 1} + \frac{|\Delta|}{2} = U - \frac{\Delta V_g^{2\leftrightarrow 1} - |\Delta|}{2} = 0. \tag{5.13b}$$

From the above equations we get

$$\Delta V_g^{1\leftrightarrow 0} = -2U - |\Delta|, \tag{5.14a}$$

$$\Delta V_g^{2\leftrightarrow 1} = 2U + |\Delta|. \tag{5.14b}$$

We see that in this case the middle of the diamond is always given by

$$\Delta V_g^{\text{mid}} = 0, \tag{5.15}$$

but the width varies depending on $|\Delta|$

$$\Delta V_g^{\text{width}} = 4U + 2|\Delta|. \tag{5.16}$$

If the second order corrections (5.9) are included then the zero-bias sequential tunneling thresholds qualitatively would be determined from:

$$(E_{1\uparrow} + E_{1\uparrow}^{(2)}) - (E_0 + E_0^{(2)}) = -U - \frac{\Delta V_g^{1\leftrightarrow 0} + |\Delta|}{2} + \Gamma_\downarrow \ln \left| \frac{1 - (\Delta V_g^{1\leftrightarrow 0} - |\Delta|)/2U}{1 + (\Delta V_g^{1\leftrightarrow 0} - |\Delta|)/2U} \right| = 0, \tag{5.17a}$$

$$(E_2 + E_2^{(2)}) - (E_{1\uparrow} + E_{1\uparrow}^{(2)}) = U - \frac{\Delta V_g^{2\leftrightarrow 1} - |\Delta|}{2} + \Gamma_\uparrow \ln \left| \frac{1 - (\Delta V_g^{2\leftrightarrow 1} + |\Delta|)/2U}{1 + (\Delta V_g^{2\leftrightarrow 1} + |\Delta|)/2U} \right| = 0. \tag{5.17b}$$

Of course the second order perturbation theory near the charge degeneracy points is not valid, but here we included it to see how the zero-bias sequential tunneling points might move due to tunneling renormalization. We see that we can get equation (5.17b) from (5.17a) by replacing $\Delta V_g^{1\leftrightarrow 0} \to -\Delta V_g^{2\leftrightarrow 1}$ and $\Gamma_\downarrow \to \Gamma_\uparrow$. In the case when $\Gamma_\downarrow = \Gamma_\uparrow$ we get $\Delta V_g^{2\leftrightarrow 1} = -\Delta V_g^{1\leftrightarrow 0}$, and this implies that the middle of the diamond still is given by $\Delta V_g^{\text{mid}} = 0$. However, when $\Gamma_\downarrow \neq \Gamma_\uparrow$, the middle of the diamond will move as a function of $|\Delta|$ (i.e. magnetic field), and even for $\Delta = 0$, will not be $\Delta V_g^{\text{mid}} = 0$.

5.3 Carbon nanotube quantum dot

In the following discussion for a quantum dot with four single particle orbitals we neglect Stoner splitting of the spin-up and spin-down bands, i.e. we assume that the bandwidth D is much larger than this splitting. We also assume that the tunneling density of states for the left and right leads is equal, i.e. $\rho_{Ls} = \rho_{Rs} = \rho_s$, and only the spin quantization direction of the two leads with respect to one another can change. Lastly, we consider asymmetric couplings to the left and right leads $t_L \neq t_R$, and in general also having a phase difference with respect to one another.

5.3.1 Zero magnetic field

The possible qualitative gate dependencies of the cotunneling threshold for a carbon nanotube coupled to ferromagnetic leads is depicted in Figure 5.2. For particular parameter values, which are discussed in the thesis, corresponding qualitative figure from Figure 5.2 is indicated in Table 5.1.

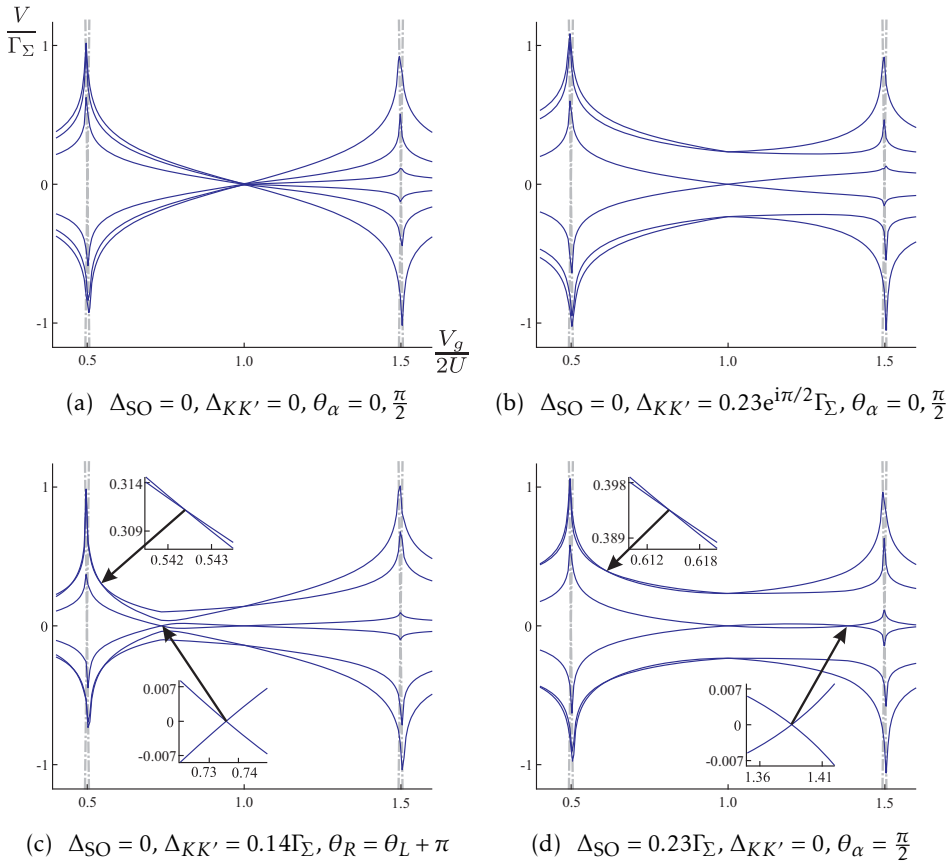

(a) $\Delta_{\mathrm{SO}} = 0, \Delta_{KK'} = 0, \theta_\alpha = 0, \frac{\pi}{2}$ (b) $\Delta_{\mathrm{SO}} = 0, \Delta_{KK'} = 0.23\mathrm{e}^{\mathrm{i}\pi/2}\Gamma_\Sigma, \theta_\alpha = 0, \frac{\pi}{2}$

(c) $\Delta_{\mathrm{SO}} = 0, \Delta_{KK'} = 0.14\Gamma_\Sigma, \theta_R = \theta_L + \pi$ (d) $\Delta_{\mathrm{SO}} = 0.23\Gamma_\Sigma, \Delta_{KK'} = 0, \theta_\alpha = \frac{\pi}{2}$

Figure 5.2: The possible qualitative gate dependencies of tunneling renormalized cotunneling threshold for a quantum dot coupled to ferromagnetic leads for different KK'-mixing, spin-orbit coupling values, and orientations of the leads θ_α. The insets show enlarged plots of crossings. The values of the other parameters are $B = 0$, $U = 47\Gamma_\Sigma$, $D = 10^9\Gamma_\Sigma$, $\frac{\rho_{\tilde{\uparrow}}}{\rho_{\tilde{\downarrow}}} = 2$, $\frac{t_{R,1/2}}{t_{L,1/2}} = \frac{3}{5}\mathrm{e}^{\mathrm{i}\pi/3}$, $\mathrm{Arg}[t_{L,1/2}] = 0$. The legend is the same as in Figure 4.1.

We start by considering the gate dependence of the cotunneling threshold for collinear configuration of the left and the right lead polarizations $\theta_L = \theta_R$. In the case when there is no spin-orbit coupling and KK'-mixing, we can find the eigenspectrum around the middle of the diamond by linearizing the logarithms in Eq. (2.29) and solving the eigenvalue problem:

$$E_{\tilde{\uparrow}} = -\frac{\Delta V_g}{2}\left(\kappa^+_{\tilde{\downarrow}} \pm \sqrt{(\kappa^-_{\tilde{\uparrow}})^2 + |\kappa^o_{\tilde{\uparrow}}|^2}\right), \tag{5.18a}$$

$$E_{\tilde{\downarrow}} = -\frac{\Delta V_g}{2}\left(\kappa^+_{\tilde{\uparrow}} \pm \sqrt{(\kappa^-_{\tilde{\downarrow}})^2 + |\kappa^o_{\tilde{\downarrow}}|^2}\right), \tag{5.18b}$$

where

$$\kappa^\pm_s = \sum_\alpha \frac{\rho_s}{U}(|t_{\alpha 1}|^2 \pm |t_{\alpha 2}|^2), \tag{5.19a}$$

$$\kappa^o_s = 2\sum_\alpha \frac{\rho_s}{U} t_{\alpha 1} t_{\alpha 2}, \tag{5.19b}$$

$$\text{with } s = \tilde{\uparrow}, \tilde{\downarrow}. \tag{5.19c}$$

Collinear				Anticollinear			
$\frac{\Delta_{SO}}{\Gamma_\Sigma}$	$\frac{\Delta_{KK'}}{\Gamma_\Sigma}$	θ	Figure 5.2	$\frac{\Delta_{SO}}{\Gamma_\Sigma}$	$\frac{\Delta_{KK'}}{\Gamma_\Sigma}$	θ	Figure 5.2
0	0	$*$	(a)	0	0	$*$	(a)
0	$0.23e^{i\pi/2}$	$*$	(b)	0	$0.23e^{i\pi/2}$	$*$	(d)
0.23	0	0	(b)	0	0.14	$*$	(c)
0.23	0	$\pi/2$	(d)	0.23	0	0	(d)
0.19	$0.14e^{i\pi/2}$	0	(b)	0.23	0	$\pi/2$	(b)
0.19	$0.14e^{i\pi/2}$	$\pi/2$	(b)	0.19	$0.14e^{i\pi/2}$	0	(d)
				0.19	0.14	0	(c)
				0.19	$0.14e^{i\pi/2}$	$\pi/2$	(b)

Table 5.1: Indication of the corresponding qualitative figure for particular Δ_{SO} and $\Delta_{KK'}$ parameters. In the case of collinear configuration we have $\theta = \theta_L = \theta_R$ and anticollinear $\theta = \theta_L = \theta_R + \pi$. Values of angle denoted with asterisk ($*$) mean that the actual plot does not depend on the angle θ.

The energies (5.18a) correspond to states with $\tilde{\uparrow}$ and (5.18b) to states with $\tilde{\downarrow}$. If $\rho_{\tilde{\uparrow}} > \rho_{\tilde{\downarrow}}$, the left side of the diamond ($\Delta V_g < 0$) has a ground state with spin $\tilde{\uparrow}$ and the right side ($\Delta V_g > 0$) with spin $\tilde{\downarrow}$. When $t_{\alpha 1} = t_{\alpha 2} = t_\alpha$ ($\kappa_s^- = 0$), which is the case for carbon nanotubes, we see that in order for the exchange field to split all cotunneling thresholds, we have to have a phase difference between the left t_L and the right t_R couplings. When only the $\Delta_{KK'}$ mixing is included, there is no dependence on the direction of the polarization of the collinear leads, as shown in Figure 5.2b. This is because there is no particular spin-quantization direction in the carbon nanotube. However, when only spin-orbit coupling is included there is qualitative difference for parallel ($\theta_\alpha = 0$) and perpendicular ($\theta_\alpha = \pi/2$) direction of the collinear leads polarization (Figure 5.2b,d). We see that for the perpendicular direction an additional crossing away from the middle of the diamond appears (Figure 5.2d). However, it can be lifted by $\Delta_{KK'}$ splitting (Figure 5.2b). We also note that the position of the crossing is always on the right side of the diamond independent of Δ_{SO} sign, tunneling amplitudes $t_{\alpha,1/2}$, and densities of states ρ_s.

For anticollinear configuration ($\theta_R = \theta_L + \pi$), similarly, as for collinear configuration, the eigenspectrum around the middle of the diamond, when there is no spin-orbit coupling and KK'-mixing, can be expressed as Eq. (5.18) by replacing $\kappa_s^\pm$ and κ_s^o by

$$\kappa_s^\pm = \frac{1}{U}\left[\rho_s(|t_{L1}|^2 \pm |t_{L2}|^2) + \rho_{\bar{s}}(|t_{R1}|^2 \pm |t_{R2}|^2)\right], \tag{5.20a}$$

$$\kappa_s^o = \frac{2}{U}\left[\rho_s t_{L1} t_{L2} + \rho_{\bar{s}} t_{R1} t_{R2}\right], \tag{5.20b}$$

$$\text{with } s = \tilde{\uparrow}, \tilde{\downarrow} \text{ and } \bar{s} = \tilde{\downarrow}, \tilde{\uparrow}. \tag{5.20c}$$

Again we set $t_{\alpha 1} = t_{\alpha 1} = t_\alpha$. In this case, we notice that all cotunneling lines are split only when there is a phase and modulus difference between the left t_L and the right t_R couplings. We also note that exchange fields from the left and right leads cancel each other if we have symmetric couplings $t_L = t_R$ (there is no splitting of cotunneling lines having different spins). This is also true when both spin-orbit coupling and KK'-mixing are included. As in the case of collinear configuration, when only KK'-mixing is included, there is no dependence on the direction of the polarization of the leads in anticollinear configuration. We also see that in this case a crossing appears (Figure 5.2d), which is lifted for the perpendicular case ($\theta_L = \pi/2$ $\theta_R = -\pi/2$, Figure 5.2b) and left intact for the parallel case ($\theta_L = 0$, $\theta_R = \pi$, Figure 5.2d) when spin-orbit coupling is included. This crossing can

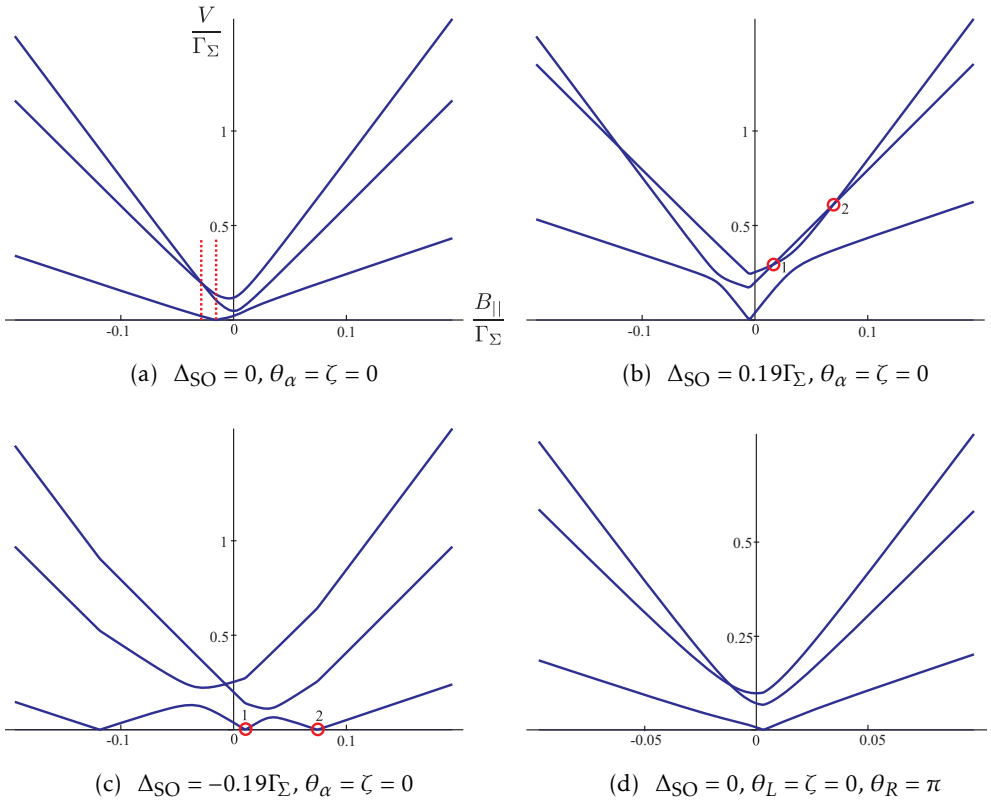

(a) $\Delta_{SO} = 0, \theta_\alpha = \zeta = 0$ (b) $\Delta_{SO} = 0.19\Gamma_\Sigma, \theta_\alpha = \zeta = 0$

(c) $\Delta_{SO} = -0.19\Gamma_\Sigma, \theta_\alpha = \zeta = 0$ (d) $\Delta_{SO} = 0, \theta_L = \zeta = 0, \theta_R = \pi$

Figure 5.3: Tunneling renormalized cotunneling threshold dependence on parallel magnetic field $B_\parallel$ for a quantum dot coupled to ferromagnetic leads, away from the middle of the diamond at gate voltage $V_g = 1.2 \times 2U$. a), b), and c) cases depict situation for the collinear lead configuration, and d) for the anticollinear lead configuration. When only KK'-mixing is included, the cotunneling thresholds qualitatively look as in case a). The values of the parameters are $\Delta_{KK'} = 0$, $U = 39\Gamma_\Sigma$, $D = 10^9\Gamma_\Sigma$, $\frac{\rho_\uparrow}{\rho_\downarrow} = 2$, $\frac{t_{R,1/2}}{t_{L,1/2}} = \frac{4}{5}e^{i\pi/3}$, $\mathrm{Arg}[t_{L,1/2}] = 0$.

also appear on the left side of the diamond, depending on the KK'-mixing phase $\phi_{KK'}$, as shown in Figure 5.2c.

5.3.2 Parallel magnetic B field

The parallel magnetic field $B_\parallel$ dependence of the cotunneling thresholds for the collinear configuration ($\theta_\alpha = 0$) is shown in Figure 5.3a,b,c. The $B < 0$ ($B > 0$) side of the plots corresponds to majority (minority) spins having the larger tunneling density of states. When only KK'-mixing is included, the cotunneling thresholds qualitatively look as in Figure 5.3a. We note that in the case of Figure 5.3a inclusion of a small $\Delta_{SO} << \Delta_{KK'}$ does not split the crossings, and in the cases of Figure 5.3b,c including a small $\Delta_{KK'} << \Delta_{SO}$ also leaves the crossings intact. However, large enough KK'-mixing can lift the crossings denoted 1 and 2 in Figure b,c. So we see that for majority spins tunneling, the parallel magnetic field $B_\parallel$ can always compensate the exchange field between ground and first excited states (ground doublet), or the second and third excited states (excited doublet), even when both Δ_{SO} and $\Delta_{KK'}$ are included. However, the compensation between the states, which would correspond to a bare Kramers doublets at zero magnetic field, appears near different values of $B_\parallel$-field, as shown by dotted (red) lines in Figure 5.3a. For minority spins tunneling, the compen-

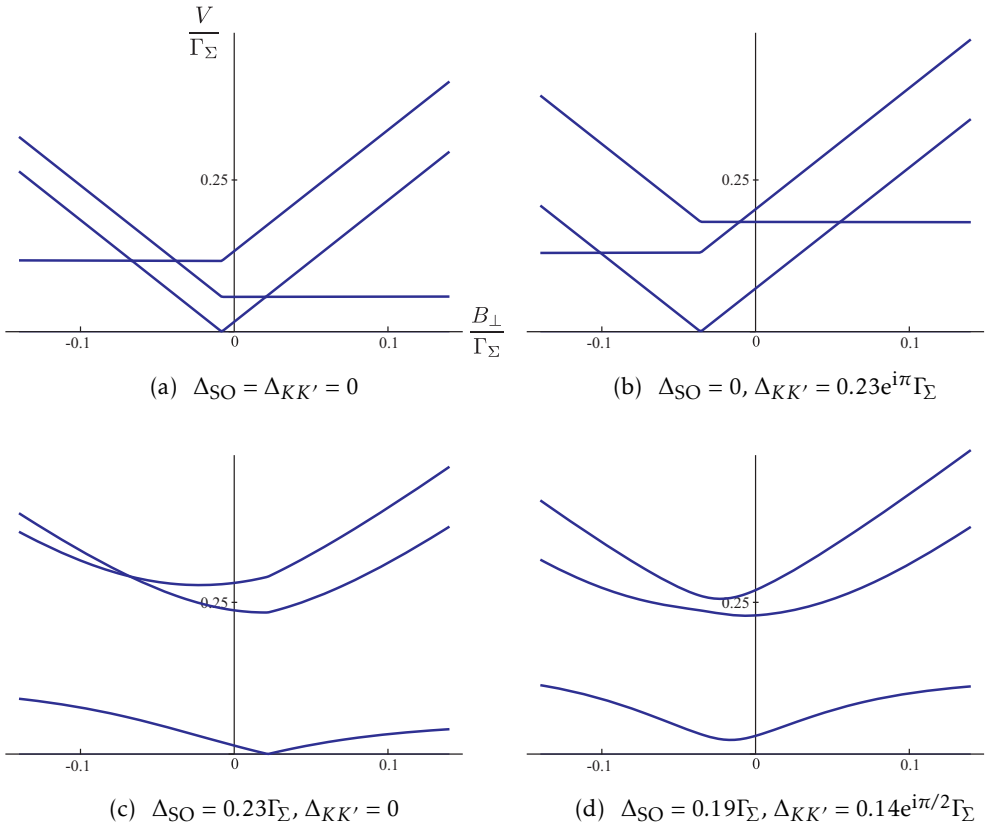

(a) $\Delta_{SO} = \Delta_{KK'} = 0$ (b) $\Delta_{SO} = 0, \Delta_{KK'} = 0.23e^{i\pi}\Gamma_\Sigma$

(c) $\Delta_{SO} = 0.23\Gamma_\Sigma, \Delta_{KK'} = 0$ (d) $\Delta_{SO} = 0.19\Gamma_\Sigma, \Delta_{KK'} = 0.14e^{i\pi/2}\Gamma_\Sigma$

Figure 5.4: Tunneling renormalized cotunneling threshold dependence on perpendicular magnetic field $B_\perp$ for a quantum dot coupled to ferromagnetic leads in the collinear configuration ($\theta_\alpha = \zeta = \pi/2$), away from the middle of the diamond at gate voltage $V_g = 1.2 \times 2U$. The values of the other parameters are $U = 47\Gamma_\Sigma$, $D = 10^9\Gamma_\Sigma$, $\frac{\rho_{\tilde{\uparrow}}}{\rho_{\tilde{\downarrow}}} = 2$, $\frac{t_{R,1/2}}{t_{L,1/2}} = \frac{3}{5}e^{i\pi/3}$, $\mathrm{Arg}[t_{L,1/2}] = 0$.

sation of exchange field is complex and depends on particular values of parameters, i.e. Δ_{SO} and the sign of it, $\Delta_{KK'}$ and its phase, and also tunneling coupling t_α. The situation for anticollinear configuration ($\theta_L = 0$, $\theta_R = \pi$) with no Δ_{SO}, $\Delta_{KK'}$ is depicted in Figure 5.3d. If we assume that the leads majority spins have largest density of states, then the $B < 0$ side of the plot corresponds to the anticollinear lead with respect to the $B_\parallel$-field direction less coupled to the dot than the collinear lead, and for $B > 0$ case *vice versa*. This means that cotunneling renormalization for antiparallel ferromagnetic leads is invariant under exchange $(\rho_{\tilde{\uparrow}}, t_L) \leftrightarrow (\rho_{\tilde{\downarrow}}, t_R)$. From Figure 5.3d, when there is no spin-orbit coupling and KK'-mixing, we see that the exchange field can be compensated only for either the ground doublet or for the excited doublet, depending on the couplings t_α to the leads. If only KK'-mixing is included, the compensation also depends on t_α phases and the phase $\phi_{KK'}$ of this KK'-mixing, and one can get cotunneling threshold looking qualitatively like the one in Figure 5.3d or its mirror image. When only spin-orbit coupling is included, the cotunneling thresholds qualitatively look exactly as in the case of collinear leads Figure 5.3b,c. Including both spin-orbit coupling and KK'-mixing again produces the situations depicted in Figure 5.3b,c, (with the possibility to lift the crossings 1 and 2 for large enough $\Delta_{KK'}$ and crossing 1 to appear in $B < 0$ region) or Figure 5.3d and its mirror image, depending on actual values of Δ_{SO}, $\Delta_{KK'}$, and t_α.

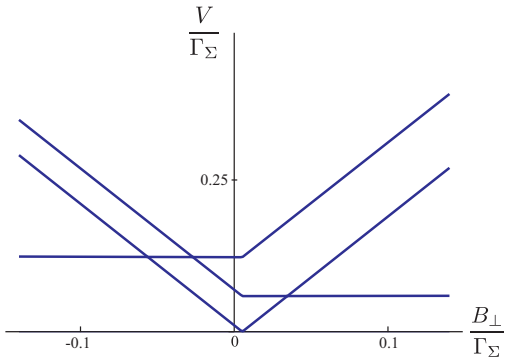

(a) $\Delta_{SO} = \Delta_{KK'} = 0$, $\frac{t_{R,1/2}}{t_{L,1/2}} = \frac{3}{5}e^{i\pi/3}$

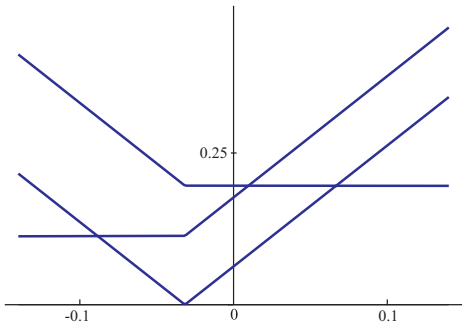

(b) $\Delta_{SO} = 0$, $\Delta_{KK'} = 0.23e^{i\pi}\Gamma_\Sigma$, $\frac{t_{R,1/2}}{t_{L,1/2}} = \frac{3}{5}e^{i\pi/3}$

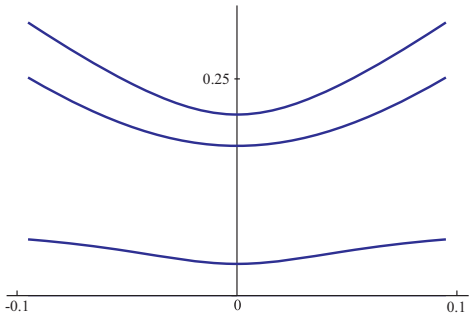

(c) $\Delta_{SO} = 0.16\Gamma_\Sigma$, $\Delta_{KK'} = 0$, $\frac{t_{R,1/2}}{t_{L,1/2}} = e^{i\pi/3}$

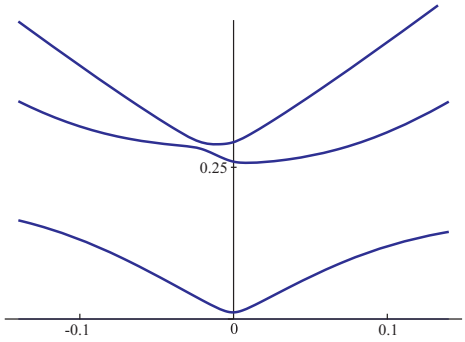

(d) $\Delta_{SO} = 0.19\Gamma_\Sigma$, $\Delta_{KK'} = 0.14e^{i\pi/2}\Gamma_\Sigma$, $\frac{t_{R,1/2}}{t_{L,1/2}} = \frac{3}{5}$

Figure 5.5: Tunneling renormalized cotunneling threshold dependence on perpendicular magnetic field $B_\perp$ for a quantum dot coupled to ferromagnetic leads in the anticollinear configuration ($\theta_L = \zeta = \pi/2$, $\theta_R = -\pi/2$), away from the middle of the diamond at gate voltage $V_g = 1.2 \times 2U$. The values of the other parameters are $U = 47\Gamma_\Sigma$, $D = 10^9\Gamma_\Sigma$, $\frac{\rho_\uparrow}{\rho_\downarrow} = 2$, $\mathrm{Arg}[t_{L,1/2}] = 0$, except for c) $U = 32\Gamma_\Sigma$.

5.3.3 Perpendicular magnetic B field

For perpendicular magnetic field $B_\perp$ and polarization of the leads ($|\theta_\alpha| = \pi/2$), we will focus on exchange field compensation for the ground doublet. With a parallel configuration of the leads ($\theta_\alpha = \pi/2$), the cotunneling thresholds are depicted in Figure 5.4. We see that for majority spin tunneling, the exchange field for the ground doublet can only be compensated if there is no spin-orbit coupling (Figure 5.4a,b), and this holds for any sign of Δ_{SO}. When only KK'-mixing is included then whether the three cotunneling thresholds qualitatively look like Figure 5.4a or Figure 5.4b depends on the phase of $\Delta_{KK'}$. For minority spin tunneling the exchange field for the ground doublet will be compensated if there is only spin-orbit coupling (Figure 5.4c). If both $\Delta_{KK'}$ and Δ_{SO} are present the exchange field is never compensated for both doublets, as shown in Figure 5.4d, and it is so even for symmetric coupling to the leads $t_L = t_R$. Lastly, the case of anticollinear configuration of the leads ($\theta_L = \pi/2$, $\theta_R = -\pi/2$) and perpendicular magnetic field $B_\perp$ is depicted in Figure 5.5. If the anticollinear lead is more coupled to the dot than the collinear one and if there is no spin-orbit coupling and KK'-mixing then the exchange field is always compensated for

the ground doublet and *vice versa*. In the case when there is only KK'-mixing the compensation depends on $\Delta_{KK'}$ and t_α phases, and the qualitative picture of the cotunneling thresholds can look as in Figure 5.5a or Figure 5.5b. If spin-orbit coupling is included, the compensation depends on the values of tunneling couplings t_α, while the sign of Δ_{SO} is irrelevant. When the tunneling couplings have a phase difference, the exchange field is never compensated and all crossings become anticrossings (Figure 5.5c). In the case of symmetric tunneling couplings there is effectively no exchange field and of course the compensation is at zero magnetic field $B_\perp = 0$. Now, when there is only spin-orbit coupling and the tunneling couplings differ only in modulus, the qualitatively situation depicted in Figure 5.4c for collinear leads configuration appears, i.e. the exchange field can be compensated. However, if in this case KK'-mixing is included, there is no compensation possible (Figure 5.5d).

Conclusions for Part I

In this first part we have examined the tunneling renormalization of quantum dot cotunneling spectrum by considering energy shifts of many-body eigenstates using quasi-degenerate perturbation theory [46, 47] in tunneling Hamiltonian H_{T}. The second order result Eq. (2.29) is applicable to any quantum dot with arbitrary number of single particle orbitals, coupled either to normal or ferromagnetic leads, when the tunneling rates Γ are much smaller than charging energy ($\Gamma << U$), and gate-voltage is far from charge degeneracy points. Using this second order result we determined energy shifts for carbon nanotube quantum dot, where fourfold "shell" structure (Section 3.3) of the single particle spectrum was assumed. It was shown that tunneling renormalization introduces gate-dependent KK'-mixing of carbon nanotube orbitals, and this in turn renormalizes g-factors for some cotunneling lines in a gate dependent way. From the energy shifts the cotunneling spectrum was obtained and we found that for asymmetric tunneling couplings to the right and left leads bias asymmetry appears, which is a second order effect in the small parameter Γ/U. By measuring the cotunneling threshold asymmetry (if the coupling to the left and to the right lead is different) between positive and negative bias and its dependence on the magnetic field angle with respect to the tube axis, it would be possible to indicate that the gate dependence of cotunneling lines appear due to tunneling renormalization and not some other effects, like the change of the local electrostatic potential. It was also found that the tunneling renormalization can be reduced by changing the relative phases between the left and right couplings to the leads. For coupling to ferromagnetic leads we showed that the exchange field can completely lift all degeneracies in a fourfold spectrum, however, at particular gate voltages the crossings of cotunneling lines may appear. Then the compensation of this exchange field by external magnetic field was examined. The most important finding was that if both spin-orbit coupling and KK'-mixing are present the exchange field can never be compensated by a perpendicular magnetic field for leads in collinear configuration, and if couplings to the left and right lead are different then it is also the case for leads in anticollinear configuration.

Part II

Sub-gap states in superconductors due to spinful quantum dots

Chapter 6

Superconductor/quantum dot/superconductor junctions

Quantum dots coupled to superconducting leads are examined in this part of the thesis. Such a setup presents an interesting research area, where the interplay between superconductivity and the Coulomb blockade physics can be examined. The state of the leads made out of conventional superconductors is described by the condensation of the so-called Cooper pairs in the ground state of the system [60]. This result in a broken symmetry state, which has the following non-vanishing expectation value

$$\Delta_\alpha = |\Delta_\alpha| e^{i\phi_\alpha} \propto \sum_{\mathbf{k}} \langle c^\dagger_{\alpha\mathbf{k}\uparrow} c^\dagger_{\alpha,-\mathbf{k}\downarrow} \rangle. \tag{6.1}$$

Here $\Delta_\alpha = |\Delta_\alpha| e^{i\phi_\alpha}$ is the superconducting order parameter, which has the modulus $|\Delta_\alpha|$, known as the superconducting gap, and the phase ϕ_α. Also $c^\dagger_{\alpha\mathbf{k}\sigma}$ denotes electron creation operator in the lead α with the momentum $\mathbf{k}$ and the spin σ.

More concretely, the system we are interested in is depicted in Figure 6.1a, where we have a quantum dot, which is in the Coulomb blockade regime, coupled to two superconducting leads, which have a phase difference $\phi = \phi_L - \phi_R$ between them. There is also a third normal lead, with which bias spectroscopy of the joint superconductor/quantum dot/superconductor (SDS) system is performed. So in order for the normal lead not to affect the joint SDS system, we want the coupling to the normal lead $\Gamma_N \ll \Gamma_{S,\alpha}$ to be much smaller than the coupling to the superconducting leads[1]. This kind of setup is motivated by the recent experiment of Chang *et al.* [62, 63], and similar experiments on superconductor/quantum dot/normal metal (SDN) systems [64–67]. Now if a single orbital quantum dot is deep in the Coulomb blockade regime and has an odd number of electrons it effectively acts as a spin-1/2 impurity, which interacts with conduction electrons of the leads through exchange interaction [68, 69]. In the case when the leads are a normal metal, a magnetic impurity induces a localized Kondo resonance at the Fermi level, if the temperature is below the so-called Kondo temperature T_K [70]. When the metal is superconducting, it has a gap $|\Delta|$ of density of states above and below the Fermi level [60] as schematically shown in Figure 6.1b, and the magnetic impurity instead gives rise to excited sub-gap states [71–78] (see Figure 6.1c).

The nature of the ground state and the excited sub-gap state depends on the ratio $T_K/|\Delta|$. If $T_K \ll |\Delta|$, which corresponds to a weak coupling, the excited state is a singlet $|S\rangle$, which is formed between the spin on the quantum dot and Bogoliubov quasiparticles in the leads, and the ground state is a doublet $|D_s\rangle$, $s = \uparrow, \downarrow$. The Bogoliubov quasiparticles correspond to superconductor's single particle excitations, which are a superposition of a particle and a hole. We also note

[1] As it was shown by Žitko et al. [61], that at zero temperature $T = 0$ the coupling to the normal lead is non-perturbative and it always induces Kondo screening. Nevertheless, we will neglect this effect by assuming that the temperature is larger than the corresponding Kondo temperature due to this normal lead.

that the presented picture of the singlet is valid when the charging energy is larger than the superconducting gap $U \gg |\Delta|$, because in the other limit $U \ll |\Delta|$ the singlet is the mixture of zero $|0\rangle$ and two $|2\rangle$ charge states on the quantum dot [79] as shown in Figure 6.2. For $T_K \ll |\Delta|$ the spin is screened resulting in a singlet ground state $|S\rangle$ and excited doublet $|D_s\rangle$. So the increasing ratio $T_K/|\Delta|$, induces a change from a doublet to a singlet ground state, as the sub-gap state crosses zero energy [80–83]. This behavior appears to be confirmed by superconducting scanning tunneling microscope (STM) measurements on an array of magnetic molecules [84] and sharp sub-gap states have also been observed in normal lead bias spectroscopy of a Coulomb blockaded carbon nanotube and InAs quantum dots [62, 64–67, 85]. The schematic of the possible sub-gap state and corresponding ground state dependence on a gate voltage for oddly occupied quantum dot is shown in Figure 6.3.[2] Our main interest in this part of the thesis is to understand the sub-gap state dependence on the phase difference ϕ between two superconductors and an external magnetic field B.[3]

6.1 The model

To describe a quantum dot in a magnetic field connected to two superconducting leads and capacitively coupled to a gate electrode, we assume that its highest partially occupied orbital is represented by a single orbital Anderson model. Then the Hamiltonian for the system is

$$H = H_0 + H_T = H_{LR} + H_D + H_T. \tag{6.2a}$$

The superconducting leads are described by the effective Bardeen-Cooper-Schrieffer (BCS) Hamiltonian [60]

$$H_{LR} = \sum_{\alpha \mathbf{k}\sigma} \xi_{\mathbf{k}\sigma} c^\dagger_{\alpha \mathbf{k}\sigma} c_{\alpha \mathbf{k}\sigma} - \sum_{\alpha \mathbf{k}} \left(\Delta_\alpha c^\dagger_{\alpha \mathbf{k}\uparrow} c^\dagger_{\alpha,-\mathbf{k}\downarrow} + \Delta^*_\alpha c_{\alpha,-\mathbf{k}\downarrow} c_{\alpha \mathbf{k}\uparrow} \right), \tag{6.2b}$$

$$\xi_{\mathbf{k}\sigma} = \xi_{\mathbf{k}} + \sigma \frac{g_{ce} B}{2}, \quad \xi_{\mathbf{k}} = \varepsilon_{\alpha \mathbf{k}} - \mu_\alpha. \tag{6.2c}$$

Here $\alpha = L, R$ stands for the left or right lead; μ_α is the chemical potential of the leads; $\sigma = \uparrow, \downarrow$ denotes the spin of the conduction electron and $\sigma = +1(-1)$ for $\uparrow$ ($\downarrow$); $\mathbf{k}$ is the momentum quantum number; $\varepsilon_{\alpha \mathbf{k}}$ is the dispersion; g_{ce} is the Landé g-factor for the conduction electrons; B denotes the applied magnetic field; and $\Delta_\alpha = |\Delta_\alpha| e^{i\phi_\alpha}$ is the superconducting gap, which has the amplitude $|\Delta_\alpha|$ and the phase ϕ_α. The quantum dot Hamiltonian is

$$H_D = \sum_{\sigma=\uparrow,\downarrow} \varepsilon_{d\sigma} d^\dagger_\sigma d_\sigma + U n_\uparrow n_\downarrow, \quad \varepsilon_{d\sigma} = \varepsilon_d + \sigma \frac{g_i B}{2}, \tag{6.2d}$$

[2] The plots in Figure 6.3 were obtained by using sub-gap state energies of Eq. (7.18) with $g \to 3g$ replacement and Eq. (6.26c) parametrization of the coupling. In Figure 6.3a and Figure 6.3b we have set $\Gamma/U = 0.1$ and $\Gamma/U = 0.2$, respectively. We note that this reproduces only qualitative behavior of the sub-gap states and such a calculation does not correspond to a formally correct result.

[3] In a transport experiment, if the SDS junction is biased it exhibits AC-Josephson effect, which manifests itself in a characteristic series of sub-gap peaks at $V = 2\Delta/ne$, $(n = 1, 2, \ldots)$ due to multiple Andreev reflections [86–88]. If, additionally, spin induced sub-gap states are present, the two effects overlap and experimental signatures of both sub-gap states and multiple Andreev reflections is not so clear. Transport experiments have shown markedly different sub-gap conductance [89–91], depending on the relative strength of tunnel couplings from the quantum dot to the source and drain leads, respectively, which can be understood as a competition between multiple Andreev reflections dominating in the nearly symmetric, and spin induced sub-gap states dominating in the strongly asymmetric coupling limit [92]. In this thesis Iwill not address such phenomena.

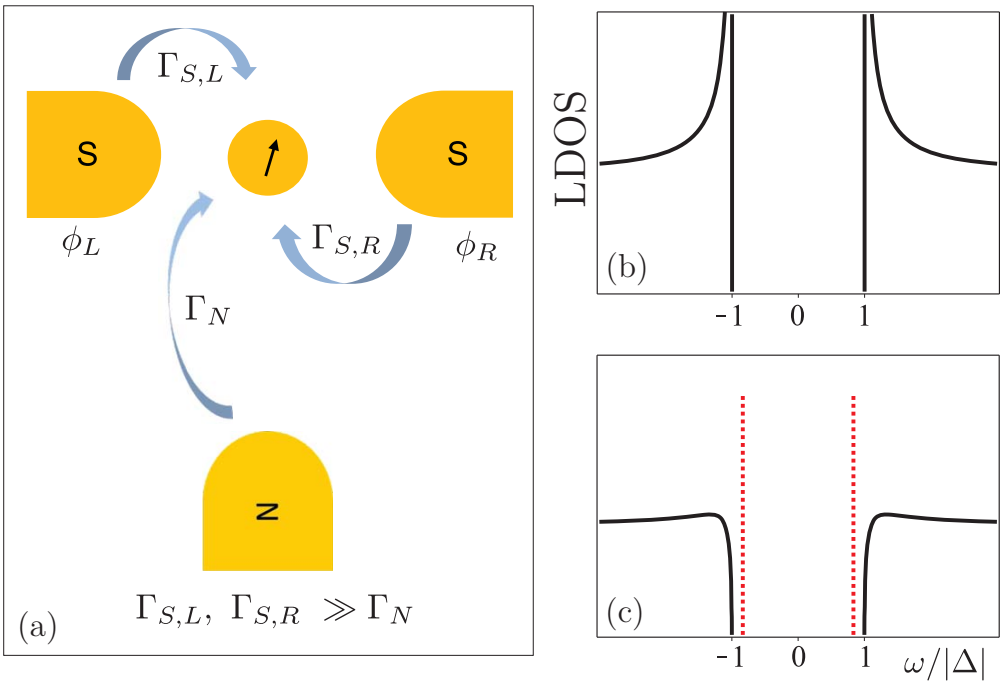

Figure 6.1: (a) Spinful quantum dot coupled to two superconducting leads, which have a phase difference $\phi = \phi_L - \phi_R$ between them, and a third normal lead, which acts as a spectroscopic tool for joint SDS system. (b) A schematic diagram of the local density of states (LDOS), which has the characteristic $\sim 1/\sqrt{1-(\omega/|\Delta|)^2}$ behavior, for a superconductor when it is not coupled to a quantum dot. (c) In the presence of a spinful quantum dot the sub-gap states with energy $\pm\omega_p$ appear, which take the spectral weight from the superconducting gap edge and LDOS behavior is modified to $\sim |\omega|\sqrt{\omega^2-|\Delta|^2}/[\omega^2-\omega_p^2]$ [93]. Here ω denotes the energy at which the system is probed and $|\Delta|$ denotes the superconducting gap.

where ε is the position of the level, g_i is the Landé g-factor, and U is the charging energy of the quantum dot. The coupling between the leads and the quantum dot is given as

$$H_T = \sum_{\alpha\mathbf{k}\sigma}\left(t_\alpha c^\dagger_{\alpha\mathbf{k}\sigma} d_\sigma + t^*_\alpha d^\dagger_\sigma c_{\alpha\mathbf{k}\sigma}\right), \tag{6.2e}$$

where t_α is the tunneling amplitude to the lead α. We note that it is possible to get rid of the phase in tunneling amplitudes $t_\alpha = |t_\alpha| e^{i\varphi_\alpha}$ by making the following gauge transformation for conduction electron operators $c_{\alpha\mathbf{k}} = \tilde{c}_{\alpha\mathbf{k}} e^{i\varphi_\alpha}$. Then the above phase φ_α goes to the order parameter phase

$$\begin{aligned} H_{\text{Pairing}} &= -\sum_{\alpha\mathbf{k}}\left(|\Delta_\alpha| e^{i\phi_\alpha} c^\dagger_{\alpha\mathbf{k}\uparrow} c^\dagger_{\alpha,-\mathbf{k}\downarrow} + |\Delta_\alpha| e^{-i\phi_\alpha} c_{\alpha,-\mathbf{k}\downarrow} c_{\alpha\mathbf{k}\uparrow}\right) \\ &= -\sum_{\alpha\mathbf{k}}\left(|\Delta_\alpha| e^{i(\phi_\alpha - 2\varphi_\alpha)} \tilde{c}^\dagger_{\alpha\mathbf{k}\uparrow} \tilde{c}^\dagger_{\alpha,-\mathbf{k}\downarrow} + |\Delta_\alpha| e^{-i(\phi_\alpha - 2\varphi_\alpha)} \tilde{c}_{\alpha,-\mathbf{k}\downarrow} \tilde{c}_{\alpha\mathbf{k}\uparrow}\right). \end{aligned} \tag{6.3}$$

So we use the tunneling Hamiltonian which has real tunneling amplitudes t_α, and redefine the order parameter Δ_α phase as $\phi_\alpha - 2\varphi_\alpha \to \phi_\alpha$.

We will express the Hamiltonians (6.2b) and (6.2e) in terms of Bogoliubov quasiparticle operators $\gamma_{\alpha\mathbf{k}\sigma}$. The conduction electron operators are expressed as

$$c_{\alpha\mathbf{k}\sigma} = u_{\alpha\mathbf{k}}\gamma_{\alpha\mathbf{k}\sigma} + \sigma v_{\alpha\mathbf{k}} e^{i\phi_\alpha}\gamma^\dagger_{\alpha,-\mathbf{k}\bar{\sigma}}, \tag{6.4a}$$

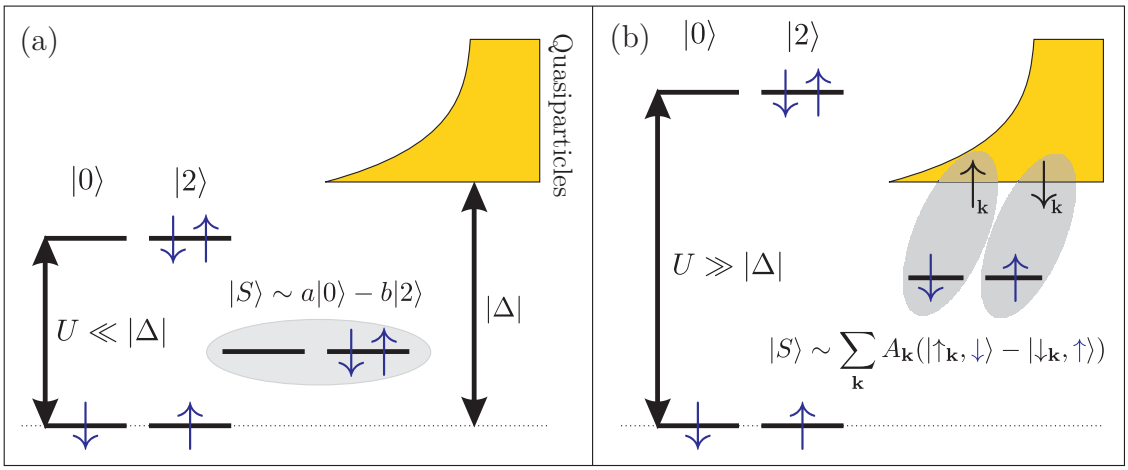

Figure 6.2: A simplified empirical distinction between two different singlets. (a) In the case when charging energy U is smaller than the superconducting gap $|\Delta|$ the singlet is a superposition of zero $|0\rangle$ and $|2\rangle$ charge states on the quantum dot, because the pairing energy gain is larger than the charging penalty. (b) In the other limit $U \gg |\Delta|$ a single electron on the quantum dot is preferred and the singlet is formed between Bogoliubov quasiparticles in the superconductor and the spin of the quantum dot. Of course, for intermediate values of $U \sim |\Delta|$ the sub-gap state has the character of both singlets.

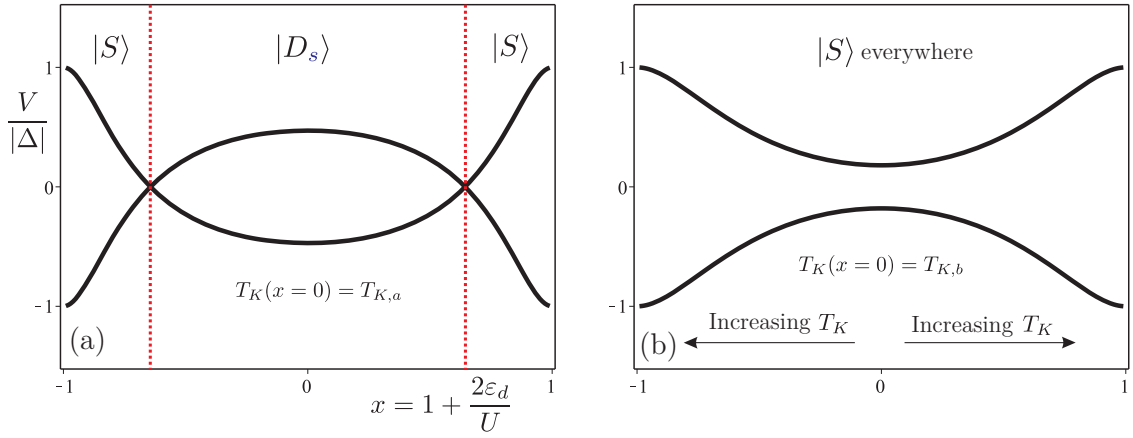

Figure 6.3: The schematic of the possible sub-gap state and corresponding ground state dependence on a gate voltage for oddly occupied quantum dot. Here x denotes dimensionless gate voltage and $x = 0$ corresponds to the middle of the diamond. (a) Situation when at the middle of the diamond the ground state is a doublet $|D_s\rangle$ and going away from $x = 0$ the increasing ratio $T_K/|\Delta|$ induces a change from a doublet $|D_s\rangle$ to a singlet $|S\rangle$ ground state, as the sub-gap state crosses zero energy. (b) The case when $T_{K,b} \gg T_{K,a}$ and we always have the singlet ground state.

where $\bar{\sigma}$ denotes the inverse spin and

$$u_{\alpha\mathbf{k}} = \sqrt{\frac{1}{2}\left(1+\frac{\xi_{\mathbf{k}}}{E_{\alpha\mathbf{k}}}\right)}, \quad v_{\alpha\mathbf{k}} = \sqrt{\frac{1}{2}\left(1-\frac{\xi_{\mathbf{k}}}{E_{\alpha\mathbf{k}}}\right)}, \quad E_{\alpha\mathbf{k}} = \sqrt{\xi_{\mathbf{k}}^2+|\Delta_\alpha|^2}. \tag{6.4b}$$

Then the leads and tunneling Hamiltonians (6.2b) and (6.2e) become

$$H_{\mathrm{LR}} = \sum_{\alpha\mathbf{k}\sigma} E_{\alpha\mathbf{k}\sigma}\gamma^\dagger_{\alpha\mathbf{k}\sigma}\gamma_{\alpha\mathbf{k}\sigma}, \quad E_{\alpha\mathbf{k}\sigma} = E_{\alpha\mathbf{k}} + \sigma\frac{g_{\mathrm{ce}}B}{2}, \tag{6.5a}$$

$$H_{\mathrm{T}} = \sum_{\alpha\mathbf{k}\sigma}\left(t_\alpha\left[u_{\alpha\mathbf{k}}\gamma^\dagger_{\alpha\mathbf{k}\sigma} + \sigma v_{\alpha\mathbf{k}}\mathrm{e}^{-\mathrm{i}\phi_\alpha}\gamma_{\alpha,-\mathbf{k}\bar{\sigma}}\right]d_\sigma + t^*_\alpha d^\dagger_\sigma\left[u_\alpha\gamma_{\alpha\mathbf{k}\sigma} + \sigma v_{\alpha\mathbf{k}}\mathrm{e}^{\mathrm{i}\phi_\alpha}\gamma^\dagger_{\alpha,-\mathbf{k}\bar{\sigma}}\right]\right). \tag{6.5b}$$

6.2 Effective cotunneling model

We want to examine the cotunneling regime well inside a Coulomb diamond, where charge fluctuations happen only virtually. This corresponds to a quantum dot level position being around $\varepsilon_d = -U/2$. To obtain the effective cotunneling model we will perform the Schrieffer-Wolff transformation [68, 69]. For the dot Hamiltonian H_{D} we have the following eigenstates

$$|\psi_d\rangle \in \{|0\rangle,\ |\uparrow\rangle,\ |\downarrow\rangle,\ |2\rangle\}, \tag{6.6}$$

with the following eigenenergies

$$E_{\psi_d} \in \left\{0,\ \varepsilon_{d\uparrow},\ \varepsilon_{d\downarrow},\ \varepsilon_{d\uparrow}+\varepsilon_{d\downarrow}+U\right\} = \left\{E_0,\ E_\uparrow,\ E_\downarrow,\ E_2\right\}. \tag{6.7}$$

The purpose of the Schrieffer-Wolff transformation is to project out the states $|0\rangle$ and $|2\rangle$, which are assumed to be well separated in energy from the states $|\uparrow\rangle$ and $|\downarrow\rangle$. To do so we will use quasi-degenerate perturbation theory as in Chapter 2. For convenience we rewrite the effective Hamiltonian to second order in H_{T}

$$\begin{aligned} H^{(0)}_{mm'} &= \langle m|H_0|m'\rangle, \\ H^{(1)}_{mm'} &= H^{\mathrm{T}}_{mm'} = \langle m|H_{\mathrm{T}}|l\rangle, \\ H^{(2)}_{mm'} &= \frac{1}{2}\sum_l H^{\mathrm{T}}_{ml}H^{\mathrm{T}}_{lm'}\left(\frac{1}{E_m-E_l}+\frac{1}{E_{m'}-E_l}\right), \end{aligned} \tag{6.8}$$

and for the states $|\uparrow\rangle$ and $|\downarrow\rangle$ we have

$$\begin{aligned} &|m\rangle, |m'\rangle \in \{|\lambda\rangle|\uparrow\rangle, |\lambda\rangle|\downarrow\rangle\}, \\ &|l\rangle \in \{|\lambda\rangle|0\rangle, |\lambda\rangle|2\rangle\}, \end{aligned} \tag{6.9}$$

with $|\lambda\rangle$ being arbitrary eigenfunction of the Hamiltonian H_{LR}. We see that the first order term vanishes $H^{(1)}_{mm'} = 0$, because the tunneling Hamiltonian H_{T} has non-vanishing matrix elements only between different charge states. The zeroth order term has the matrix elements

$$H^{(0)}_{ss'} = \delta_{ss'}(H_{\mathrm{LR}} + \varepsilon_{ds}), \quad s,s' \in \uparrow,\downarrow. \tag{6.10}$$

At second order we get the following matrix elements

$$\begin{aligned} H^{(2)}_{ss'} = -\sum_{aa'}\Big\{ &\left[u_a u_{a'}(A^{aa'}_{s-as} + A^{aa'}_{s'-a's'}) + v_a v_{a'}\mathrm{e}^{-\mathrm{i}(\phi_a-\phi_{a'})}(B^{aa'}_{s-as} + B^{aa'}_{s'-a's'})\right]\gamma_{as}\gamma^\dagger_{a's'} \\ &+s'\left[u_a v_{a'}\mathrm{e}^{-\mathrm{i}\phi_{a'}}(A^{aa'}_{s-as} + A^{aa'}_{s'+a'\bar{s}'}) - u_{a'}v_a\mathrm{e}^{-\mathrm{i}\phi_a}(B^{aa'}_{s-as} + B^{aa'}_{s'+a'\bar{s}'})\right]\gamma_{as}\gamma_{a'\bar{s}'} \\ &+s\left[u_{a'}v_a\mathrm{e}^{\mathrm{i}\phi_a}(A^{aa'}_{s+a\bar{s}} + A^{aa'}_{s'-a's'}) - u_a v_{a'}\mathrm{e}^{\mathrm{i}\phi_{a'}}(B^{aa'}_{s+a\bar{s}} + B^{aa'}_{s'-a's'})\right]\gamma^\dagger_{a\bar{s}}\gamma^\dagger_{a's'} \\ &+ss'\left[v_a v_{a'}\mathrm{e}^{\mathrm{i}(\phi_a-\phi_{a'})}(A^{aa'}_{s+a\bar{s}} + A^{aa'}_{s'+a'\bar{s}'}) + u_a u_{a'}(B^{aa'}_{s+a\bar{s}} + B^{aa'}_{s'+a'\bar{s}'})\right]\gamma^\dagger_{a\bar{s}}\gamma_{a'\bar{s}'}\Big\}, \end{aligned} \tag{6.11}$$

where we have used this notation

$$\begin{aligned} a &= \alpha, \mathbf{k}, \quad -a = \alpha, -\mathbf{k}, \\ A^{aa'}_{s\pm b\sigma} &= -\frac{1}{2} \times \frac{t_a t_{a'}}{E_s - E_0 \pm E_{b\sigma}}, \\ B^{aa'}_{s\pm b\sigma} &= -\frac{1}{2} \times \frac{t_a t_{a'}}{E_s - E_2 \pm E_{b\sigma}}. \end{aligned} \tag{6.12}$$

Note that when writing down the matrix elements in (6.11) we used the assumption $\xi_a = \xi_{-a}$, $E_{a\sigma} = E_{-a\sigma}$, $u_a = u_{-a}$, $v_a = v_{-a}$. To see the structure of the Hamiltonian (6.11) we neglect the $\mathbf{k}$ dependence of the quasiparticle energy $E_{b\sigma}$ in coefficients (6.12), i.e., $E_{b\sigma} \to |\Delta| + \sigma g_{\mathrm{ce}} B/2$ and set $\varepsilon_{ds} = (x-1)U/2 + s g_{\mathrm{i}} B/2$, where x denotes the dimensionless level position around the particle-hole symmetric point $\varepsilon_d = -U/2$:

$$x = 1 + \frac{2\varepsilon_d}{U}. \tag{6.13}$$

Then after expanding the coefficients (6.12) in B/U and $|\Delta|/U$ to lowest order we obtain

$$\begin{aligned} A^{aa'}_{s\pm\sigma} &\approx \frac{t_a t_{a'}}{U}\left[\frac{1}{1-x} + \frac{(s g_{\mathrm{i}} \pm \sigma g_{\mathrm{ce}})B \pm 2|\Delta|}{U(1-x)^2}\right], \\ B^{aa'}_{s\pm\sigma} &\approx \frac{t_a t_{a'}}{U}\left[\frac{1}{1+x} + \frac{(s g_{\mathrm{i}} \pm \sigma g_{\mathrm{ce}})B \pm 2|\Delta|}{U(1+x)^2}\right]. \end{aligned} \tag{6.14}$$

We want to write Hamiltonians (6.10) and (6.11) in terms of spin operators S^i, which satisfy the commutation relation $[S^i, S^j] = \mathrm{i}\epsilon_{ijk} S^k$, with ϵ_{ijk} being the Levi-Civita symbol. The quantum dot creation and annihilation operators can be expressed as

$$\begin{aligned} d^\dagger_\uparrow d_\uparrow &= \frac{1}{2} + S^z, \\ d^\dagger_\downarrow d_\downarrow &= \frac{1}{2} - S^z, \\ d^\dagger_\uparrow d_\downarrow &= S^x + \mathrm{i}S^y = S^+, \\ d^\dagger_\downarrow d_\uparrow &= S^x - \mathrm{i}S^y = S^-. \end{aligned} \tag{6.15}$$

Then the effective Hamiltonian (6.10), (6.11) to second order becomes

$$H^{(0)} = H_{\mathrm{LR}} + H_{\mathrm{i},B}, \tag{6.16a}$$

$$\begin{aligned} H^{(2)} &\approx H_J + H_W \\ &\quad + H_{J,\Delta} + H_{W,\Delta} + H_{J,B} + H_{W,B} + H^{(2)}_{\mathrm{i},B}. \end{aligned} \tag{6.16b}$$

where

$$H_{\mathrm{i},B} = g_{\mathrm{i}} B S^z, \tag{6.17a}$$

$$\begin{aligned} H_J = \sum_{a'a} J_{a'a} \Big\{ & S^z \left[K_{a'a}\left(\gamma^\dagger_{a'\uparrow}\gamma_{a\uparrow} - \gamma^\dagger_{a'\downarrow}\gamma_{a\downarrow}\right) + (L_{a'a} - L_{aa'})\gamma^\dagger_{a'\uparrow}\gamma^\dagger_{a\downarrow} + (L^*_{aa'} - L^*_{a'a})\gamma_{a'\downarrow}\gamma_{a\uparrow}\right] \\ & + S^+ \left[K_{a'a}\gamma^\dagger_{a'\downarrow}\gamma_{a\uparrow} + L_{a'a}\gamma^\dagger_{a'\downarrow}\gamma^\dagger_{a\downarrow} + L^*_{a'a}\gamma_{a'\uparrow}\gamma_{a\uparrow}\right] \\ & + S^- \left[K_{a'a}\gamma^\dagger_{a'\uparrow}\gamma_{a\downarrow} + L_{aa'}\gamma^\dagger_{a'\uparrow}\gamma^\dagger_{a\uparrow} + L^*_{aa'}\gamma_{a'\downarrow}\gamma_{a\downarrow}\right] \Big\}, \end{aligned} \tag{6.17b}$$

$$H_W = \sum_{a'a} W_{a'a}\left[M_{a'a}\left(\gamma^\dagger_{a'\uparrow}\gamma_{a\uparrow} + \gamma^\dagger_{a'\downarrow}\gamma_{a\downarrow}\right) + (L_{a'a} + L_{aa'})\gamma^\dagger_{a'\uparrow}\gamma^\dagger_{a\downarrow} + (L^*_{aa'} + L^*_{a'a})\gamma_{a'\downarrow}\gamma_{a\uparrow}\right], \tag{6.17c}$$

$$H_{J,\Delta} = -\sum_{a'a} J^{\Delta}_{a'a} M_{a'a}\Big[S^z(\gamma^\dagger_{a'\uparrow}\gamma_{a\uparrow} - \gamma^\dagger_{a'\downarrow}\gamma_{a\downarrow}) + S^+\gamma^\dagger_{a'\downarrow}\gamma_{a\uparrow} + S^-\gamma^\dagger_{a'\uparrow}\gamma_{a\downarrow}\Big], \tag{6.18a}$$

$$H_{W,\Delta} = -\sum_{a'a} W^{\Delta}_{a'a} K_{a'a}(\gamma^\dagger_{a'\uparrow}\gamma_{a\uparrow} + \gamma^\dagger_{a'\downarrow}\gamma_{a\downarrow}), \tag{6.18b}$$

$$H_{J,B} = \sum_{a'a} J^{B}_{a'a} S^z\Big[M_{a'a}(\gamma^\dagger_{a'\uparrow}\gamma_{a\uparrow} + \gamma^\dagger_{a'\downarrow}\gamma_{a\downarrow}) + (L_{a'a} + L_{aa'})\gamma^\dagger_{a'\uparrow}\gamma^\dagger_{a\downarrow} + (L^*_{aa'} + L^*_{a'a})\gamma_{a'\downarrow}\gamma_{a\uparrow}\Big], \tag{6.18c}$$

$$H_{W,B} = \sum_{a'a} W^{B}_{a'a}\Big[K_{a'a}(\gamma^\dagger_{a'\uparrow}\gamma_{a\uparrow} - \gamma^\dagger_{a'\downarrow}\gamma_{a\downarrow}) + (L_{a'a} - L_{aa'})\gamma^\dagger_{a'\uparrow}\gamma^\dagger_{a\downarrow} + (L^*_{aa'} - L^*_{a'a})\gamma_{a'\downarrow}\gamma_{a\uparrow}\Big], \tag{6.18d}$$

The functions $K_{a'a}$, $L_{a'a}$, $M_{a'a}$ are given as

$$\begin{aligned} K_{a'a} &= u_{a'}u_a + v_{a'}v_a e^{i(\phi_{a'}-\phi_a)}, \\ L_{a'a} &= u_{a'}v_a e^{i\phi_a}, \\ M_{a'a} &= u_{a'}u_a - v_{a'}v_a e^{i(\phi_{a'}-\phi_a)}, \end{aligned} \tag{6.19}$$

and the couplings are

$$J_{a'a} = \frac{t_{a'}t_a}{U}\frac{4}{1-x^2}, \quad W_{a'a} = \frac{t_{a'}t_a}{U}\frac{2x}{1-x^2}, \tag{6.20}$$

$$\begin{aligned} J^{\Delta}_{a'a} &= \frac{t_{a'}t_a}{U}\frac{|\Delta|}{U}\frac{16x}{(1-x^2)^2}, \quad W^{\Delta}_{a'a} = \frac{t_{a'}t_a}{U}\frac{|\Delta|}{U}\frac{4(1+x^2)}{(1-x^2)^2}, \\ J^{B}_{a'a} &= \frac{t_{a'}t_a}{U}\frac{\tilde{B}}{U}\frac{16x}{(1-x^2)^2}, \quad W^{B}_{a'a} = \frac{t_{a'}t_a}{U}\frac{\tilde{B}}{U}\frac{4(1+x^2)}{(1-x^2)^2}, \end{aligned} \tag{6.21}$$

where $\tilde{B} = (g - g_{ce})B/2$. Additionally, the term $H^{(2)}_B$ represents gate-dependent renormalization of the magnetic field

$$\begin{aligned} H^{(2)}_B &= -\sum_a \Big\{\Big[u_a u_a A^{aa}_{\uparrow -a\uparrow} + v_a v_a B^{aa}_{\uparrow -a\uparrow}\Big](1+2S^z) \\ &\qquad + \Big[u_a u_a A^{aa}_{\downarrow -a\downarrow} + v_a v_a B^{aa}_{\downarrow -a\downarrow}\Big](1-2S^z)\Big\} \\ &\approx -S^z \sum_\alpha \frac{8\nu_F|t_\alpha|^2}{U}\frac{1}{1-x^2}\tilde{B} + \text{const.} \end{aligned} \tag{6.22}$$

Here we have kept the $\mathbf{k}$ dependence of the coefficients (6.12) and have evaluated the $\mathbf{k}$-sums using the following assumptions and simplifications: symmetric conduction band $\xi \in [-D, D]$; $|\varepsilon_d \pm \tilde{B}| > |\Delta|$; $|U + \varepsilon_d \pm \tilde{B}| > |\Delta|$; the result was expanded to lowest order in $\tilde{B}/U$ and $|\Delta|/U$. When considering the effective cotunneling model this gate-dependent renormalization of the magnetic field (6.22) will not be taken into account.

In the calculations we will keep only the terms of Eq. (6.17), i.e.,

$$\boxed{H \approx H_{\mathrm{LR}} + H_{\mathrm{i},B} + H_J + H_W,} \tag{6.23}$$

because the additional terms, when superconductivity in the leads [69] and magnetic field are present, are smaller by Δ/U or B/U. The Hamiltonian H_J (6.17b) describes the interaction between the spin on the quantum dot and conduction electrons, and if expressed in terms of operators $c^\dagger_{\alpha\mathbf{k}\sigma}$ takes the usual Kondo Hamiltonian form

$$H_J = \sum_{\substack{i=x,y,z \\ \alpha'\mathbf{k}'s',\alpha\mathbf{k}s}} J_{\alpha'\alpha} S^i c^\dagger_{\alpha'\mathbf{k}'s'}\tau^i_{s's} c_{\alpha\mathbf{k}s}, \tag{6.24}$$

where τ^i are the Pauli matrices. Similarly, the term H_W (6.17c) is rewritten as

$$H_W = \sum_{\alpha'\mathbf{k}',\alpha\mathbf{k},s} W_{\alpha'\alpha} c^\dagger_{\alpha'\mathbf{k}'s} c_{\alpha\mathbf{k}s}, \tag{6.25}$$

and corresponds to the potential scattering for the conduction electrons. Lastly, $H_{\mathrm{i},B}$ (6.17a) simply gives the Zeeman splitting of the quantum dot spin.

When the effective Hamiltonian (6.23) is derived from the Anderson type model (6.2a), then the exchange coupling $J_{\alpha\alpha'}$ and the potential scattering term $W_{\alpha\alpha'}$ have the following matrix structure in the left/right lead space

$$J_{\alpha\alpha'} = J \begin{pmatrix} \cos\theta\cos\theta & \cos\theta\sin\theta \\ \sin\theta\cos\theta & \sin\theta\sin\theta \end{pmatrix}, \quad W_{\alpha\alpha'} = W \begin{pmatrix} \cos\theta\cos\theta & \cos\theta\sin\theta \\ \sin\theta\cos\theta & \sin\theta\sin\theta \end{pmatrix}, \tag{6.26a}$$

where

$$\cos\theta = \frac{t_L}{\sqrt{t_L^2 + t_R^2}}, \quad \sin\theta = \frac{t_R}{\sqrt{t_L^2 + t_R^2}}, \tag{6.26b}$$

$$J = \frac{4}{1-x^2}\frac{t_L^2 + t_R^2}{U}, \quad W = \frac{2x}{1-x^2}\frac{t_L^2 + t_R^2}{U}. \tag{6.26c}$$

We note that the exchange coupling $J > 0$ is always anti-ferromagnetic inside the oddly occupied diamond $x \in [-1..1]$, and also $J > |W|$.

Chapter 7

Sub-gap states

7.1 Review of an experiment

Before we start discussing the theoretical description of the sub-gap states, we review an experiment by Chang *et al.* [62], to see how they are observed in practice. The scanning electron microscope image of the device is shown in Figure 7.1, where ~ 100 nm diameter InAs nanowire (green) is contacted to two ends of the superconducting loop (gray) made out of aluminium (Al). Everything is deposited on the Si substrate, which has an applied gate voltage V_{BG}. The superconducting loop has an area of $A \sim 25\mu\mathrm{m}^2$ and the magnetic field B is threaded through it. The magnetic field controls the phase difference $\phi \sim BA/\Phi_0$ (here Φ_0 is the flux quantum) between two ends of the loop, introduces the Zeeman splitting of the spin in the quantum dot, and closes the superconducting gap. The quantum dot forms in the Al-InAs-Al junction, which is of the length 0.5 μm. To perform the bias spectroscopy of the system a normal metal lead (yellow), which is made out of gold (Au) and has an applied bias V_{T}, is contacted to the nanowire in the middle of the junction.

The resulting differential conductance $\mathrm{d}I/\mathrm{d}V_{\mathrm{T}}$ dependence on the gate voltage V_{BG} and on the phase difference ϕ for the odd occupations of the quantum dot is depicted in Figure 7.2, in order of increasing charging energy U. The vertical red line represents the particle-hole symmetric point. The superconducting gap is observed at $V_{\mathrm{T}} \sim 0.2$ mV. The sub-gap states (which actually become broadened resonances, when the normal lead is contacted) can be seen through enhanced values of $\mathrm{d}I/\mathrm{d}V_{\mathrm{T}}$. We see that for smaller charging energy (see Figure 7.2a) the sub-gap states do not cross the zero bias and has "anti-crossing" like behavior as a function of the gate voltage V_{BG}. Also as a function of phase for $V_{\mathrm{T}} < 0$ it has a minimum at $\phi = 0$ and a maximum at $\phi = \pi$. For large charging energy (see Figure 7.2c) the sub-gap states cross the zero bias and has an "eye" like behavior as a

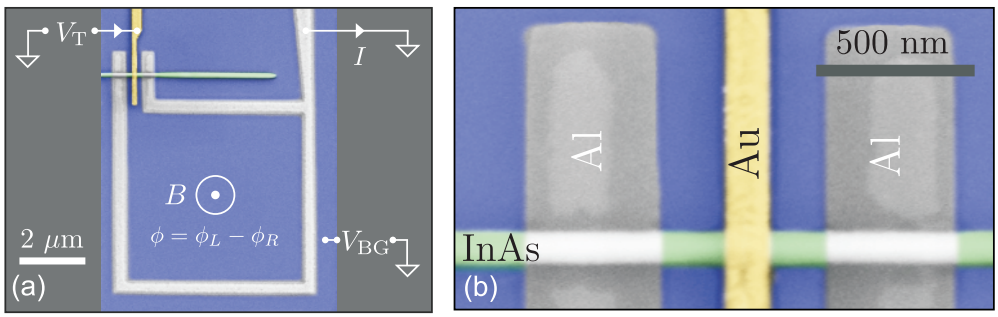

Figure 7.1: (a) Scanning electron microscope image of the device. (b) Zoom of the region where the normal lead (Au) is contacted to the SDS junction.

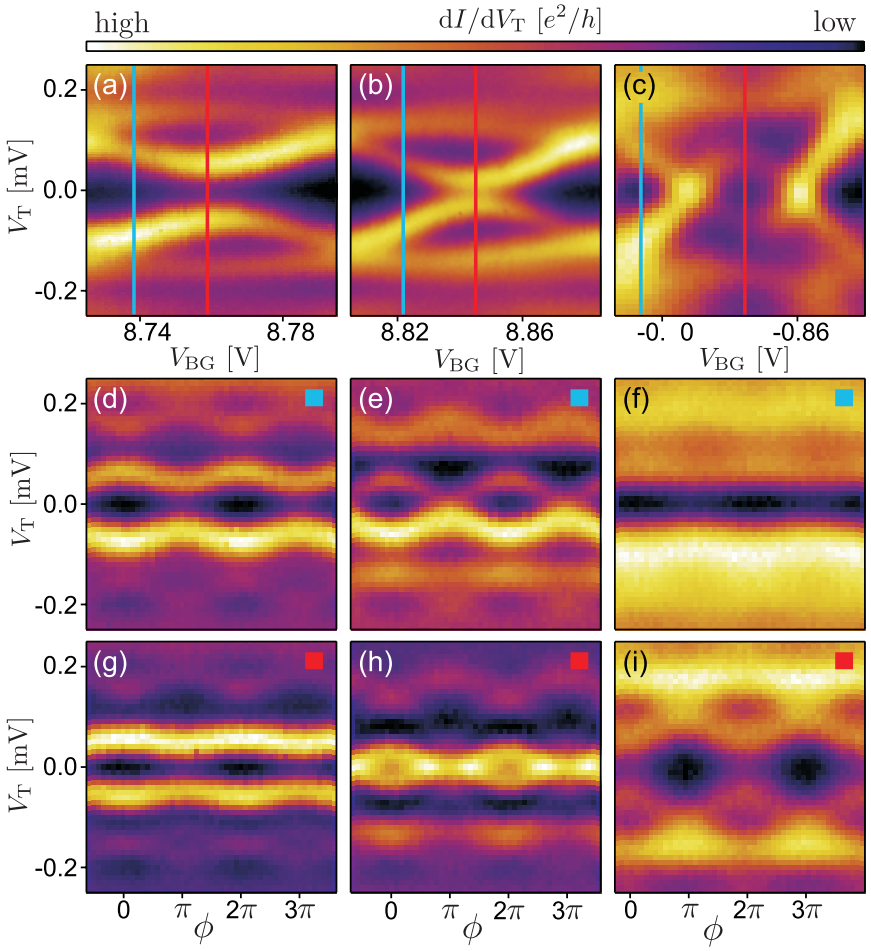

Figure 7.2: (a)-(c) Experimentally observed sub-gap state dependence on the gate voltage V_BG. The diamond in (a) has the smallest charging energy U and (c) has the largest one. The corresponding to (a)-(c) sub-gap state phase dependence is shown in (d)-(f) away from the particle-hole symmetric point (gate voltage at the blue vertical line), and (g)-(i) at the particle-hole symmetric point (gate voltage at the red vertical line).

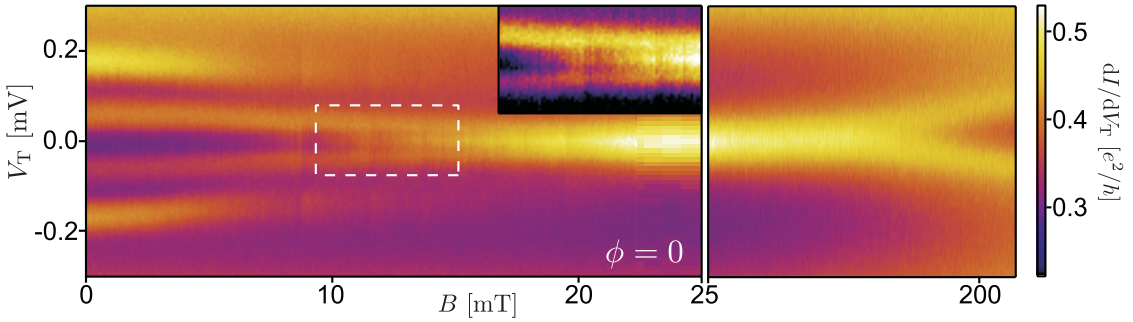

Figure 7.3: Magnetic field dependence of the sub-gap states in Figure 7.2c at the particle-hole symmetric point.

function of V_{BG}. If the gate voltage is in the region between the crossings the sub-gap states acquire reversed phase dependence, i.e., it has a minimum at $\phi = \pi$ and a maximum at $\phi = 0$ for $V_{\mathrm{T}} < 0$. Additionally, when the sub-gap states are close to the zero bias and are outside the "eye" they can cross the zero bias as a function of phase ϕ.

Theoretically we will be able to address magnetic field dependence for the situation corresponding to Figure 7.1c at the particle-hole symmetric point. Such dependence is shown in Figure 7.3. We see that the gap closes as a function of B and the sub-gap state follows the gap without crossing it. Also for higher magnetic fields (10 to 20 mT, small gap) a zero bias peak appears, which could be attributed to the Kondo peak due to normal lead [61]. For even higher magnetic fields (from 20 mT), the superconductivity is destroyed in the aluminium electrodes and also the resulting Kondo peak is being Zeeman split. In our calculations we will not address effects concerning the Kondo effect due to the normal lead, and we will not include the magnetic field dependence of the superconducting gap.

7.2 Classical spin

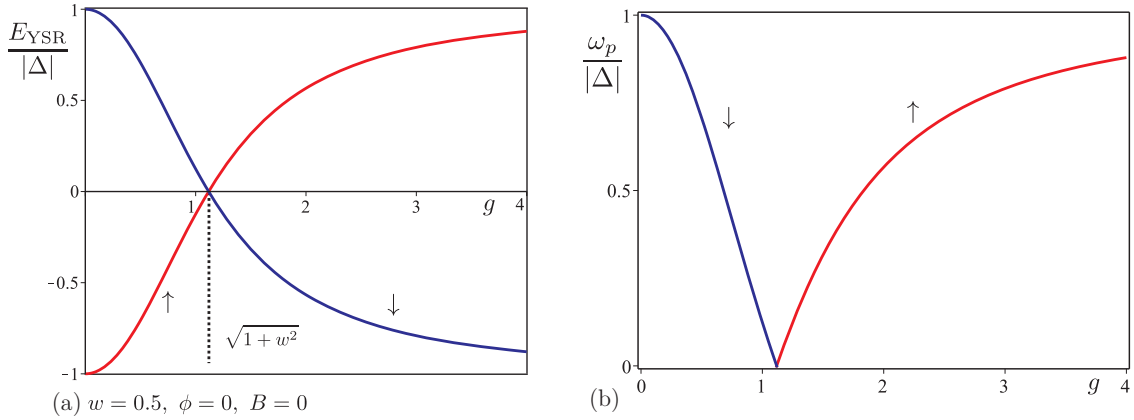

Figure 7.4: (a) Sub-gap state energy dependence on the coupling. The blue curve denotes spin ↑ state and the red curve denotes spin ↓. When the exchange coupling is anti-ferromagnetic $g > 0$ and small $g < \sqrt{1+w^2}$ then the ground-state contains quasiparticle with spin ↑ and for larger couplings $g > \sqrt{1+w^2}$ it switches to spin ↓. (b) The corresponding sub-gap excitation spectrum. The potential scattering value is $w = 0.5$.

We start by discussing the case of a classical spin, which corresponds to simplifying the exchange Hamiltonian (6.24) to a spin-dependent potential scattering term for conduction electrons:

$$H_J^{cl} = \sum_{\alpha'\mathbf{k}',\alpha\mathbf{k}} J_{\alpha'\alpha} S \left(c^\dagger_{\alpha'\mathbf{k}'\uparrow} c_{\alpha\mathbf{k}\uparrow} - c^\dagger_{\alpha'\mathbf{k}'\downarrow} c_{\alpha\mathbf{k}\downarrow} \right). \tag{7.1}$$

In this case the problem can be diagonalized exactly by using the Bogoliubov-de Gennes transformation

$$\gamma_{n\sigma} = \sum_{\beta\mathbf{q}} \left(A_{n\sigma,\beta\mathbf{q}} c_{\beta\mathbf{q}\sigma} + \sigma B_{n\sigma,\beta\mathbf{q}} c^\dagger_{\beta,-\mathbf{q}\bar{\sigma}} \right). \tag{7.2}$$

Here we denoted the lead index by the label β and the momentum by the label $\mathbf{q}$. The equations for the expansion coefficients $A_{n\sigma,\beta\mathbf{q}}$ and $B_{n\sigma,\beta\mathbf{q}}$ are generated by requiring the following commutator

$$[H, \gamma_{n\sigma}] = -E_{n\sigma} \gamma_{n\sigma}, \tag{7.3}$$

where $E_{n\sigma}$ is the quasiparticle energy with included H_J^{cl} and H_W terms. The equations for coefficients A and B are generated by taking the commutators

$$[H, c_{b\sigma}] = -\varepsilon_{b\sigma} c_{b\sigma} + \sigma\Delta_{\sigma b} c^\dagger_{-b\bar\sigma} - \sum_a (W_{ba} + \sigma J_{ba} S) c_{a\sigma}, \quad \varepsilon_{b\sigma} = \varepsilon_b + \sigma B, \tag{7.4a}$$

$$[H, c^\dagger_{b\sigma}] = \varepsilon_{b\sigma} c^\dagger_{b\sigma} - \sigma\Delta^*_{\sigma b} c_{-b\bar\sigma} + \sum_a (W_{ab} + \sigma J_{ab} S) c^\dagger_{a\sigma}, \tag{7.4b}$$

which after using transformation (7.2) and commutator (7.3) give

$$\begin{aligned}[H, \gamma_{n\sigma}] &= -E_{n\sigma} \sum_b \left(A_{n\sigma,b} c_{b\sigma} + \sigma B_{n\sigma,b} c^\dagger_{-b\bar\sigma} \right) \\ &= \sum_b \left[(-\varepsilon_{b\sigma} c_{b\sigma} + \sigma\Delta_{\sigma b} c^\dagger_{-b\bar\sigma}) A_{n\sigma,b} - c_{b\sigma} \sum_a A_{n\sigma,a} (W_{ab} + \sigma J_{ab} S) \right] \\ &\quad + \sum_b \left[(\varepsilon_{-b\bar\sigma} c^\dagger_{-b\bar\sigma} - \bar\sigma\Delta^*_{\sigma b} c_{b\sigma}) \sigma B_{n\sigma,b} + c^\dagger_{-b\bar\sigma} \sum_a (W_{-b,-a} + \bar\sigma J_{-b,-a} S) \sigma B_{n\sigma,a} \right].\end{aligned} \tag{7.5}$$

Here we used the shorthand notation $b \equiv \beta, \mathbf{q}$, $-b \equiv \beta, -\mathbf{q}$. After equating the coefficients in front of different operators $c_{\beta\mathbf{q}\sigma}$ or $c^\dagger_{\beta\mathbf{q}\sigma}$ we get

$$c_{b\sigma}: \quad E_{n\sigma} A_{n\sigma,b} = \varepsilon_{b\sigma} A_{n\sigma,b} - \Delta^*_{\sigma b} B_{n\sigma,b} + \sum_a A_{n\sigma,a} (W_{ab} + \sigma J_{ab} S), \tag{7.6a}$$

$$c^\dagger_{-b\bar\sigma}: \quad E_{n\sigma} B_{n\sigma,b} = -\varepsilon_{-b\bar\sigma} B_{n\sigma,b} - \Delta_{\sigma b} A_{n\sigma,b} - \sum_a (W_{-b,-a} + \bar\sigma J_{-b,-a} S) B_{n\sigma,a}. \tag{7.6b}$$

We see that we get two independent sets of equations, i.e., one set for coefficients $A_\uparrow, B_\uparrow$ and one set for coefficients $A_\downarrow, B_\downarrow$:

$$\begin{pmatrix} E_{n\sigma} - \varepsilon_{b\sigma} & \Delta^*_{\sigma b} \\ \Delta_{\sigma b} & E_{n\sigma} + \varepsilon_{-b\bar\sigma} \end{pmatrix} \begin{pmatrix} A_{b\sigma,n} \\ B_{b\sigma,n} \end{pmatrix} = \begin{pmatrix} \sum_a (W_{ab} + \sigma J_{ab} S) A_{a\sigma,n} \\ -\sum_a (W_{-b,-a} - \sigma J_{-b,-a} S) B_{a\sigma,n} \end{pmatrix}, \tag{7.7}$$

Solving the above equations for A and B we obtain the following integral equations

$$A_{n\sigma,\beta\mathbf{q}} = -\frac{(E_{n\sigma} + \xi_{-\mathbf{q}\bar\sigma}) \sum_{\alpha\mathbf{k}} (W_{\alpha\beta} + \sigma J_{\alpha\beta} S) A_{n\sigma,\alpha\mathbf{k}} + \Delta^*_\beta \sum_{\alpha\mathbf{k}} (W_{\beta\alpha} - \sigma J_{\beta\alpha} S) B_{n\sigma,\alpha\mathbf{k}}}{\xi_{\mathbf{q}\sigma}\xi_{-\mathbf{q}\bar\sigma} + |\Delta_\beta|^2 + (\xi_{\mathbf{q}\sigma} - \xi_{-\mathbf{q}\bar\sigma}) E_{n\sigma} - E^2_{n\sigma}}, \tag{7.8a}$$

$$B_{n\sigma,\beta\mathbf{q}} = \frac{(E_{n\sigma} - \xi_{\mathbf{q}\sigma}) \sum_{\alpha\mathbf{k}} (W_{\beta\alpha} - \sigma J_{\beta\alpha} S) B_{n\sigma,\alpha\mathbf{k}} + \Delta_\beta \sum_{\alpha\mathbf{k}} (W_{\alpha\beta} + \sigma J_{\alpha\beta} S) A_{n\sigma,\alpha\mathbf{k}}}{\xi_{\mathbf{q}\sigma}\xi_{-\mathbf{q}\bar\sigma} + |\Delta_\beta|^2 + (\xi_{\mathbf{q}\sigma} - \xi_{-\mathbf{q}\bar\sigma}) E_{n\sigma} - E^2_{n\sigma}}. \tag{7.8b}$$

By integrating the above Eqs. (7.8) over $\mathbf{q}$ we get

$$\begin{pmatrix} 1 + f_{n\sigma}\zeta^{+,\sigma}_{LL}\Omega_{n\sigma} & f_{n\sigma}\zeta^{+,\sigma}_{RL}\Omega_{n\sigma} & f_{n\sigma} e^{-i\phi_L}\zeta^{-,\sigma}_{LL} & f_{n\sigma} e^{-i\phi_L}\zeta^{-,\sigma}_{LR} \\ f_{n\sigma}\zeta^{+,\sigma}_{LR}\Omega_{n\sigma} & 1 + f_{n\sigma}\zeta^{+,\sigma}_{RR}\Omega_{n\sigma} & f_{n\sigma} e^{-i\phi_R}\zeta^{-,\sigma}_{RL} & f_{n\sigma} e^{-i\phi_R}\zeta^{-,\sigma}_{RR} \\ -f_{n\sigma} e^{i\phi_L}\zeta^{+,\sigma}_{LL} & -f_{n\sigma} e^{i\phi_L}\zeta^{+,\sigma}_{RL} & 1 - f_{n\sigma}\zeta^{-,\sigma}_{LL}\Omega_{n\sigma} & -f_{n\sigma}\zeta^{-,\sigma}_{LR}\Omega_{n\sigma} \\ -f_{n\sigma} e^{i\phi_R}\zeta^{+,\sigma}_{LR} & -f_{n\sigma} e^{i\phi_R}\zeta^{+,\sigma}_{RR} & -f_{n\sigma}\zeta^{-,\sigma}_{RL}\Omega_{n\sigma} & 1 - f_{n\sigma}\zeta^{-,\sigma}_{RR}\Omega_{n\sigma} \end{pmatrix} \begin{pmatrix} A_{n\sigma,L} \\ A_{n\sigma,R} \\ B_{n\sigma,L} \\ B_{n\sigma,R} \end{pmatrix} = 0. \tag{7.9}$$

Here the assumption $\xi_{\mathbf{q}} = \xi_{-\mathbf{q}}$ was used and the $\mathbf{q}$ sums were performed using a flat density of states approximation, i.e., $\sum_{\mathbf{q}} \ldots \to \nu_F \int_{-D}^{D} d\xi \ldots$, where the bands in the left and right leads are assumed to be symmetric $\xi \in [-D, D]$. Also we have set the amplitudes of the gaps in the left and the right lead to be equal $|\Delta_L| = |\Delta_R| = |\Delta|$. Lastly, the following notation was introduced:

$$\Omega_{n\sigma} = E_{n\sigma} - \sigma \frac{g_{ce} B}{2}, \tag{7.10}$$

$$w_{\alpha\alpha'} = \pi\nu_F W_{\alpha\alpha'}, \quad g_{\alpha\alpha'} = \pi\nu_F J_{\alpha\alpha'} S, \quad \zeta^{\pm,\sigma}_{\alpha\alpha'} = w_{\alpha\alpha'} \pm \sigma g_{\alpha\alpha'}, \tag{7.11}$$

$$A_{n\sigma,\beta} = \sum_{\mathbf{q}} A_{n\sigma,\beta\mathbf{q}}, \quad B_{n\sigma,\beta} = \sum_{\mathbf{q}} B_{n\sigma,\beta\mathbf{q}}, \tag{7.12}$$

$$\begin{aligned} f_\sigma &= \frac{1}{\pi}\int_{-D}^{D} \frac{\mathrm{d}\xi}{\xi^2 + |\Delta|^2 - \Omega_{n\sigma}^2} = \frac{2}{\pi}\frac{\arctan\left(\frac{D}{\sqrt{|\Delta|^2-\Omega_{n\sigma}^2}}\right)}{\sqrt{|\Delta|^2-\Omega_{n\sigma}^2}} \\ &\approx \frac{1}{\sqrt{|\Delta|^2-\Omega_{n\sigma}^2}}, \quad \text{for} \quad D \gg |\Delta|,\ |\Omega_{n\sigma}| < |\Delta|. \end{aligned} \tag{7.13}$$

By taking the determinant of the matrix in (7.9) we obtain the *secular* equation, that can be solved to yield sub-gap states, i.e., solutions $|\Omega_{n\sigma}| < |\Delta|$. When the couplings have the structure described by Eq. (6.26), the resulting *secular* equation is

$$\begin{aligned} &1 + 2g\sigma f_\sigma \Omega_{n\sigma} + u\left(1 - f_\sigma^2 \sin^2(2\theta)\sin^2\frac{\phi}{2}\right) = 0, \\ &u = w^2 - g^2, \quad \phi = \phi_L - \phi_R, \end{aligned} \tag{7.14}$$

which can be solved analytically to give the following sub-gap states

$$\Omega_{\pm,\sigma} = \sigma c_\pm |\Delta| \sqrt{\frac{(1+u)(1+\chi u) + 2g^2 \pm 2g\sqrt{g^2 + u(1-\chi)(1+\chi u)}}{(1+u)^2 + 4g^2}}, \tag{7.15}$$

where

$$\chi = 1 - \sin^2(2\theta)\sin^2\frac{\phi}{2}, \tag{7.16a}$$

$$c_+ = \mathrm{sgn}(u), \quad c_- = -\mathrm{sgn}(1+\chi u), \tag{7.16b}$$

and $g > 0$ was assumed. For $g < 0$ the above result holds with interchanged spins. From Eqs. (7.21) and (7.15) we see that there can be up to four sub-gap solutions.

In the rest of this section we will examine the sub-gap excitation spectrum dependence on the coupling strengths and phase difference for $B = 0$ case ($\Omega_{n\sigma} = E_{n\sigma}$). We define the excitation spectrum ω_p of the system as the energy differences between the ground-state $|\mathrm{GS}\rangle$, which has all quasiparticle states filled with negative energy $E_{n\sigma} < 0$, and the excited state $|\mathrm{ES}\rangle$, which has an additional quasiparticle at positive energy $E_{n\sigma} > 0$:

$$\omega_p = E_{\mathrm{ES}} - E_{\mathrm{GS}}, \quad |\mathrm{ES}\rangle = \gamma^\dagger_{n\sigma}|\mathrm{GS}\rangle, \quad E_{n\sigma} > 0. \tag{7.17}$$

Of course there are also sub-gap excitations corresponding to removed quasiparticles from the ground state $|\mathrm{ES}\rangle = \gamma_{n\sigma}|\mathrm{GS}\rangle$, however, we will specify the excitation spectrum only for added quasiparticles. When there is no phase difference $\phi = 0$ from Eq. (7.15) we obtain the following energies for two sub-gap states when considering anti-ferromagnetic coupling:

$$E_{\mathrm{YSR},\sigma} = -\sigma|\Delta|\frac{1 + w^2 - g^2}{\sqrt{(1+w^2-g^2)^2 + 4g^2}}, \quad g > 0. \tag{7.18}$$

This is the result obtained by Yu-Shiba-Rusinov [71–73]. The energy dependence of the two states on the coupling is shown in Figure 7.4a and the corresponding excitation spectrum is shown in

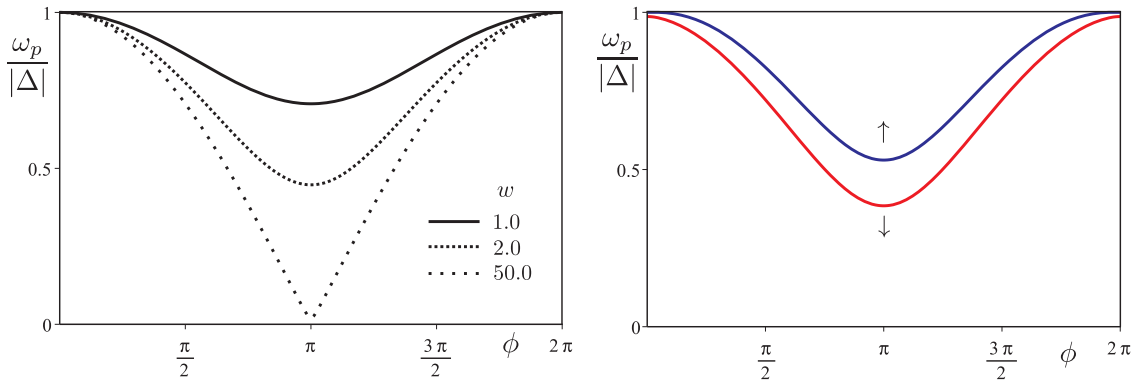

(a) $g = 0,\ \theta = \pi/4,\ B = 0$ (b) $w = 2.0,\ g = 0.4,\ \theta = \pi/4,\ B = 0$

Figure 7.5: (a) When there is no exchange coupling $g = 0$, the sub-gap excitation is spin degenerate Andreev bound state. If potential scattering is increased the excitation approaches zero energy at $\phi = \pi$ ($w \to +\infty$ corresponds to transmission $\tau = 1$). (b) The presence of exchange coupling $g < |w|$ splits the Andreev bound state. In the plot anti-ferromagnetic $g > 0$ coupling is considered and $w = 2.0$.

Figure 7.4b. For values $g < \sqrt{1+w^2}$ of the exchange coupling the sub-gap excitation is an added quasiparticle with spin $\downarrow$ and for $g > \sqrt{1+w^2}$ the excited quasiparticle changes to spin $\uparrow$.

In the case when there is no exchange coupling $g = 0$ we obtain the usual expression for the Andreev bound state [94–98]:

$$E_{\mathrm{K},\pm,\sigma} = \pm\sigma|\Delta|\sqrt{1-\tau\sin^2\frac{\phi}{2}}, \quad \tau = \frac{w^2\sin^2(2\theta)}{1+w^2}, \tag{7.19}$$

where τ is the normal state transmission of the junction. The dependence of the Andreev bound state on phase difference is shown in Figure 7.5a. We see that the sub-gap states are spin-degenerate, and if a small exchange coupling $g \ll |w|$ is introduced they are split by

$$E_{\pm,\sigma} \approx E_{\mathrm{K},\pm,\sigma} + \sigma|\Delta|\frac{g|w|}{1+w^2}\sqrt{\frac{1-\chi}{1+w^2}}. \tag{7.20}$$

which is shown in Figure 7.5b. When $g > |w|$ the phase difference dependence of the excitation spectrum from Eq. (7.15) is shown in Figure 7.6. We see that for finite phase difference two added quasiparticle sub-gap excitations are present. The crossing of two excited states at $\phi = \pi$ is lifted by potential scattering w or coupling asymmetry.

For arbitrary couplings $g_{\alpha\alpha'}$ and $w_{\alpha\alpha'}$ it is not possible to write down a simple closed form solution, so we find sub-gap states perturbatively in the couplings:

$$\Omega_{\pm,\sigma} \approx \sigma c_\pm|\Delta|(1-\eta^2_{cl,\sigma,\pm}), \tag{7.21}$$

where $c_\pm = -\mathrm{sgn}(\eta_{cl,\sigma,\pm})$ with

$$\begin{aligned}\eta_{cl,\sigma,\pm} &= \frac{1}{\sqrt{2}}\left[g_{LL} + g_{RR} \pm g_{cl,d}\right],\\ g_{cl,d} &= \Big[(g_{LL}-g_{RR})^2 + 4|g_{LR}|^2\cos^2\frac{\phi}{2} + 4|w_{LR}|^2\sin^2\frac{\phi}{2}\\ &\quad - 4\sigma|g_{LR}||w_{LR}|\sin(\phi_g-\phi_w)\sin\phi\Big]^{\frac{1}{2}},\end{aligned} \tag{7.22}$$

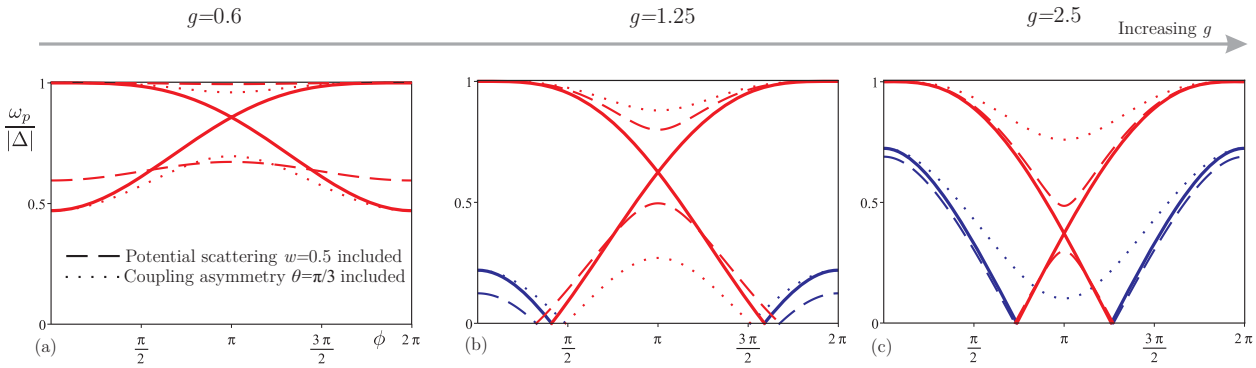

Figure 7.6: The excitation spectrum dependence on the phase difference for $B = 0$ and $g > |w|$. The dashed lines represent excitation spectrum when potential scattering $w = 0.5$ is included and the dotted lines show the situation when coupling asymmetry $\theta = \pi/3$ is present.

and $g_{LR} = g^*_{RL} = |g_{LR}|e^{i\phi_g}$, $w_{LR} = w^*_{RL} = |w_{LR}|e^{i\phi_w}$. From Eq. (7.22) we see that there are four sub-gap states (two added quasiparticle excitations) if the couplings have arbitrary form even at phase difference $\phi = 0$. This corresponds to two channels, which contribute to the sub-gap state formation, i.e., the matrix $g_{\alpha\alpha'}$ has two non-zero eigenvalues. Reverting to an Anderson model, one has $g^2_{LR} = g_{LL}g_{RR}$, which implies that

$$\eta_{cl,\pm} = \frac{\sqrt{2}}{2}\left(g \pm \sqrt{g^2\chi + w^2(1-\chi)}\right). \tag{7.23}$$

7.3 Quantum spin

In this section we obtain the sub-gap state energies perturbatively in the couplings for the case of the quantum spin. We start by presenting a simplified calculation for the case with no potential scattering term $H_W = 0$ (6.17c) and magnetic field $B = 0$. The exchange Hamiltonian (6.17b) for low energies gets simplified to

$$\begin{aligned} H_J \approx \frac{1}{2}\sum_{\alpha'\mathbf{k}'\alpha\mathbf{k}} \left(1 + e^{i(\phi_{\alpha'} - \phi_\alpha)}\right) J_{\alpha'\alpha} \\ \times \left[S^z\left(\gamma^\dagger_{\alpha'\mathbf{k}'\uparrow}\gamma_{\alpha\mathbf{k}\uparrow} - \gamma^\dagger_{\alpha'\mathbf{k}'\downarrow}\gamma_{\alpha\mathbf{k}\downarrow}\right) + S^+\gamma^\dagger_{\alpha'\mathbf{k}'\downarrow}\gamma_{\alpha\mathbf{k}\uparrow} + S^-\gamma^\dagger_{\alpha'\mathbf{k}'\uparrow}\gamma_{\alpha\mathbf{k}\downarrow}\right] = \sum_{\mathbf{k}'\mathbf{k}} \psi^\dagger_{\mathbf{k}'}\mathcal{M}\psi_{\mathbf{k}}, \end{aligned} \tag{7.24}$$

where the pairing-like terms $\gamma^\dagger_{a'\uparrow}\gamma^\dagger_{a\downarrow}$ and $\gamma_{a'\uparrow}\gamma_{a\downarrow}$ were neglected and we have set $u_{\mathbf{k}} \approx v_{\mathbf{k}} \approx \frac{1}{2}$, because the energy dependence of the $u_{\mathbf{k}}$, $v_{\mathbf{k}}$ factors is necessary only for higher order corrections for the sub-gap state energies. Also the following spinor $\psi_{\mathbf{k}}$ and matrix $\mathcal{M}$ were introduced

$$\psi^\dagger_{\mathbf{k}} = (\gamma^\dagger_{L\mathbf{k}\uparrow}, \gamma^\dagger_{R\mathbf{k}\uparrow}, \gamma^\dagger_{L\mathbf{k}\downarrow}, \gamma^\dagger_{R\mathbf{k}\downarrow}), \tag{7.25}$$

$$\mathcal{M} = \begin{pmatrix} S^z & S^+ \\ S^- & -S^z \end{pmatrix} \otimes \begin{pmatrix} J_{LL} & J_{LR}\frac{1+e^{i\phi}}{2} \\ J^*_{LR}\frac{1+e^{-i\phi}}{2} & J_{RR} \end{pmatrix} = \mathcal{M}_s \otimes \mathcal{M}_l. \tag{7.26}$$

We note that the matrix $\mathcal{M}_s$ represents the spin space of conduction electrons and $\mathcal{M}_l$ represents the lead space. The above effective Hamiltonian (7.24) corresponds to Yosida's wavefunction ansatz [99, 100] with one included quasiparticle, which is described in Appendix D.1. First the Yosida's method

was applied by Soda-Matsuura-Nagaoka [74] for a quantum magnetic impurity problem in the superconductor. Because the Hamiltonian (7.24) is written in the excitation basis ($\gamma_{\alpha\mathbf{k}\sigma}|0\rangle$=0, with $|0\rangle$ being the BCS vacuum state) it can be diagonalized exactly. After diagonalizing the lead space matrix $\mathcal{M}_l$ we obtain two decoupled channels $\delta = 1, 2$

$$\begin{aligned}\gamma_{1\mathbf{k}\sigma} &= a\gamma_{L\mathbf{k}\sigma} + b\mathrm{e}^{+\mathrm{i}\phi_d}\gamma_{R\mathbf{k}\sigma},\\ \gamma_{2\mathbf{k}\sigma} &= a\gamma_{R\mathbf{k}\sigma} - b\mathrm{e}^{-\mathrm{i}\phi_d}\gamma_{L\mathbf{k}\sigma},\end{aligned} \tag{7.27a}$$

where $\phi_d = \phi/2 + \phi_g$, $J_{LR} = |J_{LR}|\mathrm{e}^{\mathrm{i}\phi_g}$, and

$$a = \sqrt{\frac{1}{2}\left(1 + \frac{J_{LL} - J_{RR}}{J_d}\right)},\ b = \sqrt{\frac{1}{2}\left(1 - \frac{J_{LL} - J_{RR}}{J_d}\right)}. \tag{7.27b}$$

The corresponding eigenvalues for two channels are

$$\begin{aligned}J_{1/2} &= \frac{1}{2}\left(J_{LL} + J_{RR} \pm J_d\right),\\ J_d &= \sqrt{(J_{LL} - J_{RR})^2 + 4|J_{LR}|^2\cos^2\frac{\phi}{2}}.\end{aligned} \tag{7.27c}$$

The eigenstates of the spin matrix

$$\mathcal{M}_s = \begin{array}{c} \begin{matrix} |\uparrow_{\delta\mathbf{k}},\uparrow\rangle & |\uparrow_{\delta\mathbf{k}},\downarrow\rangle & |\downarrow_{\delta\mathbf{k}},\uparrow\rangle & |\downarrow_{\delta\mathbf{k}},\downarrow\rangle \end{matrix} \\ \begin{pmatrix} \frac{1}{2} & 0 & 0 & 0 \\ 0 & -\frac{1}{2} & 1 & 0 \\ 0 & 1 & -\frac{1}{2} & 0 \\ 0 & 0 & 0 & \frac{1}{2} \end{pmatrix} \end{array}, \tag{7.28}$$

are the singlet

$$|S_{\delta\mathbf{k}}\rangle = \frac{1}{\sqrt{2}}\left(|\uparrow_{\delta\mathbf{k}},\downarrow\rangle - |\downarrow_{\delta\mathbf{k}},\uparrow\rangle\right), \quad \lambda_S = -\frac{3}{2}, \tag{7.29a}$$

and triplet like solutions

$$\begin{aligned}|T^0_{\delta\mathbf{k}}\rangle &= \frac{1}{\sqrt{2}}\left(|\uparrow_{\delta\mathbf{k}},\downarrow\rangle + |\downarrow_{\delta\mathbf{k}},\uparrow\rangle\right),\\ |T^+_{\delta\mathbf{k}}\rangle &= |\uparrow_{\delta\mathbf{k}},\uparrow\rangle, \quad |T^-_{\delta\mathbf{k}}\rangle = |\downarrow_{\delta\mathbf{k}},\downarrow\rangle, \quad \lambda_T = \frac{1}{2}.\end{aligned} \tag{7.29b}$$

Here $\lambda_{S/T}$ denotes corresponding eigenvalue and

$$|\sigma_{\delta\mathbf{k}}, s\rangle = \gamma^\dagger_{\delta\mathbf{k}\sigma}|0\rangle|s\rangle, \text{ with } S^z|s\rangle = s/2|s\rangle. \tag{7.30}$$

Using the above basis $|S_{\delta\mathbf{k}}\rangle$ and $|T^j_{\delta\mathbf{k}}\rangle$ (7.29) we obtain

$$\begin{aligned}H_{\mathrm{LR}} + H_J = &\sum_{\delta\mathbf{k}} E_{\mathbf{k}}\left(|S_{\delta\mathbf{k}}\rangle\langle S_{\delta\mathbf{k}}| + \Sigma_j|T^j_{\delta\mathbf{k}}\rangle\langle T^j_{\delta\mathbf{k}}|\right)\\ &- \frac{3}{2}\sum_{\delta\mathbf{k}'\mathbf{k}} J_\delta|S_{\delta\mathbf{k}'}\rangle\langle S_{\delta\mathbf{k}}| + \frac{1}{2}\sum_{j\delta\mathbf{k}'\mathbf{k}} J_\delta|T^j_{\delta\mathbf{k}'}\rangle\langle T^j_{\delta\mathbf{k}}|,\end{aligned} \tag{7.31}$$

To get the sub-gap state from the above Hamiltonian (7.31) we make the linear superposition

$$|S_\delta\rangle = \sum_{\mathbf{q}} A_{\delta\mathbf{q}} |S_{\delta\mathbf{q}}\rangle, \tag{7.32}$$

and solve the stationary Schrödinger equation

$$(H_{\mathrm{LR}} + H_J - E_{S_\delta})|S_\delta\rangle = 0. \tag{7.33}$$

For the triplet components

$$|T^j_\delta\rangle = \sum_{\mathbf{q}} A^j_{\delta\mathbf{q}} |T^j_{\delta\mathbf{q}}\rangle, \quad j = 0, \pm, \tag{7.34}$$

the procedure is completely analogous. After projecting Eq. (7.33) to $\langle S_{\delta\kappa}|$ (or $\langle T^j_\delta|$) we obtain

$$A_{\delta\kappa} = \frac{3J_\delta}{2} \frac{\sum_{\mathbf{q}} A_{\delta\mathbf{q}}}{E_\kappa - E_{S_\delta}} \quad \rightarrow \quad 1 = 3g_\delta I_{E_{S_\delta}}, \tag{7.35a}$$

$$A^j_{\delta\kappa} = -\frac{J_\delta}{2} \frac{\sum_{\mathbf{q}} A^j_{\delta\mathbf{q}}}{E_\kappa - E_{S_\delta}} \quad \rightarrow \quad 1 = -g_\delta I_{E_{S_\delta}}, \tag{7.35b}$$

where after the arrow we have integrated over κ and defined $g_\delta = \pi \nu_F J_\delta/2$. The necessary integral I_E in (7.35) for sub-gap states $|E| < |\Delta|$ and large bandwidth $D \gg |\Delta|$ becomes

$$I_E = \frac{1}{\pi\nu_F} \sum_\kappa \frac{1}{E_\kappa - E} \approx \frac{2}{\pi} \ln\left|\frac{2D}{\Delta}\right| + \frac{2E\left(\frac{1}{2} + \frac{1}{\pi}\arcsin\frac{E}{\Delta}\right)}{\sqrt{|\Delta|^2 - E^2}}. \tag{7.36}$$

Similar integrals are performed more explicitly in Appendix D.1. By parameterizing the energy as

$$E \approx |\Delta|(1 - \eta^2), \tag{7.37}$$

we expand the integral (7.36) to lowest order in η

$$I_E \approx \frac{\sqrt{2}}{|\eta|}, \tag{7.38}$$

and obtain a perturbative solution to lowest order in g_δ

$$\begin{aligned} |\eta_{S_\delta}| &\approx 3\sqrt{2} g_\delta, \qquad \text{for singlet,} \\ |\eta_{T_\delta}| &\approx -\sqrt{2} g_\delta, \qquad \text{for triplet.} \end{aligned} \tag{7.39}$$

We see that there exists a singlet like solution if the effective channel exchange coupling is anti-ferromagnetic $g_\delta > 0$ and the triplet like solution if the coupling is ferromagnetic $g_\delta < 0$. For the triplet the above result (7.39) matches the excitation energy obtained from perturbative classical spin expression (7.21) when $S = \frac{1}{2}$, and for the singlet it matches (7.21) if in the classical expression the coupling is replaced by $g_{\alpha\alpha'} \rightarrow 3g_{\alpha\alpha'}$. If the potential scattering term H_W (6.17c) is included the previous statement is not affected (see Appendix D.1), however, such a term mixes the $\delta = 1, 2$ channels.

In the presence of a magnetic field the Zeeman term is expressed in the singlet/triplet basis as

$$\begin{aligned} H_B = &- \tilde{B}\sum_{\delta\mathbf{k}}\left(|S_{\delta\mathbf{k}}\rangle\langle T^0_{\delta\mathbf{k}}| + |T^0_{\delta\mathbf{k}}\rangle\langle S_{\delta\mathbf{k}}|\right) \\ &+ \bar{B}\sum_{\delta\mathbf{k}}\left(|T^+_{\delta\mathbf{k}}\rangle\langle T^+_{\delta\mathbf{k}}| - |T^-_{\delta\mathbf{k}}\rangle\langle T^-_{\delta\mathbf{k}}|\right), \\ &+ \frac{g_{\mathrm{i}}B}{2}\left(|D_\uparrow\rangle\langle D_\uparrow| - |D_\downarrow\rangle\langle D_\downarrow|\right), \end{aligned} \tag{7.40}$$

where

$$\tilde{B} = \frac{B}{2}(g_{\mathrm{i}} - g_{\mathrm{ce}}), \quad \bar{B} = \frac{B}{2}(g_{\mathrm{i}} + g_{\mathrm{ce}}). \tag{7.41}$$

Here the last term represents Zeeman splitting of the ground-state doublet $|D_s\rangle = |0\rangle|s\rangle$. The sub-gap states $|T^\pm_\delta\rangle$ are the eigenstates of H_B, and for $g_i \neq g_{\mathrm{ce}}$ the singlet $|S_\delta\rangle$ and the triplet $|T^0_\delta\rangle$ get mixed, so the new eigenstate is

$$|\psi_\delta\rangle = \sum_{\mathbf{q}}\left(a_{\delta\mathbf{q}}|S_{\delta\mathbf{q}}\rangle + b_{\delta\mathbf{q}}|T^0_{\delta\mathbf{q}}\rangle\right), \tag{7.42}$$

which after projecting the stationary Schrödinger equation

$$(H_{\mathrm{LR}} + H_B + H_J - E)|\psi_\delta\rangle = 0 \tag{7.43}$$

to sub-space spanned by $\langle S_{\delta\kappa}|$ and $\langle T^0_{\delta\kappa}|$ we obtain the equations

$$\begin{pmatrix} E_\kappa - E & -\tilde{B} \\ -\tilde{B} & E_\kappa - E \end{pmatrix}\begin{pmatrix} a_{\mathbf{k}} \\ b_{\mathbf{k}} \end{pmatrix} = J_\delta \sum_{\mathbf{k}}\begin{pmatrix} 3a_{\mathbf{k}} \\ -b_{\mathbf{k}} \end{pmatrix}, \tag{7.44}$$

which yield

$$\begin{aligned} a_\kappa &= J_\delta \frac{3(E_\kappa - E)a - \tilde{B}b}{(E_\kappa - E)^2 - \tilde{B}^2}, \\ b_\kappa &= J_\delta \frac{-(E_\kappa - E)b + 3\tilde{B}a}{(E_\kappa - E)^2 - \tilde{B}^2}. \end{aligned} \tag{7.45}$$

Here we introduced the notation $a = \sum_{\mathbf{k}} a_{\mathbf{k}}$, $b = \sum_{\mathbf{k}} b_{\mathbf{k}}$. We rewrite the coefficients in Eq. (7.45) as

$$\begin{aligned} a_\kappa &= \frac{J_\delta}{2}\left[3\left(\frac{1}{E_\kappa - (E+\tilde{B})} + \frac{1}{E_\kappa - (E-\tilde{B})}\right)a - \left(\frac{1}{E_\kappa - (E+\tilde{B})} - \frac{1}{E_\kappa - (E-\tilde{B})}\right)b\right], \\ b_\kappa &= \frac{J_\delta}{2}\left[-\left(\frac{1}{E_\kappa - (E+\tilde{B})} + \frac{1}{E_\kappa - (E-\tilde{B})}\right)b + 3\left(\frac{1}{E_\kappa - (E+\tilde{B})} - \frac{1}{E_\kappa - (E-\tilde{B})}\right)a\right], \end{aligned} \tag{7.46}$$

and by integrating Eqs. (7.46) over κ we obtain the following *secular* equation

$$\begin{vmatrix} 1 - \frac{3g_\delta}{2}[I_{E+\tilde{B}} + I_{E-\tilde{B}}] & \frac{g_\delta}{2}[I_{E+\tilde{B}} - I_{E-\tilde{B}}] \\ -\frac{3g_\delta}{2}[I_{E+\tilde{B}} - I_{E-\tilde{B}}] & 1 + \frac{g_\delta}{2}[I_{E+\tilde{B}} + I_{E-\tilde{B}}] \end{vmatrix} = 0. \tag{7.47}$$

We start by examining Eq. (7.47) in the small magnetic field limit, i.e., $|\tilde{B}| \ll |g^2_\delta \Delta|$. We parameterize the energy as before

$$E_l = |\Delta|(1 - \eta_l^2), \quad \eta_\pm = \sqrt{\eta_l^2 \pm \frac{\tilde{B}}{|\Delta|}}, \tag{7.48}$$

and from Eq. (7.47) to lowest order in $\eta_\pm$ we get

$$\eta_+\eta_- - \sqrt{2}g_\delta(\eta_+ + \eta_-) - 6g_\delta^2 = 0, \tag{7.49}$$

which after expanding $\eta_\pm$ to lowest order in $\tilde{B}/(\eta_l^2|\Delta|)$ yields

$$\eta_l^4 - 2\sqrt{2}g_\delta\eta_l^3 - 6g_\delta^2\eta_l^2 - \left(\frac{\tilde{B}}{2|\Delta|}\right)^2 = 0. \tag{7.50}$$

Finally, from the above Eq. (7.50) we obtain the perturbative solutions

$$\begin{aligned} |\eta_{S,l}| &\approx 3\sqrt{2}g_\delta\left(1 + \frac{3}{16}\frac{\tilde{B}^2}{\eta_{S_\delta}^4|\Delta|^2}\right), \quad \text{singlet like,} \\ |\eta_{T^0,l}| &\approx -\sqrt{2}g_\delta\left(1 + \frac{1}{16}\frac{\tilde{B}^2}{\eta_{T_\delta}^4|\Delta|^2}\right), \quad \text{triplet like.} \end{aligned} \tag{7.51}$$

We see that the energy of the sub-gap state decreases quadratically in $\tilde{B}$ for small magnetic field. In the high magnetic field limit, i.e., $|\tilde{B}| \gg |g_\delta^2\Delta|$, from Eq. (7.47) to lowest order in g_δ we obtain the solution

$$E_h = |\Delta|(1-\eta_h^2) - \tilde{B}, \quad |\eta_h| \approx \sqrt{2}g_\delta. \tag{7.52}$$

The above result (7.52) corresponds to neglected off-diagonal terms in the spin matrix (7.28). For arbitrary magnetic field the perturbative solution in g_δ is obtained by solving Eq. (7.49) numerically.

Now we examine the sub-gap excitation spectrum when it is assumed that the magnetic field in the superconducting leads is screened, i.e., $g_{ce} \approx 0$ and $\tilde{B} = \bar{B} = g_i B/2$. Note that we also do not consider closing of the superconducting gap. For positive magnetic field $\tilde{B} > 0$ the ground-state is a doublet $E_\downarrow = -\tilde{B}$ and the resulting sub-gap excitations for a particular channel δ are depicted in Figure 7.7. For anti-ferromagnetic coupling $g_\delta > 0$ (Figure 7.7a) there is a singlet like excitation, which for high magnetic fields approaches an energy consistent with the classical spin (7.21). In this case the eigenstate is $|\uparrow_\delta,\downarrow\rangle = \sum_{\mathbf{q}} A^{\uparrow}_{\delta\mathbf{q}}|\uparrow_{\delta\mathbf{q}},\downarrow\rangle$, where $A^{\uparrow}_{\delta\mathbf{k}}$ is determined by projecting the Schödinger equation to $|\uparrow_{\delta\mathbf{k}},\downarrow\rangle$ with neglected spin-flip terms S^+ and S^- in the exchange Hamiltonian (7.24). For ferromagnetic coupling $g_\delta < 0$ (Figure 7.7b) the excitation is a triplet, which gets split by the magnetic field. The $|T_\delta^+\rangle$ and $|T_\delta^0\rangle$ components approaches the gap and crosses it, and $|T_\delta^-\rangle$ component does not move with $\tilde{B}$. Changing the sign of the magnetic field simply reverses all spins in the previous discussion.

So far we have examined the excitation spectrum when a single quasi-particle is included, i.e., the system is effectively described by the Hamiltonian (7.24). Now the question is, whether the pairing-like terms $\gamma^\dagger_{a'\uparrow}\gamma^\dagger_{a\downarrow}$ in (6.17b) and (6.17c) modify the perturbative result for the energy difference between the ground-state $|D_s\rangle$ and the sub-gap states. There is a second order energy correction for the ground-state

$$\begin{aligned} E_s^{(2)} &= \sum_{\lambda\neq D_s}\frac{|\langle l|H'|D_s\rangle|^2}{E_s^{(0)} - E_\lambda} \\ &= \sum_{aa'}\Bigg(-\frac{1}{4}\frac{J_{a'a}J_{aa'}|L_{a'a} - L_{aa'}|^2}{E_a + E_{a'}} - \frac{1}{2}\frac{J_{a'a}J_{aa'}|L_{a'a} - L_{aa'}|^2}{E_a + E_{a'} - s(g-g_{ce})B} \\ &\qquad - \frac{W_{a'a}W_{aa'}|L_{a'a} + L_{aa'}|^2}{E_a + E_{a'}} + 2\mathrm{i}s\frac{J_{a'a}W_{aa'}\,\mathrm{Im}[L_{a'a}L^*_{aa'}]}{E_a + E_{a'}}\Bigg), \end{aligned} \tag{7.53}$$

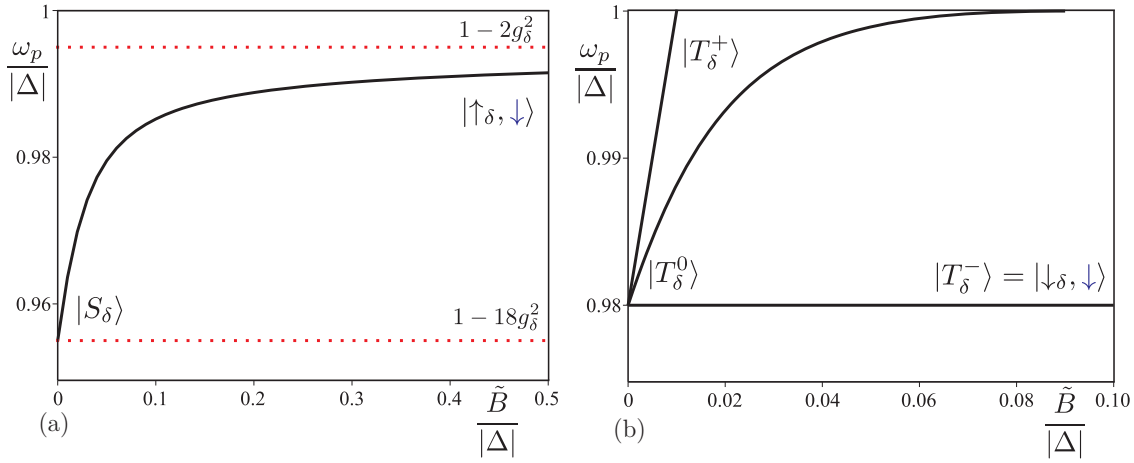

Figure 7.7: Sub-gap excitation spectrum from the ground-state doublet $|D_\downarrow\rangle$ when it is assumed that the magnetic field in the superconductor is screened $g_{\text{ce}} \approx 0$. (a) For anti-ferromagnetic coupling $g_\delta > 0$ the sub-gap state is singlet like state, which for high magnetic fields becomes classical spin like state $|\uparrow_\delta,\downarrow\rangle$. (b) For ferromagnetic coupling $g_\delta < 0$ the sub-gap state is a triplet. The $|T_\delta^+\rangle$ and $|T_\delta^0\rangle$ components approaches the gap and crosses it, and $|T_\delta^-\rangle$ component does not move with $\tilde{B}$.

where $|l\rangle$ are all possible intermediate states and $H' = H_J + H_W$. However, such a term gets canceled for the energy difference, because the sub-gap states get the same second-order shift when three quasiparticles are included in the wavefunction ansatz (see Appendix D.2). The Yosida's wavefunction ansatz generates a well defined perturbative expansion in the couplings g, w for the energy differences. Also with the included three quasiparticles a higher order correction Eq. (D.30) for the energy difference is found, which contains leading-logarithmic contribution $\ln \frac{2D}{|\Delta|}$. These logarithms can be resummed using the usual poor man's scaling approach [see Eq. (D.31)-(D.33)], which yields the running coupling $g^* = \frac{\pi}{4\ln(D^*/T_K)}$, with $T_K = De^{-\frac{\pi}{4g}}$ being the Kondo temperature, and $D^* \gg |\Delta|$. The expression of g^* shows that the perturbative expansion is valid only when the Kondo temperature is much smaller than the superconducting gap $T_K \ll |\Delta|$.

Chapter 8

Supercurrent

The supercurrent $\mathbf{j}_S$ is a dissipationless current flowing in the superconductor if there is an order parameter phase $\phi(\mathbf{r})$ gradient, i.e., $\mathbf{j}_S \sim \nabla\phi(\mathbf{r})$. In this chapter we examine a type of the supercurrent due to the Josephson effect [101], which arises in two superconductors, which have a phase difference between them $\phi = \phi_L - \phi_R$, coupled by a weak link. This phenomenon appears in the SDS junctions (see Figure 6.1). Various measurements of the supercurrent through Coulomb blockaded quantum dots [102–105] have shown that odd-occupied spin degenerate quantum dots may lead to a negative (π-phase) supercurrent. Also a supercurrent sign-reversal, i.e. a $\pi - 0$ transition, has been shown to take place, when moving the gate voltage from odd occupancy (moving away particle-hole symmetric point), or when increasing the ratio $T_K/|\Delta|$. This observation is consistent with a number of theoretical predictions [106–115]. Here we examine the relation between the sub-gap states and the supercurrent, and present the phase diagram for SDS junction.

At zero temperature $T = 0$ the supercurrent is generally given as the ground-state energy E_{GS} derivative with respect to the phase difference $\phi = \phi_L - \phi_R$ between two superconducting

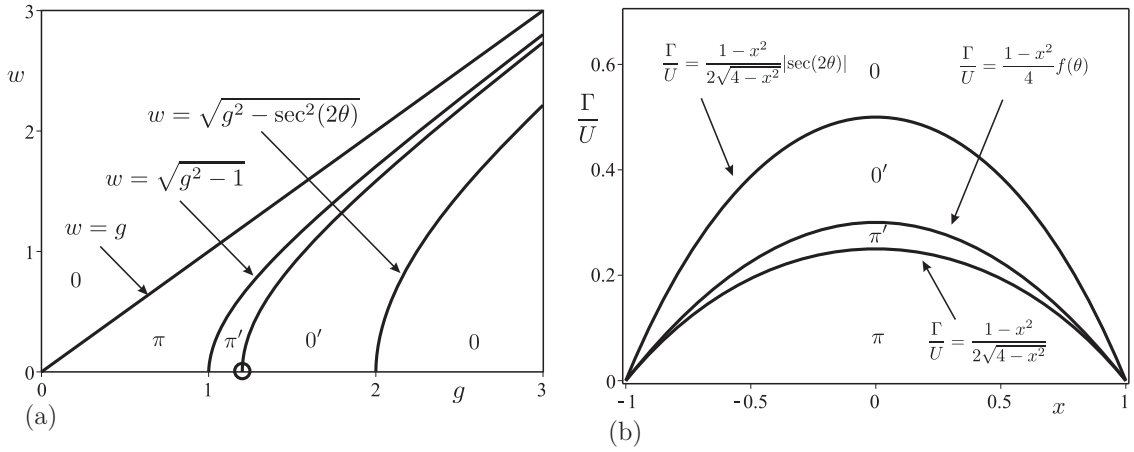

Figure 8.1: (a) Phase diagram as a function of couplings g and w for a junction with a classical spin. The coupling asymmetry is $\theta = \pi/3$. The transition from π' to $0'$ for $w = 0$ is denoted by a circle and is given by $g = f(\theta)$, where $f(\theta) = [1/2\left\{\sin^2(2\theta) + \sqrt{4 + \sin^4(2\theta)}\right\}]^{1/2}$. When there is no coupling asymmetry $\theta = \pi/4$ for $g > w$ the junction never goes to 0-junction for increasing g. (b) Phase diagram when the couplings are parameterized by Eq. (6.26c), where $\Gamma = \nu_F(t_L^2 + t_R^2)$, and the dimensionless level position (gate voltage) x is given by Eq. (6.13).

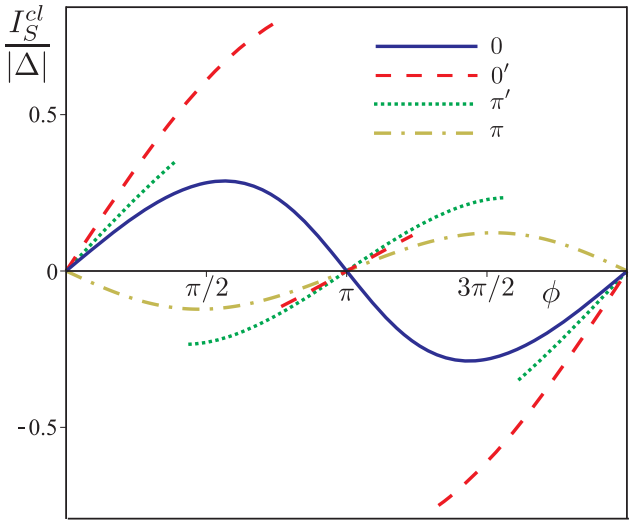

Figure 8.2: Examples of supercurrent for different junctions with a classical spin. Potential scattering is set to $w = 0$. The values of other parameters are $g = 2.5$, $\theta = 1.15$ for 0, $g = 2.5$, $\theta = \pi/4$ for 0′, $g = 1.25$, $\theta = \pi/4$ for π', and $g = 0.6$, $\theta = \pi/4$ for π-junction.

leads [116], i.e.,

$$I_S(\phi) = 2\frac{\partial E_{\rm GS}}{\partial \phi}. \tag{8.1}$$

The above relation Eq. (8.1) for the considered model can be obtained by performing gauge transformation for the conduction electrons„

$$c_{\alpha \mathbf{k}\sigma} \quad \rightarrow \quad c_{\alpha \mathbf{k}\sigma} e^{i\phi_\alpha/2}, \tag{8.2}$$

which transfers the phase difference from the Hamiltonian $H_{\rm LR}$ into $H_W + H_J$, i.e.,

$$\begin{aligned} J_{\alpha\alpha'} \quad &\rightarrow \quad J_{\alpha\alpha'} e^{i(\phi_\alpha - \phi_{\alpha'})/2}, \\ W_{\alpha\alpha'} \quad &\rightarrow \quad W_{\alpha\alpha'} e^{i(\phi_\alpha - \phi_{\alpha'})/2}. \end{aligned} \tag{8.3}$$

Then the current operator can be expressed as

$$\hat{I}_S(\phi) = i[H_W + H_J, N_L] = \frac{1}{2}\frac{\partial (H_W + H_J)}{\partial \phi}, \tag{8.4}$$

where $N_L = \sum_{\mathbf{k}\sigma} c^\dagger_{L\mathbf{k}\sigma} c_{L\mathbf{k}\sigma}$ is the particle number operator in the left lead. By using the relation (8.4) and the Hellmann-Feynman theorem

$$\frac{\partial E_{\rm GS}}{\partial \phi} = \langle {\rm GS} | \frac{\partial H}{\partial \phi} | {\rm GS} \rangle, \tag{8.5}$$

we obtain the supercurrent expression (8.1). For the case of a junction with a classical spin the supercurrent can also be found by using the sub-gap excitation spectrum as [98]

$$I_S^{cl} = -\sum_p \tanh\left(\frac{\omega_p}{2T}\right)\frac{{\rm d}\omega_p}{{\rm d}\phi} \overset{T\to 0}{=} -\frac{{\rm d}|E_+|}{{\rm d}\phi} - \frac{{\rm d}|E_-|}{{\rm d}\phi}, \tag{8.6}$$

where after the second equality in Eq. (8.6) we have used the zero temperature limit, and $E_\pm$ is given by Eq. (7.15) for $B = 0$. To lowest order in g and w the expression (8.6) yields

$$I_S^{cl} \approx (|\Delta|/2)\sin^2(2\theta)\left(w^2 - g^2\right)\sin\phi. \tag{8.7}$$

From Eqs. (8.1) and (8.6) we see that the phase ϕ dependent part of the ground state is

$$E_{\rm GS} = -\frac{1}{2}\left(|E_+| + |E_-|\right) + \text{const.} \tag{8.8}$$

If the ground state energy has one global minimum at $\phi = 0$, then the junction is classified as 0-junction, and the supercurrent is a continuous function of ϕ, has a positive slope at $\phi = 0$, and negative slope at $\phi = \pi$. When the global minimum is at π we have a π-junction. Then the supercurrent is a continuous function of ϕ, has a negative slope at 0, and a positive slope at π. The situation when there are minima at both phases 0 and π can also arise. If 0 corresponds to a global minimum and π to a local minimum, then the junction is called 0′-junction. For π being a global minimum and 0 being a local minimum the junction is called π′-junction. In both previous cases the supercurrent is a discontinuous function [with one discontinuity in the interval $\phi \in (0, \pi)$ and one in the interval $\phi \in (\pi, 2\pi)$] and it has positive slopes at 0 and π. This discontinuous behavior of the supercurrent is directly related to the sub-gap states crossing the zero energy and changing their spin as can be seen from Figure 7.6b,c. The resulting phase diagram as a function of couplings w and g is depicted in Figure 8.1, and examples of the supercurrent for different junctions is shown in Figure 8.2.

For a junction with a quantum spin we can calculate the supercurrent perturbatively from Eq. (7.53). For $B > 0$ the ground state is $|D_\downarrow\rangle$ and we have

$$I_S \approx 2|\Delta|\sin^2(2\theta)\left[\left(w^2 - g^2\right)F(0) - 2g^2F(\tilde{B})\right]\sin\phi, \tag{8.9}$$

where

$$F(\tilde{B}) = \frac{1}{|\Delta|\pi^2\nu_F^2}\sum_{\mathbf{k}\mathbf{k}'}\frac{u_{\mathbf{k}}v_{\mathbf{k}}u_{\mathbf{k}'}v_{\mathbf{k}'}}{E_{\mathbf{k}} + E_{\mathbf{k}'} + \tilde{B}}, \quad F(0) \overset{D\gg|\Delta|}{\approx} \frac{1}{4}, \tag{8.10}$$

and we also used Eq. (6.26) form of the coupling. When there is no magnetic field the supercurrent becomes

$$I_S \approx (|\Delta|/2)\sin^2(2\theta)\left(w^2 - 3g^2\right)\sin\phi. \tag{8.11}$$

We see that this result is not given by the dispersion of the sub-gap states, i.e.,

$$I_S \neq -\sum_{i=\pm}\frac{d|E_i|}{d\phi} = \begin{cases} \dfrac{|\Delta|}{2}\sin^2(2\theta)\left(w^2 - 9g^2\right)\sin\phi, & g > 0, \\ \dfrac{|\Delta|}{2}\sin^2(2\theta)\left(w^2 - g^2\right)\sin\phi, & g < 0. \end{cases} \tag{8.12}$$

as in the case of a classical spin Eq. (8.6). For the coupling derived from the Anderson model we have $g > |w|$ and in this case the junction is always π for perturbative values of g and w. When the magnetic field is present and $|\tilde{B}| \ll |\Delta|$ we have

$$F(\tilde{B}) - F(0) \approx -\frac{\tilde{B}}{2\pi^2|\Delta|}. \tag{8.13}$$

From Eq. (8.9) we see that when $\tilde{B} > 0$ the supercurrent $|I_S|$ decreases for a π-junction and increases for a 0-junction, and *vice versa* for $\tilde{B} < 0$. We note that $\tilde{B}$ can become negative for positive B when $g_{\rm ce} > g_{\rm i}$.

Conclusions for Part II

The second part of the thesis is dedicated to the examination of the sub-gap states and corresponding excitation spectrum for spin coupled to two superconducting leads, which have a phase difference ϕ. The interaction between spin and conduction electrons is described by a Kondo model. Because of the two leads, there can be up to two interaction channels between conduction electrons and spin, which result in four sub-gap excitations (two quasiparticle like $\gamma^{\dagger}_{n\sigma}$ and two quasihole like $\gamma_{n\sigma}$). If the Kondo model is derived from Anderson's model, at zero phase difference $\phi = 0$ there is only one channel, and thus two sub-gap states. However, at finite phase difference the problem effectively becomes two channel, and four sub-gap states appear. If the spin is assumed to be classical the Kondo interaction effectively becomes spin dependent potential scattering for conduction electrons and the problem can be solved exactly [Eq. (7.15)]. For the quantum spin case a perturbative result in couplings g and w can be obtained using Yosida's wavefunction ansatz. The analysis is valid when the ground-state is one of the doublet $|D_s\rangle$ components and when the Kondo temperature is much larger then the superconducting gap $T_K \ll |\Delta|$. If the potential scattering w and the magnetic field B are neglected, then for effective channel exchange coupling $g_\delta > 0$ the sub-gap states are singlets $|S_\delta\rangle$ and for $g_\delta < 0$ the states are triplets $|T^{0,\pm}_\delta\rangle$. Perturbatively, the energy of the triplet state $|T^{0,\pm}_\delta\rangle$ matches the classical result (7.21) and for the singlet state it matches if the exchange coupling in the classical expression is replaced by $g_{\alpha\alpha'} \to 3g_{\alpha\alpha'}$. The inclusion of the magnetic field mixes the singlet $|S_\delta\rangle$ and the triplet $|T^0_\delta\rangle$ if the g-factors of the spin and conduction electrons are different, i.e., $g_{\rm i} \neq g_{\rm ce}$. Assuming that the magnetic field is screened in the superconducting leads $g_{\rm ce} \approx 0$, this mixing results in the transition energy from the ground-state doublet $|D_\downarrow\rangle$ ($B > 0$) to the singlet $|S_\delta\rangle$ approaching classical value for high magnetic field $B \gg g^2_\delta|\Delta|$. For the triplet $|T^0_\delta\rangle$ the transition energy approaches the gap value $|\Delta|$. Because of the phase difference ϕ there is a supercurrent running through the junction. In the case of a classical spin it can be directly related to the sub-gap excitation spectrum, which can be calculated exactly. The phase diagram as a function of exchange g and potential scattering w is shown in Figure 8.1. For the quantum spin case the supercurrent is obtained perturbatively and it is found that there is no direct relation between supercurrent and the sub-gap excitation spectrum. Also, if the Kondo model is derived from Anderson's model ($g > |w|$), the perturbative expression (8.9) always will yield a π-junction behavior.

Part III

Designing π-stacked molecules as phonon insulators

Chapter 9

Molecular junctions as thermoelectric devices

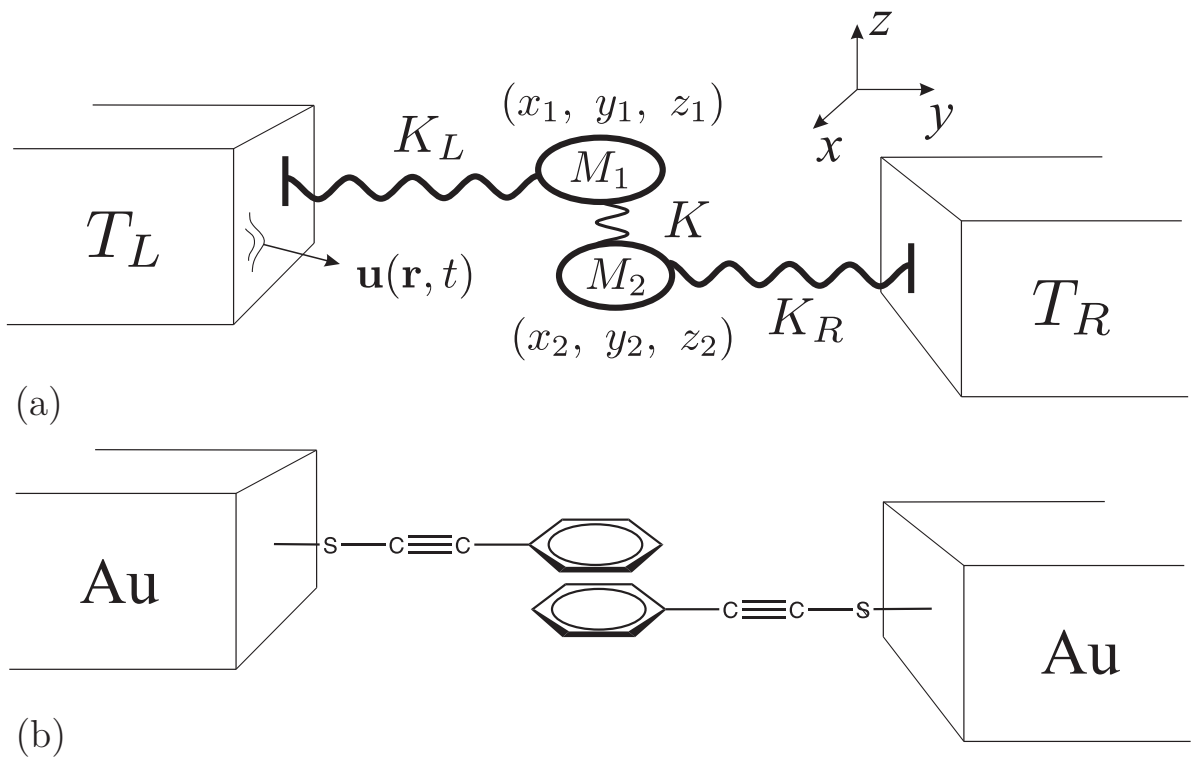

Figure 9.1: a) An effective description of the center of mass vibrational degrees of freedom in the system as two large masses M_1 and M_2, which have coordinates (x_1, y_1, x_1) and (x_2, y_2, z_2), coupled to each other by a spring K_i and to the leads by springs K_{iL} and K_{iR}. The substrate is modelled as an elastic continuum described by the displacement vector $\mathbf{u}(\mathbf{r}, t)$. T_L and T_R denote the temperatures of the left and the right lead, respectively. b) A schematic diagram of a junction consisting of two π-stacked 2-phenylethyne-1-thiol molecules, which are coupled to the gold (Au) electrodes.

In this third part of the thesis we are concerned with the performance of molecular junctions (see Figure 9.1) used as thermoelectric devices, in which a temperature gradient is used to produce an electrical current or voltage. Recent studies showed that such devices give a large thermoelectric effect because of sharp electronic resonances appearing due to molecular orbitals [117, 118] or due to interference effects [119, 120]. At the same time, it has been argued that molecular junctions should have a very small phonon contribution to the heat conductance because, in small molecules,

the quantized molecular vibrational modes have frequencies above the Debye frequency of the electrodes, preventing phonons from being transported from the hot to the cold electrode via the molecule. However, this argument does not take into account that when a molecule is bonded between two electrodes, additional vibrational modes appear which are associated with center of mass motion of the entire molecule [121]. Since the mass of the entire molecule is very large compared to that of individual atoms, these modes have a low frequency, well inside the band of acoustic phonons in the electrodes, and might be detrimental for the thermoelectric performance.

So we propose a simple mechanism to reduce thermal conductance of the molecular junction due to center of mass vibrational modes. We call such a thermal conductance the phonon conductance. The idea is to have a system effectively consisting of two large masses M_1 and M_2 coupled by the spring K to each other and by springs K_L, K_R to the leads as shown in Figure 9.1a. When the spring constant between the masses is weak the phonon conductance is reduced compared to the situation with a single mass in the junction $M = M_1 + M_2$. For thermoelectric purposes the molecule should also maintain the electrical conductivity. As a possible realization of such a system having such properties we consider π-stacked molecules in the junction as depicted in Figure 9.1b. Here by π-stacking we mean attractive, noncovalent interactions between aromatic rings, which in the case of Figure 9.1b are two sandwiched benzene rings [122].

9.1 The model

We describe the vibrational degrees of freedom in a molecule and the coupling to the leads using the harmonic approximation and it is assumed that the molecule couples to a particular lead only at a single point $(x_\alpha, y_\alpha, z_\alpha)$, with $\alpha = L, R$. So the system under consideration is a junction consisting of two leads described by vibrational modes of a continuum and a molecule (middle region) described by harmonic oscillators. The Hamiltonian for the vibrational degrees of the system is

$$H = H_0 + V, \tag{9.1a}$$

$$H_0 = \sum_{i,m} \frac{p_{im}^2}{2M_m} + H_{\mathrm{L}} + H_{\mathrm{R}}, \quad i = x, y, z, \quad m = 1, 2, \tag{9.1b}$$

$$H_\alpha = \sum_\nu \hbar\omega_{\alpha\nu} a_{\alpha\nu}^\dagger a_{\alpha\nu}, \quad \alpha = \mathrm{L}, \mathrm{R}, \tag{9.1c}$$

$$V = \frac{1}{4} \sum_{ii'mm'} K_{im,i'm'} (r_{im} - r_{i'm'})^2 + \frac{1}{2} \sum_{ii'm\alpha\mathbf{r}} K_{im,i'\alpha}(\mathbf{r}) [r_{im} - u_{i'\alpha}(\mathbf{r})]^2, \tag{9.1d}$$

where $\mathbf{r}_m = (x_m, y_m, z_m)$ are the coordinates of the mass M_m; $\mathbf{p}_m$ is the corresponding momentum; $u_{i'\alpha}(\mathbf{r}) \equiv u_{i'\alpha}(\mathbf{r}, 0)$ is the displacement vector in the lead α at time $t = 0$; $K_{im,i'm'}$ are the spring constants between masses and $K_{im,i'\alpha}(\mathbf{r})$ are the couplings to the leads. The operator $a_{\alpha\nu}^\dagger$ creates a vibrational mode ν in the lead α with energy $\hbar\omega_{\alpha\nu}$, and it satisfies the canonical commutation relation $[a_{\alpha\nu}, a_{\alpha'\nu'}^\dagger] = \delta_{\alpha\alpha'}\delta_{\nu\nu'}$. The description of elastic continuum modes and quantization of displacement vector $\mathbf{u}_\alpha(\mathbf{r}, t)$ is given in Chapter 10. For the system depicted in Figure 9.1a we have the following non-zero couplings

$$K_{i1,i2} = K_{i2,i1} \equiv K_i, \quad K_{i1,iL}(\mathbf{r}) \equiv K_{iL}\delta(\mathbf{r} - \mathbf{r}_L), \quad K_{i2,iR}(\mathbf{r}) \equiv K_{iR}\delta(\mathbf{r} - \mathbf{r}_R), \tag{9.2}$$

where $\mathbf{r}_\alpha \equiv (x_\alpha, y_\alpha, z_\alpha)$ denotes points of attachment of the molecules to the leads. The validity of the approximation that the molecule couples to a single point of the lead is discussed in Appendix F.2.

We transform the coordinates into mass weighted coordinates, i.e.,

$$\begin{aligned} r_n \quad &\to \quad \frac{r_n}{\sqrt{M_n}}, \quad p_n \quad \to \quad p_n\sqrt{M_n}, \\ u_\beta \quad &\to \quad \frac{u_\beta}{\sqrt{M_\beta}}, \quad \pi_\beta \quad \to \quad \pi_\beta\sqrt{M_\beta}, \end{aligned} \tag{9.3}$$

where we have introduced the following shorthand notation $n \equiv i, m$, $\beta \equiv i', \alpha, \mathbf{r}$ for the labels and M_β denotes the mass of the lead atoms. Then the Hamiltonian (9.1d) is rewritten in mass weighted coordinates as

$$V = \frac{1}{2}\sum_{nn'} V_{nn'} r_n r_{n'} + \frac{1}{2}\sum_{\beta} V_\beta u_\beta^2 + \sum_{n\beta} V_{n\beta} r_n u_\beta(), \tag{9.4}$$

$$\begin{aligned} V_{nn} &= \frac{1}{M_n}\Big(\sum_{n'} K_{nn'} + \sum_{\beta} K_{n\beta}\Big), \quad V_{nn'} = -\frac{K_{nn'}}{\sqrt{M_n M_{n'}}}, \quad n \neq n', \\ V_\beta &= \frac{1}{M_\beta}\sum_{n'} K_{n'\beta}, \quad V_{n\beta} = -\frac{K_{n\beta}}{\sqrt{M_n M_\beta}}, \end{aligned} \tag{9.5}$$

which is more convenient for the current calculation described in Section 11.1.

Chapter 10

Eigenmodes of the leads described as elastic continuum

In this chapter we describe the eigenmodes of the leads, when there is no coupling to the molecule, where we closely follow Ezawa [123]. The same method to describe the semiconducting leads with a weak link between them was also applied extensively by Patton and Gellar [124–126].

10.1 General equations

The equation of motion for an elastic medium is given by

$$\rho \frac{\partial^2 u_i}{\partial t^2} = \frac{\partial \sigma_{ij}}{\partial x_j}, \tag{10.1}$$

where ρ is the mass density of the medium, $u_i = u_i(\mathbf{r}, t)$ is a displacement vector component in the i direction, $x_j \in \{x, y, z\}$ denotes Cartesian coordinate, and σ_{ij} is a stress tensor given by

$$\frac{\sigma_{ij}}{\rho} = (c_l^2 - 2c_t^2)\frac{\partial u_k}{\partial x_k}\delta_{ij} + c_t^2\left(\frac{\partial u_i}{\partial x_j} + \frac{\partial u_j}{\partial x_i}\right) \tag{10.2}$$

for an isotropic medium. Note that the Einstein summation convention over all repeated indices is implied. Here c_l is the velocity of a longitudinal wave in an infinite isotropic medium (displacement is in the direction of propagation), and c_t is the velocity of a transverse wave in an infinite isotropic medium (displacement is perpendicular to the direction of propagation). The velocities c_l and c_t are given in terms of Young modulus E and Poisson ratio σ as [127]

$$c_l = \sqrt{\frac{E(1-\sigma)}{\rho(1+\sigma)(1-2\sigma)}}, \tag{10.3}$$

$$c_t = \sqrt{\frac{E}{2\rho(1+\sigma)}}. \tag{10.4}$$

Note that the allowed values for the coefficients are

$$E > 0, \quad -1 < \sigma < \frac{1}{2}, \qquad c_l > \sqrt{\frac{4}{3}}c_t, \tag{10.5}$$

and that E, σ correspond to an adiabatic measurement (constant entropy) values [127]. More generally the stress tensor is expressed through the strain tensor u_{ij} as

$$\sigma_{ij} = K u_{kk}\delta_{ij} + 2\mu\left(u_{ij} - \frac{1}{3}\delta_{ij}u_{kk}\right), \tag{10.6}$$

where the strain tensor to second order in the displacement derivatives is given as

$$u_{ij} = \frac{1}{2}\left(\frac{\partial u_i}{\partial x_j} + \frac{\partial u_j}{\partial x_i} + \frac{\partial u_k}{\partial x_i}\frac{\partial u_k}{\partial x_j}\right). \tag{10.7}$$

We consider only the harmonic approximation, i.e. no second order term in the strain tensor.

Equation (10.1) with stress tensor (10.2) can be conveniently rewritten as

$$\frac{\partial^2 \mathbf{u}}{\partial t^2} = c_t^2 \nabla^2 \mathbf{u} + (c_l^2 - c_t^2)\nabla(\nabla \cdot \mathbf{u}). \tag{10.8}$$

Using Helmholtz decomposition we can represent the vector $\mathbf{u}$ as a sum of two components

$$\mathbf{u} = \mathbf{u}_l + \mathbf{u}_t, \tag{10.9}$$

which satisfy the conditions

$$\nabla \times \mathbf{u}_l = 0, \tag{10.10a}$$
$$\nabla \cdot \mathbf{u}_t = 0, \tag{10.10b}$$

i.e. $\mathbf{u}_l$ is an irrotational vector field and $\mathbf{u}_t$ is a solenoidal vector field. Taking the divergence of both sides of the expression (10.8) and using (10.10b) we obtain the equation

$$\nabla \cdot \left(\frac{\partial^2 \mathbf{u}_l}{\partial t^2} - c_l^2 \nabla^2 \mathbf{u}_l\right) = 0, \tag{10.11a}$$

and using relation (10.10a) we also have to satisfy

$$\nabla \times \left(\frac{\partial^2 \mathbf{u}_l}{\partial t^2} - c_l^2 \nabla^2 \mathbf{u}_l\right) = 0. \tag{10.11b}$$

If the curl and the divergence of a vector vanish in all space, then the vector has to be zero identically. So from equations (10.11) the wave equation for the longitudinal part $\mathbf{u}_l$ is obtained:

$$\left(\frac{\partial^2}{\partial t^2} - c_l^2 \nabla^2\right)\mathbf{u}_l = 0. \tag{10.12}$$

For the transversal part $\mathbf{u}_t$ we get the equation

$$\nabla \times \left(\frac{\partial^2 \mathbf{u}_t}{\partial t^2} - c_t^2 \nabla^2 \mathbf{u}_t\right) = 0, \tag{10.13a}$$

when taking the curl of both sides of the equation (10.8) and satisfying the relation (10.10a), and the equation

$$\nabla \cdot \left(\frac{\partial^2 \mathbf{u}_t}{\partial t^2} - c_t^2 \nabla^2 \mathbf{u}_t\right) = 0, \tag{10.13b}$$

by using the relation (10.10b). From equations (10.13) the wave equation for transversal part $\mathbf{u}_t$ is obtained:

$$\left(\frac{\partial^2}{\partial t^2} - c_t^2 \nabla^2\right)\mathbf{u}_t = 0. \tag{10.14}$$

The displacement vector also can be written in terms of the scalar potential ϕ and the vector potential $\boldsymbol{\psi}$:

$$\mathbf{u}_l = \nabla\phi, \tag{10.15a}$$

$$\mathbf{u}_t = \nabla\times\boldsymbol{\psi}, \quad \text{with} \quad \nabla\cdot\boldsymbol{\psi} = 0. \tag{10.15b}$$

The potentials also satisfy the wave equations

$$\left(\frac{\partial^2}{\partial t^2} - c_t^2\nabla^2\right)\phi = 0, \tag{10.16a}$$

$$\left(\frac{\partial^2}{\partial t^2} - c_l^2\nabla^2\right)\boldsymbol{\psi} = 0, \quad \text{with} \quad \nabla\cdot\boldsymbol{\psi} = 0. \tag{10.16b}$$

10.2 Eigenmodes of a half space filled with an isotropic elastic medium

We want to find the eigenmodes of a half space $y \le 0$ filled with an isotropic elastic medium, which has a stress-free surface. For every point of a stress-free surface we have to satisfy the boundary condition

$$\sigma_{ij}n_j = 0, \tag{10.17}$$

where $\mathbf{n}$ is the outward normal at each point of the surface. For a half space $y \le 0$ we have

$$\mathbf{n} = \{0, 0, 1\}. \tag{10.18}$$

So we need to solve equation (10.8) with the boundary condition (10.17). We start by choosing the following ansatz for the displacement vector

$$\mathbf{u}(\mathbf{r}, t) = \frac{1}{2\pi}\mathbf{f}(y)\mathrm{e}^{\mathrm{i}(k_z z + k_x x - \omega t)}, \quad \mathbf{f} = \{f_z, f_x, f_y\}, \quad [\mathbf{u}(\mathbf{r}, t)] = [\mathbf{f}(y)] = L, \tag{10.19}$$

where $[A]$ denotes the dimension of the quantity A, and dimensions L, T, and M stand for length, time, and mass dimension, respectively. For definiteness we assume $\omega \ge 0$. Inserting (10.19) into equation (10.8) and the boundary condition (10.17) we obtain

$$\left[\mathcal{M}_0 + \mathcal{M}_1\left(-\mathrm{i}\frac{\partial}{\partial y}\right) + \mathcal{M}_2\left(-\mathrm{i}\frac{\partial}{\partial y}\right)^2\right]\mathbf{f}(y) = \omega^2\mathbf{f}(y), \tag{10.20}$$

$$\left[\mathcal{N}_0 + \mathcal{N}_1\left(-\mathrm{i}\frac{\partial}{\partial y}\right)\right]\mathbf{f}(y) = 0, \quad \text{for } y = 0, \tag{10.21}$$

where

$$\mathcal{M}_0 = \begin{pmatrix} c_l^2k_z^2 + c_t^2k_x^2 & (c_l^2 - c_t^2)k_zk_x & 0 \\ (c_l^2 - c_t^2)k_zk_x & c_l^2k_x^2 + c_t^2k_z^2 & 0 \\ 0 & 0 & c_t^2(k_z^2 + k_x^2) \end{pmatrix}, \tag{10.22a}$$

$$\mathcal{M}_1 = (c_l^2 - c_t^2)\begin{pmatrix} 0 & 0 & k_z \\ 0 & 0 & k_x \\ k_z & k_x & 0 \end{pmatrix}, \tag{10.22b}$$

$$\mathcal{M}_2 = \mathcal{N}_1 = \begin{pmatrix} c_t^2 & 0 & 0 \\ 0 & c_t^2 & 0 \\ 0 & 0 & c_l^2 \end{pmatrix}, \tag{10.22c}$$

$$\mathcal{N}_0 = \begin{pmatrix} 0 & 0 & c_t^2k_z \\ 0 & 0 & c_t^2k_x \\ (c_l^2 - 2c_t^2)k_z & (c_l^2 - 2c_t^2)k_x & 0 \end{pmatrix}. \tag{10.22d}$$

We anticipate that the eigenmodes, which we label as ν, will be classified using the following quantities ("quantum numbers")

$$\nu = (\mathbf{k}, k_y, m), \quad \mathbf{k} = \{k_z, k_x\}. \tag{10.23}$$

where $\mathbf{k}$ is the wavevector in zx plane, k_y wavevector perpendicular to the surface, and $m \in \{H, \pm, 0, R\}$ labels type of the mode, where there will be four types as discussed in forthcoming sections.

The solutions will be normalized in the following way:

$$\langle \mathbf{u}^{(\nu')}, \mathbf{u}^{(\nu)} \rangle = [\chi_\nu] \int \mathrm{d}\mathbf{r} \mathbf{u}^{\dagger(\nu')}(\mathbf{r}) \mathbf{u}^{(\nu)}(\mathbf{r}) = \delta_{\nu'\nu}[\chi_\nu], \quad [\langle \mathbf{u}^{(\nu')}, \mathbf{u}^{(\nu)} \rangle] = L^5, \tag{10.24}$$

where $\delta_{\nu'\nu}$ denotes Dirac delta function for continuous variables and Kroenecker delta for discrete variables. The quantity $[\chi_\nu]$ denotes particular dimension depending on whether ν contains discrete or continuous labels. Note that

$$[\mathbf{u}(\mathbf{r}, t)] \neq [\mathbf{u}^{(\nu)}(\mathbf{r})]. \tag{10.25}$$

The normalization condition (10.24) can be written more explicitly as

$$\begin{aligned} \langle \mathbf{u}^{(\mathbf{k}', k_y', m')}, \mathbf{u}^{(\mathbf{k}, k_y, m)} \rangle &= [\chi_m] \frac{1}{2\pi} \int_{-\infty}^{\infty} \mathrm{d}z \mathrm{e}^{\mathrm{i}(k_z' - k_z)z} \frac{1}{2\pi} \int_{-\infty}^{\infty} \mathrm{d}x \mathrm{e}^{\mathrm{i}(k_x' - k_x)x} \int_{-\infty}^{0} \mathrm{d}y \mathbf{f}^{\dagger(\mathbf{k}, k_y', m')}(y) \mathbf{f}^{(\mathbf{k}, k_y, m)}(y) \\ &= [\chi_m] \delta_{\mathbf{k}', \mathbf{k}} \int_{-\infty}^{0} \mathrm{d}y \mathbf{f}^{\dagger(\mathbf{k}, k_y', m')}(y) \mathbf{f}^{(\mathbf{k}, k_y, m)}(y) = \delta_{\mathbf{k}', \mathbf{k}} \delta_{k_y', k_y} \delta_{m', m} [\chi_m], \end{aligned} \tag{10.26}$$

and we get

$$(\mathbf{f}^{(\mathbf{k}, k_y', m')}, \mathbf{f}^{(\mathbf{k}, k_y, m)}) = \int_{-\infty}^{0} \mathrm{d}y \mathbf{f}^{\dagger(\mathbf{k}, k_y', m')}(y) \mathbf{f}^{(\mathbf{k}, k_y, m)}(y) = \delta_{k_y', k_y} \delta_{m', m}. \tag{10.27}$$

Here

$$\mathbf{u}^{(\nu)}(\mathbf{r}) = \mathbf{u}^{(\mathbf{k}, k_y, m)}(\mathbf{r}) = \frac{1}{2\pi} \mathbf{f}^{(\mathbf{k}, k_y, m)}(z) \mathrm{e}^{\mathrm{i}(k_z z + k_x x)}, \quad \mathbf{k} = \{k_z, k_x\}, \tag{10.28}$$

and $\langle A, B \rangle$ denotes the inner product in the whole space, and (A, B) in y direction. We have the following dimensions of $\mathbf{u}^{(\mathbf{k}, k_y, m)}$, $\mathbf{f}^{(\mathbf{k}, k_y, m)}$, and $[\chi_m]$:

$$\begin{aligned} &[\mathbf{u}^{(\mathbf{k}, k_y, m)}] = [\mathbf{f}^{(\mathbf{k}, k_y, m)}] = 1, \quad [\chi_m] = L^2 \quad \text{for} \quad m = H, \pm, 0, \\ &[\mathbf{u}^{(\mathbf{k}, k_R, R)}] = [\mathbf{f}^{(\mathbf{k}, k_R, R)}] = L^{-1/2}, \quad [\chi_R] = L^3, \quad \text{for} \quad m = R, \end{aligned} \tag{10.29}$$

where the first line is the dimensions for the modes with continuous k_y and the second line for the modes with discrete k_y. For some of the derivations we will use the potentials ϕ and $\boldsymbol{\psi}$. In analogy with (10.19) we use the following ansatz

$$\phi(\mathbf{r}, t) = \frac{1}{2\pi} f_\phi(y) \mathrm{e}^{\mathrm{i}(k_z z + k_x x - \omega t)}, \tag{10.30a}$$

$$\boldsymbol{\psi}(\mathbf{r}, t) = \frac{1}{2\pi} \mathbf{f}_{\boldsymbol{\psi}}(y) \mathrm{e}^{\mathrm{i}(k_z z + k_x x - \omega t)}, \tag{10.30b}$$

and we find that $\mathbf{f}$ is expressed in terms of f_ϕ and $\mathbf{f}_{\boldsymbol{\psi}}$ as

$$f_z = \mathrm{i}k_z f_\phi + \mathrm{i}k_x f_{\psi_y} - \frac{d}{dy} f_{\psi_x}, \tag{10.31a}$$

$$f_x = \mathrm{i}k_x f_\phi + \frac{d}{dy} f_{\psi_z} - \mathrm{i}k_z f_{\psi_y}, \tag{10.31b}$$

$$f_y = \frac{d}{dy} f_\phi + \mathrm{i}k_z f_{\psi_x} - \mathrm{i}k_x f_{\psi_z}. \tag{10.31c}$$

Inserting the potentials into the wave equations (10.16) we obtain

$$c_l^2\left[k_z^2+k_x^2-\frac{\partial^2}{\partial y^2}\right]f_\phi=\omega^2 f_\phi, \tag{10.32a}$$

$$c_t^2\left[k_z^2+k_x^2-\frac{\partial^2}{\partial y^2}\right]\mathbf{f}_\psi=\omega^2\mathbf{f}_\psi, \tag{10.32b}$$

$$\mathrm{i}k_z f_{\psi_z}+\mathrm{i}k_x f_{\psi_x}+\frac{\partial}{\partial y}f_{\psi_y}=0, \tag{10.32c}$$

and from the boundary condition (10.21) we get

$$\left[\mathcal{K}_0+\mathcal{K}_1\left(-\mathrm{i}\frac{\partial}{\partial y}\right)+\mathcal{K}_2\left(-\mathrm{i}\frac{\partial}{\partial y}\right)^2\right]\mathbf{F}=0,\quad \text{for } y=0,\quad \text{with}\quad \mathbf{F}=\{f_\phi,f_{\psi_z},f_{\psi_x},f_{\psi_y}\}, \tag{10.33}$$

where

$$\mathcal{K}_0=\begin{pmatrix}0 & -c_t^2k_zk_x & c_t^2k_z^2 & 0\\ 0 & -c_t^2k_x^2 & c_t^2k_zk_x & 0\\ (c_l^2-2c_t^2)(k_z^2+k_x^2) & 0 & 0 & 0\end{pmatrix}, \tag{10.34a}$$

$$\mathcal{K}_1=\begin{pmatrix}2c_t^2k_z & 0 & 0 & c_t^2k_x\\ 2c_t^2k_x & 0 & 0 & -c_t^2k_z\\ 0 & -2c_t^2k_x & 2c_t^2k_z & 0\end{pmatrix}, \tag{10.34b}$$

$$\mathcal{K}_2=\begin{pmatrix}0 & 0 & -c_t^2 & 0\\ 0 & c_t^2 & 0 & 0\\ c_l^2 & 0 & 0 & 0\end{pmatrix}. \tag{10.34c}$$

We will perform calculations and will find the modes, where z and x axes are rotated such that the vector $\mathbf{k}$ gets transformed into

$$\mathbf{k}=\{k_z,k_x\}\quad\rightarrow\quad\{\kappa,0\},\quad \text{with } \kappa=\sqrt{k_z^2+k_x^2}. \tag{10.35}$$

10.2.1 SH-mode, $m=H$

For this mode we set $f_z=f_y=0$, and then the wave is polarized both to the direction of $\mathbf{k}=\{\kappa,0\}$ and the y-axis, i.e. we get shear wave with horizontal polarization (SH-mode), which we label as

$$m=H. \tag{10.36}$$

For this polarization the equation of motion (10.20) and the boundary condition (10.21) reads as

$$\left(c_t^2\frac{d^2}{dy^2}+\omega^2-c_t^2\kappa^2\right)f_x=0, \tag{10.37a}$$

$$\left.\frac{df_x}{dy}\right|_{y=0}=0. \tag{10.37b}$$

As always for linear differential equation with constant coefficients we guess solution of the form $\mathrm{e}^{\mathrm{i}k_\beta y}$, which yields the following characteristic equation for (10.37a)

$$-c_t^2k_\beta^2+\omega^2-c_t^2\kappa^2=0\quad\rightarrow\quad\omega=c_t\sqrt{k_\beta^2+\kappa^2}. \tag{10.38}$$

Then we construct the following general solution

$$2f_x = Ae^{ik_\beta y} + Be^{-ik_\beta y} \quad \rightarrow \quad f_x = A\cos(k_\beta y), \quad k_\beta > 0, \tag{10.39}$$

where after the arrow we have satisfied the boundary condition (10.37b), which requires $A = B$. We see that k_β has to be real, because if k_β is imaginary then the above solution grows exponentially in y direction, which is not physical.

Now we normalize the solution (10.39) using condition (10.27)

$$\begin{aligned} |A|^2 \int_{-\infty}^{0} \mathrm{d}y \cos(k'_\beta y)\cos(k_\beta y) &= \frac{|A|^2}{2}\int_{-\infty}^{+\infty} \mathrm{d}y \cos(k'_\beta y)\cos(k_\beta y) \\ = \frac{|A|^2}{8}\int_{-\infty}^{+\infty} \mathrm{d}y \left(e^{i(k'_\beta+k_\beta)y} + e^{i(k'_\beta-k_\beta)y} + e^{-i(k'_\beta-k_\beta)y} + e^{-i(k'_\beta+k_\beta)y}\right) \\ = \frac{\pi|A|^2}{2}\delta(k'_\beta - k_\beta) \quad \rightarrow \quad A = \sqrt{\frac{2}{\pi}}. \end{aligned} \tag{10.40}$$

We note that terms with $e^{\pm i(k'_\beta+k_\beta)y}$ vanish, because k'_β and k_β always have the same sign. So we get the final expression for the SH-mode

$$\boxed{f_z^{(\kappa,k_\beta,H)} = f_y^{(\kappa,k_\beta,H)} = 0, \quad f_x^{(\kappa,k_\beta,H)} = \sqrt{\frac{2}{\pi}}\cos(k_\beta y), \quad m = H.} \tag{10.41}$$

10.2.2 Mixed $P-SV$ mode, $m = \pm$

We proceed with the calculation using the potentials ϕ and ψ, and the corresponding equations of motion (10.32). In the coordinate system where $\mathbf{k} = \{\kappa, 0\}$ we get that f_ϕ with f_{ψ_x} gets decoupled from f_{ψ_z} with f_{ψ_y}, i.e. equation of motion (10.32) and the boundary condition (10.33) simplifies to

$$c_t^2\left[\kappa^2 - \frac{d^2}{dy^2}\right] f_{\psi_{z,y}} = \omega^2 f_{\psi_{z,y}}, \tag{10.42a}$$

$$i\kappa f_{\psi_z} + \frac{d}{dy} f_{\psi_y} = 0, \tag{10.42b}$$

$$i\kappa \frac{d}{dy} f_{\psi_y} - \frac{d^2}{dy^2} f_{\psi_z} = 0, \quad \text{at } y = 0. \tag{10.42c}$$

and

$$c_l^2\left[\kappa^2 - \frac{d^2}{dy^2}\right] f_\phi = \omega^2 f_\phi, \tag{10.43a}$$

$$c_t^2\left[\kappa^2 - \frac{d^2}{dy^2}\right] f_{\psi_x} = \omega^2 f_{\psi_x}, \tag{10.43b}$$

$$\kappa^2 f_{\psi_x} - 2i\kappa \frac{d}{dy} f_\phi + \frac{d^2}{dy^2} f_{\psi_x} = 0, \quad \text{at } y = 0, \tag{10.43c}$$

$$(c_l^2 - 2c_t^2)\kappa^2 f_\phi - 2c_t^2 i\kappa \frac{d}{dy} f_{\psi_x} - c_l^2 \frac{d^2}{dy^2} f_\phi = 0, \quad \text{at } y = 0. \tag{10.43d}$$

Solution of equations (10.42) corresponds to the SH-mode, when $f_\phi = f_{\psi_x} = 0 \rightarrow f_z = f_y = 0$. For mixed $P-SV$ mode (as also for modes in next sections) we set $f_x = 0 \rightarrow f_{\psi_z} = f_{\psi_z} = 0$, and use the

following ansatz for f_ϕ and f_{ψ_x}

$$f_\phi = A\mathrm{e}^{\mathrm{i}k_\alpha y} + B\mathrm{e}^{-\mathrm{i}k_\alpha y}, \tag{10.44a}$$

$$f_{\psi_x} = C\mathrm{e}^{\mathrm{i}k_\beta y} + D\mathrm{e}^{-\mathrm{i}k_\beta y}, \tag{10.44b}$$

Inserting these solutions in the equations (10.43a,b) we get

$$\omega_\alpha = c_l\sqrt{k_\alpha^2 + \kappa^2}, \tag{10.45a}$$

$$\omega_\beta = c_t\sqrt{k_\beta^2 + \kappa^2}, \tag{10.45b}$$

and the boundary condition (10.43c,d) gives

$$-2\kappa k_\alpha[A - B] + (k_\beta^2 - \kappa^2)[C + D] = 0, \tag{10.46a}$$

$$(k_\beta^2 - \kappa^2)[A + B] + 2\kappa k_\beta[C - D] = 0. \tag{10.46b}$$

After requiring that $\omega_\alpha = \omega_\beta$ we obtain

$$k_\alpha = \frac{c_t}{c_l}\sqrt{k_\beta^2 + \kappa^2\left[1 - \frac{c_l^2}{c_t^2}\right]}. \tag{10.47}$$

There are two independent solutions for the above system of equations. We note that in this case the wave coming from ϕ is called a P-wave (pressure wave) and the one from ψ a SV-wave (shear wave with vertical polarization). Also for a mixed $P - SV$ wave we have

$$k_\alpha^2,\ k_\beta^2 > 0, \quad k_\alpha,\ k_\beta > 0, \quad \rightarrow \quad k_\beta > \kappa\sqrt{\frac{c_l^2}{c_t^2} - 1}. \tag{10.48}$$

As a first solution we pick a P-wave incident upon the surface

$$A = 1, \quad C = 0, \tag{10.49}$$

and from (10.46) we find

$$B = -a, \quad D = \sqrt{\frac{k_\alpha}{k_\beta}}b, \tag{10.50}$$

where we introduced coefficients

$$a = \frac{(k_\beta^2 - \kappa^2)^2 - 4\kappa^2 k_\alpha k_\beta}{(k_\beta^2 - \kappa^2)^2 + 4\kappa^2 k_\alpha k_\beta}, \quad b = \frac{4\kappa\sqrt{k_\alpha k_\beta}(k_\beta^2 - \kappa^2)}{(k_\beta^2 - \kappa^2)^2 + 4\kappa^2 k_\alpha k_\beta}. \tag{10.51}$$

So for an incident P-wave we get

$$f_\phi^{(\kappa,c,P)} = \mathrm{e}^{\mathrm{i}k_\alpha y} - a\mathrm{e}^{-\mathrm{i}k_\alpha y}, \tag{10.52a}$$

$$f_{\psi_x}^{(\kappa,c,P)} = \sqrt{\frac{k_\alpha}{k_\beta}}b\mathrm{e}^{-\mathrm{i}k_\beta y}. \tag{10.52b}$$

Using the relations (10.31) we find the corresponding displacement vector $\mathbf{f}(y)$ for P-wave

$$f_z^{(\kappa,c,P)} = \mathrm{i}A^{(\kappa,c,P)}\kappa\left[\mathrm{e}^{\mathrm{i}k_\alpha y} - a\mathrm{e}^{-\mathrm{i}k_\alpha y} + \sqrt{\frac{k_\alpha k_\beta}{\kappa^2}}b\mathrm{e}^{-\mathrm{i}k_\beta y}\right], \tag{10.53a}$$

$$f_x^{(\kappa,c,P)} = 0, \tag{10.53b}$$

$$f_y^{(\kappa,c,P)} = \mathrm{i}A^{(\kappa,c,P)}\kappa\left[\frac{k_\alpha}{\kappa}\left(\mathrm{e}^{\mathrm{i}k_\alpha y} + a\mathrm{e}^{-\mathrm{i}k_\alpha y}\right) + \sqrt{\frac{k_\alpha}{k_\beta}}b\mathrm{e}^{-\mathrm{i}k_\beta y}\right]. \tag{10.53c}$$

Here we introduced the normalization constant A, which we determine from condition (10.27). When calculating normalization constant we will need the integral

$$I = \int_{-\infty}^{0}\mathrm{d}y\mathrm{e}^{\pm\mathrm{i}(q\mp\mathrm{i}\eta)y} = \frac{\mathrm{i}}{\mp q + \mathrm{i}\eta} = \mp\frac{\mathrm{i}\mathcal{P}}{q} + \pi\delta(q), \tag{10.54}$$

where $\eta = +0$ is positive infinitesimal, and $\mathcal{P}$ denotes principal part. The normalization condition (10.27) for the P-wave (10.53) gives:

$$\begin{aligned}
&|A^{(\kappa,c,P)}|^2\pi\left[(\kappa^2+k_\alpha^2)(1+a^2)\delta(k'_\alpha-k_\alpha) + \left(k_\alpha k_\beta + \kappa^2\frac{k_\alpha}{k_\beta}\right)b^2\delta(k'_\beta-k_\beta)\right]\\
&= |A^{(\kappa,c,P)}|^2\pi\left[(\kappa^2+k_\alpha^2)(1+a^2)\left(\frac{c_l}{c_t}\right)^2\frac{k_\alpha}{k_\beta} + \left(k_\alpha k_\beta + \kappa^2\frac{k_\alpha}{k_\beta}\right)b^2\right]\delta(k'_\beta-k_\beta)\\
&= |A^{(\kappa,c,P)}|^2 2\pi\frac{k_\alpha}{k_\beta}(k_\beta^2+\kappa^2)\delta(k'_\beta-k_\beta) \quad\rightarrow\quad A^{(\kappa,c,P)} = \sqrt{\frac{k_\beta}{2\pi k_\alpha(k_\beta^2+\kappa^2)}}.
\end{aligned} \tag{10.55}$$

Here we used the identity

$$\delta(f(x)) = \sum_{j=1}^{n}\frac{\delta(x-x_j)}{|f'(x_j)|}, \quad \text{with } f(x_j)=0 \text{ and } f'(x_j)\neq 0, \tag{10.56}$$

which yields

$$\frac{\partial k_\alpha}{\partial k_\beta} = \left(\frac{c_t}{c_l}\right)^2\frac{k_\beta}{k_\alpha}, \quad \delta(k'_\alpha-k_\alpha) = \frac{\delta(k'_\beta-k_\beta)}{|\partial k_\alpha/\partial k_\beta|} = \left(\frac{c_l}{c_t}\right)^2\frac{k_\alpha}{k_\beta}\delta(k'_\beta-k_\beta). \tag{10.57}$$

We note that all the terms with a principal value cancel each other, and there were many δ-functions, which cannot be satisfied, so we have not specified them. Using the above normalization constant the normalized displacement vector $\mathbf{f}(y)$ for a P-wave becomes:

$$\boxed{\begin{aligned}
f_z^{(\kappa,c,P)} &= \mathrm{i}\sqrt{\frac{k_\beta}{2\pi k_\alpha(1+k_\beta^2/\kappa^2)}}\left[\mathrm{e}^{\mathrm{i}k_\alpha y} - a\mathrm{e}^{-\mathrm{i}k_\alpha y} + \sqrt{\frac{k_\alpha k_\beta}{\kappa^2}}b\mathrm{e}^{-\mathrm{i}k_\beta y}\right],\\
f_x^{(\kappa,c,P)} &= 0,\\
f_y^{(\kappa,c,P)} &= \mathrm{i}\sqrt{\frac{k_\beta}{2\pi k_\alpha(1+k_\beta^2/\kappa^2)}}\left[\frac{k_\alpha}{\kappa}\left(\mathrm{e}^{\mathrm{i}k_\alpha y} + a\mathrm{e}^{-\mathrm{i}k_\alpha y}\right) + \sqrt{\frac{k_\alpha}{k_\beta}}b\mathrm{e}^{-\mathrm{i}k_\beta y}\right], \quad m = P.
\end{aligned}} \tag{10.58}$$

When a SV-wave is the incident wave we have

$$A = 0, \quad C = 1, \tag{10.59}$$

and equations (10.46) yields

$$B = -\sqrt{\frac{k_\beta}{k_\alpha}}b, \quad D = -a, \tag{10.60}$$

so the incident SV-wave becomes

$$f_\phi^{(\kappa,c,SV)} = -\sqrt{\frac{k_\beta}{k_\alpha}}b\mathrm{e}^{-\mathrm{i}k_\alpha y}, \tag{10.61a}$$

$$f_{\psi_x}^{(\kappa,c,SV)} = \mathrm{e}^{\mathrm{i}k_\beta y} - a\mathrm{e}^{-\mathrm{i}k_\beta y}. \tag{10.61b}$$

The corresponding displacement vector $\mathbf{f}(y)$ for SV-wave is

$$f_z^{(\kappa,c,SV)} = \mathrm{i}A^{(\kappa,c,SV)}\kappa\left[-\sqrt{\frac{k_\beta}{k_\alpha}}b\mathrm{e}^{-\mathrm{i}k_\alpha y} - \frac{k_\beta}{\kappa}\left(\mathrm{e}^{\mathrm{i}k_\beta y} + a\mathrm{e}^{-\mathrm{i}k_\beta y}\right)\right], \tag{10.62a}$$

$$f_x^{(\kappa,c,SV)} = 0, \tag{10.62b}$$

$$f_y^{(\kappa,c,SV)} = \mathrm{i}A^{(\kappa,c,SV)}\kappa\left[\sqrt{\frac{k_\alpha k_\beta}{\kappa^2}}b\mathrm{e}^{-\mathrm{i}k_\alpha y} + \mathrm{e}^{\mathrm{i}k_\beta y} - a\mathrm{e}^{-\mathrm{i}k_\beta y}\right], \tag{10.62c}$$

and we find the normalization constant $A^{(\kappa,c,SV)}$ from

$$\begin{aligned}
&|A^{(\kappa,c,SV)}|^2\pi\left[k_\beta\left(k_\alpha + \frac{\kappa^2}{k_\alpha}\right)b^2\delta(k'_\alpha - k_\alpha) + (\kappa^2 + k_\beta^2)(1+a^2)\delta(k'_\beta - k_\beta)\right] \\
&= |A^{(\kappa,c,SV)}|^2\pi\left[k_\beta\left(k_\alpha + \frac{\kappa^2}{k_\alpha}\right)b^2\left(\frac{c_l}{c_t}\right)^2\frac{k_\alpha}{k_\beta} + (\kappa^2 + k_\beta^2)(1+a^2)\right]\delta(k'_\beta - k_\beta) \\
&= |A^{(\kappa,c,SV)}|^2 2\pi(k_\beta^2 + \kappa^2)\delta(k'_\beta - k_\beta) \quad \rightarrow \quad A^{(\kappa,c,SV)} = \frac{1}{\sqrt{2\pi(k_\beta^2 + \kappa^2)}}.
\end{aligned} \tag{10.63}$$

which yields the final expression for the SV-wave

$$\boxed{\begin{aligned}
f_z^{(\kappa,c,SV)} &= \mathrm{i}\frac{1}{\sqrt{2\pi(1 + k_\beta^2/\kappa^2)}}\left[-\sqrt{\frac{k_\beta}{k_\alpha}}b\mathrm{e}^{-\mathrm{i}k_\alpha y} - \frac{k_\beta}{\kappa}\left(\mathrm{e}^{\mathrm{i}k_\beta y} + a\mathrm{e}^{-\mathrm{i}k_\beta y}\right)\right], \\
f_x^{(\kappa,c,SV)} &= 0, \\
f_y^{(\kappa,c,SV)} &= \mathrm{i}\frac{1}{\sqrt{2\pi(1 + k_\beta^2/\kappa^2)}}\left[\sqrt{\frac{k_\alpha k_\beta}{\kappa^2}}b\mathrm{e}^{-\mathrm{i}k_\alpha y} + \mathrm{e}^{\mathrm{i}k_\beta y} - a\mathrm{e}^{-\mathrm{i}k_\beta y}\right], \quad m = SV.
\end{aligned}} \tag{10.64}$$

Note that the P-wave and the SV-wave are orthogonal to each other:

$$\begin{aligned}
(\mathbf{f}^{(\kappa,c,P)}, \mathbf{f}^{(\kappa,c,SV)}) &\sim ab\sqrt{\frac{k_\alpha k_\beta}{\kappa^2}}\left[\left(\frac{k_\alpha}{\kappa} + \frac{\kappa}{k_\alpha}\right)\delta(k'_\alpha - k_\alpha) - \left(\frac{k_\beta}{\kappa} + \frac{\kappa}{k_\beta}\right)\delta(k'_\beta - k_\beta)\right] \\
&= ab\sqrt{\frac{k_\alpha k_\beta}{\kappa^2}}\left[\left(\frac{k_\alpha}{\kappa} + \frac{\kappa}{k_\alpha}\right)\left(\frac{c_l}{c_t}\right)^2\frac{k_\alpha}{k_\beta} - \left(\frac{k_\beta}{\kappa} + \frac{\kappa}{k_\beta}\right)\right]\delta(k'_\beta - k_\beta) = 0.
\end{aligned} \tag{10.65}$$

Having the P-wave and the SV-wave we will construct a so-called mixed $P-SV$ wave in the following way

$$f^{(\kappa,c,\pm)}_{\phi,\psi_x} = \mp \mathrm{i}\sqrt{\frac{\kappa}{k_\alpha}} f^{(\kappa,c,P)}_{\phi,\psi_x} + \sqrt{\frac{\kappa}{k_\beta}} f^{(\kappa,c,SV)}_{\phi,\psi_x}, \tag{10.66}$$

or more explicitly

$$f^{(\kappa,c,\pm)}_{\phi} = \mp \mathrm{i}\sqrt{\frac{\kappa}{k_\alpha}} \left(\mathrm{e}^{\mathrm{i}k_\alpha y} - \zeta_\pm \mathrm{e}^{-\mathrm{i}k_\alpha y}\right), \tag{10.67a}$$

$$f^{(\kappa,c,\pm)}_{\psi_x} = \sqrt{\frac{\kappa}{k_\beta}} \left(\mathrm{e}^{\mathrm{i}k_\beta y} - \zeta_\pm \mathrm{e}^{-\mathrm{i}k_\beta y}\right), \tag{10.67b}$$

where

$$\zeta_\pm = a \pm \mathrm{i}b, \quad |\zeta_\pm|^2 = a^2 + b^2 = 1. \tag{10.68}$$

The displacement vector $\mathbf{f}^\pm$ for mixed $P-SV$ mode is

$$\mathbf{f}^{(\kappa,c,\pm)} = \frac{1}{\sqrt{2}}\left[\mp \mathrm{i}\mathbf{f}^{(\kappa,c,P)} + \mathbf{f}^{(\kappa,c,SV)}\right], \tag{10.69}$$

or more explicitly

$$\boxed{\begin{aligned} f_z^{(\kappa,c,\pm)} &= \frac{1}{\sqrt{4\pi(1+k_\beta^2/\kappa^2)}}\left[\pm\sqrt{\frac{k_\beta}{k_\alpha}}\left(\mathrm{e}^{\mathrm{i}k_\alpha y} - \zeta_\pm \mathrm{e}^{-\mathrm{i}k_\alpha y}\right) - \mathrm{i}\frac{k_\beta}{\kappa}\left(\mathrm{e}^{\mathrm{i}k_\beta y} + \zeta_\pm \mathrm{e}^{-\mathrm{i}k_\beta y}\right)\right], \\ f_x^{(\kappa,c,\pm)} &= 0, \\ f_y^{(\kappa,c,\pm)} &= \frac{1}{\sqrt{4\pi(1+k_\beta^2/\kappa^2)}}\left[\pm\sqrt{\frac{k_\alpha k_\beta}{\kappa^2}}\left(\mathrm{e}^{\mathrm{i}k_\alpha y} + \zeta_\pm \mathrm{e}^{-\mathrm{i}k_\alpha y}\right) + \mathrm{i}\left(\mathrm{e}^{\mathrm{i}k_\beta y} - \zeta_\pm \mathrm{e}^{-\mathrm{i}k_\beta y}\right)\right], \quad m = \pm. \end{aligned}} \tag{10.70}$$

10.2.3 Mode with total reflection, $m = 0$

In this section we examine the modes which have

$$k_\alpha^2 < 0,\ k_\beta^2 > 0 \quad \rightarrow \quad 0 < k_\beta < \kappa\sqrt{\frac{c_l^2}{c_t^2} - 1}, \tag{10.71}$$

and define

$$k_\alpha = \mathrm{i}k_\gamma = \mathrm{i}\frac{c_t}{c_l}\sqrt{\kappa^2\left[\frac{c_l^2}{c_t^2} - 1\right] - k_\beta^2}, \quad 0 < k_\gamma < \kappa\sqrt{1 - \frac{c_t^2}{c_l^2}}. \tag{10.72}$$

From the solution of equation (10.44) we see that we need to set $A = 0$, because otherwise we would get exponentially increasing solution as $y \to -\infty$, which is unphysical. So we start with incident SV-wave, i.e.

$$A = 0, \quad C = 1, \tag{10.73}$$

and from (10.46) we find

$$B = -b, \quad D = -a, \tag{10.74}$$

with

$$a = \frac{(k_\beta^2 - \kappa^2)^2 - 4\mathrm{i}\kappa^2 k_\gamma k_\beta}{(k_\beta^2 - \kappa^2)^2 + 4\mathrm{i}\kappa^2 k_\gamma k_\beta}, \quad b = \frac{4\kappa k_\beta (k_\beta^2 - \kappa^2)}{(k_\beta^2 - \kappa^2)^2 + 4\mathrm{i}\kappa^2 k_\gamma k_\beta}. \tag{10.75}$$

The following potentials are obtained

$$f_{\phi}^{(\kappa,c,0)} = -b\mathrm{e}^{k_\gamma y}, \tag{10.76a}$$

$$f_{\psi_x}^{(\kappa,c,0)} = \mathrm{e}^{\mathrm{i}k_\beta y} - a\mathrm{e}^{-\mathrm{i}k_\beta y}, \tag{10.76b}$$

and the displacement vector becomes

$$f_z^{(\kappa,c,0)} = -\mathrm{i}A^{(\kappa,c,0)}\kappa\left[b\mathrm{e}^{k_\gamma y} + \frac{k_\beta}{\kappa}\left(\mathrm{e}^{\mathrm{i}k_\beta y} + a\mathrm{e}^{-\mathrm{i}k_\beta y}\right)\right], \tag{10.77a}$$

$$f_x^{(\kappa,c,0)} = 0, \tag{10.77b}$$

$$f_y^{(\kappa,c,0)} = A^{(\kappa,c,0)}\kappa\left[-\frac{k_\gamma}{\kappa}b\mathrm{e}^{k_\gamma y} + \mathrm{i}\left(\mathrm{e}^{\mathrm{i}k_\beta y} - a\mathrm{e}^{-\mathrm{i}k_\beta y}\right)\right]. \tag{10.77c}$$

In this case the normalization constant is

$$\begin{aligned} &|A^{(\kappa,c,0)}|^2\pi\left(1+|a|^2\right)(\kappa^2+k_\beta^2)\delta(k'_\beta - k_\beta) \\ &= |A^{(\kappa,c,0)}|^2 2\pi(\kappa^2+k_\beta^2)\delta(k'_\beta - k_\beta) \quad \rightarrow \quad A^{(\kappa,c,0)} = \frac{1}{\sqrt{2\pi(\kappa^2+k_\beta^2)}}, \end{aligned} \tag{10.78}$$

and we get the following final expression for a mode with total reflection

$$\boxed{\begin{aligned} f_z^{(\kappa,c,0)} &= -\mathrm{i}\frac{1}{\sqrt{2\pi(1+k_\beta^2/\kappa^2)}}\left[b\mathrm{e}^{k_\gamma y} + \frac{k_\beta}{\kappa}\left(\mathrm{e}^{\mathrm{i}k_\beta y} + a\mathrm{e}^{-\mathrm{i}k_\beta y}\right)\right], \\ f_x^{(\kappa,c,0)} &= 0, \\ f_y^{(\kappa,c,0)} &= \frac{1}{\sqrt{2\pi(1+k_\beta^2/\kappa^2)}}\left[-\frac{k_\gamma}{\kappa}b\mathrm{e}^{k_\gamma y} + \mathrm{i}\left(\mathrm{e}^{\mathrm{i}k_\beta y} - a\mathrm{e}^{-\mathrm{i}k_\beta y}\right)\right], \quad m = 0. \end{aligned}} \tag{10.79}$$

10.2.4 Rayleigh mode, $m = R$

In the case of this mode we have

$$k_\alpha^2 < 0,\ k_\beta^2 < 0, \tag{10.80}$$

and we define

$$k_\beta = \mathrm{i}k_\eta, \quad k_\alpha = \mathrm{i}k_\gamma = \mathrm{i}\frac{c_t}{c_l}\sqrt{\kappa^2\left[\frac{c_l^2}{c_t^2} - 1\right] + k_\eta^2}. \tag{10.81}$$

We need to set $A = C = 0$ in order not to have exponentially increasing terms in (10.44), and then set of equations (10.46) become

$$2\mathrm{i}\kappa k_\gamma B - (\kappa^2 + k_\eta^2)D = 0, \tag{10.82a}$$

$$(\kappa^2 + k_\eta^2)B + 2\mathrm{i}\kappa k_\eta D = 0. \tag{10.82b}$$

In order to have non-trivial solutions the determinant of this set of equations has to be equal to zero, i.e.

$$(\kappa^2 + k_\eta^2)^2 - 4\kappa^2 k_\gamma k_\eta = 0, \tag{10.83}$$

which requires the wavevector k_η to be a root k_R of

$$\xi^4 + 4\xi^3 + 2(3-8\nu)\xi^2 - 4(3-4\nu)\xi + 1 = 0, \quad \text{with} \quad \xi = \frac{k_R^2}{\kappa^2},\ \nu = \left(\frac{c_t}{c_l}\right)^2 = \frac{1-2\sigma}{2(1-\sigma)}, \tag{10.84}$$

known as the Rayleigh condition. Note that ξ has to be in the interval $\xi \in [0,1]$.

We set the following coefficients for the Rayleigh mode

$$A = 0, \quad B = 1, \quad C = 0, \tag{10.85}$$

which from (10.82) yields

$$D = \frac{2\mathrm{i}\kappa k_\gamma}{\kappa^2 + k_\eta^2}, \tag{10.86}$$

and we get the following potentials

$$f_\phi^{(\kappa,c,R)} = \mathrm{e}^{k_\gamma y}, \tag{10.87a}$$

$$f_{\psi_x}^{(\kappa,c,R)} = \frac{2\mathrm{i}\kappa k_\gamma}{\kappa^2 + k_\eta^2}\mathrm{e}^{k_\eta y}. \tag{10.87b}$$

The corresponding displacement vector $\mathbf{f}(y)$ for the Rayleigh mode is

$$f_z^{(\kappa,c,R)} = \mathrm{i}A^{(\kappa,c,R)}\kappa\left[\mathrm{e}^{k_\gamma y} - \frac{2k_\gamma k_\eta}{\kappa^2 + k_\eta^2}\mathrm{e}^{k_\eta y}\right], \tag{10.88a}$$

$$f_x^{(\kappa,c,R)} = 0, \tag{10.88b}$$

$$f_y^{(\kappa,c,R)} = A^{(\kappa,c,R)}\kappa\left[\frac{k_\gamma}{\kappa}\mathrm{e}^{k_\gamma y} - \frac{2\kappa k_\gamma}{\kappa^2 + k_\eta^2}\mathrm{e}^{k_\eta y}\right]. \tag{10.88c}$$

Because the velocity k_R is discrete for given κ, we choose the mode to be normalized to 1 instead of a δ-function:

$$\begin{aligned}
&|A^{(\kappa,c,R)}|^2\kappa^2\int_{-\infty}^{0}\mathrm{d}y\left[\left(1+\frac{k_\gamma^2}{\kappa^2}\right)\mathrm{e}^{2k_\gamma y} + \frac{4k_\gamma^2}{\kappa^2+k_\eta^2}\mathrm{e}^{2k_\eta y} - \frac{2k_\gamma}{\kappa^2+k_\eta^2}\left(k_\gamma + k_\eta\right)\mathrm{e}^{(k_\gamma+k_\eta)y}\right] \\
&= |A^{(\kappa,c,R)}|^2\kappa\left[\frac{\kappa^2+k_\gamma^2}{2\kappa k_\gamma} + \left(\frac{k_\gamma}{k_\eta} - 2\right)\frac{2\kappa k_\gamma}{\kappa^2+k_\eta^2}\right] \\
&= |A^{(\kappa,c,R)}|^2\kappa\left[\frac{\kappa^2+k_\gamma^2}{2\kappa k_\gamma} + \left(\frac{k_\gamma}{k_\eta} - 2\right)\frac{\kappa^2+k_\eta^2}{2\kappa k_\eta}\right] \\
&= |A^{(\kappa,c,R)}|^2\kappa\frac{(k_\gamma-k_\eta)(\kappa^2 k_\gamma - \kappa^2 k_\eta + 2k_\gamma k_\eta^2)}{2\kappa k_\gamma k_\eta^2} = |A^{(\kappa,c,R)}|^2\kappa K(\sigma) \quad \rightarrow \quad A^{(\kappa,c,R)} = \frac{1}{\sqrt{\kappa K(\sigma)}},
\end{aligned} \tag{10.89}$$

with

$$K(\sigma) = \frac{(k_\gamma - k_\eta)(\kappa^2 k_\gamma - \kappa^2 k_\eta + 2k_\gamma k_\eta^2)}{2\kappa k_\gamma k_\eta^2}. \tag{10.90}$$

Here we also used relation (10.83). The final expression for the displacement vector of Rayleigh mode is:

$$\boxed{\begin{aligned} f_z^{(\kappa,c,R)} &= \mathrm{i}\sqrt{\frac{\kappa}{K(\sigma)}}\left[\mathrm{e}^{k_\gamma y} - \frac{2k_\gamma k_\eta}{\kappa^2+k_\eta^2}\mathrm{e}^{k_\eta y}\right], \\ f_x^{(\kappa,c,R)} &= 0, \\ f_y^{(\kappa,c,R)} &= \sqrt{\frac{\kappa}{K(\sigma)}}\left[\frac{k_\gamma}{\kappa}\mathrm{e}^{k_\gamma y} - \frac{2\kappa k_\gamma}{\kappa^2+k_\eta^2}\mathrm{e}^{k_\eta y}\right], \quad m = R. \end{aligned}} \tag{10.91}$$

10.3 The complete set of eigenfunctions

The completeness of eigenfunctions is proven in [123] and here we will only state the result. Firstly, the following completeness in a subspace of y is satisfied with any constant κ:

$$\sum_{m,k_\beta} f_i^{(\kappa,k_\beta,m)}(y) f_j^{*(\kappa,k_\beta,m)}(y') = \delta_{ij}\delta(y-y'), \tag{10.92}$$

or more explicitly

$$\begin{aligned} &f_i^{(\kappa,k_R,R)}(y) f_j^{*(\kappa,k_R,R)}(y') + \int_0^{+\infty} \mathrm{d}k_\beta f_i^{(\kappa,k_\beta,H)}(y) f_j^{*(\kappa,k_\beta,H)}(y') \\ &+ \int_0^{\kappa\sqrt{(c_l/c_t)^2-1}} \mathrm{d}k_\beta f_i^{(\kappa,k_\beta,0)}(y) f_j^{*(\kappa,k_\beta,0)}(y') \\ &+ \int_{\kappa\sqrt{(c_l/c_t)^2-1}}^{+\infty} \mathrm{d}k_\beta \left[f_i^{(\kappa,k_\beta,+)}(y) f_j^{*(\kappa,k_\beta,+)}(y') + f_i^{(\kappa,k_\beta,-)}(y) f_j^{*(\kappa,k_\beta,-)}(y')\right] = \delta_{ij}\delta(y-y'). \end{aligned} \tag{10.93}$$

If we sum over κ we get completeness in subspace zy

$$\sum_{\kappa,m,k_\beta} u_i^{(\kappa,k_\beta,m)}(\mathbf{r}) u_j^{*(\kappa,k_\beta,m)}(\mathbf{r}') = \frac{1}{(2\pi)^2}\delta_{ij}\delta(y-y')\int_{-\infty}^{+\infty}\mathrm{d}\kappa \mathrm{e}^{\mathrm{i}\kappa(z-z')} = \frac{1}{2\pi}\delta_{ij}\delta(y-y')\delta(z-z'). \tag{10.94}$$

To obtain completeness in full half-space xyz we need to construct eigenfunctions $f_i^{(\kappa,k_\beta,m)}$ for an arbitrary direction of the wavevector $\mathbf{k} = \{k_z, k_x\}$. This we obtain by rotating the coordinate plane $z'x'$, where we have the wavevector $\mathbf{k}' = \{\kappa, 0\}$, to zx, where the wavevector becomes $\mathbf{k} = \{k_z, k_x\}$ with $\kappa = \sqrt{k_z^2 + k_x^2}$. This is achieved by making the transformation

$$f_i^{(\mathbf{k},k_\beta,m)}(y) = R_{ij} f_j^{(\kappa,k_\beta,m)}(y), \quad u_i^{(\mathbf{k},k_\beta,m)}(\mathbf{r}) = \frac{1}{2\pi} f_i^{(\mathbf{k},k_\beta,m)}(y)\mathrm{e}^{\mathrm{i}(k_z z + k_x x)}, \tag{10.95}$$

where the rotation matrix R_{ij} is

$$R_{ij} = \begin{pmatrix} \cos\theta & 0 & \sin\theta \\ 0 & 1 & 0 \\ -\sin\theta & 0 & \cos\theta \end{pmatrix}, \tag{10.96}$$

and θ is the angle of rotation around the y axis with

$$k_z = \kappa\cos\theta, \quad k_x = \kappa\sin\theta. \tag{10.97}$$

Because the Kroenecker δ_{ij} is a second rank tensor and is invariant under rotations the subspace completeness (10.92) is carried over to the new coordinate system, and we have

$$\begin{aligned}\sum_{\mathbf{k},m,k_\beta} u_i^{(\mathbf{k},k_\beta,m)}(\mathbf{r})u_j^{*(\mathbf{k},k_\beta,m)}(\mathbf{r}') &= \frac{1}{(2\pi)^2}\delta_{ij}\delta(y-y')\int_{-\infty}^{+\infty}\mathrm{d}k_z\mathrm{e}^{\mathrm{i}k_z(z-z')}\int_{-\infty}^{+\infty}\mathrm{d}k_x\mathrm{e}^{\mathrm{i}k_x(x-x')} \\ &= \delta_{ij}\delta(y-y')\delta(z-z')\delta(x-x') = \delta_{ij}\delta(\mathbf{r}-\mathbf{r}').\end{aligned} \tag{10.98}$$

10.4 Quantization of eigenmodes

The equation (10.8) with the boundary condition (10.17), which we rewrite again for convenience

$$\frac{\partial^2\mathbf{u}}{\partial t^2} = c_t^2\nabla^2\mathbf{u} + (c_l^2 - c_t^2)\nabla(\nabla\cdot\mathbf{u}), \tag{10.99a}$$

$$\sigma_{ij}n_j = 0, \quad \sigma_{ij} = \rho(c_l^2 - 2c_t^2)\frac{\partial u_k}{\partial x_k}\delta_{ij} + \rho c_t^2\left(\frac{\partial u_i}{\partial x_j} + \frac{\partial u_j}{\partial x_i}\right), \tag{10.99b}$$

can be formulated as a variational problem with the following Lagrangian

$$L[\mathbf{v},\mathbf{u}] = \frac{\rho}{2}\left(-\Phi[\mathbf{v},\mathbf{u}] + \int_V \mathrm{d}\mathbf{r}\frac{\partial\mathbf{v}^\dagger}{\partial t}\cdot\frac{\partial\mathbf{u}}{\partial t}\right), \tag{10.100}$$

where the following sesquilinear form was used:

$$\Phi[\mathbf{v},\mathbf{u}] = \int_V \mathrm{d}\mathbf{r}\left[(c_l^2 - 2c_t^2)(\nabla\cdot\mathbf{v})^*(\nabla\cdot\mathbf{u}) + c_t^2(\nabla\times\mathbf{v})^*(\nabla\times\mathbf{u}) + 2c_t^2\frac{\partial v_i^*}{\partial x_j}\frac{\partial u_j}{\partial x_i}\right] \tag{10.101}$$

To get the equations of motion we need to use the variational principle for $L[\mathbf{u},\mathbf{u}]$. From the above Lagrangian we get the following Hamiltonian

$$H[\mathbf{v},\mathbf{u}] = \frac{\rho}{2}\Phi[\mathbf{v},\mathbf{u}] + \frac{1}{2\rho}\int_V \mathrm{d}\mathbf{r}\boldsymbol{\pi}_v^\dagger\cdot\boldsymbol{\pi}_u, \quad \text{with} \quad \boldsymbol{\pi}_v = \rho\frac{\partial\mathbf{v}}{\partial t},\ \boldsymbol{\pi}_u = \rho\frac{\partial\mathbf{u}}{\partial t}, \tag{10.102}$$

where $\boldsymbol{\pi}$ is the canonical momentum. Note that the energy of the eigenmode is determined from the general relation

$$H[\mathbf{u}^{(\nu)},\mathbf{u}^{(\nu')}] = \rho\omega_\nu^2\langle\mathbf{u}^{(\nu)},\mathbf{u}^{(\nu')}\rangle = \rho\omega_\nu^2\delta_{\nu\nu'}[\chi_\nu]. \tag{10.103}$$

Having the complete set of eigenfunctions (10.98) we expand the phonon field $\hat{\mathbf{u}}(\mathbf{r},t)$ as

$$\hat{\mathbf{u}}(\mathbf{r},t) = \sum_\nu\sqrt{\frac{\hbar}{2\rho\omega_\nu}}\left[\mathbf{u}^{(\nu)}(\mathbf{r})\mathrm{e}^{-\mathrm{i}\omega_\nu t}a_\nu + \mathbf{u}^{*(\nu)}(\mathbf{r})\mathrm{e}^{\mathrm{i}\omega_\nu t}a_\nu^\dagger\right], \quad \text{with} \quad \omega_{\mathbf{k},k_\beta} = c_l\sqrt{k_\beta^2 + |\mathbf{k}|^2} > 0, \tag{10.104}$$

in terms of the operators a_ν and $a_\nu^\dagger$, which satisfy the following commutation relations

$$[a_\nu, a_{\nu'}^\dagger] = \delta_{\nu\nu'}, \quad [a_\nu, a_{\nu'}] = 0, \quad [a_\nu^\dagger, a_{\nu'}^\dagger] = 0, \tag{10.105}$$

or more concretely

$$[a_{\mathbf{k},k_\beta,m}, a_{\mathbf{k}',k_\beta',m'}^\dagger] = \delta_{m,m'}\delta_{k_\beta,k_\beta'}\delta_{\mathbf{k},\mathbf{k}'}. \tag{10.106}$$

Note that the dimensions of the quantities entering the phonon field are

$$[\hat{\mathbf{u}}(\mathbf{r},t)] = L, \quad [\rho] = ML^{-3}, \quad [\hbar] = ML^2T^{-1}, \quad [\omega_\nu] = T^{-1}, \quad \left[\sqrt{\frac{\hbar}{2\rho\omega_\nu}}\right] = L^{5/2}, \tag{10.107}$$

and for modes ν with continuous c we have

$$\left[\sum_{\nu}\right] = \left[\int \mathrm{d}k_z \int \mathrm{d}k_x \int \mathrm{d}k_\beta\right] = L^{-3}, \quad [\mathbf{u}^{(\nu)}(\mathbf{r})] = 1, \quad [a_\nu] = L^{3/2}, \tag{10.108}$$

and for modes ν with discrete c we have

$$\left[\sum_{\nu}\right] = \left[\int \mathrm{d}k_z \int \mathrm{d}k_x\right] = L^{-2}, \quad [\mathbf{u}^{(\nu)}(\mathbf{r})] = L^{-1/2}, \quad [a_\nu] = L. \tag{10.109}$$

The canonical momentum for the phonon field (10.104) is

$$\hat{\boldsymbol{\pi}}(\mathbf{r},t) = \rho\frac{\partial\hat{\mathbf{u}}(\mathbf{r},t)}{\partial t} = -\mathrm{i}\sum_{\nu}\sqrt{\frac{\hbar\rho\omega_\nu}{2}}\left[\mathbf{u}^{(\nu)}(\mathbf{r})\mathrm{e}^{-\mathrm{i}\omega_\nu t}a_\nu - \mathbf{u}^{*(\nu)}(\mathbf{r})\mathrm{e}^{\mathrm{i}\omega_\nu t}a_\nu^\dagger\right], \tag{10.110}$$

and the following commutation relation is satisfied

$$[\hat{u}_i(\mathbf{r},t), \hat{\pi}_j(\mathbf{r}',t)] = \mathrm{i}\hbar\delta_{ij}\delta(\mathbf{r}-\mathbf{r}'), \tag{10.111}$$

because of the completeness relation (10.98). We specify the Hamiltonian operator for phonons as

$$\hat{H}[\hat{\mathbf{u}}(\mathbf{r},t), \hat{\mathbf{u}}(\mathbf{r},t)] =: \frac{\rho}{2}\Phi[\hat{\mathbf{u}}(\mathbf{r},t), \hat{\mathbf{u}}(\mathbf{r},t)] + \frac{1}{2\rho}\int_V \mathrm{d}\mathbf{r}\hat{\boldsymbol{\pi}}^\dagger(\mathbf{r},t)\hat{\boldsymbol{\pi}}(\mathbf{r},t) :, \tag{10.112}$$

where $:A:$ denotes a normal ordered (Wick ordered) operator. Using relation (10.103) we find that the Hamiltonian operator becomes

$$\hat{H} = \sum_{\nu}\hbar\omega_\nu a_\nu^\dagger a_\nu. \tag{10.113}$$

Chapter 11

Transport through the molecular junction

11.1 Heat current and phonon conductance

When there is a temperature difference $\Delta T = T_L - T_R$ between the leads, the heat current is running through the device. If the electron-phonon coupling is neglected we can define the heat current due to phonons as the rate of change of the energy [as described by Hamiltonian (9.1a)] in one particular lead α [128–131]:

$$Q_{\alpha,t} = -\langle \partial_t H_\alpha(t)\rangle = -\frac{\mathrm{i}}{\hbar}\langle [H, H_\alpha](t)\rangle. \tag{11.1}$$

Here $A(t) = \mathrm{e}^{\mathrm{i}Ht} A \mathrm{e}^{-\mathrm{i}Ht}$ denotes the Heisenberg evolution of an operator. The commutator in Eq. (11.1) yields

$$Q_{\alpha,t} = \frac{1}{\rho_\alpha}\sum_{ni\mathbf{r}} V_{n,i\alpha}(\mathbf{r})\langle \pi_{i\alpha}(\mathbf{r},t) r_n(t)\rangle = \frac{\mathrm{i}\hbar}{\rho_\alpha}\sum_{ni\mathbf{r}} V_{n,i\alpha}(\mathbf{r}) G^{r\pi,<}_{n,i\alpha\mathbf{r},tt}, \tag{11.2}$$

where $G^{r\pi,<}_{n\beta,tt'} = -\mathrm{i}/\hbar\langle \pi_\beta(t') r_n(t)\rangle$ is the lesser Green's function. Note that the shorthand notation $n \equiv i, m$, $\beta \equiv i', \alpha, \mathbf{r}$ for the labels is used. The same time function $G^{r\pi,<}_{n\beta,tt}$ can be expressed in terms of $G^{ru,<}_{n\beta,tt'} = -\mathrm{i}/\hbar\langle u_\beta(,t') r_n(t)\rangle$ as

$$G^{r\pi,<}_{n\beta,tt} = \lim_{t'\to t}\frac{\partial}{\partial t'}\rho_\beta G^{ru,<}_{n\beta,tt'}. \tag{11.3}$$

In the steady state the current becomes time independent and can be expressed in the following way

$$Q_\alpha = Q_{\alpha,t=0} = \frac{\mathrm{i}\hbar}{\rho_\alpha}\int_{-\infty}^{+\infty}\frac{\mathrm{d}\omega}{2\pi}\sum_{ni\mathbf{r}} V_{n,i\alpha}(\mathbf{r}) G^{r\pi,<}_{n,i\alpha\mathbf{r},\omega} = -\hbar\int_{-\infty}^{+\infty}\frac{\mathrm{d}\omega}{2\pi}\omega\sum_{ni\mathbf{r}} V_{n,i\alpha}(\mathbf{r}) G^{ru,<}_{n,i\alpha\mathbf{r},\omega}, \tag{11.4}$$

where we have the Fourier transformation $G^{ru,<}_{n\beta,\omega} = \int_{-\infty}^{+\infty}\mathrm{d}(t-t')\mathrm{e}^{\mathrm{i}\omega(t-t')} G^{ru,<}_{n\beta,tt'}$. We calculate the above Green's function entering the current using the Keldysh technique [132] and closely follow Wang *et al.* [131].

So we need to consider such bosonic contour-ordered Green's functions

$$G^c_{ab}(\tau,\tau') = -\frac{\mathrm{i}}{\hbar}\langle T_c a(\tau) b(\tau')\rangle =, \begin{cases} G^>_{ab}(\tau,\tau'), & \tau >_c \tau', \\ G^<_{ab}(\tau,\tau'), & \tau <_c \tau' \end{cases} \tag{11.5}$$

with the following definition of the greater $G^>$ and the lesser $G^<$ Green's functions

$$G^>_{ab}(t,t') = -\frac{\mathrm{i}}{\hbar}\langle b(t') a(t)\rangle, \tag{11.6a}$$

$$G^<_{ab}(t,t') = -\frac{\mathrm{i}}{\hbar}\langle a(t) b(t')\rangle, \tag{11.6b}$$

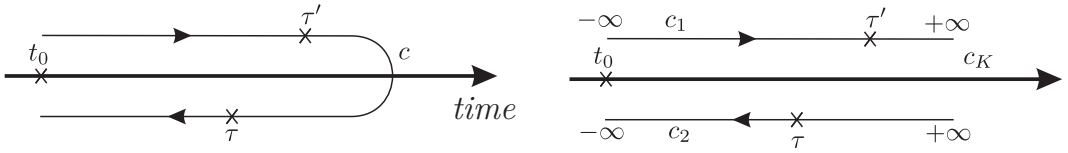

(a) The ''closed time path'' contour (b) The Keldysh contour

Figure 11.1: Different contours for the computation of the contour-ordered Green's function.

where a and b are bosonic operators, and c is the contour along the real time axis that starts and ends at t_0 by passing through τ and τ' once (see Figure 11.1a). The contour-ordering operator T_c orders the operators according to the position on the contour of their time arguments, and the relation $\tau >_c \tau'$ means that τ is further along the contour than τ'. We are interested in the stationary state of the system so the initial time is put to $t_0 \to -\infty$, and we extend the largest time along the contour to infinity to obtain the Keldysh contour depicted in Figure 11.1b. Now we consider the following contour-ordered Green's functions

$$S^c_{\beta\beta',\tau\tau'} = -\frac{\mathrm{i}}{\hbar}\langle T_c u_\beta(\tau) u_{\beta'}(\tau')\rangle, \tag{11.7a}$$

$$G^{ur,c}_{\beta n,\tau\tau'} = -\frac{\mathrm{i}}{\hbar}\langle T_c u_\beta(\tau) r_n(\tau')\rangle, \tag{11.7b}$$

$$G^{ru,c}_{n\beta\tau\tau'} = -\frac{\mathrm{i}}{\hbar}\langle T_c r_n(\tau) u_\beta(\tau')\rangle, \tag{11.7c}$$

$$D^c_{nn',\tau\tau'} = -\frac{\mathrm{i}}{\hbar}\langle T_c r_n(\tau) r_{n'}(\tau')\rangle, \tag{11.7d}$$

which satisfy the equations

$$G^{ur,c}_{\beta n',\tau\tau'} = \sum_{\beta_1 n_2,\tau_1} S^{0,c}_{\beta\beta_1,\tau\tau_1} V_{\beta_1 n_2} D^c_{n_2 n',\tau_1\tau'} + \sum_{\beta_1,\tau_1} S^{0,c}_{\beta\beta_1,\tau\tau_1} V_{\beta_1} G^{ur,c}_{\beta_1 n',\tau_1\tau'}, \tag{11.8a}$$

$$G^{ru,c}_{n\beta',\tau\tau'} = \sum_{n_1\beta_2,\tau_1} D^c_{nn_1,\tau\tau_1} V_{n_1\beta_2} S^{0,c}_{\beta_2\beta',\tau_1\tau'} + \sum_{\beta_1,\tau_1} G^{ru,c}_{n\beta_1,\tau\tau_1} V_{\beta_1} S^{0,c}_{\beta_1\beta',\tau_1\tau'}, \tag{11.8b}$$

$$D^c_{nn',\tau\tau'} = D^{0,c}_{nn',\tau\tau'} + \sum_{n_1\neq n_2,\tau_1} D^{0,c}_{nn_1,\tau\tau_1} V_{n_1 n_2} D^c_{n_2 n',\tau_1\tau'} + \sum_{n_1\beta_2,\tau_1} D^{0,c}_{nn_1,\tau\tau_1} V_{n_1\beta_2} G^{ur,c}_{\beta_2 n',\tau_1\tau'}, \tag{11.8c}$$

on the Keldysh contour and $\sum_{\tau_1} \to \int_{c_K} \mathrm{d}\tau_1 \ldots$ denotes integration along this contour. The derivation of Eqs. (11.8) is presented in Appendix E. The Green's functions D^0 and S^0 are calculated in Appendix F and correspond to Hamiltonian consisting of (9.1b) and the terms V_{nn} in (9.4). Using the Larkin-Ovchinnikov representation for contour-ordered Green's functions [133, 134]

$$G^c \quad \to \quad G = \begin{pmatrix} G^R & G^K \\ 0 & G^A \end{pmatrix}, \tag{11.9}$$

we can Fourier transform Eqs. (11.8) with respect to the time difference $t-t'$, to give

$$G^{ur}_{\beta n',\omega} = \sum_{\beta_1 n_2} S^0_{\beta\beta_1,\omega} V_{\beta_1 n_2} D_{n_2 n',\omega} + \sum_{\beta_1} S^0_{\beta\beta_1,\omega} V_{\beta_1} G^{ur}_{\beta_1 n',\omega}, \tag{11.10a}$$

$$G^{ru}_{n\beta',\omega} = \sum_{n_1\beta_2} D_{nn_1,\omega} V_{n_1\beta_2} S^0_{\beta_2\beta',\omega} + \sum_{\beta_1} G^{ru}_{n\beta_1,\omega} V_{\beta_1} S^0_{\beta_1\beta',\omega}, \tag{11.10b}$$

$$D_{nn',\omega} = D^0_{nn',\omega} + \sum_{n_1\neq n_2} D^0_{nn_1,\omega} V_{n_1 n_2} D_{n_2 n',\omega} + \sum_{n_1\beta_2} D^0_{nn_1,\omega} V_{n_1\beta_2} G^{ur}_{\beta_2 n',\omega}. \tag{11.10c}$$

In Eq. (11.9) $G^R/G^A/G^K$ denote respectively retarded/advanced/Keldysh Green's functions, which for bosonic operators a and b are defined as

$$G^R_{ab}(t,t') = -\frac{\mathrm{i}}{\hbar}\theta(t-t')\langle[a(t),b(t')]\rangle, \tag{11.11a}$$

$$G^A_{ab}(t,t') = \frac{\mathrm{i}}{\hbar}\theta(t'-t)\langle[a(t),b(t')]\rangle, \tag{11.11b}$$

$$G^K_{ab}(t,t') = -\frac{\mathrm{i}}{\hbar}\langle\{a(t),b(t')\}\rangle. \tag{11.11c}$$

By neglecting the subscripts in the equations (11.8) and (11.10), they can be written more abstractly

$$G^{ur} = S^0 V D + S^0 V G^{ur}, \tag{11.12a}$$

$$G^{ru} = D V S^0 + G^{ru} V S^0, \tag{11.12b}$$

$$D = D^0 + D^0 V D + D^0 V G^{ur}, \tag{11.12c}$$

which can be expressed as

$$G^{ur} = \tilde{S}^0 V D, \tag{11.13a}$$

$$G^{ru} = D V \tilde{S}^0, \tag{11.13b}$$

$$D = \tilde{D}^0 + \tilde{D}^0 V G^{ur}, \tag{11.13c}$$

where we have introduced frequency shifted lead Green's function $\tilde{S}^0 = [1 - S^0 V]^{-1} S^0$ and molecule Green's function in the normal mode basis $\tilde{D}^0 = [1 - D^0 V]^{-1} D^0$. After inserting Eq. (11.13a) into Eq. (11.13c) we obtain the Dyson equation for the molecule

$$D = \tilde{D}^0 + \tilde{D}^0 \Sigma D, \quad \Sigma = V \tilde{S}^0 V, \tag{11.14}$$

with the self-energy Σ. In the calculation we will need separately the self-energy due to left and right lead, which explicitly reads

$$\Sigma_{nn',\alpha} = \sum_{i_1\mathbf{r}_1 i_2\mathbf{r}_2} V_{n,i_1\alpha}(\mathbf{r}_1) \tilde{S}^0_{i_1\alpha\mathbf{r}_1, i_2\alpha\mathbf{r}_2,\omega} V_{i_2\alpha,n'}(\mathbf{r}_2), \quad \alpha = L,R, \tag{11.15}$$

where we have suppressed the frequency subscript for the self-energy.

Now we will express the heat current in terms of the molecule Green's function D. Using Eq. (11.13b) and the following Langreth rule $G^{ru,K} = D^R V \tilde{S}^{0,K} + D^K V \tilde{S}^{0,A}$, which can be seen from the Larkin-Ovchinnikov representation (11.9), we obtain

$$Q_\alpha = -\hbar \int_{-\infty}^{+\infty} \frac{\mathrm{d}\omega}{2\pi} \frac{\omega}{2} \mathrm{Tr}[D^R \Sigma^K_\alpha + D^K \Sigma^A_\alpha]. \tag{11.16}$$

We note that we have the relation $2G^{ru,<}_{n\beta,tt} = G^{ru,K}_{n\beta,tt}$ for the same time lesser Green's function. Because the heat current is real $Q_\alpha = Q^*_\alpha$ and conserved $Q_L = -Q_R$, Eq. (11.16) can be cast into a more symmetric form

$$\begin{aligned} Q &= \frac{1}{4}(Q_L + Q^*_L - Q_R - Q^*_R) \\ &= \frac{\hbar}{4}\int_0^{+\infty}\frac{\mathrm{d}\omega}{2\pi}\omega\,\mathrm{Tr}[(D^R - D^A)(\Sigma^K_{\mathrm{R}} - \Sigma^K_{\mathrm{L}}) + \mathrm{i}D^K(\Gamma_{\mathrm{R}} - \Gamma_{\mathrm{L}})], \end{aligned} \tag{11.17}$$

where we have introduced

$$\Gamma_\alpha = \mathrm{i}(\Sigma^R_\alpha - \Sigma^A_\alpha), \tag{11.18}$$

and used the following properties $\left[D^R_\omega\right]^\dagger = D^A_\omega$, $\left[\Sigma^A_{\alpha,\omega}\right]^\dagger = \Sigma^R_{\alpha,\omega}$, $\left[D^K_\omega\right]^\dagger = -D^K_\omega$, $\left[\Sigma^K_{\alpha,\omega}\right]^\dagger = -\Sigma^K_{\alpha,\omega}$. For a quadratic model, like the one we consider in this paper Eq. (9.1), the heat current (11.17) can be rewritten in terms of transmission $\mathcal{T}_{\mathrm{p}}(\omega)$, which is a temperature independent function, i.e., we get a Landauer-Büttiker type expression [135–137]

$$Q_{\mathrm{p}} = \hbar\int_0^{+\infty}\frac{\mathrm{d}\omega}{2\pi}\omega\mathcal{T}_{\mathrm{p}}(\omega)(n_L - n_R), \tag{11.19}$$

where $n_\alpha = 1/\{\exp[\beta_\alpha\hbar\omega] - 1\}$ is the Bose-Einstein distribution with $\beta_\alpha = 1/(k_B T_\alpha)$ denoting the inverse temperature. The phonon transmission function $\mathcal{T}_{\mathrm{p}}(\omega)$ is given by a Caroli type formula [138]

$$\mathcal{T}_{\mathrm{p}}(\omega) = \mathrm{Tr}[\Gamma_{\mathrm{L}}(\omega)D^R(\omega)\Gamma_{\mathrm{R}}(\omega)D^A(\omega)], \tag{11.20}$$

When the temperature difference ΔT is small the Eq. (11.19) yields the following linear phonon conductance

$$\kappa_{\mathrm{p}} = \hbar\int_0^{+\infty}\frac{\mathrm{d}\omega}{2\pi}\omega\mathcal{T}_{\mathrm{p}}(\omega)\frac{\partial n(\omega,T)}{\partial T}, \quad \frac{\partial n(T)}{\partial T} = \frac{k_B}{\hbar\omega}\frac{x^2\mathrm{e}^x}{(\mathrm{e}^x-1)^2}, \quad x = \frac{\hbar\omega}{k_B T}. \tag{11.21}$$

We consider the operation of the device at room temperature $T = 300$ K. For molecules examined in this paper the typical energies of the center of mass vibrational modes are smaller than room temperature, so the phonon conductance corresponding to these modes saturates and becomes temperature independent, i.e.,

$$\kappa_{\mathrm{p}} \overset{T\to+\infty}{=} k_B\int_0^{+\infty}\frac{\mathrm{d}\omega}{2\pi}\mathcal{T}_{\mathrm{p}}(\omega), \quad \frac{\partial n(T)}{\partial T} \to \frac{k_B}{\hbar\omega}. \tag{11.22}$$

11.1.1 Single mass model

When there is a single mass M_1 (see Figure 11.2) in the junction we have only coupling to the leads

$$K_{i1,iL}(\mathbf{r}) \equiv K_{iL}\delta(\mathbf{r} - \mathbf{r}_L), \quad K_{i1,iR}(\mathbf{r}) \equiv K_{iR}\delta(\mathbf{r} - \mathbf{r}_R), \tag{11.23}$$

which gives the following mass weighted coordinate couplings V to a single point

$$V_{i1,i1} = \frac{K_{iL} + K_{iR}}{M_1} \equiv \omega_i^2, \quad V_{i\alpha} = \frac{K_{i\alpha}}{M_\alpha}, \quad V_{i1,i\alpha} = -\frac{K_{i\alpha}}{\sqrt{M_1 M_\alpha}}. \tag{11.24}$$

In such a case we obtain the following phonon transmission function

$$\mathcal{T}^i_{\mathrm{one}}(\omega) = \left(\frac{K_{iL}K_{iR}}{M_1}\right)^2 \frac{2\tilde{b}_{iL}\tilde{b}_{iR}}{\left[\omega^2 - \omega_i^2 - \frac{K^2_{iL}}{M_1}\tilde{a}_{iL} - \frac{K^2_{iR}}{M_1}\tilde{a}_{iR}\right]^2 + \left[\frac{K^2_{iL}}{M}\tilde{b}_{iL} + \frac{K^2_{iR}}{M}\tilde{b}_{iR}\right]^2}, \tag{11.25}$$

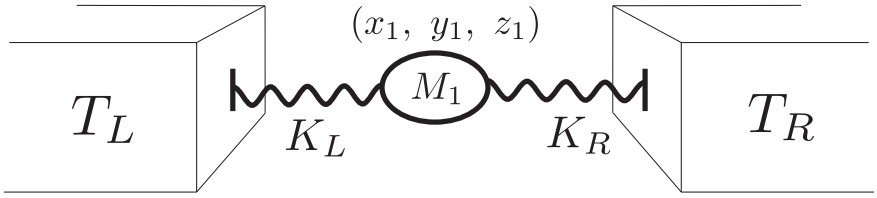

Figure 11.2: Model for single mass in the junction.

where $\tilde{a}_{i\alpha}$ and $\tilde{b}_{i\alpha}$ describe real and imaginary parts of frequency shifted lead Green's function

$$\tilde{S}^{0,R}_{i\alpha\mathbf{r}_\alpha,i\alpha\mathbf{r}_\alpha,\omega} = M_\alpha(\tilde{a}_{i\alpha} + \mathrm{i}\tilde{b}_{i\alpha}), \tag{11.26a}$$

$$\tilde{a}_{i\alpha} = \frac{a_{i\alpha} - K_{i\alpha}(a_{i\alpha}^2 + b_{i\alpha}^2)}{(1 - K_{i\alpha}a_{i\alpha})^2 + (K_{i\alpha}b_{i\alpha})^2}, \quad \tilde{b}_{i\alpha} = \frac{b_{i\alpha}}{(1 - K_{i\alpha}a_{i\alpha})^2 + (K_{i\alpha}b_{i\alpha})^2}, \tag{11.26b}$$

with $a_{i\alpha}$ and $b_{i\alpha}$ being real and imaginary parts of non-interacting lead Green's function

$$S^{0,R}_{i\alpha\mathbf{r}_\alpha,i\alpha\mathbf{r}_\alpha,\omega} = M_\alpha(a_{i\alpha} + \mathrm{i}b_{i\alpha}), \tag{11.27}$$

where

$$a_{i\alpha} = -\frac{A_{i\alpha}}{\pi}\left(2\omega_D + \omega\ln\left|\frac{\omega_D - \omega}{\omega_D + \omega}\right|\right), \quad b_{i\alpha} = -A_{i\alpha}\omega\theta(|\omega| - \omega_D), \tag{11.28}$$

and the coefficients $A_{i\alpha}$ for gold (Au) substrate are obtained in Appendix F.1. We use the transmission (11.25) to get black dotted lines in Figure 11.3.

11.1.2 Two masses model

When there are two masses M_1 and M_2 (see Figure 9.1a) in the junction we have the spring constants (9.2) which give the following mass weighted coordinate couplings V to a single point

$$\begin{aligned} &V_{i1,i1} = \frac{K_i + K_{iL}}{M_1} \equiv \omega_{i1}^2, \quad V_{i2,i2} = \frac{K_i + K_{iR}}{M_2} \equiv \omega_{i2}^2, \quad V_{i\alpha} = \frac{K_{i\alpha}}{M_\alpha}, \\ &V_{i1,i2} = -\frac{K_i}{\sqrt{M_1 M_2}}, \quad V_{i1,iL} = -\frac{K_{iL}}{\sqrt{M_1 M_L}}, \quad V_{i2,iR} = -\frac{K_{iR}}{\sqrt{M_2 M_R}}. \end{aligned} \tag{11.29}$$

Then we get such a phonon transmission function

$$\mathcal{T}^i_{\mathrm{two}}(\omega) = \left(\frac{K_{iL}K_iK_{iR}}{M_1M_2}\right)^2 \frac{2\tilde{b}_{iL}\tilde{b}_{iR}}{\mathcal{R}^2 + \mathcal{I}^2}, \tag{11.30}$$

where all relevant functions entering the above transmission are expressed as

$$\begin{aligned} \mathcal{R} = {} & (\omega^2 - \omega_{i+}^2)(\omega^2 - \omega_{i-}^2) + \frac{K_{iL}^2}{M_1}\frac{K_{iR}^2}{M_2}(\tilde{a}_{iL}\tilde{a}_{iR} - \tilde{b}_{iL}\tilde{b}_{iR}) \\ & - \left(\omega^2 - \frac{\omega_{i+}^2 + \omega_{i-}^2}{2}\right)\left(\frac{K_{iL}^2}{M_1}\tilde{a}_{iL} + \frac{K_{iR}^2}{M_2}\tilde{a}_{iR}\right) - \delta_i\left(\frac{K_{iL}^2}{M_1}\tilde{a}_{iL} - \frac{K_{iR}^2}{M_2}\tilde{a}_{iR}\right), \end{aligned} \tag{11.31a}$$

$$\mathcal{I} = \left(\omega^2 - \frac{\omega_{i+}^2 + \omega_{i-}^2}{2}\right)\left(\frac{K_{iL}^2}{M_1}\tilde{b}_{iL} + \frac{K_{iR}^2}{M_2}\tilde{b}_{iR}\right) + \delta_i\left(\frac{K_{iL}^2}{M_1}\tilde{b}_{iL} - \frac{K_{iR}^2}{M_2}\tilde{b}_{iR}\right) - \frac{K_{iL}^2}{M_1}\frac{K_{iR}^2}{M_2}(\tilde{b}_{iL}\tilde{a}_{iR} + \tilde{b}_{iR}\tilde{a}_{iL}), \tag{11.31b}$$

$$\omega_{i\pm}^2 = \frac{\omega_{i1}^2 + \omega_{i2}^2}{2} \pm \Delta_i, \quad \Delta_i = \sqrt{\delta_i^2 + V_{i1,i2}^2}, \quad \delta_i = \frac{\omega_{i1}^2 - \omega_{i2}^2}{2}, \tag{11.31c}$$

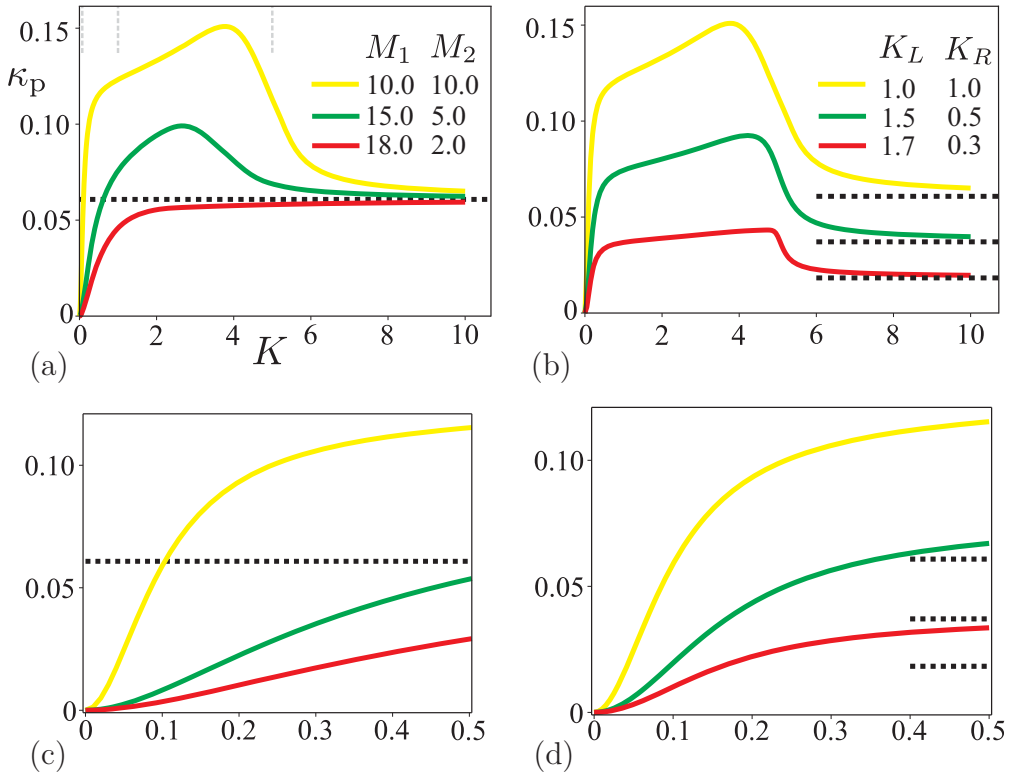

Figure 11.3: Phonon conductance κ_p dependence on the middle spring constant in y direction. The units of phonon conductance κ_p and spring constant K are $\kappa_0 = 49$ pW/K and $K_0 = 12.7$ N/m. Also in a) the couplings to the leads are $K_L = K_R = 1.0$ and in b) the masses are $M_1 = M_2 = 10.0$. Figures c) and d) show zoom of phonon conductance for small values of K of e) and f), respectively. We want to use particular molecules, which have spring constants below the black dotted lines, corresponding to a model with a single mass in the junction.

The frequencies $\omega^2_{i\pm}$ correspond to normal vibrational modes and are derived in Appendix G.

Now we will discuss the saturated phonon conductance (11.22) dependence on the parameters of the model. We note that in calculations we use elastic parameters for gold (Au), which has mass density $\rho = 19.3$ kg/cm^3, Young modulus $E_Y = 77.5$ GPa, and Poisson ratio $\sigma = 0.42$ [139, 140]. These elastic parameters yield the longitudinal velocity $c_l = \sqrt{E_Y(1-\sigma)/\rho(1+\sigma)(1-2\sigma)} \approx 3.20$ km/s and transverse velocity $c_t = \sqrt{E_Y/\rho(1+\sigma)} \approx 1.19$ km/s. We use bulk Debye temperature $T_D = 170$ K for frequency cut-off, which corresponds to $\omega_D \approx 22.2$ THz [54]. The units of spring constant, mass, and heat conductance respectively are: $K_0 = 1/A_\perp \omega_D \approx 12.7$ N/m, $M_0 = 1/A_\perp \omega_D^3 \approx 15.3 m_H$, $\kappa_0 = k_B \omega_D / 2\pi \approx 49$ pW/K, where m_H is the mass of a hydrogen atom and $A_\perp = 1.445/4\pi\rho c_t^3$.

Figure 11.3 shows the typical phonon conductance dependence on the middle spring constant in the y direction. Figure 11.3a depicts this dependence for different masses asymmetry, fixed total mass $M = M_1 + M_2$, and symmetric coupling to the leads $K_L = K_R$. In the case of symmetric masses $M_1 = M_2$ the conductance overshoots the value of conductance compared to when there is a single mass in the junction. However, if the masses are very asymmetric, this overshooting does not happen. The situation when masses are symmetric $M_1 = M_2$, but the coupling to the leads is changed is shown in Figure 11.3b. In this case we see that the more asymmetric the couplings the more the phonon conductance is reduced (the sum of the couplings to the left K_L and the right K_R

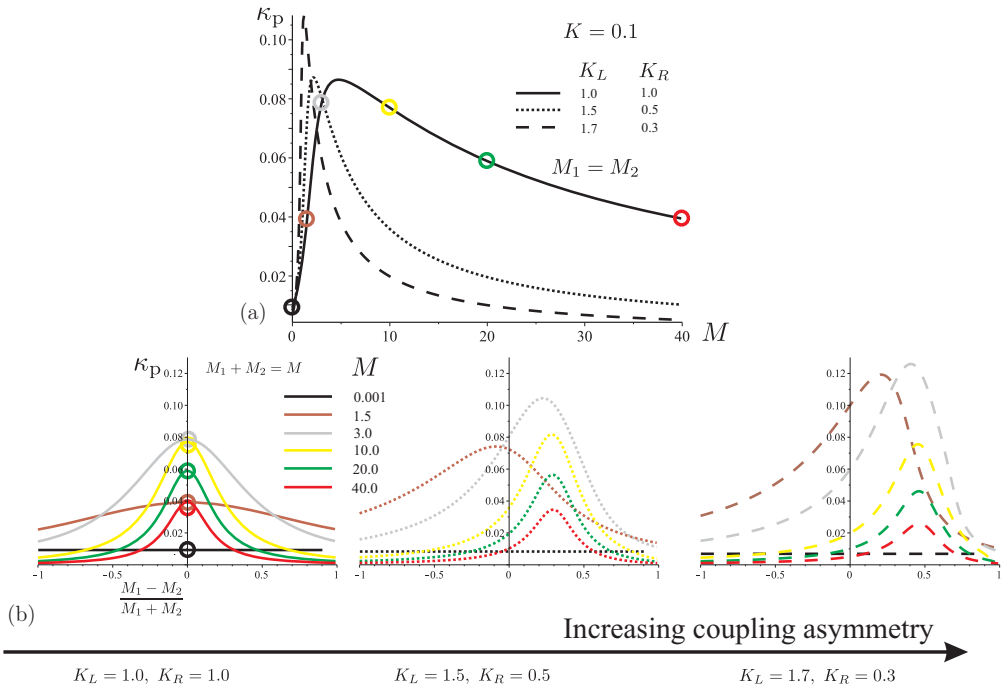

Figure 11.4: a) Conductance dependence on total mass $M = M_1 + M_2$, when the masses are symmetric $M/2 = M_1 = M_2$. b) Conductance dependence on masses asymmetry when total mass is being fixed.

leads is being kept constant). We note that in the considered model the transmission separates for different directions $\mathcal{T}_\mathrm{p} = \mathcal{T}_\mathrm{p}^x + \mathcal{T}_\mathrm{p}^y + \mathcal{T}_\mathrm{p}^z$ and that for z and x directions the dependence is analogous. As we can see from the typical behavior in Figure 11.3c,d our aim is to have phonon conductance below the dotted black line corresponding to conductance with single mass $M = M_1 + M_2$ in the junction.

The dependence on the total mass when the masses are symmetric is depicted in Figure 11.4a, 11.5a, 11.6a for different middle spring constants K corresponding to values shown by gray vertical lines in Figure 11.3a. The heat conductance decreases with increasing total mass, except for the region of very small masses, which correspond to the case when the frequencies $\omega_{i\pm}$ are pushed out of the interval $[0, \omega_D]$. For symmetric coupling to the leads for fixed mass sum $M = M_1 + M_2$ the conductance tends to go down with increased masses asymmetry as can be seen in Figure 11.4b, 11.5b, 11.6b. However, if the coupling to the leads is asymmetric the heat conductance maximum is being shifted. For example, if $K_L > K_R$, then the maximum will appear for $M_1 > M_2$ [the relevant parameters to determine this are K_L/M_1 and K_R/M_2 as can be seen from expressions (11.31a) and (11.31b)]. The effect of coupling strength to the leads is shown in Figure 11.7a, 11.8a, and on coupling asymmetry in Figure 11.7b, 11.8b. It can have all sorts of behaviors depending on the actual values of K and $K_l = K_L + K_R$.

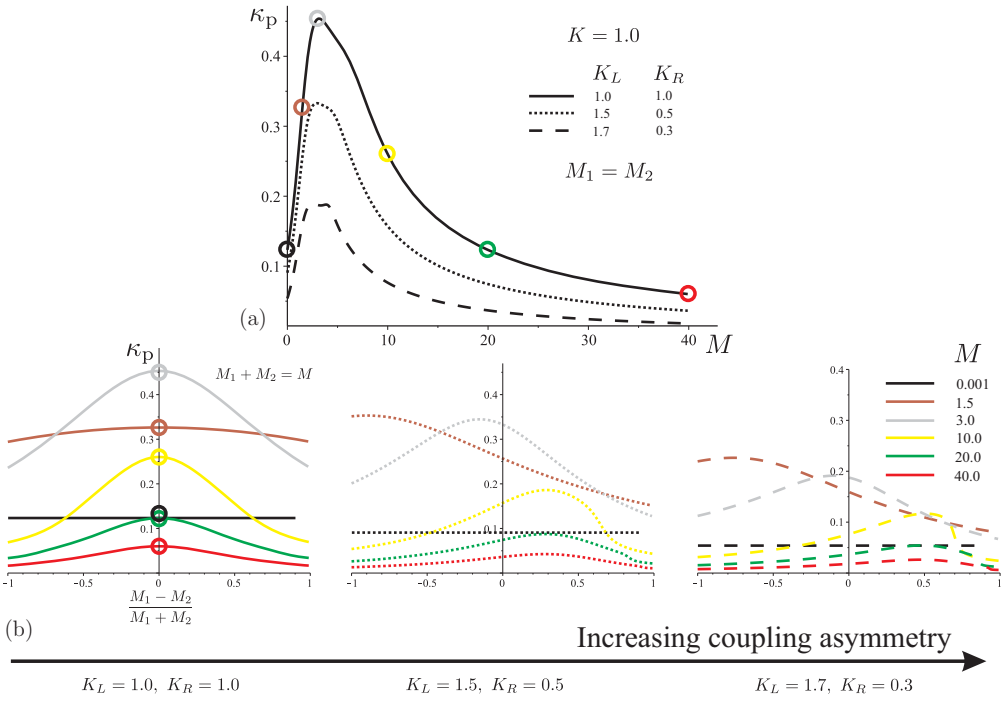

Figure 11.5: The same as Figure 11.4 only with $K = 1.0$

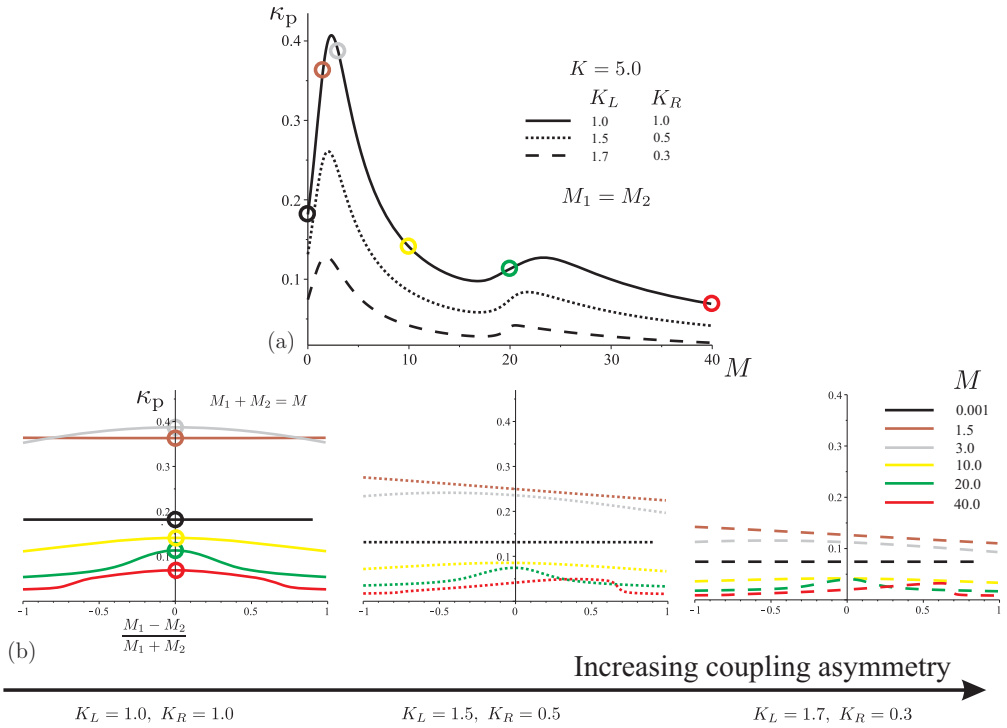

Figure 11.6: The same as Figure 11.4 only with $K = 5.0$

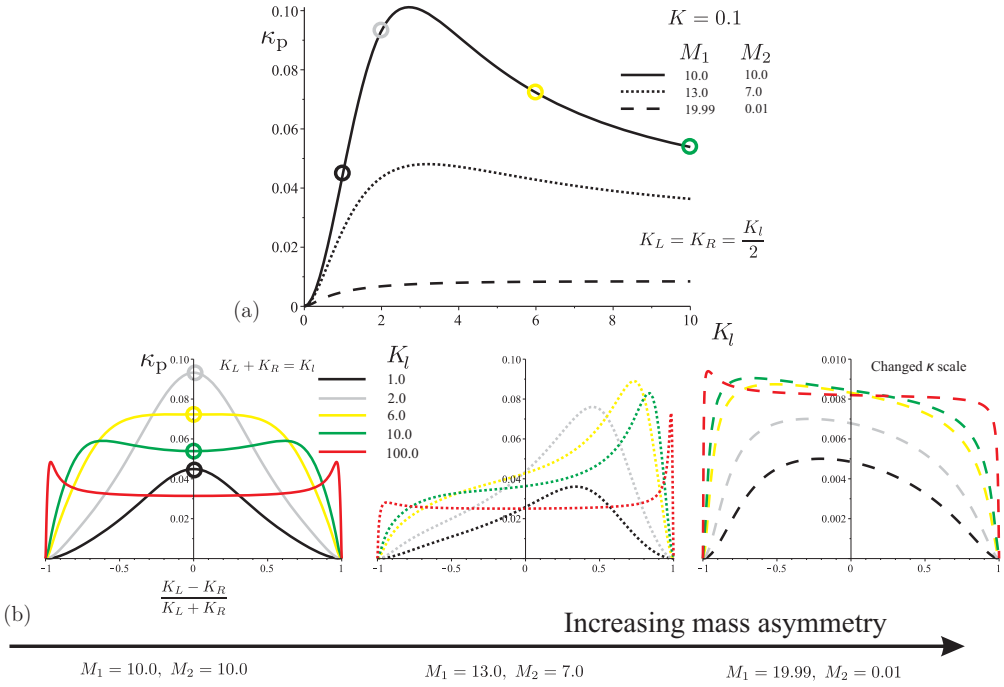

Figure 11.7: a) Conductance dependence on total coupling to the leads $K_l = K_L + K_R$, when the couplings are symmetric $K_l/2 = K_L = K_R$. b) Conductance dependence on coupling asymmetry when total coupling is being fixed.

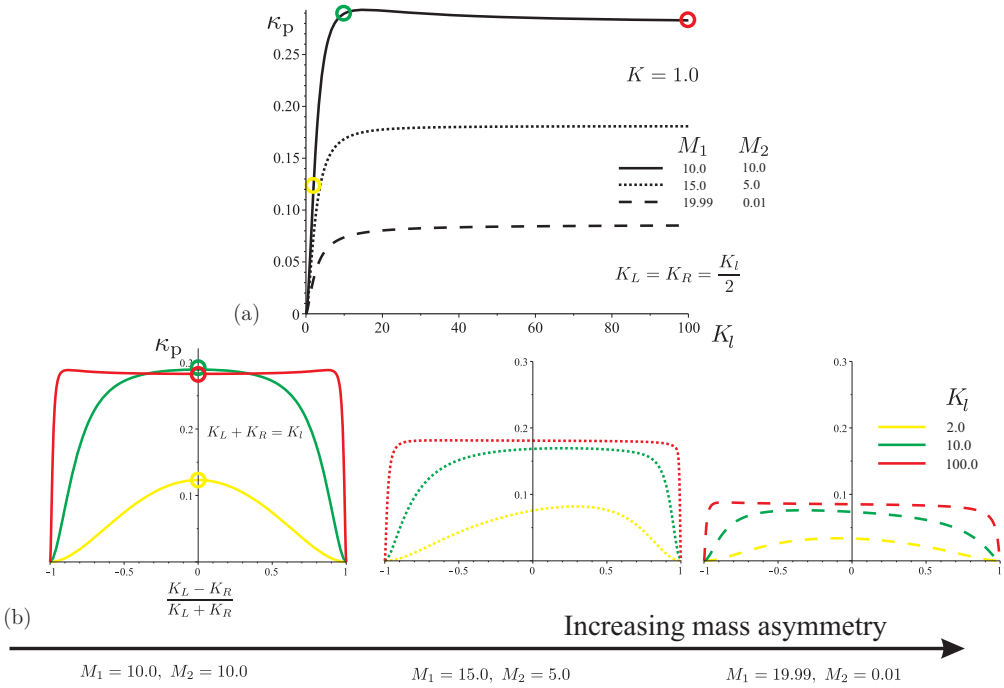

Figure 11.8: The same as Figure 11.7 only with $K = 1.0$

11.2 Figure of merit ZT

To describe the thermoelectric efficiency of the molecules in the junction, we will calculate the dimensionless figure of merit ZT, which is given by [141]

$$ZT = \frac{S^2 \sigma_e T}{\kappa_e + \kappa_p}, \tag{11.32}$$

where S is the Seebeck coefficient, σ_e is the electronic conductance, κ_e is the electron contribution to the thermal conductance, and T denotes temperature. The numerator in Eq. (11.32) gives the power production of the device and the denominator is a measure of the heat current. Because we neglect the electron-phonon coupling in our calculations, the quantities S, σ_e, and κ_e will be expressed through the electron transmission $\mathcal{T}_e(E)$ [142–144]. Once the electron transmission function $\mathcal{T}_e(E)$ is known the electric and heat currents due to electrons can be expressed using Landauer-Büttiker type expressions

$$I_e = -\frac{2e}{h}\int_{-\infty}^{+\infty} \mathrm{d}E (f_L - f_R)\mathcal{T}_e(E), \tag{11.33a}$$

$$Q_e = \frac{2}{h}\int_{-\infty}^{+\infty} \mathrm{d}E (E - \mu_{\mathrm{hot}})(f_L - f_R)\mathcal{T}_e(E), \tag{11.33b}$$

where $f_\alpha = 1/\{\exp[\beta_\alpha(E-\mu_\alpha)]+1\}$ is the Fermi-Dirac distribution, e denotes the absolute value of the electron charge, and μ_{hot} is the chemical potential of the hot lead. If the temperature difference $\Delta T = T_L - T_R$ and the applied bias $\Delta V = -\Delta\mu/e = -(\mu_L - \mu_R)/e$ are small compared to $T = (T_L + T_R)/2$ and $\mu = (\mu_L + \mu_R)/2$, i.e., $|\Delta T/T| \ll 1$ and $|\Delta\mu/\mu| \ll 1$, then we can expand the distribution function f_α to lowest order around a point (μ, T) as

$$\begin{aligned} f(\mu_\alpha, T_\alpha) &\approx f(\mu,T) + \frac{\partial f(\mu,T)}{\partial \mu}(\mu_\alpha - \mu) + \frac{\partial f(\mu,T)}{\partial T}(T_\alpha - T) \\ &= f(\mu,T) - \frac{\partial f(\mu,T)}{\partial E}(\mu_\alpha - \mu) - \frac{\partial f(\mu,T)}{\partial E}(E-\mu)\frac{T_\alpha - T}{T}. \end{aligned} \tag{11.34}$$

Using the above relation the difference between Fermi-Dirac distributions becomes

$$-(f_L - f_R) \approx \frac{\partial f(E,\mu,T)}{\partial E}\Delta\mu + \frac{\partial f(E,\mu,T)}{\partial E}(E-\mu)\frac{\Delta T}{T}, \tag{11.35}$$

and the electrical with the heat currents given in Eq. (11.33) can be expressed as

$$I_e \approx e^2 L_0 \Delta V - eL_1 \frac{\Delta T}{T}, \tag{11.36a}$$

$$Q_e \approx -eL_1 \Delta V + L_2 \frac{\Delta T}{T}, \tag{11.36b}$$

where

$$L_m = \frac{2}{h}\int_{-\infty}^{+\infty} \mathrm{d}E (E-\mu)^m \left(-\frac{\partial f(E,\mu,T)}{\partial E}\right)\mathcal{T}_e(E). \tag{11.37}$$

Then the linear transport coefficients S, σ_e, and κ_e are determined in the following way

$$\sigma_e = \left.\frac{I_e}{\Delta V}\right|_{\Delta T = 0} = e^2 L_0, \tag{11.38a}$$

$$S = -\left.\frac{\Delta V}{\Delta T}\right|_{I_e = 0} = -\frac{1}{eT}\frac{L_1}{L_0}, \tag{11.38b}$$

$$\kappa_e = \left.\frac{Q_e}{\Delta T}\right|_{I_e = 0} = \frac{1}{T}\left(L_2 - \frac{L_1^2}{L_0}\right). \tag{11.38c}$$

11.3 π-stacked molecules

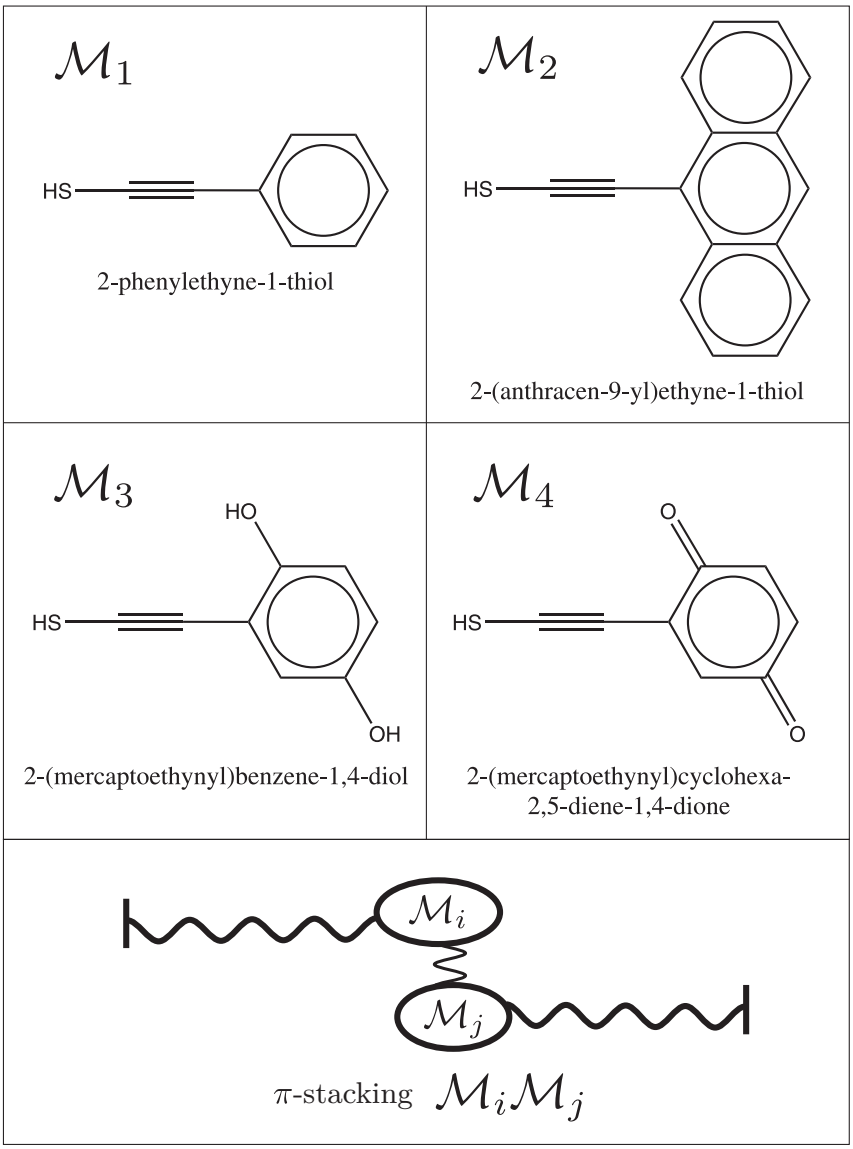

Figure 11.9: The considered molecules for π-stacking.

Having discussed in Section 11.1.2 how the molecules can be divided into two parts to reduce the phonon conductance κ_p we try to come up with some molecular structures where these conditions are realized (see Figure 11.3). In this section we propose that this could be achieved by π-stacked molecules, where we hope that π-stacking yields soft mechanical connection (weak spring constant) between two masses. The considered molecules for π-stacking are shown in Figure 11.9. We examine the following four stackings $\mathcal{M}_1\mathcal{M}_1$, $\mathcal{M}_1\mathcal{M}_2$, $\mathcal{M}_2\mathcal{M}_2$, and $\mathcal{M}_3\mathcal{M}_4$. We note that all spring constants were obtained using density functional theory (DFT) by finding the energy landscape for the molecules and then it is fitted to Hook's law.[1] The obtained coupling to the leads for all

[1]The DFT calculations were performed by Qian Li and Gemma C. Solomon and details of the calculations are presented in Ref. [145].

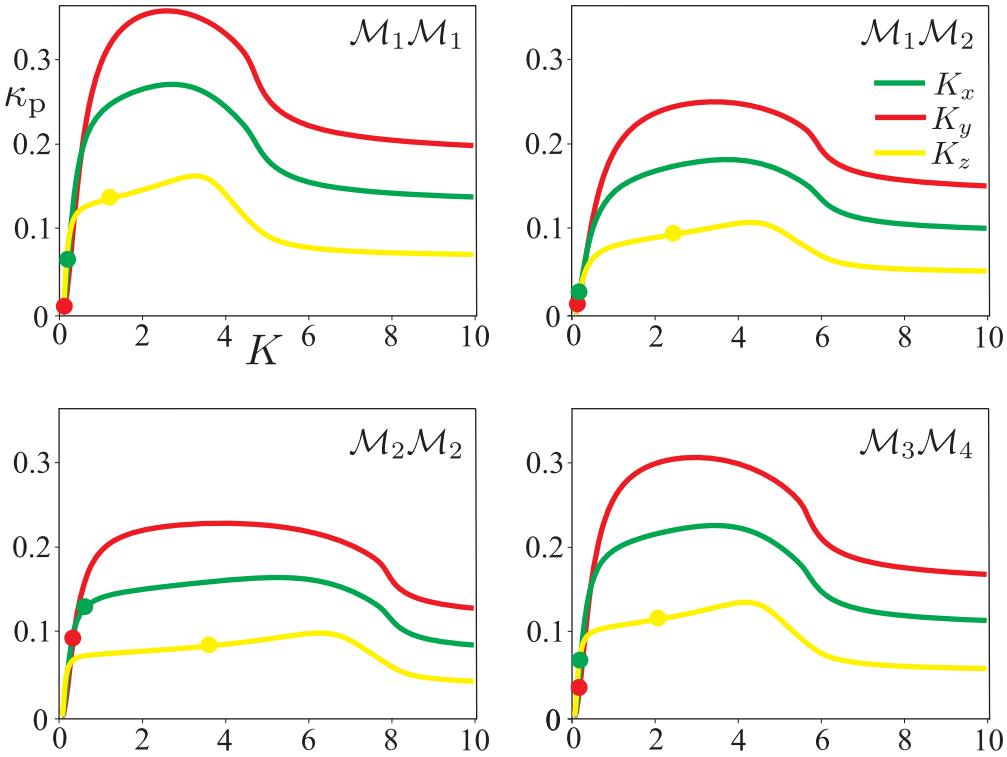

Figure 11.10: The dependence of the phonon conductance for arbitrary middle spring constants K_i in different directions for considered stackings. Solid circles denote the conductance calculated with the middle spring constants obtained from DFT, which are summarized in Table 11.1. The units of phonon conductance κ_p and spring constant K are $\kappa_0 = 49$ pW/K and $K_0 = 12.7$ N/m.

stackings is symmetric $K_{iL} = K_{iR} = K_{iS}$ and the same: $K_{xS} = 1.789K_0$, $K_{yS} = 3.349K_0$, $K_{zS} = 0.945K_0$. The dependence of the phonon conductance for arbitrary middle spring constants K_i for considered stackings is shown in Figure 11.10, where solid circles denote the conductance calculated with the middle spring constants obtained from DFT. The values of K_i, the resulting phonon conductances κ^i_{two}, κ^i_{one} in three different directions, and comparison of total phonon conductance κ_{two} between two masses and a single mass $M = M_1 + M_2$ conductance κ_{one} is summarized in Table 11.1.

We see that for all molecules, due to the small middle spring constant, the conductance is significantly reduced in the y direction compared to the case if there would be a single mass in the junction. Also the phonon density of states and the coupling to the leads is the largest in the y direction. In all cases in the z direction and for stackings $\mathcal{M}_2\mathcal{M}_2$, $\mathcal{M}_3\mathcal{M}_3$ in the x direction the conductance is larger than in the single mass case. However, due to the large reduction in the y direction the overall phonon conductance becomes smaller for the stackings $\mathcal{M}_1\mathcal{M}_1$, $\mathcal{M}_1\mathcal{M}_2$, $\mathcal{M}_3\mathcal{M}_4$. Note that the largest reduction is for stacking $\mathcal{M}_1\mathcal{M}_2$, which has asymmetric masses. So the suggested mechanism for reduction of phonon conductance is partially exploited with π-stacked molecules.

To describe the thermoelectric efficiency of π-stacked molecules in the junction, we calculate the dimensionless figure of merit ZT, which is given by Eq. (11.32). The resulting ZT as a function of chemical potential μ at room temperature $T = 300$ K for all considered stackings is depicted in Figure 11.11, when the electron transmission $\mathcal{T}_e(E)$ is calculated using DFT. For the stacking $\mathcal{M}_1\mathcal{M}_2$, which had the largest reduction in phonon conductance, we see that the optimized values

	$\mathcal{M}_1\mathcal{M}_1$	$\mathcal{M}_1\mathcal{M}_2$	$\mathcal{M}_2\mathcal{M}_2$	$\mathcal{M}_3\mathcal{M}_4$
K_x	0.137	0.129	0.568	0.147
K_y	0.056	0.090	0.275	0.129
K_z	1.161	2.414	3.586	2.041
κ^x_{two}	0.062	0.024	0.129	0.065
κ^y_{two}	0.007	0.010	0.092	0.033
κ^z_{two}	0.135	0.093	0.083	0.114
κ^x_{one}	0.126	0.093	0.073	0.103
κ^y_{one}	0.182	0.138	0.111	0.152
κ^z_{one}	0.066	0.047	0.037	0.053
κ_{two}	0.204	0.127	0.304	0.212
κ_{one}	0.374	0.278	0.221	0.308

Table 11.1: The values of the middle spring constant K_i obtained from DFT, the resulting phonon conductances κ^i_{two}, κ^i_{one} in three different directions, and comparison of total phonon conductance κ_{two} between two masses and a single mass phonon conductance κ_{one}. The blue values of conductance denote situation when $\kappa_{\text{two}} < \kappa_{\text{one}}$ and the red ones *vice versa*.

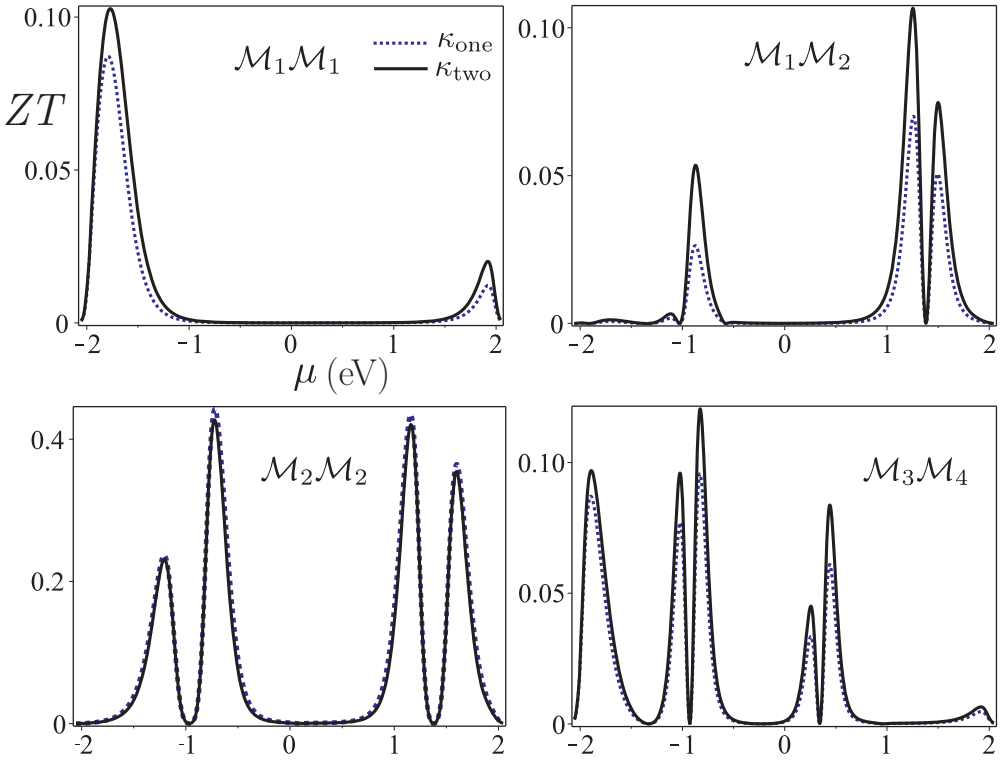

Figure 11.11: The figure of merit ZT dependence on the chemical potential μ at room temperature $T = 300$ K for all considered stackings with electronic transmission $\mathcal{T}_e(E)$ obtained from DFT. The solid black curves show ZT when system has a weak link in the middle (two masses model) and dashed blue curves show ZT when the center of mass vibrational degrees of freedom are described by single mass in the junction.

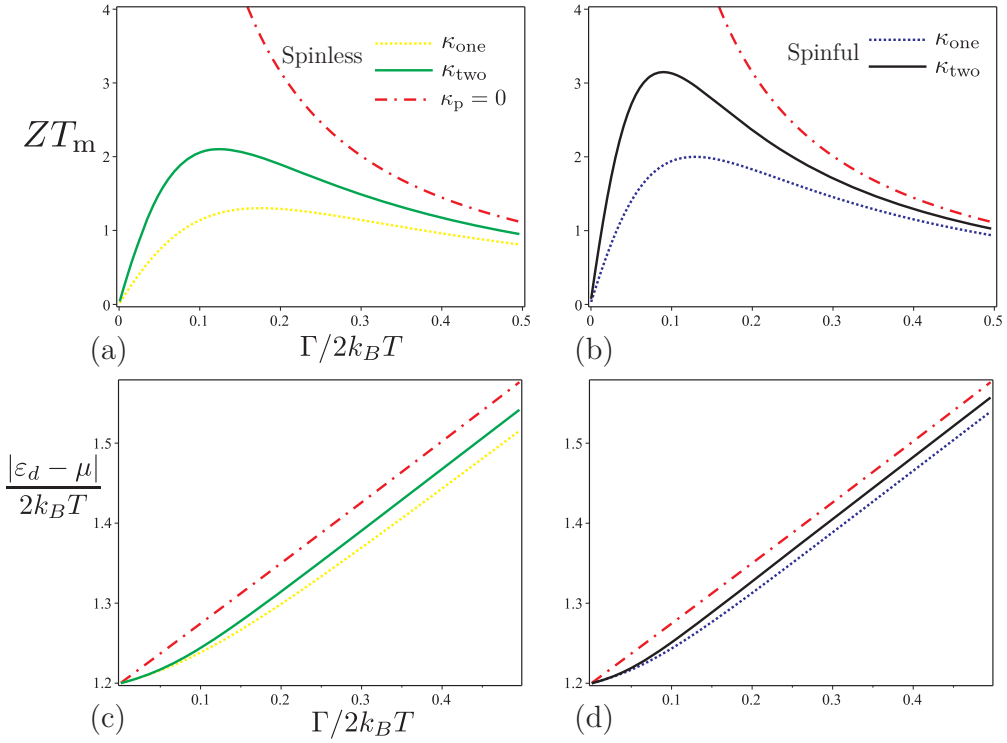

Figure 11.12: a), b) Maximal figure of merit $ZT_{\rm m}$ dependence on the coupling strength Γ, for the stacking $\mathcal{M}_1\mathcal{M}_2$, when spinful resonant level electronic transmission $\mathcal{T}_{\rm e}(E)$ is used. The red dashed-dotted line gives behavior of $ZT_{\rm m}$ when there is no phonon conductance $\kappa_{\rm p}=0$. c), d) The position of the level ε_d with respect to the chemical potential of the leads μ at which ZT is maximized.

of ZT are considerably increased compared to the case of a single mass in the junction. For all other stackings the main contribution to the thermal transport comes from electrons, and the effect of a change in the phonon conductance is not substantial. We also see that the values of ZT for the examined molecules are not large, which is, however, mainly due to the electronic properties. One possibility of increasing ZT is to reduce the electronic coupling to the leads, which can be done without significantly altering the mechanical coupling. It has been shown [7, 117, 146, 147] that in the limit of a small electronic coupling, ZT in Eq. (11.32) becomes infinite if the molecular resonances can be correctly positioned relative to the lead Fermi level and if $\kappa_{\rm p}$ is neglected. In this case, the efficiency is limited only by the phonon heat current and our mechanism can lead to a large improvement. To illustrate this we show in Figure 11.12 the maximal $ZT_{\rm m}$ value dependence on the coupling strength, for the stacking $\mathcal{M}_1\mathcal{M}_2$, when the electron transmission has the form of resonant level, i.e.,

$$\mathcal{T}_{\rm e}(E)=\frac{\Gamma^2}{(E-\varepsilon_d)^2+\Gamma^2}, \tag{11.39}$$

where ε_d is the position of the level and Γ denotes coupling strength to the leads. Here the difference between spinful and spinless cases is that for spinless case we use functions L_m Eq. (11.37) without a factor of 2. We note that the Coulomb interactions do not alter the result very much, the only thing is that the resonant level effectively becomes spinless, as was shown by Leijnse *et al.* [148].

Conclusions for Part III

In the third part of the thesis we have examined molecular junctions used as thermoelectric devices, where we have addressed a question of reducing the phonon conductance due to center of mass vibrational modes of the molecule. So we have proposed a simple mechanism, which is based on the idea of vibrationally decoupling the left lead from the right lead (see Figure 9.1). This is achieved by dividing the system into two sub-units, which have a soft mechanical connection between them (small spring constant). Of course, in order to be a good thermoelectric device the junction should maintain electrical conductivity. To describe and to analyze the possible reduction of the phonon conductance as a function of different parameters (masses of the molecules and spring constants) we have set up a simplified model for which the exact transmission for phonons is obtained. As a possible realization of the mechanism we have examined π-stacked molecules, which partially exploit the suggested mechanism. The relevant spring constants needed to describe the junction with π-stacked molecules were obtained using density functional theory (DFT).

Part IV

Appendices

Appendix A

Finite temperature integral appearing in second order expansion

In this Appendix we describe the calculation of the integral

$$I = \int_{-D}^{D} \frac{f(\xi)\mathrm{d}\xi}{\xi + a + \mathrm{i}\eta} = \int_{-\beta D}^{\beta D} \frac{f(x/\beta)\mathrm{d}x}{x + \beta a + \mathrm{i}\beta\eta} \quad \rightarrow \quad \int_{-R}^{R} \frac{\mathrm{d}x}{(\mathrm{e}^{x}+1)(x+\alpha+\mathrm{i}\eta)} \tag{A.1}$$

for finite temperature. Here $\mathrm{i}\eta = +\mathrm{i}0$ is infinitesimal imaginary part so after the arrow we have replaced $\mathrm{i}\beta\eta \rightarrow \mathrm{i}\eta$, and denoted $\alpha = \beta a$, $R = \beta D$. We are interested in asymptotic value of integral I, when $R \rightarrow +\infty$ and $R >> |\alpha|$. We go to complex plane and apply contour depicted in Figure A.1, where we will let $j \rightarrow +\infty$, $j \in \mathbb{N}$. According to residue theorem the integral around this contour is equal to $2\pi\mathrm{i}$ times the sum of all residues enclosed by this contour, which yields

$$I + I_1 + I_2 + I_3 = -2\pi\mathrm{i} \sum_{n=0}^{j-1} \frac{1}{(2n+1)\pi\mathrm{i} + \alpha + \mathrm{i}\eta} \overset{\eta\rightarrow+0}{=} \Psi_0\left(\frac{1}{2} + \frac{\alpha}{2\pi\mathrm{i}}\right) - \Psi_0\left(j + \frac{1}{2} + \frac{\alpha}{2\pi\mathrm{i}}\right), \tag{A.2}$$

where we used that all residues appear due to poles of Fermi function $\frac{1}{\mathrm{e}^{z}+1}$, which are at $z_0 = (2n+1)\pi\mathrm{i}$, $k \in \mathbb{N}$, and

$$\operatorname{Res} \frac{(\mathrm{e}^{z_0}+1)^{-1}}{(z_0+\alpha+\mathrm{i}\eta)} = -\frac{1}{(2n+1)\pi\mathrm{i} + \alpha + \mathrm{i}\eta}. \tag{A.3}$$

We also expressed the sum in (A.2) in terms of digamma function defined as

$$\Psi_0(z) = -\gamma + \sum_{n=0}^{\infty} \left(\frac{1}{n+1} - \frac{1}{n+z}\right) \tag{A.4}$$

where $\gamma \approx 0.577$ is Euler-Mascheroni constant.

$$I_1 \overset{\substack{j\rightarrow+\infty \\ \eta\rightarrow+0}}{=} \int_0^{+\infty} \frac{\mathrm{i}\mathrm{d}y}{(\mathrm{e}^{\mathrm{i}y+R}+1)(\mathrm{i}y+R+\alpha)} \approx \mathrm{i}\mathrm{e}^{-R} \int_0^{+\infty} \frac{\mathrm{e}^{-\mathrm{i}y}\mathrm{d}y}{\mathrm{i}y+R+\alpha} = \mathrm{E}_1(R+\alpha)\mathrm{e}^{\alpha} \approx \frac{\mathrm{e}^{-R}}{R} \rightarrow 0, \tag{A.5a}$$

$$I_2 \overset{\eta\rightarrow+0}{=} -\int_{-R}^{R} \frac{\mathrm{d}x}{(\mathrm{e}^{2\pi\mathrm{i}j+x}+1)(2\pi\mathrm{i}j+x+\alpha)} \overset{j\rightarrow+\infty}{\longrightarrow} 0, \tag{A.5b}$$

$$I_3 \overset{\eta\rightarrow+0}{=} -\int_0^{+2\pi j} \frac{\mathrm{i}\mathrm{d}y}{(\mathrm{e}^{\mathrm{i}y-R}+1)(\mathrm{i}y-R+\alpha)} \approx -\int_0^{+2\pi j} \frac{\mathrm{i}\mathrm{d}y}{\mathrm{i}y-R} = -\ln\sqrt{1+\left(\frac{2\pi j}{R}\right)^2} + \mathrm{i}\arctan\left(\frac{2\pi j}{R}\right), \tag{A.5c}$$

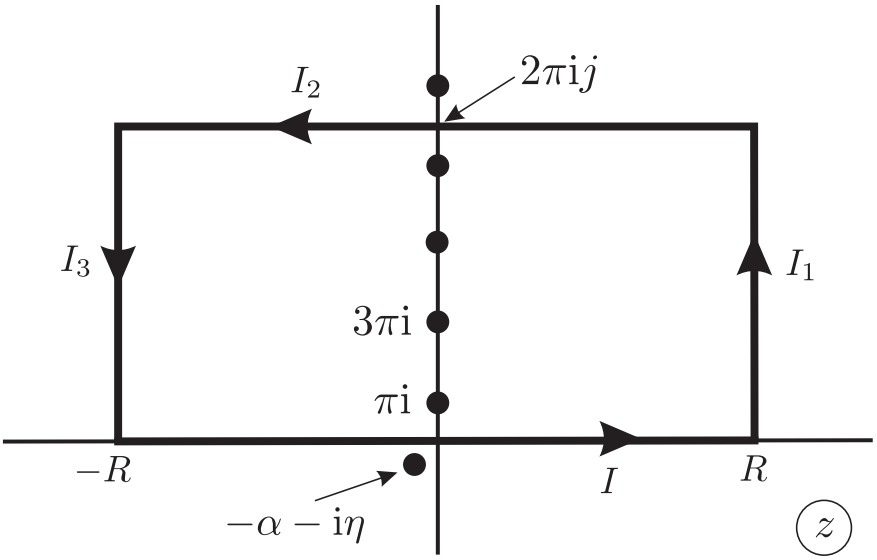

Figure A.1: Contour, which is used to calculate the integral (A.1).

where we used the following asymptotic expansion

$$\mathrm{E}_1(x) \overset{x\to+\infty}{=} \mathrm{e}^{-x}\left[\frac{1}{x} + O\left(\frac{1}{x^2}\right)\right]. \tag{A.6}$$

Now combining (A.2) with (A.5) and taking the $j \to +\infty$ limit afterwards we get

$$\boxed{I \approx \Psi_0\left(\frac{1}{2} + \frac{\alpha}{2\pi\mathrm{i}}\right) - \ln\frac{R}{2\pi} - \mathrm{i}\frac{\pi}{2} = \mathrm{Re}\left[\Psi_0\left(\frac{1}{2} + \frac{\alpha}{2\pi\mathrm{i}}\right)\right] - \ln\frac{R}{2\pi} - \mathrm{i}\pi f(\alpha)}, \tag{A.7}$$

where the following asymptotic expansion was used

$$\Psi_0(x) \overset{x\to+\infty}{=} \ln(x) + O\left(\frac{1}{x}\right), \tag{A.8}$$

and the identity

$$\mathrm{Im}\left[\Psi_0\left(\frac{1}{2} + \mathrm{i}x\right)\right] = \frac{\pi}{2}\tanh(\pi x) = \pi\left(\frac{1}{2} - f(2\pi x)\right), \quad f(x) = \frac{1}{\mathrm{e}^x + 1}. \tag{A.9}$$

Appendix B

Fourth order corrections to energy shifts

In this Appendix we examine fourth order term

$$
\begin{aligned}
H^{(4)}_{mm'} = \frac{1}{2}\sum_{l,l',l''} H^{\mathrm{T}}_{ml}H^{\mathrm{T}}_{ll'}H^{\mathrm{T}}_{l'l''}H^{\mathrm{T}}_{l''m'}\left[\frac{1}{(E_m-E_l)(E_m-E_{l'})(E_m-E_{l''})}+\frac{1}{(E_{m'}-E_l)(E_{m'}-E_{l'})(E_{m'}-E_{l''})}\right] \\
+\sum_{l,l',m''} H^{\mathrm{T}}_{ml}H^{\mathrm{T}}_{lm''}H^{\mathrm{T}}_{m''l'}H^{\mathrm{T}}_{l'm'}\left[\frac{8}{(E_m-E_l)(E_m-E_{l'})(E_{m''}-E_{l'})}+\frac{8}{(E_{m'}-E_l)(E_{m'}-E_{l'})(E_{m''}-E_l)}\right. \\
+\frac{4}{(E_m-E_{l'})(E_{m''}-E_l)}\left(\frac{1}{E_m-E_l}+\frac{1}{E_{m''}-E_{l'}}\right)+\frac{4}{(E_{m'}-E_l)(E_{m''}-E_{l'})}\left(\frac{1}{E_{m'}-E_{l'}}+\frac{1}{E_{m''}-E_l}\right) \\
\left.-\frac{1}{(E_{m''}-E_l)(E_{m''}-E_{l'})}\left(\frac{1}{E_m-E_l}+\frac{1}{E_{m'}-E_{l'}}\right)-\frac{3}{(E_m-E_l)(E_{m'}-E_{l'})}\left(\frac{1}{E_{m''}-E_l}+\frac{1}{E_{m''}-E_{l'}}\right)\right].
\end{aligned}
\tag{B.1}
$$

of perturbation expansion in tunneling Hamiltonian H_{T}.

B.1 1st Expression

We start by considering term of the form

$$
\frac{1}{2}\sum_{l,l',l''} H^{\mathrm{T}}_{ml}H^{\mathrm{T}}_{ll'}H^{\mathrm{T}}_{l'l''}H^{\mathrm{T}}_{l''m'}\left[\frac{1}{(E_m-E_l)(E_m-E_{l'})(E_m-E_{l''})}+\frac{1}{(E_{m'}-E_l)(E_{m'}-E_{l'})(E_{m'}-E_{l''})}\right], \tag{B.2}
$$

where we will use following notation for tunneling Hamiltonian

$$
H_{\mathrm{T}} = \sum_{ab}\left(t_{ab}c^{\dagger}_a d_b + t^{*}_{ab}d^{\dagger}_b c_a\right), \tag{B.3}
$$

with short-hand notations:

$$
a = \alpha\nu\sigma, \quad b = n, \quad t_{ab} = t^{n}_{\alpha\nu\sigma}. \tag{B.4}
$$

The only non-vanishing terms are of the type

$$
t_{a_1b_1}t_{a_2b_2}t^{*}_{a_3b_3}t^{*}_{a_4b_4}\langle m|c^{\dagger}_1d_1|l\rangle\langle l|c^{\dagger}_2d_2|l'\rangle\langle l'|d^{\dagger}_3c_3|l''\rangle\langle l''|d^{\dagger}_4c_4|m'\rangle \tag{B.5a}
$$

$$
t^{*}_{a_1b_1}t^{*}_{a_2b_2}t_{a_3b_3}t_{a_4b_4}\langle m|d^{\dagger}_1c_1|l\rangle\langle l|d^{\dagger}_2c_2|l'\rangle\langle l'|c^{\dagger}_3d_3|l''\rangle\langle l''|c^{\dagger}_4d_4|m'\rangle \tag{B.5b}
$$

$$
t_{a_1b_1}t^{*}_{a_2b_2}t_{a_3b_3}t^{*}_{a_4b_4}\langle m|c^{\dagger}_1d_1|l\rangle\langle l|d^{\dagger}_2c_2|l'\rangle\langle l'|c^{\dagger}_3d_3|l''\rangle\langle l''|d^{\dagger}_4c_4|m'\rangle \tag{B.5c}
$$

$$
t^{*}_{a_1b_1}t_{a_2b_2}t^{*}_{a_3b_3}t_{a_4b_4}\langle m|d^{\dagger}_1c_1|l\rangle\langle l|c^{\dagger}_2d_2|l'\rangle\langle l'|d^{\dagger}_3c_3|l''\rangle\langle l''|c^{\dagger}_4d_4|m'\rangle \tag{B.5d}
$$

$$
t_{a_1b_1}t^{*}_{a_2b_2}t^{*}_{a_3b_3}t_{a_4b_4}\langle m|c^{\dagger}_1d_1|l\rangle\langle l|d^{\dagger}_2c_2|l'\rangle\langle l'|d^{\dagger}_3c_3|l''\rangle\langle l''|c^{\dagger}_4d_4|m'\rangle \tag{B.5e}
$$

$$
t^{*}_{a_1b_1}t_{a_2b_2}t_{a_3b_3}t^{*}_{a_4b_4}\langle m|d^{\dagger}_1c_1|l\rangle\langle l|c^{\dagger}_2d_2|l'\rangle\langle l'|c^{\dagger}_3d_3|l''\rangle\langle l''|d^{\dagger}_4c_4|m'\rangle, \tag{B.5f}
$$

and they can be rewritten as

$$t_{a_1b_1}t_{a_2b_2}t^*_{a_3b_3}t^*_{a_4b_4}\langle\mathcal{D}|d_1|\delta\rangle\langle\delta|d_2|\delta'\rangle\langle\delta'|d_3^\dagger|\delta''\rangle\langle\delta''|d_4^\dagger|\mathcal{D}'\rangle\times\langle\mathrm{LR}|c_1^\dagger|\lambda\rangle\langle\lambda|c_2^\dagger|\lambda'\rangle\langle\lambda'|c_3|\lambda''\rangle\langle\lambda''|c_4|\mathrm{LR}\rangle \tag{B.6a}$$

$$t^*_{a_1b_1}t^*_{a_2b_2}t_{a_3b_3}t_{a_4b_4}\langle\mathcal{D}|d_1^\dagger|\delta\rangle\langle\delta|d_2^\dagger|\delta'\rangle\langle\delta'|d_3|\delta''\rangle\langle\delta''|d_4|\mathcal{D}'\rangle\times\langle\mathrm{LR}|c_1|\lambda\rangle\langle\lambda|c_2|\lambda'\rangle\langle\lambda'|c_3^\dagger|\lambda''\rangle\langle\lambda''|c_4^\dagger|\mathrm{LR}\rangle \tag{B.6b}$$

$$t_{a_1b_1}t^*_{a_2b_2}t_{a_3b_3}t^*_{a_4b_4}\langle\mathcal{D}|d_1|\delta\rangle\langle\delta|d_2^\dagger|\delta'\rangle\langle\delta'|d_3|\delta''\rangle\langle\delta''|d_4^\dagger|\mathcal{D}'\rangle\times\langle\mathrm{LR}|c_1^\dagger|\lambda\rangle\langle\lambda|c_2|\lambda'\rangle\langle\lambda'|c_3^\dagger|\lambda''\rangle\langle\lambda''|c_4|\mathrm{LR}\rangle \tag{B.6c}$$

$$t^*_{a_1b_1}t_{a_2b_2}t^*_{a_3b_3}t_{a_4b_4}\langle\mathcal{D}|d_1^\dagger|\delta\rangle\langle\delta|d_2|\delta'\rangle\langle\delta'|d_3^\dagger|\delta''\rangle\langle\delta''|d_4|\mathcal{D}'\rangle\times\langle\mathrm{LR}|c_1|\lambda\rangle\langle\lambda|c_2^\dagger|\lambda'\rangle\langle\lambda'|c_3|\lambda''\rangle\langle\lambda''|c_4^\dagger|\mathrm{LR}\rangle \tag{B.6d}$$

$$t_{a_1b_1}t^*_{a_2b_2}t^*_{a_3b_3}t_{a_4b_4}\langle\mathcal{D}|d_1|\delta\rangle\langle\delta|d_2^\dagger|\delta'\rangle\langle\delta'|d_3^\dagger|\delta''\rangle\langle\delta''|d_4|\mathcal{D}'\rangle\times\langle\mathrm{LR}|c_1^\dagger|\lambda\rangle\langle\lambda|c_2|\lambda'\rangle\langle\lambda'|c_3|\lambda''\rangle\langle\lambda''|c_4^\dagger|\mathrm{LR}\rangle \tag{B.6e}$$

$$t^*_{a_1b_1}t_{a_2b_2}t_{a_3b_3}t^*_{a_4b_4}\langle\mathcal{D}|d_1^\dagger|\delta\rangle\langle\delta|d_2|\delta'\rangle\langle\delta'|d_3|\delta''\rangle\langle\delta''|d_4^\dagger|\mathcal{D}'\rangle\times\langle\mathrm{LR}|c_1|\lambda\rangle\langle\lambda|c_2^\dagger|\lambda'\rangle\langle\lambda'|c_3^\dagger|\lambda''\rangle\langle\lambda''|c_4|\mathrm{LR}\rangle, \tag{B.6f}$$

where $|\mathcal{D}\rangle$, $|\delta\rangle$ correspond to the dot states and $|\mathrm{LR}\rangle$, $|\lambda\rangle$ to the lead states. We also use short-hand notation

$$c_i = c_{a_i}, \quad d_i = d_{b_i}. \tag{B.7}$$

1. Let's evaluate (B.6a) term. We see that the matrix element with the lead states will not vanish if either

$$a_1 = a_3,\ a_2 = a_4 \quad \text{or} \quad a_1 = a_4,\ a_2 = a_3, \quad \text{and} \quad a_1 \neq a_2. \tag{B.8}$$

so we end up with

$$\sum_{\lambda,\lambda',\lambda''}\langle\mathrm{LR}|c_1^\dagger|\lambda\rangle\langle\lambda|c_2^\dagger|\lambda'\rangle\langle\lambda'|c_1|\lambda''\rangle\langle\lambda''|c_2|\mathrm{LR}\rangle = \langle\mathrm{LR}|c_1^\dagger\boxed{c_1|\mathrm{LR}\rangle}\langle\mathrm{LR}|c_1^\dagger c_2^\dagger\boxed{c_2c_1|\mathrm{LR}\rangle}\langle\mathrm{LR}|c_1^\dagger c_2^\dagger c_1\boxed{c_2|\mathrm{LR}\rangle}\langle\mathrm{LR}|c_2^\dagger c_2|\mathrm{LR}\rangle, \tag{B.9}$$

$$\sum_{\lambda,\lambda',\lambda''}\langle\mathrm{LR}|c_1^\dagger|\lambda\rangle\langle\lambda|c_2^\dagger|\lambda'\rangle\langle\lambda'|c_2|\lambda''\rangle\langle\lambda''|c_1|\mathrm{LR}\rangle = \langle\mathrm{LR}|c_1^\dagger\boxed{c_1|\mathrm{LR}\rangle}\langle\mathrm{LR}|c_1^\dagger c_2^\dagger\boxed{c_2c_1|\mathrm{LR}\rangle}\langle\mathrm{LR}|c_1^\dagger c_2^\dagger c_2\boxed{c_1|\mathrm{LR}\rangle}\langle\mathrm{LR}|c_1^\dagger c_1|\mathrm{LR}\rangle, \tag{B.10}$$

which at finite temperature will give the following contribution

$$\begin{aligned}\frac{1}{2}\sum f_1 f_2\Bigg\{&-\frac{\mathcal{M}(\frac{a_1,a_2,a_1,a_2}{1,1,\dagger,\dagger})}{(\varepsilon_1+E_i-E_\delta)(\varepsilon_1+\varepsilon_2+E_i-E_{\delta'})(\varepsilon_2+E_i-E_{\delta''})}\\&+\frac{\mathcal{M}(\frac{a_1,a_2,a_2,a_1}{1,1,\dagger,\dagger})}{(\varepsilon_1+E_i-E_\delta)(\varepsilon_1+\varepsilon_2+E_i-E_{\delta'})(\varepsilon_1+E_i-E_{\delta''})}\Bigg\},\end{aligned} \tag{B.11}$$

where

$$\mathcal{M}\left(\frac{a_1,a_2,a_3,a_4}{s_1,s_2,s_3,s_4}\right) = t^{s_1}_{a_1b_1}t^{s_2}_{a_2b_2}t^{s_3}_{a_3b_3}t^{s_4}_{a_4b_4}\langle\mathcal{D}|d_1^{s_1}|\delta\rangle\langle\delta|d_2^{s_2}|\delta'\rangle\langle\delta'|d_3^{s_3}|\delta''\rangle\langle\delta''|d_4^{s_4}|\mathcal{D}'\rangle, \tag{B.12}$$

and $s_i \in \{1, \dagger\}$ corresponds to either performing Hermitian conjugate $\dagger$ or doing nothing 1. Also summation over all possible indices is implied and

$$E_i \in \{E_\mathcal{D}, E_{\mathcal{D}'}\}. \tag{B.13}$$

2. As in previous case term (B.6b) will not vanish if either

$$a_1 = a_3,\ a_2 = a_4 \quad \text{or} \quad a_1 = a_4,\ a_2 = a_3, \quad \text{and} \quad a_1 \neq a_2. \tag{B.14}$$

so we end up with

$$\sum_{\lambda,\lambda',\lambda''}\langle\mathrm{LR}|c_1|\lambda\rangle\langle\lambda|c_2|\lambda'\rangle\langle\lambda'|c_1^\dagger|\lambda''\rangle\langle\lambda''|c_2^\dagger|\mathrm{LR}\rangle = \langle\mathrm{LR}|c_1\boxed{c_1^\dagger|\mathrm{LR}\rangle}\langle\mathrm{LR}|c_1c_2\boxed{c_2^\dagger c_1^\dagger|\mathrm{LR}\rangle}\langle\mathrm{LR}|c_1c_2c_1^\dagger\boxed{c_2^\dagger|\mathrm{LR}\rangle}\langle\mathrm{LR}|c_2c_2^\dagger|\mathrm{LR}\rangle, \tag{B.15}$$

$$\sum_{\lambda,\lambda',\lambda''}\langle\mathrm{LR}|c_1|\lambda\rangle\langle\lambda|c_2|\lambda'\rangle\langle\lambda'|c_2^\dagger|\lambda''\rangle\langle\lambda''|c_1^\dagger|\mathrm{LR}\rangle = \langle\mathrm{LR}|c_1\boxed{c_1^\dagger|\mathrm{LR}\rangle}\langle\mathrm{LR}|c_1c_2\boxed{c_2^\dagger c_1^\dagger|\mathrm{LR}\rangle}\langle\mathrm{LR}|c_1c_2c_2^\dagger\boxed{c_1^\dagger|\mathrm{LR}\rangle}\langle\mathrm{LR}|c_1c_1^\dagger|\mathrm{LR}\rangle, \tag{B.16}$$

and the contribution of this term is

$$\frac{1}{2}\sum(1-f_1)(1-f_2)\Bigg\{-\frac{\mathcal{M}(\frac{a_1,a_2,a_1,a_2}{\dagger,\dagger,1,1})}{(-\varepsilon_1+E_i-E_\delta)(-\varepsilon_1-\varepsilon_2+E_i-E_{\delta'})(-\varepsilon_2+E_i-E_{\delta''})} + \frac{\mathcal{M}(\frac{a_1,a_2,a_2,a_1}{\dagger,\dagger,1,1})}{(-\varepsilon_1+E_i-E_\delta)(-\varepsilon_1-\varepsilon_2+E_i-E_{\delta'})(-\varepsilon_1+E_i-E_{\delta''})}\Bigg\}. \tag{B.17}$$

3. The term (B.6c) will not vanish if

$$a_1 = a_4,\ a_2 = a_3 \quad \text{and} \quad a_1 \neq a_2. \tag{B.18}$$

We note that the other term

$$a_1 = a_2,\ a_3 = a_4, \tag{B.19}$$

would survive if we projected only to one particular state of the dot, and then would have only the diagonal contributions. But we will see that this term is behaving badly, if single particle spacing is becoming smaller than $\rho|t|^2$. So we end up with

$$\sum_{\lambda,\lambda',\lambda''}\langle \mathrm{LR}|c_1^\dagger|\lambda\rangle\langle\lambda|c_2|\lambda'\rangle\langle\lambda'|c_2^\dagger|\lambda''\rangle\langle\lambda''|c_1|\mathrm{LR}\rangle = \langle \mathrm{LR}|c_1^\dagger\boxed{c_1|\mathrm{LR}\rangle}\langle \mathrm{LR}|c_1^\dagger c_2\boxed{c_2^\dagger c_1|\mathrm{LR}\rangle}\langle \mathrm{LR}|c_1^\dagger c_2 c_2^\dagger\boxed{c_1|\mathrm{LR}\rangle}\langle \mathrm{LR}|c_1^\dagger c_1|\mathrm{LR}\rangle, \tag{B.20}$$

$$\sum_{\lambda,\lambda',\lambda''}\langle \mathrm{LR}|c_1^\dagger|\lambda\rangle\langle\lambda|c_1|\lambda'\rangle\langle\lambda'|c_2^\dagger|\lambda''\rangle\langle\lambda''|c_2|\mathrm{LR}\rangle = \langle \mathrm{LR}|c_1^\dagger\boxed{c_1|\mathrm{LR}\rangle}\langle \mathrm{LR}|c_1^\dagger c_1\boxed{|\mathrm{LR}\rangle}\langle \mathrm{LR}|c_2^\dagger\boxed{c_2|\mathrm{LR}\rangle}\langle \mathrm{LR}|c_2^\dagger c_2|\mathrm{LR}\rangle. \tag{B.21}$$

We see that (B.21) would vanish if we project to particular lead state $|\mathrm{LR}\rangle$ and all other possible dot states, because then we are not allowed to have $|\mathrm{LR}\rangle$ as an intermediate state. The contribution of (B.6c) term is

$$\frac{1}{2}\sum\Bigg\{\frac{f_1(1-f_2)\mathcal{M}(\frac{a_1,a_2,a_2,a_1}{1,\dagger,1,\dagger})}{(\varepsilon_1+E_i-E_\delta)(\varepsilon_1-\varepsilon_2+E_i-E_{\delta'})(\varepsilon_1+E_i-E_{\delta''})} + \frac{f_1 f_2\mathcal{M}(\frac{a_1,a_1,a_2,a_2}{1,\dagger,1,\dagger})}{(\varepsilon_1+E_i-E_\delta)(E_i-E_{\delta'})(\varepsilon_2+E_i-E_{\delta''})}\Bigg\}. \tag{B.22}$$

We see that the term in red has $(E_i - E_{\delta'})^{-1}$ factor, where E_i and $E_{\delta'}$ in this case are in the same charge state, and the difference between two corresponds to single particle level spacing, which of course blows up if we have degenerate levels. This term is not included if we project to all dot states and particular lead state $|\mathrm{LR}\rangle$.

4. As in (B.6c) The term (B.6d) will not vanish if

$$a_1 = a_4,\ a_2 = a_3 \quad \text{and} \quad a_1 \neq a_2. \tag{B.23}$$

but we will also keep

$$a_1 = a_2,\ a_3 = a_4, \tag{B.24}$$

and we end up with

$$\sum_{\lambda,\lambda',\lambda''}\langle \mathrm{LR}|c_1|\lambda\rangle\langle\lambda|c_2^\dagger|\lambda'\rangle\langle\lambda'|c_2|\lambda''\rangle\langle\lambda''|c_1^\dagger|\mathrm{LR}\rangle = \langle \mathrm{LR}|c_1\boxed{c_1^\dagger|\mathrm{LR}\rangle}\langle \mathrm{LR}|c_1 c_2^\dagger\boxed{c_2 c_1^\dagger|\mathrm{LR}\rangle}\langle \mathrm{LR}|c_1 c_2^\dagger c_2\boxed{c_1^\dagger|\mathrm{LR}\rangle}\langle \mathrm{LR}|c_1 c_1^\dagger|\mathrm{LR}\rangle, \tag{B.25}$$

$$\sum_{\lambda,\lambda',\lambda''}\langle \mathrm{LR}|c_1|\lambda\rangle\langle\lambda|c_1^\dagger|\lambda'\rangle\langle\lambda'|c_2|\lambda''\rangle\langle\lambda''|c_2^\dagger|\mathrm{LR}\rangle = \langle \mathrm{LR}|c_1\boxed{c_1^\dagger|\mathrm{LR}\rangle}\langle \mathrm{LR}|c_1 c_1^\dagger\boxed{|\mathrm{LR}\rangle}\langle \mathrm{LR}|c_2\boxed{c_2^\dagger|\mathrm{LR}\rangle}\langle \mathrm{LR}|c_2 c_2^\dagger|\mathrm{LR}\rangle. \tag{B.26}$$

The contribution of this term is

$$\frac{1}{2}\sum\Bigg\{\frac{(1-f_1)f_2\mathcal{M}(\frac{a_1,a_2,a_2,a_1}{\dagger,1,\dagger,1})}{(-\varepsilon_1+E_i-E_\delta)(-\varepsilon_1+\varepsilon_2+E_i-E_{\delta'})(-\varepsilon_1+E_i-E_{\delta''})} + \frac{(1-f_1)(1-f_2)\mathcal{M}(\frac{a_1,a_1,a_2,a_2}{\dagger,1,\dagger,1})}{(-\varepsilon_1+E_i-E_\delta)(E_i-E_{\delta'})(-\varepsilon_2+E_i-E_{\delta''})}\Bigg\}. \tag{B.27}$$

5. The term (B.6e) will not vanish if

$$a_1 = a_3,\ a_2 = a_4 \quad \text{and} \quad a_1 \neq a_2, \tag{B.28}$$

but we will also keep

$$a_1 = a_2,\ a_3 = a_4, \quad \text{and} \quad a_2 \neq a_3, \tag{B.29}$$

and we end up with

$$\sum_{\lambda,\lambda',\lambda''} \langle \mathrm{LR}|c_1^\dagger|\lambda\rangle\langle\lambda|c_2|\lambda'\rangle\langle\lambda'|c_1|\lambda''\rangle\langle\lambda''|c_2^\dagger|\mathrm{LR}\rangle = \langle \mathrm{LR}|c_1^\dagger \boxed{c_1|\mathrm{LR}\rangle}\langle \mathrm{LR}|c_1^\dagger c_2 \boxed{c_2^\dagger c_1|\mathrm{LR}\rangle}\langle \mathrm{LR}|c_1^\dagger c_2 c_1 \boxed{c_2^\dagger|\mathrm{LR}\rangle}\langle \mathrm{LR}|c_2 c_2^\dagger|\mathrm{LR}\rangle, \tag{B.30}$$

$$\sum_{\lambda,\lambda',\lambda''} \langle \mathrm{LR}|c_1^\dagger|\lambda\rangle\langle\lambda|c_1|\lambda'\rangle\langle\lambda'|c_2|\lambda''\rangle\langle\lambda''|c_2^\dagger|\mathrm{LR}\rangle = \langle \mathrm{LR}|c_1^\dagger \boxed{c_1|\mathrm{LR}\rangle}\langle \mathrm{LR}|c_1^\dagger c_1 \boxed{|\mathrm{LR}\rangle}\langle \mathrm{LR}|c_2 \boxed{c_2^\dagger|\mathrm{LR}\rangle}\langle \mathrm{LR}|c_2 c_2^\dagger|\mathrm{LR}\rangle, \tag{B.31}$$

The contribution of this term is

$$\frac{1}{2}\sum f_1(1-f_2)\Bigg\{-\frac{\mathcal{M}(\frac{a_1,a_2,a_1,a_2}{1,\dagger,\dagger,1})}{(\varepsilon_1+E_i-E_\delta)(\varepsilon_1-\varepsilon_2+E_i-E_{\delta'})(-\varepsilon_2+E_i-E_{\delta''})} + \frac{\mathcal{M}(\frac{a_1,a_1,a_2,a_2}{1,\dagger,\dagger,1})}{(\varepsilon_1+E_i-E_\delta)(E_i-E_{\delta'})(-\varepsilon_2+E_i-E_{\delta''})}\Bigg\}. \tag{B.32}$$

6. As in (B.6e) the term (B.6f) will not vanish if

$$a_1 = a_3,\ a_2 = a_4 \quad \text{and} \quad a_1 \neq a_2, \tag{B.33}$$

but we will also keep

$$a_1 = a_2,\ a_3 = a_4, \quad \text{and} \quad a_2 \neq a_3, \tag{B.34}$$

and we end up with

$$\sum_{\lambda,\lambda',\lambda''} \langle \mathrm{LR}|c_1|\lambda\rangle\langle\lambda|c_2^\dagger|\lambda'\rangle\langle\lambda'|c_1^\dagger|\lambda''\rangle\langle\lambda''|c_2|\mathrm{LR}\rangle = \langle \mathrm{LR}|c_1 \boxed{c_1^\dagger|\mathrm{LR}\rangle}\langle \mathrm{LR}|c_1 c_2^\dagger \boxed{c_2 c_1^\dagger|\mathrm{LR}\rangle}\langle \mathrm{LR}|c_1 c_2^\dagger c_1^\dagger \boxed{c_2|\mathrm{LR}\rangle}\langle \mathrm{LR}|c_2^\dagger c_2|\mathrm{LR}\rangle, \tag{B.35}$$

$$\sum_{\lambda,\lambda',\lambda''} \langle \mathrm{LR}|c_1|\lambda\rangle\langle\lambda|c_1^\dagger|\lambda'\rangle\langle\lambda'|c_2^\dagger|\lambda''\rangle\langle\lambda''|c_2|\mathrm{LR}\rangle = \langle \mathrm{LR}|c_1 \boxed{c_1^\dagger|\mathrm{LR}\rangle}\langle \mathrm{LR}|c_1 c_1^\dagger \boxed{|\mathrm{LR}\rangle}\langle \mathrm{LR}|c_2^\dagger \boxed{c_2|\mathrm{LR}\rangle}\langle \mathrm{LR}|c_2^\dagger c_2|\mathrm{LR}\rangle, \tag{B.36}$$

The contribution of this term is

$$\frac{1}{2}\sum (1-f_1)f_2\Bigg\{-\frac{\mathcal{M}(\frac{a_1,a_2,a_1,a_2}{\dagger,1,1,\dagger})}{(-\varepsilon_1+E_i-E_\delta)(-\varepsilon_1+\varepsilon_2+E_i-E_{\delta'})(\varepsilon_2+E_i-E_{\delta''})} + \frac{\mathcal{M}(\frac{a_1,a_1,a_2,a_2}{\dagger,1,1,\dagger})}{(-\varepsilon_1+E_i-E_\delta)(E_i-E_{\delta'})(\varepsilon_2+E_i-E_{\delta''})}\Bigg\}. \tag{B.37}$$

B.2 2nd Expression

In this section we will consider term of the form

$$\sum_{l,l',m''} C_{m_i} H^{\mathrm{T}}_{ml} H^{\mathrm{T}}_{lm''} H^{\mathrm{T}}_{m''l'} H^{\mathrm{T}}_{l'm'} \left[\frac{1}{(E_{m_1}-E_l)(E_{m_2}-E_l)(E_{m_3}-E_{l'})} + \frac{1}{(E_{m_4}-E_l)(E_{m_5}-E_{l'})(E_{m_6}-E_{l'})}\right], \tag{B.38}$$

where

$$m_i \in \{m, m', m''\}. \tag{B.39}$$

and C_{m_i} is some prefactor smaller than 1. Again the only non-vanishing terms are of the type

$$t_{a_1b_1}t^*_{a_2b_2}t_{a_3b_3}t^*_{a_4b_4}\langle m|c_1^\dagger d_1|l\rangle\langle l|d_2^\dagger c_2|m''\rangle\langle m''|c_3^\dagger d_3|l'\rangle\langle l'|d_4^\dagger c_4|m'\rangle \tag{B.40a}$$

$$t^*_{a_1b_1}t_{a_2b_2}t^*_{a_3b_3}t_{a_4b_4}\langle m|d_1^\dagger c_1|l\rangle\langle l|c_2^\dagger d_2|m''\rangle\langle m''|d_3^\dagger c_3|l'\rangle\langle l'|c_4^\dagger d_4|m'\rangle \tag{B.40b}$$

$$t_{a_1b_1}t^*_{a_2b_2}t^*_{a_3b_3}t_{a_4b_4}\langle m|c_1^\dagger d_1|l\rangle\langle l|d_2^\dagger c_2|m''\rangle\langle m''|d_3^\dagger c_3|l'\rangle\langle l'|c_4^\dagger d_4|m'\rangle \tag{B.40c}$$

$$t^*_{a_1b_1}t_{a_2b_2}t_{a_3b_3}t^*_{a_4b_4}\langle m|d_1^\dagger c_1|l\rangle\langle l|c_2^\dagger d_2|m''\rangle\langle m''|c_3^\dagger d_3|l'\rangle\langle l'|d_4^\dagger c_4|m'\rangle, \tag{B.40d}$$

and they can be rewritten as

$$t_{a_1b_1}t^*_{a_2b_2}t_{a_3b_3}t^*_{a_4b_4}\langle\mathcal{D}|d_1|\delta\rangle\langle\delta|d_2^\dagger|\mathcal{D}''\rangle\langle\mathcal{D}''|d_3|\delta'\rangle\langle\delta'|d_4^\dagger|\mathcal{D}'\rangle\times\langle \mathrm{LR}|c_1^\dagger|\lambda\rangle\langle\lambda|c_2|\mathrm{LR}\rangle\langle\mathrm{LR}|c_3^\dagger|\lambda'\rangle\langle\lambda'|c_4|\mathrm{LR}\rangle \tag{B.41a}$$

$$t^*_{a_1b_1}t_{a_2b_2}t^*_{a_3b_3}t_{a_4b_4}\langle\mathcal{D}|d_1^\dagger|\delta\rangle\langle\delta|d_2|\mathcal{D}''\rangle\langle\mathcal{D}''|d_3^\dagger|\delta'\rangle\langle\delta'|d_4|\mathcal{D}'\rangle\times\langle \mathrm{LR}|c_1|\lambda\rangle\langle\lambda|c_2^\dagger|\mathrm{LR}\rangle\langle\mathrm{LR}|c_3|\lambda'\rangle\langle\lambda'|c_4^\dagger|\mathrm{LR}\rangle \tag{B.41b}$$

$$t_{a_1b_1}t^*_{a_2b_2}t^*_{a_3b_3}t_{a_4b_4}\langle\mathcal{D}|d_1|\delta\rangle\langle\delta|d_2^\dagger|\mathcal{D}''\rangle\langle\mathcal{D}''|d_3^\dagger|\delta'\rangle\langle\delta'|d_4|\mathcal{D}'\rangle\times\langle \mathrm{LR}|c_1^\dagger|\lambda\rangle\langle\lambda|c_2|\mathrm{LR}\rangle\langle\mathrm{LR}|c_3|\lambda'\rangle\langle\lambda'|c_4^\dagger|\mathrm{LR}\rangle \tag{B.41c}$$

$$t^*_{a_1b_1}t_{a_2b_2}t_{a_3b_3}t^*_{a_4b_4}\langle\mathcal{D}|d_1^\dagger|\delta\rangle\langle\delta|d_2|\mathcal{D}''\rangle\langle\mathcal{D}''|d_3|\delta'\rangle\langle\delta'|d_4^\dagger|\mathcal{D}'\rangle\times\langle \mathrm{LR}|c_1|\lambda\rangle\langle\lambda|c_2^\dagger|\mathrm{LR}\rangle\langle\mathrm{LR}|c_3^\dagger|\lambda'\rangle\langle\lambda'|c_4|\mathrm{LR}\rangle. \tag{B.41d}$$

7. Let's evaluate (B.41a) term. We see that the matrix element with the lead states will not vanish if (and that is also the case for all other terms in (B.41))

$$a_1 = a_2,\ a_3 = a_4, \tag{B.42}$$

so we end up with

$$\sum_{\lambda,\lambda'}\langle \mathrm{LR}|c_1^\dagger|\lambda\rangle\langle\lambda|c_1|\mathrm{LR}\rangle\langle\mathrm{LR}|c_2^\dagger|\lambda'\rangle\langle\lambda'|c_2|\mathrm{LR}\rangle = \langle\mathrm{LR}|c_1^\dagger\boxed{c_1|\mathrm{LR}\rangle}\langle\mathrm{LR}|c_1^\dagger c_1|\mathrm{LR}\rangle\langle\mathrm{LR}|c_2^\dagger\boxed{c_2|\mathrm{LR}\rangle}\langle\mathrm{LR}|c_2^\dagger c_2|\mathrm{LR}\rangle, \tag{B.43}$$

which at finite temperature will give the following contribution

$$\begin{aligned}\sum C_{m_i} f_1 f_2 \mathcal{M}\left(\frac{a_1,a_1,a_2,a_2}{1,\dagger,1,\dagger}\right)\Bigg\{&\frac{1}{(\varepsilon_1+E_{m_1}-E_\delta)(\varepsilon_1+E_{m_2}-E_\delta)(\varepsilon_2+E_{m_3}-E_{\delta'})}\\ &+\frac{1}{(\varepsilon_1+E_{m_4}-E_\delta)(\varepsilon_2+E_{m_5}-E_{\delta'})(\varepsilon_2+E_{m_6}-E_{\delta'})}\Bigg\}.\end{aligned} \tag{B.44}$$

8. The lead sums in term (B.41b)

$$\sum_{\lambda,\lambda'}\langle \mathrm{LR}|c_1|\lambda\rangle\langle\lambda|c_1^\dagger|\mathrm{LR}\rangle\langle\mathrm{LR}|c_2|\lambda'\rangle\langle\lambda'|c_2^\dagger|\mathrm{LR}\rangle = \langle\mathrm{LR}|c_1\boxed{c_1^\dagger|\mathrm{LR}\rangle}\langle\mathrm{LR}|c_1c_1^\dagger|\mathrm{LR}\rangle\langle\mathrm{LR}|c_2\boxed{c_2^\dagger|\mathrm{LR}\rangle}\langle\mathrm{LR}|c_2c_2^\dagger|\mathrm{LR}\rangle, \tag{B.45}$$

and its contribution

$$\begin{aligned}\sum C_{m_i}(1-f_1)(1-f_2)\mathcal{M}\left(\frac{a_1,a_1,a_2,a_2}{\dagger,1,\dagger,1}\right)\Bigg\{&\frac{1}{(-\varepsilon_1+E_{m_1}-E_\delta)(-\varepsilon_1+E_{m_2}-E_\delta)(-\varepsilon_2+E_{m_3}-E_{\delta'})}\\ &+\frac{1}{(-\varepsilon_1+E_{m_4}-E_\delta)(-\varepsilon_2+E_{m_5}-E_{\delta'})(-\varepsilon_2+E_{m_6}-E_{\delta'})}\Bigg\}.\end{aligned} \tag{B.46}$$

9. The lead sums in term (B.41c)

$$\sum_{\lambda,\lambda'}\langle \mathrm{LR}|c_1^\dagger|\lambda\rangle\langle\lambda|c_1|\mathrm{LR}\rangle\langle\mathrm{LR}|c_2|\lambda'\rangle\langle\lambda'|c_2^\dagger|\mathrm{LR}\rangle = \langle\mathrm{LR}|c_1^\dagger\boxed{c_1|\mathrm{LR}\rangle}\langle\mathrm{LR}|c_1^\dagger c_1|\mathrm{LR}\rangle\langle\mathrm{LR}|c_2\boxed{c_2^\dagger|\mathrm{LR}\rangle}\langle\mathrm{LR}|c_2c_2^\dagger|\mathrm{LR}\rangle, \tag{B.47}$$

and its contribution

$$\begin{aligned}\sum C_{m_i} f_1(1-f_2)\mathcal{M}\left(\frac{a_1,a_1,a_2,a_2}{1,\dagger,\dagger,1}\right)\Bigg\{&\frac{1}{(\varepsilon_1+E_{m_1}-E_\delta)(\varepsilon_1+E_{m_2}-E_\delta)(-\varepsilon_2+E_{m_3}-E_{\delta'})}\\ &+\frac{1}{(\varepsilon_1+E_{m_4}-E_\delta)(-\varepsilon_2+E_{m_5}-E_{\delta'})(-\varepsilon_2+E_{m_6}-E_{\delta'})}\Bigg\}.\end{aligned} \tag{B.48}$$

10. The lead sums in term (B.41d)

$$\sum_{\lambda,\lambda'}\langle \mathrm{LR}|c_1|\lambda\rangle\langle\lambda|c_1^\dagger|\mathrm{LR}\rangle\langle \mathrm{LR}|c_2^\dagger|\lambda'\rangle\langle\lambda'|c_2|\mathrm{LR}\rangle = \langle \mathrm{LR}|c_1\boxed{c_1^\dagger|\mathrm{LR}\rangle}\langle \mathrm{LR}|c_1c_1^\dagger|\mathrm{LR}\rangle\langle \mathrm{LR}|c_2^\dagger\boxed{c_2|\mathrm{LR}\rangle}\langle \mathrm{LR}|c_2^\dagger c_2|\mathrm{LR}\rangle, \tag{B.49}$$

and its contribution

$$\begin{aligned}\sum C_{m_i}(1-f_1)f_2\mathcal{M}\left(\begin{matrix}a_1,a_1,a_2,a_2\\ \dagger,1,1,\dagger\end{matrix}\right)\Bigg\{&\frac{1}{(-\varepsilon_1+E_{m_1}-E_\delta)(-\varepsilon_1+E_{m_2}-E_\delta)(\varepsilon_2+E_{m_3}-E_{\delta'})}\\ &+\frac{1}{(-\varepsilon_1+E_{m_4}-E_\delta)(\varepsilon_2+E_{m_5}-E_{\delta'})(\varepsilon_2+E_{m_6}-E_{\delta'})}\Bigg\}.\end{aligned} \tag{B.50}$$

B.3 Evaluation of the integrals

B.3.1 1st Expression

From above analysis for 1st expression we see that we need to evaluate integrals of the type

$$\begin{aligned}I_1(a,b,c) &= \lim_{\eta_x,\eta_y\to+0}\mathrm{Re}\int_{-D+\mathrm{i}\eta_x}^{D+\mathrm{i}\eta_x}\int_{-D+\mathrm{i}\eta_y}^{D+\mathrm{i}\eta_y}\frac{f(x)f(y)\mathrm{d}x\mathrm{d}y}{(x+a)(x+b)(x+y+c)}\\ &\overset{T=0}{\to}\lim_{\eta_x,\eta_y\to+0}\mathrm{Re}\int_{-D+\mathrm{i}\eta_x}^{0+\mathrm{i}\eta_x}\int_{-D+\mathrm{i}\eta_y}^{0+\mathrm{i}\eta_y}\frac{\mathrm{d}x\mathrm{d}y}{(x+a)(x+b)(x+y+c)},\end{aligned} \tag{B.51}$$

$$\begin{aligned}I_2(a,b,c) &= \lim_{\eta_x,\eta_y\to+0}\mathrm{Re}\int_{-D+\mathrm{i}\eta_x}^{D+\mathrm{i}\eta_x}\int_{-D+\mathrm{i}\eta_y}^{D+\mathrm{i}\eta_y}\frac{f(x)f(y)\mathrm{d}x\mathrm{d}y}{(x+a)(y+b)(x+y+c)}\\ &\overset{T=0}{\to}\lim_{\eta_x,\eta_y\to+0}\mathrm{Re}\int_{-D+\mathrm{i}\eta_x}^{0+\mathrm{i}\eta_x}\int_{-D+\mathrm{i}\eta_y}^{0+\mathrm{i}\eta_y}\frac{\mathrm{d}x\mathrm{d}y}{(x+a)(y+b)(x+y+c)}.\end{aligned} \tag{B.52}$$

Here $\eta=+0$ gives infinitesimally small imaginary part. From now on we will skip the indication of the limit and of the real part of the integral. Let's calculate integral I_1 for zero temperature. Firstly, we integrate with respect to y, which yields

$$I_1=\int_{-D+\mathrm{i}\eta_x}^{0+\mathrm{i}\eta_x}\frac{\mathrm{d}x\ln(x+y+c)}{(x+a)(x+b)}\bigg|_{y=-D+\mathrm{i}\eta_y}^{y=0+\mathrm{i}\eta_y}=-\int_{-D+\mathrm{i}\eta_x}^{0+\mathrm{i}\eta_x}\frac{\mathrm{d}x\ln(x+y+c)}{a-b}\left(\frac{1}{x+a}-\frac{1}{x+b}\right)\bigg|_{y=-D}^{y=0}. \tag{B.53}$$

Here in the last step we have taken limit of $\eta_y\to+0$, which also corresponds to taking the following branch of logarithm:

$$\ln(-x)=\ln(x)+\mathrm{i}\pi,\quad x>0. \tag{B.54}$$

We see that we need to perform integral of the type (we neglect subscript x in η_x)

$$\begin{aligned}\mathcal{I}(y,a,c)=\int_{-D+\mathrm{i}\eta}^{0+\mathrm{i}\eta}\frac{\mathrm{d}x\ln\left(\frac{x+y+c}{D}\right)}{x+a}&=\int_{-D+\mathrm{i}\eta}^{0+\mathrm{i}\eta}\mathrm{d}x\left(\underbrace{\frac{\ln\left(\frac{x+a}{a-c-y}\right)}{(a-c-y)\left(1-\frac{x+a}{a-c-y}\right)}+\frac{\ln\left(\frac{x+a}{a-c-y}\right)}{x+y+c}}_{0}+\frac{\ln\left(\frac{x+y+c}{D}\right)}{x+a}\right)\\ &=\int_{\frac{-D+a+\mathrm{i}\eta}{a-c-y}}^{\frac{a+\mathrm{i}\eta}{a-c-y}}\frac{\mathrm{d}t\ln t}{1-t}+\int_{-D+\mathrm{i}\eta}^{0+\mathrm{i}\eta}\mathrm{d}x\frac{\mathrm{d}}{\mathrm{d}x}\left\{\ln\left(\frac{x+a}{a-c-y}\right)\ln\left(\frac{x+y+c}{D}\right)\right\}\\ &=\left(\int_1^{\frac{a+\mathrm{i}\eta}{a-c-y}}-\int_1^{\frac{-D+a+\mathrm{i}\eta}{a-c-y}}\right)\frac{\mathrm{d}t\ln t}{1-t}+\left\{\ln\left(\frac{x+a}{a-c-y}\right)\ln\left(\frac{x+y+c}{D}\right)\right\}\bigg|_{x=-D+\mathrm{i}\eta}^{x=0+\mathrm{i}\eta}\\ &=\mathrm{dilog}\left(\frac{a+\mathrm{i}\eta}{a-c-y}\right)-\mathrm{dilog}\left(\frac{-D+a+\mathrm{i}\eta}{a-c-y}\right)\\ &+\ln\left(\frac{a+\mathrm{i}\eta}{a-c-y}\right)\ln\left(\frac{y+c}{D}\right)-\ln\left(\frac{-D+a+\mathrm{i}\eta}{a-c-y}\right)\ln\left(\frac{-D+y+c}{D}\right).\end{aligned} \tag{B.55}$$

where

$$\mathrm{dilog}(x) = \int_1^x \frac{\mathrm{d}t \ln t}{1-t}. \tag{B.56}$$

In the last step of (B.55) we again took the limit $\eta \to +0$ where possible. The limit of $\eta \to +0$ in the $\mathrm{dilog}(x)$ functions (and also in some of log's) depends on the sign of $a-c-y$, because we have the following branches of the $\mathrm{dilog}(x)$ and $\ln(x)$ functions

$$\lim_{\epsilon\to\pm 0} \mathrm{dilog}(-x+\mathrm{i}\epsilon) = \frac{1}{6}\pi^2 - \mathrm{dilog}(1-x) - \{\ln(-x) \pm \mathrm{i}\pi\}\ln(1-x), \quad x>0, \tag{B.57}$$

$$\lim_{\epsilon\to\pm 0} \ln(-x+\mathrm{i}\epsilon) = \ln(x) \pm \mathrm{i}\pi, \quad x>0. \tag{B.58}$$

However, by choosing the incorrect branch we will only affect the imaginary part of the expression, so we can make the calculation with any branch, and then take the real part of the expression, which is the desired result. So we will choose the upper branch (i.e. $\epsilon \to +0$)

$$\mathcal{I}(y,a,c) = \mathrm{Re}\left\{\mathrm{dilog}\left(\frac{a}{a-c-y}\right) - \mathrm{dilog}\left(\frac{-D+a}{a-c-y}\right) + \ln\left(\frac{a}{a-c-y}\right)\ln\left(\frac{y+c}{D}\right) - \ln\left(\frac{-D+a}{a-c-y}\right)\ln\left(\frac{-D+y+c}{D}\right)\right\}. \tag{B.59}$$

Integral I_1 can be expressed through $\mathcal{I}$ as

$$I_1 = -\frac{1}{a-b}\{\mathcal{I}(0,a) - \mathcal{I}(-D,a) - \mathcal{I}(0,b) + \mathcal{I}(-D,b)\}. \tag{B.60}$$

Integral I_2 can be performed in a similar manner, and here we write only its final expression

$$I_2 = -\frac{1}{a+b-c}\,\mathrm{Re}\left\{\ln\left(\frac{y+b}{D}\right)\Big|_{y=-D}^{y=0} \ln\left(\frac{x+a}{x+c-b}\right)\Big|_{x=-D}^{x=0}\right\} - I_1(a,c-b,c). \tag{B.61}$$

Note that in particular cases (i.e. $a=b$, $c=0$ and etc.) one has to take a limit to find an actual closed form expression (or perform the integrals for those particular values) and the good thing is that those limits exist.

Again we rewrite the full expressions of integrals for convenience without indication of real part:

$$\begin{aligned} I_1 = -\frac{1}{a-b}\Bigg\{ & \mathrm{dilog}\left(\frac{a}{a-c}\right) - \mathrm{dilog}\left(\frac{-D+a}{a-c}\right) + \ln\left(\frac{a}{a-c}\right)\ln\left(\frac{c}{D}\right) - \ln\left(\frac{-D+a}{a-c}\right)\ln\left(\frac{-D+c}{D}\right) \\ & - \mathrm{dilog}\left(\frac{b}{b-c}\right) + \mathrm{dilog}\left(\frac{-D+b}{b-c}\right) - \ln\left(\frac{b}{b-c}\right)\ln\left(\frac{c}{D}\right) + \ln\left(\frac{-D+b}{b-c}\right)\ln\left(\frac{-D+c}{D}\right) \\ & - \mathrm{dilog}\left(\frac{a}{a-c+D}\right) + \mathrm{dilog}\left(\frac{-D+a}{a-c+D}\right) - \ln\left(\frac{a}{a-c+D}\right)\ln\left(\frac{-D+c}{D}\right) + \ln\left(\frac{-D+a}{a-c+D}\right)\ln\left(\frac{-2D+c}{D}\right) \\ & + \mathrm{dilog}\left(\frac{b}{b-c+D}\right) - \mathrm{dilog}\left(\frac{-D+b}{b-c+D}\right) + \ln\left(\frac{b}{b-c+D}\right)\ln\left(\frac{-D+c}{D}\right) - \ln\left(\frac{-D+b}{b-c+D}\right)\ln\left(\frac{-2D+c}{D}\right)\Bigg\}, \end{aligned} \tag{B.62}$$

$$I_2 = -\frac{1}{a+b-c}\left\{\ln\left(\frac{b}{D}\right) - \ln\left(\frac{-D+b}{D}\right)\right\}\left\{\ln\left(\frac{a}{c-b}\right) - \ln\left(\frac{-D+a}{-D+c-b}\right)\right\} - I_1(a,c-b,c), \tag{B.63}$$

and in very large D limit, which we will be interested in, they become (also keeping the terms that do not depend on D)

$$\begin{aligned} I_1 \overset{D\to+\infty}{=} -\frac{1}{a-b}\Bigg\{ & \mathrm{dilog}\left(\frac{a}{a-c}\right) - \mathrm{dilog}\left(\frac{-D}{a-c}\right) + \ln\left(\frac{a}{a-c}\right)\ln\left(\frac{c}{D}\right) \\ & - \mathrm{dilog}\left(\frac{b}{b-c}\right) + \mathrm{dilog}\left(\frac{-D}{b-c}\right) - \ln\left(\frac{b}{b-c}\right)\ln\left(\frac{c}{D}\right)\Bigg\}, \end{aligned} \tag{B.64}$$

$$I_2 \overset{D\to+\infty}{=} -\frac{1}{a+b-c}\ln\left(\frac{b}{D}\right)\ln\left(\frac{a}{c-b}\right) - I_1(a,c-b,c). \tag{B.65}$$

B.3.2 2nd Expression

For 2nd expression we need to evaluate integral of the type

$$\begin{aligned} I_3(a,b,c) &= \lim_{\eta_x,\eta_y\to+0} \mathrm{Re}\int_{-D+\mathrm{i}\eta_x}^{D+\mathrm{i}\eta_x}\int_{-D+\mathrm{i}\eta_y}^{D+\mathrm{i}\eta_y} \frac{f(x)f(y)\mathrm{d}x\mathrm{d}y}{(x+a)(x+b)(y+c)} \\ &\overset{T=0}{\to} \lim_{\eta_x,\eta_y\to+0} \mathrm{Re}\int_{-D+\mathrm{i}\eta_x}^{0+\mathrm{i}\eta_x}\int_{-D+\mathrm{i}\eta_y}^{0+\mathrm{i}\eta_y} \frac{\mathrm{d}x\mathrm{d}y}{(x+a)(x+b)(y+c)}, \end{aligned} \tag{B.66}$$

which is straightforward to do for zero temperature

$$\begin{aligned} I_3 &= -\int_{-D+\mathrm{i}\eta_x}^{0+\mathrm{i}\eta_x} \frac{\mathrm{d}x\ln(y+c)}{a-b}\left(\frac{1}{x+a}-\frac{1}{x+b}\right)\Big|_{y=-D+\mathrm{i}\eta_y}^{y=0+\mathrm{i}\eta_y} \\ &= -\frac{1}{a-b}\ln(y+c)\Big|_{y=-D}^{y=0}\ln\left(\frac{x+a}{x+b}\right)\Big|_{x=-D}^{x=0}, \end{aligned} \tag{B.67}$$

and explicitly it looks like

$$I_3 = -\frac{1}{a-b}\,\mathrm{Re}\left\{\ln\left(\frac{c}{-D+c}\right)\ln\frac{a(D-b)}{b(D-a)}\right\}. \tag{B.68}$$

B.4 Taylor expansion of the result for a single charge state

In this section we will expand the result for a single charge state and will examine it in the middle of the first diamond, i.e. $V_g = 2U + \Delta V_g$. We also assume that the bandwidth is extremely large $D \to +\infty$ and charging energy $U >> E_i$ is much bigger than the single particle energies.

1. We start by examining term (B.11). For a single charge state the energy differences in the denominator takes the form

$$a = E_i - E_\delta = -3U + V_g + \Delta_a^{(1)} = -U + \Delta V_g + \Delta_a^{(1)}, \tag{B.69}$$

$$c = E_i - E_{\delta'} = -8U + 2V_g + \Delta_c^{(1)} = -4U + 2\Delta V_g + \Delta_c^{(2)}, \tag{B.70}$$

$$b = E_i - E_{\delta''} = -3U + V_g + \Delta_b^{(1)} = -U + \Delta V_g + \Delta_b^{(1)}, \tag{B.71}$$

Here $\Delta^{(n)}$ corresponds to sum of single particle energies

$$\Delta^{(n)} = \sum_{j=1}^{n} E_n, \tag{B.72}$$

with special case

$$\Delta^{(0)} = E_i - E_j, \tag{B.73}$$

being single particle energy difference. The expansion of results will be performed in small parameter values

$$x = \frac{\Delta^{(n)} + \Delta V_g}{U}. \tag{B.74}$$

The expansion of integrals I_1 and I_2 becomes

$$I_1 \approx \frac{1}{U}\ln\left(\frac{U}{D}\right) + \frac{8\ln(2)}{3U} \quad \to \quad \frac{8\ln(2)}{3U}, \tag{B.75}$$

$$I_2 \approx \frac{2[\mathrm{dilog}(4) - \mathrm{dilog}(4/3)] - \ln^2(3)}{4U}. \tag{B.76}$$

Here for I_1 we have neglected term dependent on D, because for very large bandwidth the result (tunneling renormalized energy differences) does not depend on it. Actually, the matrix elements themselves for fourth order do not depend on D. This was checked numerically, because it is too tedious to do that analytically.

2. For single charge states all (B.17) type terms vanish.

3. For term (B.22) the energy differences in the denominator takes the form

$$a = E_i - E_\delta = -U + \Delta V_g + \Delta_a^{(1)}, \tag{B.77}$$

$$c = E_i - E_{\delta'} = \Delta_c^{(0)}, \tag{B.78}$$

$$b = E_i - E_{\delta''} = -U + \Delta V_g + \Delta_b^{(1)}. \tag{B.79}$$

The expansion of integral I_1 becomes

$$\begin{aligned} I_1 &\approx \frac{1}{U}\ln\left(\frac{U}{D}\right) + \frac{\Delta_c^{(0)}}{U^2}\ln\left|\frac{\Delta_c^{(0)}}{U}\right| + \frac{(\Delta_a^{(1)} + \Delta_b^{(1)} + 2V_g)}{2U^2}\ln\left(\frac{U}{\mathrm{e}D}\right), \\ &\to \frac{\Delta_c^{(0)}}{U^2}\ln\left|\frac{\Delta_c^{(0)}}{U}\right| - \frac{(\Delta_a^{(1)} + \Delta_b^{(1)} + 2V_g)}{2U^2}. \end{aligned} \tag{B.80}$$

We again have neglected D dependent terms.

4. For term (B.27) the energy differences in the denominator take the form

$$a = E_i - E_\delta = -U - \Delta V_g - \Delta_a^{(1)}, \tag{B.81}$$

$$c = E_i - E_{\delta'} = \Delta_c^{(0)}, \tag{B.82}$$

$$b = E_i - E_{\delta''} = -U - \Delta V_g - \Delta_b^{(1)}. \tag{B.83}$$

The expansion of integral I_1 becomes

$$\begin{aligned} I_1 &\approx \frac{1}{U}\ln\left(\frac{U}{D}\right) + \frac{\Delta_c^{(0)}}{U^2}\ln\left|\frac{\Delta_c^{(0)}}{U}\right| - \frac{(\Delta_a^{(1)} + \Delta_b^{(1)} + 2V_g)}{2U^2}\ln\left(\frac{U}{\mathrm{e}D}\right), \\ &\to \frac{\Delta_c^{(0)}}{U^2}\ln\left|\frac{\Delta_c^{(0)}}{U}\right| + \frac{(\Delta_a^{(1)} + \Delta_b^{(1)} + 2V_g)}{2U^2}. \end{aligned} \tag{B.84}$$

5. For term (B.32) the energy differences in the denominator take the form

$$a = E_i - E_\delta = -U + \Delta V_g + \Delta_a^{(1)}, \tag{B.85}$$

$$c = E_i - E_{\delta'} = \Delta_c^{(0)}, \tag{B.86}$$

$$b = E_i - E_{\delta''} = -U - \Delta V_g - \Delta_b^{(1)}. \tag{B.87}$$

The expansion of integral I_2 becomes

$$I_2 \approx -\frac{\pi^2}{4U} + \frac{\Delta_c^{(0)}}{U^2}\ln\left|\frac{\Delta_c^{(0)}}{\mathrm{e}U}\right| - \frac{\pi^2(\Delta_a^{(1)} - \Delta_b^{(1)} - \Delta_c^{(0)})}{8U^2}. \tag{B.88}$$

6. For term (B.37) the energy differences in the denominator take the form

$$a = E_i - E_\delta = -U - \Delta V_g - \Delta_a^{(1)}, \tag{B.89}$$

$$c = E_i - E_{\delta'} = \Delta_c^{(0)}, \tag{B.90}$$

$$b = E_i - E_{\delta''} = -U + \Delta V_g + \Delta_b^{(1)}. \tag{B.91}$$

The expansion of integral I_2 becomes

$$I_2 \approx -\frac{\pi^2}{4U} + \frac{\Delta_c^{(0)}}{U^2} \ln\left|\frac{\Delta_c^{(0)}}{eU}\right| - \frac{\pi^2(\Delta_b^{(1)} - \Delta_a^{(1)} - \Delta_c^{(0)})}{8U^2}. \tag{B.92}$$

We can get this result from (B.88) by interchanging a with b.

2nd Expression. For second expression terms the energy differences in the denominator take the form

$$a = -U \pm (\Delta V_g + \Delta_a^{(1)}), \tag{B.93}$$

$$b = -U \pm (\Delta V_g + \Delta_b^{(1)}), \tag{B.94}$$

$$c = -U \pm (\Delta V_g + \Delta_c^{(1)}), \tag{B.95}$$

where all possible sign combinations can be taken. We will examine only the term with all pluses, because result for other signs does not differ qualitatively. The expansion of integral I_3 becomes

$$\begin{aligned} I_3 &\approx \frac{1}{U}\ln\left(\frac{U}{D}\right) + \frac{\Delta_a^{(1)} + \Delta_b^{(1)} + 2\Delta V_g}{2U^2}\ln\left(\frac{U}{D}\right) - \frac{\Delta_c^{(1)} + \Delta V_g}{U^2} \\ &\to -\frac{\Delta_c^{(1)} + \Delta V_g}{U^2}. \end{aligned} \tag{B.96}$$

Appendix C

Analytical expressions for a single charge in a "shell" eigenspectrum

If we consider quantum dot consisting of four single particle orbitals of single "shell", the second order effective Hamiltonian (2.29) acquires the following matrix-block structure, where different blocks correspond to different charge states:

$$H^{(2)}_{DD'} \to \begin{pmatrix}
\cdot & & & & & & & & & & & & & & & \\
 & \cdot & \cdot & \cdot & \cdot & & & & & & & & & & & \\
 & \cdot & \cdot & \cdot & \cdot & & & & & & & & & & & \\
 & \cdot & \cdot & \cdot & \cdot & & & & & & & & & & & \\
 & \cdot & \cdot & \cdot & \cdot & & & & & & & & & & & \\
 & & & & & \cdot & \cdot & \cdot & \cdot & \cdot & 0 & & & & & \\
 & & & & & \cdot & \cdot & \cdot & \cdot & 0 & \cdot & & & & & \\
 & & & & & \cdot & \cdot & \cdot & 0 & \cdot & \cdot & & & & & \\
 & & & & & \cdot & \cdot & 0 & \cdot & \cdot & \cdot & & & & & \\
 & & & & & \cdot & 0 & \cdot & \cdot & \cdot & \cdot & & & & & \\
 & & & & & 0 & \cdot & \cdot & \cdot & \cdot & \cdot & & & & & \\
 & & & & & & & & & & & \cdot & \cdot & \cdot & \cdot & \\
 & & & & & & & & & & & \cdot & \cdot & \cdot & \cdot & \\
 & & & & & & & & & & & \cdot & \cdot & \cdot & \cdot & \\
 & & & & & & & & & & & \cdot & \cdot & \cdot & \cdot & \\
 & & & & & & & & & & & \cdot & \cdot & \cdot & \cdot & \\
 & & & & & & & & & & & & & & & \cdot
\end{pmatrix}. \tag{C.1}$$

We examine the first 4×4 block corresponding to a single charge many-body states. The elements of this 4×4 matrix, which we will call $\mathcal{H}_{i,j}$ can be expressed as

$$\mathcal{H}_{i,j} = (U - V_g + E_i)\delta_{i,j} + \sum_{\alpha\sigma}\rho_{\alpha\sigma}\begin{cases} |t^i_{\alpha\sigma}|^2 \ln\left|\dfrac{U - V_g + E_i - \mu_\alpha}{D}\right| + \displaystyle\sum_{k\neq i}|t^k_{\alpha\sigma}|^2 \ln\left|\dfrac{3U - V_g + E_k - \mu_\alpha}{D}\right|, & i = j, \\ \dfrac{1}{2}(t^i_{\alpha\sigma})^* t^j_{\alpha\sigma} \ln\left|\dfrac{(U - V_g + E_i - \mu_\alpha)(U - V_g + E_j - \mu_\alpha)}{(3U - V_g + E_i - \mu_\alpha)(3U - V_g + E_j - \mu_\alpha)}\right|, & i \neq j. \end{cases} \tag{C.2}$$

Here $V_g = 2UN_g$. We will rewrite this expression by shifting diagonals by a constant

$$-\left(U - V_g + \sum_{\alpha\sigma k}\rho_{\alpha\sigma}|t^k_{\alpha\sigma}|\ln\frac{U}{D}\right). \tag{C.3}$$

and by changing $V_g = 2U + \frac{\Delta V_g}{2}$. This yields

$$\mathcal{H}_{i,j} = E_i\delta_{i,j} + \sum_{\alpha\sigma}\rho_{\alpha\sigma}\begin{cases} |t^i_{\alpha\sigma}|^2 \ln\left|1 - \dfrac{E_i - \Delta V_g/2 - \mu_\alpha}{U}\right| + \displaystyle\sum_{k\neq i}|t^k_{\alpha\sigma}|^2 \ln\left|1 + \dfrac{E_k - \Delta V_g/2 - \mu_\alpha}{U}\right|, & i = j, \\ \dfrac{1}{2}(t^i_{\alpha\sigma})^* t^j_{\alpha\sigma} \ln\left|\dfrac{\left(1 - \frac{E_i - \Delta V_g/2 - \mu_\alpha}{U}\right)\left(1 - \frac{E_j - \Delta V_g/2 - \mu_\alpha}{U}\right)}{\left(1 + \frac{E_i - \Delta V_g/2 - \mu_\alpha}{U}\right)\left(1 + \frac{E_j - \Delta V_g/2 - \mu_\alpha}{U}\right)}\right|, & i \neq j. \end{cases} \tag{C.4}$$

In the calculations we will also need expressions of the form

$$\mathcal{H}_{i,i} - \mathcal{H}_{j,j} = E_i - E_j + \sum_{\alpha\sigma} \rho_{\alpha\sigma} \left\{ |t^i_{\alpha\sigma}|^2 \ln \left| \frac{1 - \frac{E_i - \Delta V_g/2 - \mu_\alpha}{U}}{1 + \frac{E_i - \Delta V_g/2 - \mu_\alpha}{U}} \right| - |t^j_{\alpha\sigma}|^2 \ln \left| \frac{1 - \frac{E_j - \Delta V_g/2 - \mu_\alpha}{U}}{1 + \frac{E_j - \Delta V_g/2 - \mu_\alpha}{U}} \right| \right\}, \tag{C.5a}$$

$$\begin{aligned} \mathcal{H}_{i,i} + \mathcal{H}_{j,j} = E_i + E_j + \sum_{\alpha\sigma} \rho_{\alpha\sigma} \Bigg\{ & |t^i_{\alpha\sigma}|^2 \ln \left| \left(1 - \frac{E_i - \Delta V_g/2 - \mu_\alpha}{U}\right) \left(1 + \frac{E_i - \Delta V_g/2 - \mu_\alpha}{U}\right) \right| \\ & + |t^j_{\alpha\sigma}|^2 \ln \left| \left(1 - \frac{E_j - \Delta V_g/2 - \mu_\alpha}{U}\right) \left(1 + \frac{E_j - \Delta V_g/2 - \mu_\alpha}{U}\right) \right| \\ & + 2 \sum_{k \neq i,j} |t^k_{\alpha\sigma}|^2 \ln \left| 1 + \frac{E_k - \Delta V_g/2 - \mu_\alpha}{U} \right| \Bigg\}. \end{aligned} \tag{C.5b}$$

Now we will expand logarithms in

$$x_{\alpha i} = \frac{E_i - \Delta V_g/2 - \mu_\alpha}{U}. \tag{C.6}$$

We see that we need to deal with expansion of the functions

$$\ln|1 + x| = \sum_{n=1}^{\infty} (-1)^{n+1} \frac{x^n}{n} = x - \frac{1}{2}x^2 + \ldots, \tag{C.7a}$$

$$\ln \left| \frac{1 - x}{1 + x} \right| = -2 \sum_{n=0}^{\infty} \frac{x^{2n+1}}{2n+1} = -2\left(x + \frac{1}{3}x^3 + \ldots\right), \tag{C.7b}$$

$$\ln|(1 - x)(1 + x)| = -\sum_{n=1}^{\infty} \frac{x^{2n}}{n} = -\left(x^2 + \frac{1}{2}x^4 + \ldots\right). \tag{C.7c}$$

So the expressions (C.5) to lowest order in $x_{\alpha i}$ become

$$\mathcal{H}_{i,i} - \mathcal{H}_{j,j} \approx E_i - E_j - 2 \sum_{\alpha\sigma} \rho_{\alpha\sigma} \left\{ |t^i_{\alpha\sigma}|^2 x_{\alpha i} - |t^j_{\alpha\sigma}|^2 x_{\alpha j} \right\}, \tag{C.8a}$$

$$\mathcal{H}_{i,i} + \mathcal{H}_{j,j} \approx E_i + E_j + 2 \sum_{k \neq i,j} \sum_{\alpha\sigma} \rho_{\alpha\sigma} |t^k_{\alpha\sigma}|^2 x_{\alpha k}. \tag{C.8b}$$

and off-diagonals

$$\mathcal{H}_{i,j} \approx -\sum_{\alpha\sigma} \rho_{\alpha\sigma} (t^i_{\alpha\sigma})^* t^j_{\alpha\sigma} \left(x_{\alpha i} + x_{\alpha j} \right), \quad i \neq j. \tag{C.9}$$

Note that we will also use the following notation

$$V_\alpha = \frac{\Delta V_g}{2} + \mu_\alpha. \tag{C.10}$$

C.1 Zero and parallel magnetic B field

Here we will do explicit calculations of the tunneling renormalized eigenspectrum, when magnetic field is parallel to the tube axis ($\zeta = 0$). In such a case the single particle Hamiltonian (3.58) is

$$H = \begin{array}{c} \begin{matrix} |K\uparrow\rangle & |K'\downarrow\rangle & |K\downarrow\rangle & |K'\uparrow\rangle \end{matrix} \\ \begin{pmatrix} E_{+1,+1} + \frac{1}{2}g_s B_\parallel & & & \frac{1}{2}\Delta_{KK'} e^{i\phi_{KK'}} \\ & E_{-1,-1} - \frac{1}{2}g_s B_\parallel & \frac{1}{2}\Delta_{KK'} e^{-i\phi_{KK'}} & \\ & \frac{1}{2}\Delta_{KK'} e^{i\phi_{KK'}} & E_{+1,-1} - \frac{1}{2}g_s B_\parallel & \\ \frac{1}{2}\Delta_{KK'} e^{-i\phi_{KK'}} & & & E_{-1,+1} + \frac{1}{2}g_s B_\parallel \end{pmatrix} \end{array}, \tag{C.11}$$

where $\Delta_{KK'}$ denotes modulus of KK' mixing. After diagonalizing the above Hamiltonian we find the eigenspectrum of the "shell" and the new eigenstates in terms of KK'-basis states, which are:

$$E_i \in \left\{\frac{1}{2}(B_s+\Delta_1), \frac{1}{2}(-B_s+\Delta_2), \frac{1}{2}(-B_s-\Delta_2), \frac{1}{2}(B_s-\Delta_1)\right\}, \tag{C.12}$$

$$\mathcal{P}_{i,n} = \begin{pmatrix} \mathcal{P}_{1,1} & 0 & 0 & \mathcal{P}_{1,4} \\ 0 & \mathcal{P}_{2,2} & \mathcal{P}_{2,3} & 0 \\ 0 & \mathcal{P}_{3,2} & \mathcal{P}_{3,3} & 0 \\ \mathcal{P}_{4,1} & 0 & 0 & \mathcal{P}_{4,4} \end{pmatrix} = \begin{pmatrix} u_1 & 0 & 0 & -v_1 e^{i\phi_{KK'}} \\ 0 & u_2 & -v_2 e^{-i\phi_{KK'}} & 0 \\ 0 & v_2 e^{i\phi_{KK'}} & u_2 & 0 \\ v_1 e^{-i\phi_{KK'}} & 0 & 0 & u_1 \end{pmatrix}, \tag{C.13}$$

where

$$\begin{aligned} &u_i = \sqrt{\frac{1}{2}\left(1+\frac{\delta_i}{\Delta_i}\right)}, \quad v_i = \sqrt{\frac{1}{2}\left(1-\frac{\delta_i}{\Delta_i}\right)}, \quad u_i v_i = \frac{\Delta_{KK'}}{2\Delta_i}, \quad i=1,2, \\ &\Delta_i = \sqrt{\delta_i^2+\Delta_{KK'}^2}, \quad \delta_1 = \Delta_{\mathrm{SO}} - B_{\mathrm{orb}}, \quad \delta_2 = \Delta_{\mathrm{SO}} + B_{\mathrm{orb}}, \\ &B_s = g_s B, \quad B_{\mathrm{orb}} = g_{\mathrm{orb}} B, \end{aligned} \tag{C.14}$$

In this case the Hamiltonian $\mathcal{H}_{i,j}$ simplifies to

$$\mathcal{H}_{i,j} = \begin{pmatrix} \mathcal{H}_{1,1} & 0 & 0 & \mathcal{H}_{1,4} \\ 0 & \mathcal{H}_{2,2} & \mathcal{H}_{2,3} & 0 \\ 0 & \mathcal{H}_{2,3}^* & \mathcal{H}_{3,3} & 0 \\ \mathcal{H}_{1,4}^* & 0 & 0 & \mathcal{H}_{4,4} \end{pmatrix}, \tag{C.15}$$

and has the eigenvalues

$$\frac{1}{2}\left(\mathcal{H}_{1,1}+\mathcal{H}_{4,4} \pm \sqrt{(\mathcal{H}_{1,1}-\mathcal{H}_{4,4})^2+4|\mathcal{H}_{1,4}|^2}\right), \tag{C.16a}$$

$$\frac{1}{2}\left(\mathcal{H}_{2,2}+\mathcal{H}_{3,3} \pm \sqrt{(\mathcal{H}_{2,2}-\mathcal{H}_{3,3})^2+4|\mathcal{H}_{2,3}|^2}\right), \tag{C.16b}$$

and eigenvectors

$$\mathcal{P} = \begin{pmatrix} \tilde{u}_1 & -\tilde{v}_1 e^{i\phi_{\mathcal{H}_{1,4}}} & 0 & 0 \\ 0 & 0 & \tilde{u}_2 & -\tilde{v}_2 e^{i\phi_{\mathcal{H}_{2,3}}} \\ 0 & 0 & \tilde{v}_2 e^{-i\phi_{\mathcal{H}_{2,3}}} & \tilde{u}_2 \\ \tilde{v}_1 e^{-i\phi_{\mathcal{H}_{1,4}}} & \tilde{u}_1 & 0 & 0 \end{pmatrix}, \quad \phi_{\mathcal{H}} = \mathrm{Arg}\,\mathcal{H}, \tag{C.17}$$

with

$$\tilde{u}_1, \tilde{v}_1 = \sqrt{\frac{1}{2}\left(1 \pm \frac{\mathcal{H}_{1,1}-\mathcal{H}_{4,4}}{\sqrt{(\mathcal{H}_{1,1}-\mathcal{H}_{4,4})^2+4|\mathcal{H}_{1,4}|^2}}\right)}, \quad \tilde{u}_2, \tilde{v}_2 = \sqrt{\frac{1}{2}\left(1 \pm \frac{\mathcal{H}_{2,2}-\mathcal{H}_{3,3}}{\sqrt{(\mathcal{H}_{2,2}-\mathcal{H}_{3,3})^2+4|\mathcal{H}_{2,3}|^2}}\right)}. \tag{C.18}$$

The tunneling amplitudes to the "shell" single particle sates after the inclusions of KK'-mixing take the following form

$$\begin{aligned} t_{\alpha\sigma}^1 &= \delta_{\sigma\uparrow}\left(u_1 t_{\alpha 1} + v_1 e^{-i\phi_{KK'}} t_{\alpha 2}^*\right), \\ t_{\alpha\sigma}^2 &= \delta_{\sigma\downarrow}\left(u_2 t_{\alpha 1}^* + v_2 e^{i\phi_{KK'}} t_{\alpha 2}\right), \\ t_{\alpha\sigma}^3 &= \delta_{\sigma\downarrow}\left(-v_2 e^{-i\phi_{KK'}} t_{\alpha 1}^* + u_2 t_{\alpha 2}\right), \\ t_{\alpha\sigma}^4 &= \delta_{\sigma\uparrow}\left(-v_1 e^{i\phi_{KK'}} t_{\alpha 1} + u_1 t_{\alpha 2}^*\right), \end{aligned} \tag{C.19}$$

where it is assumed that (3.64) are only non-zero tunneling amplitudes. In such a case the spin sums become:

$$\sum_\sigma \rho_{\alpha\sigma}|t^1_{\alpha\sigma}|^2 = \rho_{\alpha\uparrow}\left\{u_1^2|t_{\alpha1}|^2 + v_1^2|t_{\alpha2}|^2 + 2u_1v_1\,\mathrm{Re}[\mathrm{e}^{\mathrm{i}\phi_{KK'}}t_{\alpha1}t_{\alpha2}]\right\}, \tag{C.20a}$$

$$\sum_\sigma \rho_{\alpha\sigma}|t^2_{\alpha\sigma}|^2 = \rho_{\alpha\downarrow}\left\{u_2^2|t_{\alpha1}|^2 + v_2^2|t_{\alpha2}|^2 + 2u_2v_2\,\mathrm{Re}[\mathrm{e}^{-\mathrm{i}\phi_{KK'}}t^*_{\alpha1}t^*_{\alpha2}]\right\}, \tag{C.20b}$$

$$\sum_\sigma \rho_{\alpha\sigma}|t^3_{\alpha\sigma}|^2 = \rho_{\alpha\downarrow}\left\{v_2^2|t_{\alpha1}|^2 + u_2^2|t_{\alpha2}|^2 - 2u_2v_2\,\mathrm{Re}[\mathrm{e}^{-\mathrm{i}\phi_{KK'}}t^*_{\alpha1}t^*_{\alpha2}]\right\}, \tag{C.20c}$$

$$\sum_\sigma \rho_{\alpha\sigma}|t^4_{\alpha\sigma}|^2 = \rho_{\alpha\uparrow}\left\{v_1^2|t_{\alpha1}|^2 + u_1^2|t_{\alpha2}|^2 - 2u_1v_1\,\mathrm{Re}[\mathrm{e}^{\mathrm{i}\phi_{KK'}}t_{\alpha1}t_{\alpha2}]\right\}, \tag{C.20d}$$

$$\sum_\sigma \rho_{\alpha\sigma}(t^1_{\alpha\sigma})^* t^4_{\alpha\sigma} = \rho_{\alpha\uparrow}\left\{-u_1v_1\mathrm{e}^{\mathrm{i}\phi_{KK'}}|t_{\alpha1}|^2 + u_1^2t^*_{\alpha1}t^*_{\alpha2} - v_1^2\mathrm{e}^{\mathrm{i}2\phi_{KK'}}t_{\alpha1}t_{\alpha2} + u_1v_1\mathrm{e}^{\mathrm{i}\phi_{KK'}}|t_{\alpha2}|^2\right\}, \tag{C.20e}$$

$$\sum_\sigma \rho_{\alpha\sigma}(t^2_{\alpha\sigma})^* t^3_{\alpha\sigma} = \rho_{\alpha\downarrow}\left\{-u_2v_2\mathrm{e}^{-\mathrm{i}\phi_{KK'}}|t_{\alpha1}|^2 + u_2^2t_{\alpha1}t_{\alpha2} - v_2^2\mathrm{e}^{-\mathrm{i}2\phi_{KK'}}t^*_{\alpha1}t^*_{\alpha2} + u_2v_2\mathrm{e}^{-\mathrm{i}\phi_{KK'}}|t_{\alpha2}|^2\right\}. \tag{C.20f}$$

Using the above relations we evaluate (C.5) type expressions

$$\begin{aligned}\mathcal{H}_{1,1}-\mathcal{H}_{4,4} &= \Delta_1 - \sum_{\alpha\sigma}\frac{\rho_{\alpha\sigma}}{U}\left\{\Delta_1(|t^1_{\alpha\sigma}|^2+|t^4_{\alpha\sigma}|^2)+(B_s-2V_\alpha)(|t^1_{\alpha\sigma}|^2-|t^4_{\alpha\sigma}|^2)\right\}\\ &= \Delta_1 - \sum_{\alpha}\frac{\rho_{\alpha\uparrow}}{U}\left\{\Delta_1(|t_{\alpha1}|^2+|t_{\alpha2}|^2)+(B_s-2V_\alpha)\left[\frac{\delta_1}{\Delta_1}(|t_{\alpha1}|^2-|t_{\alpha2}|^2)+2\frac{\Delta_{KK'}}{\Delta_1}\,\mathrm{Re}[\mathrm{e}^{\mathrm{i}\phi_{KK'}}t_{\alpha1}t_{\alpha2}]\right]\right\},\end{aligned} \tag{C.21a}$$

$$\begin{aligned}\mathcal{H}_{2,2}-\mathcal{H}_{3,3} &= \Delta_2 - \sum_{\alpha\sigma}\frac{\rho_{\alpha\sigma}}{U}\left\{\Delta_2(|t^2_{\alpha\sigma}|^2+|t^3_{\alpha\sigma}|^2)-(B_s+2V_\alpha)(|t^2_{\alpha\sigma}|^2-|t^3_{\alpha\sigma}|^2)\right\}\\ &= \Delta_2 - \sum_{\alpha}\frac{\rho_{\alpha\downarrow}}{U}\left\{\Delta_2(|t_{\alpha1}|^2+|t_{\alpha2}|^2)-(B_s+2V_\alpha)\left[\frac{\delta_2}{\Delta_2}(|t_{\alpha1}|^2-|t_{\alpha2}|^2)+2\frac{\Delta_{KK'}}{\Delta_2}\,\mathrm{Re}[\mathrm{e}^{-\mathrm{i}\phi_{KK'}}t^*_{\alpha1}t^*_{\alpha2}]\right]\right\},\end{aligned} \tag{C.21b}$$

$$\begin{aligned}\mathcal{H}_{1,1}+\mathcal{H}_{4,4} &= B_s + \sum_{\alpha\sigma}\frac{\rho_{\alpha\sigma}}{U}\left\{\Delta_2(|t^2_{\alpha\sigma}|^2-|t^3_{\alpha\sigma}|^2)-(B_s+2V_\alpha)(|t^2_{\alpha\sigma}|^2+|t^3_{\alpha\sigma}|^2)\right\}\\ &= B_s + \sum_{\alpha}\frac{\rho_{\alpha\downarrow}}{U}\left\{\Delta_2\left[\frac{\delta_2}{\Delta_2}(|t_{\alpha1}|^2-|t_{\alpha2}|^2)+2\frac{\Delta_{KK'}}{\Delta_2}\,\mathrm{Re}[\mathrm{e}^{-\mathrm{i}\phi_{KK'}}t^*_{\alpha1}t^*_{\alpha2}]\right]-(B_s+2V_\alpha)(|t_{\alpha1}|^2+|t_{\alpha2}|^2)\right\},\end{aligned} \tag{C.21c}$$

$$\begin{aligned}\mathcal{H}_{2,2}+\mathcal{H}_{3,3} &= -B_s + \sum_{\alpha\sigma}\frac{\rho_{\alpha\sigma}}{U}\left\{\Delta_1(|t^1_{\alpha\sigma}|^2-|t^4_{\alpha\sigma}|^2)+(B_s-2V_\alpha)(|t^1_{\alpha\sigma}|^2+|t^4_{\alpha\sigma}|^2)\right\}\\ &= -B_s + \sum_{\alpha}\frac{\rho_{\alpha\uparrow}}{U}\left\{\Delta_1\left[\frac{\delta_1}{\Delta_1}(|t_{\alpha1}|^2-|t_{\alpha2}|^2)+2\frac{\Delta_{KK'}}{\Delta_1}\,\mathrm{Re}[\mathrm{e}^{\mathrm{i}\phi_{KK'}}t_{\alpha1}t_{\alpha2}]\right]+(B_s-2V_\alpha)(|t_{\alpha1}|^2+|t_{\alpha2}|^2)\right\},\end{aligned} \tag{C.21d}$$

and off-diagonals

$$\begin{aligned}\mathcal{H}_{1,4} &= -\sum_{\alpha\sigma}\frac{\rho_{\alpha\sigma}}{U}(t^1_{\alpha\sigma})^*t^4_{\alpha\sigma}(B_s-2V_\alpha)\\ &= \sum_{\alpha}\frac{\rho_{\alpha\uparrow}}{U}\mathrm{e}^{\mathrm{i}\phi_{KK'}}\left\{\frac{\Delta_{KK'}}{2\Delta_1}(|t^2_{\alpha1}|-|t^2_{\alpha_2}|)-\left[u_1^2\mathrm{e}^{-\mathrm{i}\phi_{KK'}}t^*_{\alpha1}t^*_{\alpha2}-v_1^2\mathrm{e}^{\mathrm{i}\phi_{KK'}}t_{\alpha1}t_{\alpha2}\right]\right\}(B_s-2V_\alpha),\end{aligned} \tag{C.22a}$$

$$\begin{aligned}\mathcal{H}_{2,3} &= \sum_{\alpha\sigma}\frac{\rho_{\alpha\sigma}}{U}(t^2_{\alpha\sigma})^*t^3_{\alpha\sigma}(B_s+2V_\alpha)\\ &= -\sum_{\alpha}\frac{\rho_{\alpha\downarrow}}{U}\mathrm{e}^{-\mathrm{i}\phi_{KK'}}\left\{\frac{\Delta_{KK'}}{2\Delta_2}(|t^2_{\alpha1}|-|t^2_{\alpha_2}|)-\left[u_2^2\mathrm{e}^{\mathrm{i}\phi_{KK'}}t_{\alpha1}t_{\alpha2}-v_2^2\mathrm{e}^{-\mathrm{i}\phi_{KK'}}t^*_{\alpha1}t^*_{\alpha2}\right]\right\}(B_s+2V_\alpha).\end{aligned} \tag{C.22b}$$

Often we will be rewriting expression in square brackets in (C.22) using relation:

$$\begin{aligned}&u^2\mathrm{e}^{\mathrm{i}\phi}-v^2\mathrm{e}^{-\mathrm{i}\phi} = \mathrm{i}\sin\phi+\frac{\delta}{\Delta}\cos\phi,\\ &\text{when } u^2=\frac{1}{2}\left(1+\frac{\delta}{\Delta}\right),\ v^2=\frac{1}{2}\left(1-\frac{\delta}{\Delta}\right).\end{aligned} \tag{C.23}$$

Now let's see how these expressions change for different parameters. Here throughout we assume normal leads $\rho_{\alpha\sigma}=\rho$ and applied symmetric bias $\mu_L=-\mu_R=V/2$:

Case 1: $t = |t|e^{i\phi_t} = t_{L/R,1/2}$, $\Delta_{SO} = \Delta_{KK'} = B = 0$:

$$\mathcal{H}_{1,1} - \mathcal{H}_{4,4} = \mathcal{H}_{2,2} - \mathcal{H}_{3,3} = 0, \tag{C.24a}$$

$$\mathcal{H}_{1,1} + \mathcal{H}_{4,4} = \mathcal{H}_{2,2} + \mathcal{H}_{3,3} = -\frac{4\rho|t|^2}{U}\Delta V_g, \tag{C.24b}$$

$$\mathcal{H}^*_{1,4} = \mathcal{H}_{2,3} = \frac{4\rho t^2}{U}\frac{\Delta V_g}{2}. \tag{C.24c}$$

The eigenvalues and eigenvectors in this case are

$$-\frac{2\rho|t|^2}{U}\left(\Delta V_g \mp |\Delta V_g|\right), -\frac{2\rho|t|^2}{U}\left(\Delta V_g \mp |\Delta V_g|\right) \quad \rightarrow \quad 0, -\frac{4\rho|t|^2}{U}\Delta V_g, \tag{C.25}$$

$$\mathcal{P} = \frac{1}{\sqrt{2}}\begin{pmatrix} 1 & -e^{-i\phi} & 0 & 0 \\ 0 & 0 & 1 & -e^{i\phi} \\ 0 & 0 & e^{-i\phi} & 1 \\ e^{i\phi} & 1 & 0 & 0 \end{pmatrix}, \tag{C.26}$$

where

$$\phi = 2\phi_t + \mathrm{Arg}(\Delta V_g). \tag{C.27}$$

The order of eigenstates corresponds to eigenvalues written in the order of (C.25) before the arrow. The modulus of the energy differences is

$$\Delta E = 2|\mathcal{H}_{2,3}| = \frac{4\rho|t|^2}{U}|\Delta V_g| = \frac{\Gamma}{\pi U}|\Delta V_g|, \quad \Gamma = 4\pi\rho|t|^2. \tag{C.28}$$

We see that cotunneling threshold acquires gate dependence due to the tunneling renormalization. Also from (C.26) we get the new effective "single particle states"

$$|a\uparrow\rangle = \frac{1}{\sqrt{2}}\left(|K\uparrow\rangle + e^{i\phi}|K'\uparrow\rangle\right), \tag{C.29a}$$

$$|b\uparrow\rangle = \frac{1}{\sqrt{2}}\left(-e^{-i\phi}|K\uparrow\rangle + |K'\uparrow\rangle\right), \tag{C.29b}$$

$$|a\downarrow\rangle = \frac{1}{\sqrt{2}}\left(|K'\downarrow\rangle + e^{-i\phi}|K\downarrow\rangle\right), \tag{C.29c}$$

$$|b\downarrow\rangle = \frac{1}{\sqrt{2}}\left(-e^{i\phi}|K'\downarrow\rangle + |K\downarrow\rangle\right), \tag{C.29d}$$

which have the following tunneling amplitudes and tunneling rates

$$t^{a\uparrow}_{\alpha\uparrow} = \frac{1}{\sqrt{2}}\left(1 + e^{i\,\mathrm{Arg}(\Delta V_g)}\right)t, \quad \Gamma^{a\uparrow}_{\alpha\uparrow} = \rho|t|^2\left(1 + \cos[\mathrm{Arg}(\Delta V_g)]\right), \tag{C.30a}$$

$$t^{b\uparrow}_{\alpha\uparrow} = \frac{1}{\sqrt{2}}\left(1 - e^{-i\,\mathrm{Arg}(\Delta V_g)}\right)t^*, \quad \Gamma^{b\uparrow}_{\alpha\uparrow} = \rho|t|^2\left(1 - \cos[\mathrm{Arg}(\Delta V_g)]\right), \tag{C.30b}$$

$$t^{a\downarrow}_{\alpha\downarrow} = \frac{1}{\sqrt{2}}\left(1 + e^{-i\,\mathrm{Arg}(\Delta V_g)}\right)t^*, \quad \Gamma^{a\downarrow}_{\alpha\downarrow} = \rho|t|^2\left(1 + \cos[\mathrm{Arg}(\Delta V_g)]\right), \tag{C.30c}$$

$$t^{b\downarrow}_{\alpha\downarrow} = \frac{1}{\sqrt{2}}\left(1 - e^{i\,\mathrm{Arg}(\Delta V_g)}\right)t, \quad \Gamma^{b\downarrow}_{\alpha\downarrow} = \rho|t|^2\left(1 - \cos[\mathrm{Arg}(\Delta V_g)]\right). \tag{C.30d}$$

Case 2: $t_L = |t_L|e^{i\phi_L} = t_{L,1/2}$, $t_R = |t_R|e^{i\phi_R} = t_{R,1/2}$, $\Delta_{SO} = \Delta_{KK'} = B = 0$:

$$\mathcal{H}_{1,1} - \mathcal{H}_{4,4} = \mathcal{H}_{2,2} - \mathcal{H}_{3,3} = 0, \tag{C.31a}$$

$$\mathcal{H}_{1,1} + \mathcal{H}_{4,4} = \mathcal{H}_{2,2} + \mathcal{H}_{3,3} = -\frac{2\rho}{U}\left\{(|t_L|^2 + |t_R|^2)\Delta V_g + (|t_L|^2 - |t_R|^2)V\right\}, \tag{C.31b}$$

$$\mathcal{H}^*_{1,4} = \mathcal{H}_{2,3} = \frac{\rho}{U}\left\{(t_L^2 + t_R^2)\Delta V_g + (t_L^2 - t_R^2)V\right\}, \tag{C.31c}$$

and the modulus of energy difference is

$$\Delta E = 2|\mathcal{H}_{2,3}| = \frac{2\rho}{U}\left|(t_L^2 + t_R^2)\Delta V_g + (t_L^2 - t_R^2)V\right|. \tag{C.32}$$

Using this energy difference we find the threshold voltage

$$V_{th} = |A\Delta V_g + BV_{th}|, \quad A = \frac{2\rho}{U}(t_L^2 + t_R^2), \quad B = \frac{2\rho}{U}(t_L^2 - t_R^2), \quad B << 1, \tag{C.33}$$

by solving quadratic equation (here D denotes discriminant)

$$\begin{aligned}
&(1 - |B|^2)V_{th}^2 - 2\,\mathrm{Re}[AB^*]\Delta V_g V_{th} - |A|^2\Delta V_g^2 = 0, \quad D = |2A\Delta V_g|^2,\\
&V_{th} = \frac{\mathrm{Re}[AB^*]\Delta V_g \pm |A|\Delta V_g}{1 - |B|^2} \approx (\mathrm{Re}[AB^*] \pm |A|)\Delta V_g,\\
&\downarrow \text{ and for real tunneling amplitudes it can be written as}\\
&V_{th} = \pm\frac{\Gamma_L + \Gamma_R}{\pi U}\left(1 \pm \frac{\Gamma_L - \Gamma_R}{\pi U}\right)\Delta V_g, \quad \text{where} \quad \Gamma_\alpha = 2\pi\rho|t_\alpha|^2.
\end{aligned} \tag{C.34}$$

From above expression we see that there is asymmetry between positive and negative bias threshold.

Case 3: $t = |t|e^{i\phi_t} = t_{L/R,1/2}$, $\Delta_{SO} \neq 0$, $B \neq 0$, $\Delta_{KK'} = 0$:

$$\mathrm{sgn}(\delta_1)(\mathcal{H}_{1,1} - \mathcal{H}_{4,4}) = \delta_1(1 - \kappa), \tag{C.35a}$$

$$\mathrm{sgn}(\delta_2)(\mathcal{H}_{2,2} - \mathcal{H}_{3,3}) = \delta_2(1 - \kappa), \tag{C.35b}$$

$$\mathcal{H}_{1,1} + \mathcal{H}_{4,4} = -\kappa\Delta V_g + B_s(1 - \kappa), \tag{C.35c}$$

$$\mathcal{H}_{2,2} + \mathcal{H}_{3,3} = -\kappa\Delta V_g - B_s(1 - \kappa), \tag{C.35d}$$

$$\mathcal{H}^*_{1,4} = \frac{\kappa}{2}e^{2i\phi_t}\left(\Delta V_g - B_s\right), \tag{C.35e}$$

$$\mathcal{H}_{2,3} = \frac{\kappa}{2}e^{2i\phi_t}\left(\Delta V_g + B_s\right), \tag{C.35f}$$

where we have denoted

$$\kappa = \frac{4\rho|t|^2}{U} = \frac{\Gamma}{\pi U}. \tag{C.36}$$

The four eigenenergies are

$$-\kappa\frac{\Delta V_g}{2} + \frac{B_s}{2}(1 - \kappa) \pm \frac{1}{2}\sqrt{(1 - \kappa)^2(\Delta_{SO} - B_{orb})^2 + \kappa^2\left(\Delta V_g + B_s\right)^2}, \tag{C.37a}$$

$$-\kappa\frac{\Delta V_g}{2} - \frac{B_s}{2}(1 - \kappa) \pm \frac{1}{2}\sqrt{(1 - \kappa)^2(\Delta_{SO} + B_{orb})^2 + \kappa^2\left(\Delta V_g - B_s\right)^2}. \tag{C.37b}$$

Thereinafter we will neglect constant shift $-\kappa\Delta V_g/2$ of all energies. When there is no magnetic field B_s, then $\delta_1 = \delta_2 = \Delta_{SO}$, and the energy splitting between two pairs of degenerate states becomes

$$\Delta E_{B=0} = \sqrt{(1 - \kappa)^2\Delta_{SO}^2 + \left(\kappa\Delta V_g\right)^2}. \tag{C.38}$$

Table C.1: Bare and renormalized g-factors for carbon nanotube quantum dot, when $\Delta_{SO} = 0$, $g_{orb} > g_s$, and $\kappa\Delta V_g >> B_s, B_{orb} > 0$

Cotunneling line	Bare transition from $K\downarrow$ to	Bare g-factor	Renormalized g-factor
1^{st}	$K\uparrow$	g_s	$(1-\kappa)g_s$
2^{nd}	$K'\downarrow$	g_{orb}	$\kappa g_s + (1-\kappa)^2 \frac{g_{orb}^2 B}{2\kappa\Delta V_g}$
3^{rd}	$K'\uparrow$	$g_s + g_{orb}$	$g_s + (1-\kappa)^2 \frac{g_{orb}^2 B}{2\kappa\Delta V_g}$

We see that in this case there is no more crossing, when $\Delta V_g = 0$, and we get splitting $2\Delta E_{B=0}$ for cotunneling threshold between negative and positive bias. When magnetic field is included and we are exactly around the middle of the diamond $\Delta V_g \approx 0$, we get the following energies after expanding square root when $\kappa << 1$

$$\frac{1}{2}(sB_s + \tau s\Delta_{SO} - \tau B_{orb})(1-\kappa), \tag{C.39}$$

with all possible sign combinations of $s = \pm 1$, $\tau = \pm 1$. This result is almost the same as for the bare spectrum case without tunneling renormalization, except for the factor $(1-\kappa)$.

Let's look at the case when $\Delta V_g > 0$ and $|\kappa\Delta V_g| >> |\Delta_{SO}|, |B|$, i.e. we expand

$$\sqrt{x^2 + (1+y)^2} \approx 1 + y + \frac{1}{2}x^2 \quad \text{with} \quad x = (1-\kappa)\frac{\Delta_{SO} \mp B_{orb}}{\kappa\Delta V_g},\ y = \pm\frac{B_s}{\Delta V_g}, \tag{C.40}$$

and then the energies become

$$4.\quad \frac{B_s}{2} + \frac{\kappa\Delta V_g}{2}\left(1 + \frac{(1-\kappa)^2}{2}\left[\frac{\Delta_{SO} - B_{orb}}{\kappa\Delta V_g}\right]^2\right), \tag{C.41a}$$

$$2.\quad \frac{B_s}{2}(1-2\kappa) - \frac{\kappa\Delta V_g}{2}\left(1 + \frac{(1-\kappa)^2}{2}\left[\frac{\Delta_{SO} - B_{orb}}{\kappa\Delta V_g}\right]^2\right), \tag{C.41b}$$

$$3.\quad -\frac{B_s}{2}(1-2\kappa) + \frac{\kappa\Delta V_g}{2}\left(1 + \frac{(1-\kappa)^2}{2}\left[\frac{\Delta_{SO} + B_{orb}}{\kappa\Delta V_g}\right]^2\right), \tag{C.41c}$$

$$1.\quad -\frac{B_s}{2} - \frac{\kappa\Delta V_g}{2}\left(1 + \frac{(1-\kappa)^2}{2}\left[\frac{\Delta_{SO} + B_{orb}}{\kappa\Delta V_g}\right]^2\right). \tag{C.41d}$$

Here the number labels correspond to sorting from the lowest energy to the highest, when $\Delta V_g > 0$ and $\Delta_{SO} = 0$. The comparison between bare g-factors and renormalized ones for different cotunneling lines, when $g_{orb} > g_s$ and $\Delta_{SO} = 0$, is given in Table C.1. We see that g-factor corresponding to g_{orb} now depends on magnetic B field and vanishes for $B = 0$. For finite B field orbital factor g_{orb} depends on the gate voltage ΔV_g. We note that in this case bare energies are

$$E_{K\downarrow} = -(g_{orb} + g_s)\frac{B}{2},\quad E_{K\uparrow} = -(g_{orb} - g_s)\frac{B}{2},\quad E_{K'\downarrow} = (g_{orb} - g_s)\frac{B}{2},\quad E_{K'\uparrow} = (g_{orb} + g_s)\frac{B}{2}. \tag{C.42}$$

Now we will expand (C.37) energies in B_s and B_{orb} assuming that $\Delta_{SO}, \Delta V_g >> |B_s|, |B_{orb}| > 0$. We need the expansion of the function

$$\begin{aligned}&\sqrt{a^2(1+x)^2 + b^2(1+y)^2} \approx \sqrt{a^2+b^2} + \frac{|a|x}{\sqrt{1+b^2/a^2}} + \frac{|b|y}{\sqrt{1+a^2/b^2}},\\ &\text{with} \quad a = (1-\kappa)\Delta_{SO},\ b = \kappa\Delta V_g,\ x = \frac{B_{orb}}{\Delta_{SO}},\ y = \frac{B_s}{\Delta V_g},\end{aligned} \tag{C.43}$$

Table C.2: Bare and renormalized g-factors for carbon nanotube quantum dot, when $g_{\rm orb} > g_s$, $\tilde{g}_{\rm orb} > \tilde{g}_s^{\pm}$, and $\kappa\Delta V_g > \Delta_{\rm SO} >> B_s, B_{\rm orb} > 0$

Cotunneling line	Bare transition from $K\downarrow$ to	Bare g-factor	Renormalized g-factor
$1^{\rm st}$	$K'\uparrow$	$g_s + g_{\rm orb}$	$(1-\kappa-\tilde{\kappa})g_s + \tilde{g}_{\rm orb}$
$2^{\rm nd}$	$K\uparrow$	g_s	$(1-\kappa)g_s$
$3^{\rm rd}$	$K'\downarrow$	$g_{\rm orb}$	$-\tilde{\kappa}g_s + \tilde{g}_{\rm orb}$

in x and y. Then the energies (C.37) become

$$\frac{B_s}{2}(1-\kappa) \pm \frac{1}{2}\left(\Delta E_{B=0} - \frac{(1-\kappa))}{\sqrt{1+\left(\frac{\kappa}{1-\kappa}\frac{\Delta V_g}{\Delta_{\rm SO}}\right)^2}} B_{\rm orb} + \frac{\kappa}{\sqrt{1+\left(\frac{1-\kappa}{\kappa}\frac{\Delta_{\rm SO}}{\Delta V_g}\right)^2}} B_s\right), \tag{C.44a}$$

$$-\frac{B_s}{2}(1-\kappa) \pm \frac{1}{2}\left(\Delta E_{B=0} + \frac{(1-\kappa)}{\sqrt{1+\left(\frac{\kappa}{1-\kappa}\frac{\Delta V_g}{\Delta_{\rm SO}}\right)^2}} B_{\rm orb} - \frac{\kappa}{\sqrt{1+\left(\frac{1-\kappa}{\kappa}\frac{\Delta_{\rm SO}}{\Delta V_g}\right)^2}} B_s\right). \tag{C.44b}$$

We will rewrite the above energies as

$$3.\quad \frac{\Delta E_{B=0}}{2} - (\tilde{g}_{\rm orb} - \tilde{g}_s^+)\frac{B}{2}, \tag{C.45a}$$

$$2.\ -\frac{\Delta E_{B=0}}{2} + (\tilde{g}_{\rm orb} + \tilde{g}_s^-)\frac{B}{2}, \tag{C.45b}$$

$$4.\quad \frac{\Delta E_{B=0}}{2} + (\tilde{g}_{\rm orb} - \tilde{g}_s^+)\frac{B}{2}, \tag{C.45c}$$

$$1.\ -\frac{\Delta E_{B=0}}{2} - (\tilde{g}_{\rm orb} + \tilde{g}_s^-)\frac{B}{2}, \tag{C.45d}$$

where

$$\tilde{\kappa} \approx \kappa\left[1+\left(\frac{1-\kappa}{\kappa}\frac{\Delta_{\rm SO}}{\Delta V_g}\right)^2\right]^{-1/2}, \tag{C.46a}$$

$$\tilde{g}_s^{\pm} \approx g_s(1-\kappa\pm\tilde{\kappa}), \tag{C.46b}$$

$$\tilde{g}_{\rm orb} \approx g_{\rm orb}(1-\kappa)\left[1+\left(\frac{\kappa}{1-\kappa}\frac{\Delta V_g}{\Delta_{\rm SO}}\right)^2\right]^{-1/2}. \tag{C.46c}$$

The number labels in (C.45) correspond to sorted energies from low to high for $\kappa\Delta V_g > \Delta_{\rm SO} >> B > 0$, and $\tilde{g}_{\rm orb} > \tilde{g}_s^{\pm}$. We again see gate voltage renormalization of $g_{\rm orb}$. In this case the comparison between bare g-factors and renormalized ones for different cotunneling lines, are given in Table C.2. We note that in this case bare energies are

$$\begin{aligned} E_{K\downarrow} &= -\frac{\Delta_{\rm SO}}{2} - (g_{\rm orb}+g_s)\frac{B}{2}, \quad E_{K'\uparrow} = -\frac{\Delta_{\rm SO}}{2} + (g_{\rm orb}+g_s)\frac{B}{2}, \\ E_{K\uparrow} &= \frac{\Delta_{\rm SO}}{2} - (g_{\rm orb}-g_s)\frac{B}{2}, \quad E_{K'\downarrow} = \frac{\Delta_{\rm SO}}{2} + (g_{\rm orb}-g_s)\frac{B}{2}. \end{aligned} \tag{C.47}$$

Case 4: $\Delta_{\mathrm{SO}} \neq 0$, $\Delta_{KK'} = B = V = 0$:

$$\mathrm{sgn}(\delta_1)(\mathcal{H}_{1,1} - \mathcal{H}_{4,4}) = \mathrm{sgn}(\delta_2)(\mathcal{H}_{2,2} - \mathcal{H}_{3,3}) = (1-\kappa^+)\Delta_{\mathrm{SO}} + \kappa^- \Delta V_g, \tag{C.48a}$$

$$\mathcal{H}_{1,1} + \mathcal{H}_{4,4} = \mathcal{H}_{2,2} + \mathcal{H}_{3,3} = \kappa^- \Delta_{\mathrm{SO}} - \kappa^+ \Delta V_g, \tag{C.48b}$$

$$\mathcal{H}^*_{1,4} = \mathcal{H}_{2,3} = \kappa_{12} \frac{\Delta V_g}{2}, \tag{C.48c}$$

where

$$\kappa^{\pm} = \sum_{\alpha} \frac{\rho}{U} \left(|t_{\alpha 1}|^2 \pm |t_{\alpha 2}|^2 \right), \; \kappa_{12} = \sum_{\alpha} \frac{2\rho}{U} t_{\alpha 1} t_{\alpha 2}. \tag{C.49}$$

We have set the chemical potentials to zero (i.e. bias $V = 0$), because we want to figure out whether we can get a crossing in the cotunneling threshold. Also all tunneling amplitudes are arbitrary. The modulus of the energy difference in this case is

$$\Delta E = \sqrt{\left\{ (1-\kappa^+)\Delta_{\mathrm{SO}} + \kappa^- \Delta V_g \right\}^2 + \left(|\kappa_{12}| \Delta V_g \right)^2}. \tag{C.50}$$

It is possible to get a crossing in cotunneling threshold if

$$\kappa_{12} = 0 \quad \rightarrow \quad t_{L1} t_{L2} + t_{R1} t_{R2} = 0, \tag{C.51a}$$

$$\Delta V_g = -\frac{1-\kappa^+}{\kappa^-} \Delta_{\mathrm{SO}}. \tag{C.51b}$$

One possible solution is

$$\begin{aligned} &t_1 = t_{L1} = t_{R1}, \quad t_2 = t_{L2} = \mathrm{e}^{\mathrm{i}\pi} t_{R2} = -t_{R2}, \\ &\Delta V_g \approx \frac{\pi U}{\Gamma_2 - \Gamma_1} \Delta_{\mathrm{SO}}, \quad \text{where} \quad \Gamma_i = 2\pi\rho |t_i|^2. \end{aligned} \tag{C.52}$$

Case 5: $t = |t| \mathrm{e}^{\mathrm{i}\phi_t} = t_{L/R,1/2}$, $\Delta_{\mathrm{SO}} \neq 0$, $\Delta_{KK'} \neq 0$, $B = 0$:

$$\mathcal{H}_{1,1} - \mathcal{H}_{4,4} = \mathcal{H}_{2,2} - \mathcal{H}_{3,3} = (1-\kappa)\Delta_{\Sigma} + \kappa \cos(\phi) \frac{\Delta_{KK'}}{\Delta_{\Sigma}} \Delta V_g, \tag{C.53a}$$

$$\mathcal{H}_{1,1} + \mathcal{H}_{4,4} = \mathcal{H}_{2,2} + \mathcal{H}_{3,3} = \kappa(\Delta_{KK'} \cos(\phi) - \Delta V_g), \tag{C.53b}$$

$$\mathcal{H}^*_{1,4} = \mathcal{H}_{2,3} = \kappa \mathrm{e}^{-\mathrm{i}\phi_{KK'}} \left(\frac{\Delta_{\mathrm{SO}}}{\Delta_{\Sigma}} \cos(\phi) + \mathrm{i} \sin(\phi) \right) \frac{\Delta V_g}{2}, \tag{C.53c}$$

where

$$\phi = \phi_{KK'} + 2\phi_t, \quad \Delta_{\Sigma} = \sqrt{\Delta_{\mathrm{SO}}^2 + \Delta_{KK'}^2}. \tag{C.54}$$

We note that one has to be careful when taking limit $\Delta_{\mathrm{SO}}, \Delta_{KK'} \to 0$. In this case the energy difference becomes

$$\Delta E = \sqrt{\left[(1-\kappa)\Delta_{\Sigma} + \kappa \cos(\phi) \frac{\Delta_{KK'}}{\Delta_{\Sigma}} \Delta V_g \right]^2 + \left| \kappa \left(\frac{\Delta_{\mathrm{SO}}}{\Delta_{\Sigma}} \cos(\phi) + \mathrm{i} \sin(\phi) \right) \Delta V_g \right|^2}. \tag{C.55}$$

The minimal value of splitting between positive and negative bias appears near gate voltage

$$\Delta V_g^{\min} = -\frac{1-\kappa}{\kappa} \Delta_{KK'} \cos(\phi), \tag{C.56}$$

and the value of this splitting is

$$\Delta E_{\min} = (1-\kappa) \sqrt{\Delta_{\mathrm{SO}}^2 + \Delta_{KK'}^2 \sin^2(\phi)}. \tag{C.57}$$

If $\Delta_{KK'} >> |\Delta_{SO}| \approx 0$ it is possible to get an approximate crossing, when $\phi = 0$ (or $\phi = \pi$) near the point

$$\Delta V_g^{\text{cross}} \approx \mp \frac{1-\kappa}{\kappa} \Delta_{KK'}. \tag{C.58}$$

Upper sign corresponds to $\phi = 0$, lower corresponds to $\phi = \pi$.

Case 6: $\Delta_{SO} \neq 0$, $\Delta_{KK'} \neq 0$, $B = V = 0$:

$$\mathcal{H}_{1,1} - \mathcal{H}_{4,4} = \mathcal{H}_{2,2} - \mathcal{H}_{3,3} = (1-\kappa^+)\Delta_\Sigma + \left(\kappa^- \frac{\Delta_{SO}}{\Delta_\Sigma} + \kappa_c \frac{\Delta_{KK'}}{\Delta_\Sigma}\right)\Delta V_g, \tag{C.59a}$$

$$\mathcal{H}_{1,1} + \mathcal{H}_{4,4} = \mathcal{H}_{2,2} + \mathcal{H}_{3,3} = \kappa^- \Delta_{SO} + \kappa_c \Delta_{KK'} - \kappa \Delta V_g, \tag{C.59b}$$

$$\mathcal{H}_{1,4}^* = \mathcal{H}_{2,3} = e^{-i\phi_{KK'}} \left(-\kappa^- \frac{\Delta_{KK'}}{\Delta_\Sigma} + \kappa_c \frac{\Delta_{SO}}{\Delta_\Sigma} + i\kappa_s\right) \frac{\Delta V_g}{2}, \tag{C.59c}$$

where

$$\kappa^\pm = \sum_\alpha \frac{\rho}{U}\left(|t_{\alpha 1}|^2 \pm |t_{\alpha 2}|^2\right) \quad \rightarrow \quad \frac{2\rho}{U}\left(|t_1|^2 \pm |t_2|^2\right), \tag{C.60a}$$

$$\kappa_c = \frac{2\rho}{U}\left(\cos(\phi_L)|t_{L1}t_{L2}| + \cos(\phi_R)|t_{R1}t_{R2}|\right) \quad \rightarrow \quad \frac{4\rho}{U}|t_1 t_2|\cos(\phi), \tag{C.60b}$$

$$\kappa_s = \frac{2\rho}{U}\left(\sin(\phi_L)|t_{L1}t_{L2}| + \sin(\phi_R)|t_{R1}t_{R2}|\right) \quad \rightarrow \quad \frac{4\rho}{U}|t_1 t_2|\sin(\phi), \tag{C.60c}$$

$$\phi_{L,R} = \phi_{KK'} + \phi_{L1,R1} + \phi_{L2,R2}, \tag{C.60d}$$

We have set chemical potentials to zero (i.e. bias $V = 0$), because we want to figure out whether we can get a crossing in the cotunneling threshold. Relations after the arrow correspond to symmetric coupling to the leads. By choosing all phases equal to zero, i.e. $\phi_L = \phi_R = 0$, we have to satisfy the condition

$$\kappa_c \Delta_{SO} = \kappa^- \Delta_{KK'} \quad \rightarrow \quad \frac{2\Delta_{SO}}{\Delta_{KK'}} = \frac{|t_1|^2 - |t_2|^2}{|t_1 t_2|}, \tag{C.61}$$

to get a crossing at

$$\Delta V_g^{\text{cross}} = -\frac{(1-\kappa^+)\Delta^2}{\kappa_c \Delta_{KK'} + \kappa^- \Delta_{SO}}. \tag{C.62}$$

Also we can get rid of the tunneling renormalization by removing the gate voltage ΔV_g dependence from the eigenspectrum. This is achieved by requiring

$$\kappa^- = 0, \quad \kappa_c = 0, \quad \kappa_s = 0 \quad \rightarrow \quad \kappa^- = 0, \quad \kappa_c + i\kappa_s = 0, \tag{C.63a}$$

which can be rewritten into conditions (4.13).

C.2 Perpendicular magnetic B field

Here we will perform calculation using spectrum and eigenstates, when magnetic field is perpendicular to the tube axis ($\zeta = \pi/2$). In such a case the single particle Hamiltonian (3.58) is

$$H = \begin{array}{c} \begin{matrix} |K\uparrow\rangle & |K'\downarrow\rangle & |K\downarrow\rangle & |K'\uparrow\rangle \end{matrix} \\ \begin{pmatrix} E_1 & & \frac{1}{2}g_s B_\perp & \frac{1}{2}\Delta_{KK'} e^{i\phi_{KK'}} \\ & E_1 & \frac{1}{2}\Delta_{KK'} e^{-i\phi_{KK'}} & \frac{1}{2}g_s B_\perp \\ \frac{1}{2}g_s B_\perp & \frac{1}{2}\Delta_{KK'} e^{i\phi_{KK'}} & E_2 & \\ \frac{1}{2}\Delta_{KK'} e^{-i\phi_{KK'}} & \frac{1}{2}g_s B_\perp & & E_2 \end{pmatrix} \end{array}, \tag{C.64}$$

where

$$E_1 = E_{+1,+1} = E_{-1,-1} = E^0 + \frac{\Delta_{\mathrm{SO}}}{2}, \quad E_2 = E_{+1,-1} = E_{-1,+1} = E^0 - \frac{\Delta_{\mathrm{SO}}}{2}. \tag{C.65}$$

Neglecting a constant shift in the energies E^0 the eigenvalues of the above Hamiltonian are

$$\pm\frac{1}{2}\sqrt{(B_s \pm \Delta_{KK'})^2 + \Delta_{\mathrm{SO}}^2}, \quad B_s = g_s B_\perp \tag{C.66}$$

with all possible sign combinations.

In order to get simple analytical results we will consider only a particular case, when there is no $\Delta_{KK'}$ mixing, and orbitals are equally coupled to the leads, i.e. $t_{1\alpha} = t_{2\alpha} = t_\alpha$. When $\Delta_{KK'} = 0$ the single particle eigenspectrum becomes

$$\pm\frac{1}{2}\sqrt{B_s^2 + \Delta_{\mathrm{SO}}^2}, \tag{C.67}$$

which is doubly degenerate. The corresponding eigenstates are

$$|K\bar{\uparrow}\rangle = +u|K\uparrow\rangle + v|K\downarrow\rangle, \tag{C.68a}$$
$$|K'\bar{\uparrow}\rangle = +u|K'\downarrow\rangle + v|K'\uparrow\rangle, \tag{C.68b}$$
$$|K\bar{\downarrow}\rangle = -v|K\uparrow\rangle + u|K\downarrow\rangle, \tag{C.68c}$$
$$|K'\bar{\downarrow}\rangle = -v|K'\downarrow\rangle + u|K'\uparrow\rangle, \tag{C.68d}$$

or written in a matrix form

$$\mathcal{P}_{i,n} = \begin{pmatrix} \mathcal{P}_{1,1} & 0 & \mathcal{P}_{1,3} & 0 \\ 0 & \mathcal{P}_{2,2} & 0 & \mathcal{P}_{2,4} \\ \mathcal{P}_{3,1} & 0 & \mathcal{P}_{3,3} & 0 \\ 0 & \mathcal{P}_{4,2} & 0 & \mathcal{P}_{4,4} \end{pmatrix} = \begin{pmatrix} u & 0 & -v & 0 \\ 0 & u & 0 & -v \\ v & 0 & u & 0 \\ 0 & v & 0 & u \end{pmatrix}, \tag{C.69}$$

where

$$u = \sqrt{\frac{1}{2}\left(1 + \frac{\Delta_{\mathrm{SO}}}{\Delta}\right)}, \quad v = \sqrt{\frac{1}{2}\left(1 - \frac{\Delta_{\mathrm{SO}}}{\Delta}\right)}\mathrm{sgn}(B_s), \quad \Delta = \sqrt{B_s^2 + \Delta_{\mathrm{SO}}^2}, \quad 2uv = \frac{B_s}{\Delta}. \tag{C.70}$$

The tunneling amplitudes take the following form

$$\begin{aligned} t^1_{\alpha\uparrow} &= +ut_{\alpha 1}, \quad t^1_{\alpha\downarrow} = +vt_{\alpha 2}, \\ t^2_{\alpha\uparrow} &= +vt^*_{\alpha 1}, \quad t^2_{\alpha\downarrow} = +ut^*_{\alpha 2}, \\ t^3_{\alpha\uparrow} &= -vt_{\alpha 1}, \quad t^3_{\alpha\downarrow} = +ut_{\alpha 2}, \\ t^4_{\alpha\uparrow} &= +ut^*_{\alpha 1}, \quad t^4_{\alpha\downarrow} = -vt^*_{\alpha 2}, \end{aligned} \tag{C.71}$$

and the spin sums become (taking $\rho_{\alpha\sigma} = \rho$ and $t_{1\alpha} = t_{2\alpha} = t_\alpha$):

$$\sum_\sigma \rho_{\alpha\sigma} |t^n_{\alpha\sigma}|^2 = \rho |t_\alpha|^2, \tag{C.72a}$$

$$\sum_\sigma \rho_{\alpha\sigma} (t^1_{\alpha\sigma})^* t^2_{\alpha\sigma} = \rho 2uv (t^*_\alpha)^2 = \rho \frac{B_s}{\Delta} (t^*_\alpha)^2, \tag{C.72b}$$

$$\sum_\sigma \rho_{\alpha\sigma} (t^1_{\alpha\sigma})^* t^3_{\alpha\sigma} = 0, \tag{C.72c}$$

$$\sum_\sigma \rho_{\alpha\sigma} (t^1_{\alpha\sigma})^* t^4_{\alpha\sigma} = \rho (u^2 - v^2)(t^*_\alpha)^2 = \rho \frac{\Delta_{\mathrm{SO}}}{\Delta} (t^*_\alpha)^2, \tag{C.72d}$$

$$\sum_\sigma \rho_{\alpha\sigma} (t^2_{\alpha\sigma})^* t^3_{\alpha\sigma} = \rho (u^2 - v^2) t^2_\alpha = \rho \frac{\Delta_{\mathrm{SO}}}{\Delta} t^2_\alpha, \tag{C.72e}$$

$$\sum_\sigma \rho_{\alpha\sigma} (t^2_{\alpha\sigma})^* t^4_{\alpha\sigma} = 0, \tag{C.72f}$$

$$\sum_\sigma \rho_{\alpha\sigma} (t^3_{\alpha\sigma})^* t^4_{\alpha\sigma} = -\rho 2uv (t^*_\alpha)^2 = -\rho \frac{B_s}{\Delta} (t^*_\alpha)^2. \tag{C.72g}$$

In this case Hamiltonian $\mathcal{H}_{i,j}$ simplifies to

$$\mathcal{H}_{i,j} = \begin{pmatrix} \mathcal{H}_{1,1} & \mathcal{H}_{1,2} & 0 & \mathcal{H}_{1,4} \\ \mathcal{H}^*_{1,2} & \mathcal{H}_{1,1} & \mathcal{H}_{2,3} & 0 \\ 0 & \mathcal{H}^*_{2,3} & \mathcal{H}_{3,3} & \mathcal{H}_{3,4} \\ \mathcal{H}^*_{1,4} & 0 & \mathcal{H}^*_{3,4} & \mathcal{H}_{3,3} \end{pmatrix} \rightarrow \begin{pmatrix} \frac{\mathcal{H}_{1,1} - \mathcal{H}_{3,3}}{2} & \mathcal{H}_{1,2} & 0 & \mathcal{H}_{1,4} \\ \mathcal{H}^*_{1,2} & \frac{\mathcal{H}_{1,1} - \mathcal{H}_{3,3}}{2} & \mathcal{H}_{2,3} & 0 \\ 0 & \mathcal{H}^*_{2,3} & -\frac{\mathcal{H}_{1,1} - \mathcal{H}_{3,3}}{2} & \mathcal{H}_{3,4} \\ \mathcal{H}^*_{1,4} & 0 & \mathcal{H}^*_{3,4} & -\frac{\mathcal{H}_{1,1} - \mathcal{H}_{3,3}}{2} \end{pmatrix}. \tag{C.73}$$

Here in the diagonal after the arrow we neglect constant factor $\frac{\mathcal{H}_{1,1} + \mathcal{H}_{3,3}}{2}$. After using relations (C.8a) and (C.9) we get the diagonal term

$$\mathcal{H}_{1,1} - \mathcal{H}_{3,3} = (1 - \kappa)\Delta, \quad \kappa = \frac{2\rho}{U}(|t_L|^2 + |t_R|^2), \tag{C.74}$$

and off-diagonals

$$\mathcal{H}_{1,2} = -\sum_\alpha \frac{\rho (t^*_\alpha)^2}{U} \frac{B_s}{\Delta} (\Delta - 2V_\alpha) = \frac{\kappa^*_+}{2} \frac{B_s}{\Delta} \left(\Delta V_g - \Delta \right) + \frac{\kappa^*_-}{2} \frac{B_s}{\Delta} V, \tag{C.75a}$$

$$\mathcal{H}_{1,4} = \mathcal{H}^*_{2,3} = -\sum_\alpha \frac{\rho (t^*_\alpha)^2}{U} \frac{\Delta_{\mathrm{SO}}}{\Delta} (\Delta - 2V_\alpha) = \frac{\kappa^*_+}{2} \frac{\Delta_{\mathrm{SO}}}{\Delta} \Delta V_g + \frac{\kappa^*_-}{2} \frac{\Delta_{\mathrm{SO}}}{\Delta} V, \tag{C.75b}$$

$$\mathcal{H}_{3,4} = +\sum_\alpha \frac{\rho (t^*_\alpha)^2}{U} \frac{B_s}{\Delta} (-\Delta - 2V_\alpha) = -\frac{\kappa^*_+}{2} \frac{B_s}{\Delta} \left(\Delta V_g + \Delta \right) - \frac{\kappa^*_-}{2} \frac{B_s}{\Delta} V, \tag{C.75c}$$

where

$$\kappa_+ = \frac{2\rho}{U}(t_L^2 + t_R^2), \quad \kappa_- = \frac{2\rho}{U}(t_L^2 - t_R^2). \tag{C.76}$$

To get simple analytical relations for solution of characteristic equation of (C.73) we also assume that tunneling amplitudes are real, i.e. $t_\alpha = t^*_\alpha$. In this case the Hamiltonian (C.73) can be written as

$$\mathcal{H}_{i,j} = \begin{pmatrix} \frac{z}{2} & x & 0 & w \\ x & \frac{z}{2} & w & 0 \\ 0 & w & -\frac{z}{2} & y \\ w & 0 & y & -\frac{z}{2} \end{pmatrix}, \quad \text{with} \quad \begin{aligned} z &= \mathcal{H}_{1,1} - \mathcal{H}_{3,3}, \\ x &= \mathcal{H}_{1,2}, \\ y &= \mathcal{H}_{3,4}, \\ w &= \mathcal{H}_{1,4}. \end{aligned} \tag{C.77}$$

Table C.3: Bare and renormalized g-factors for carbon nanotube with applied perpendicular field, when $\Delta_{SO} = 0$ and $\kappa\Delta V_g >> B_s > 0$

Cotunneling line	Bare g-factor	Renormalized g-factor
1^{st}	0	g_s
2^{nd}	g_s	κg_s
3^{rd}	g_s	$(1-\kappa)g_s$

The eigenvalues of the above Hamiltonian are

$$\frac{1}{2}\left(x+y\pm\sqrt{(x-y+z)^2+(2w)^2}\right),\quad -\frac{1}{2}\left(x+y\pm\sqrt{(x-y-z)^2+(2w)^2}\right). \tag{C.78}$$

Now we consider case when couplings to the left and right leads are equal $t_L = t_R$. In such a case $\kappa_- = 0$ and we get

$$x+y=-\kappa B_s,\quad x-y=\frac{B_s}{\Delta}\kappa\Delta V_g,\quad 2w=\frac{\Delta_{SO}}{\Delta}\kappa\Delta V_g,\quad z=(1-\kappa)\Delta. \tag{C.79}$$

If there is no spin-orbit coupling $\Delta_{SO} = 0$ and we are in the middle of the diamond $\Delta V_g = 0$, we get the following eigenspectrum, sorted from low to high energies ($B_s > 0$):

$$1.\ -\frac{B_s}{2},\quad 2.\ -(1-2\kappa)\frac{B_s}{2},\quad 3.\ (1-2\kappa)\frac{B_s}{2},\quad 4.\ \frac{B_s}{2}, \tag{C.80}$$

The corresponding g-factors for the above eigenspectrum are

$$1.\ \kappa g_s,\quad 2.\ (1-\kappa)g_s,\quad 3.\ g_s. \tag{C.81}$$

When there is still no spin-orbit coupling, but $\kappa\Delta V_g >> B > 0$ we get the following eigenspectrum

$$1.\ -\kappa\Delta V_g - B_s, \tag{C.82a}$$

$$2.\ -\kappa\Delta V_g + B_s, \tag{C.82b}$$

$$3.\ \ \kappa\Delta V_g - (1-2\kappa)B_s, \tag{C.82c}$$

$$4.\ \ \kappa\Delta V_g + (1+2\kappa)B_s. \tag{C.82d}$$

The comparison between bare and renormalized g-factors in this case is given in Table C.3.

When $\kappa\Delta V_g, \Delta_{SO} >> |B_s| > 0$ we can expand square root in spectrum (C.78). We rewrite this square root as

$$\sqrt{\left(\frac{ax}{\sqrt{1+x^2}}\pm b\sqrt{1+x^2}\right)^2+\left(\frac{a}{\sqrt{1+x^2}}\right)^2}\approx\sqrt{a^2+b^2}\pm\frac{ab}{\sqrt{a^2+b^2}}x, \tag{C.83}$$

$$\text{where}\quad x=\frac{B_s}{\Delta_{SO}},\ a=\kappa\Delta V_g,\ b=(1-\kappa)\Delta_{SO},$$

and then the spectrum becomes

$$1.\ -\frac{\Delta E_{B=0}}{2}-(\tilde{g}_s+\kappa g_s)\frac{B}{2}, \tag{C.84}$$

$$2.\ -\frac{\Delta E_{B=0}}{2}+(\tilde{g}_s+\kappa g_s)\frac{B}{2}, \tag{C.85}$$

$$3.\ \ \frac{\Delta E_{B=0}}{2}-(\tilde{g}_s-\kappa g_s)\frac{B}{2}, \tag{C.86}$$

$$4.\ \ \frac{\Delta E_{B=0}}{2}+(\tilde{g}_s-\kappa g_s)\frac{B}{2}, \tag{C.87}$$

Table C.4: Bare and renormalized g-factors for carbon nanotube with applied perpendicular field, when $\kappa\Delta V_g > \Delta_{\rm SO} >> B_s > 0$

Cotunneling line	Bare g-factor	Renormalized g-factor
$1^{\rm st}$	0	$\tilde{g}_s + \kappa g_s$
$2^{\rm nd}$	$\frac{g_s B}{2\Delta_{\rm SO}}$	κg_s
$3^{\rm rd}$	$\frac{g_s B}{2\Delta_{\rm SO}}$	$\tilde{g}_s$

where

$$\Delta E_{B=0} = \sqrt{(1-\kappa)^2\Delta_{\rm SO}^2 + \left(\kappa\Delta V_g\right)^2}, \tag{C.88a}$$

$$\tilde{g}_s \approx g_s(1-\kappa)\left[1+\left(\frac{1-\kappa}{\kappa}\frac{\Delta_{\rm SO}}{\Delta V_g}\right)^2\right]^{-1/2}. \tag{C.88b}$$

The comparison of g-factor in this case is given in Table C.4.

C.3 Ferromagnetic leads

If the leads are ferromagnetic, then the tunneling density of states is different for spin-up and spin-down $\rho_{\alpha\sigma}$, which has an effect on spin sums:

$$\begin{aligned}\sum_\sigma \rho_{\alpha\sigma}\,(t^n_{\alpha\sigma})^*\,t^{n'}_{\alpha\sigma} &= (t^n_{\alpha\uparrow})^* t^{n'}_{\alpha\uparrow}\left(\rho_{\alpha\tilde{\uparrow}}\cos^2(\theta_\alpha/2) + \rho_{\alpha\tilde{\downarrow}}\sin^2(\theta_\alpha/2)\right)\\ &+ (t^n_{\alpha\downarrow})^* t^{n'}_{\alpha\downarrow}\left(\rho_{\alpha\tilde{\uparrow}}\sin^2(\theta_\alpha/2) + \rho_{\alpha\tilde{\downarrow}}\cos^2(\theta_\alpha/2)\right)\\ &+ \left((t^n_{\alpha\uparrow})^* t^{n'}_{\alpha\downarrow}e^{-i\varphi_\alpha} + (t^n_{\alpha\downarrow})^* t^{n'}_{\alpha\uparrow}e^{i\varphi_\alpha}\right)\left(\rho_{\alpha\tilde{\uparrow}} - \rho_{\alpha\tilde{\downarrow}}\right)\sin(\theta_\alpha/2)\cos(\theta_\alpha/2).\end{aligned} \tag{C.89}$$

When there is no magnetic field $B = 0$, then the above sums become

$$\sum_\sigma \rho_{\alpha\sigma}|t^1_{\alpha\sigma}|^2 = \left\{\rho_{\alpha\tilde{\uparrow}}\cos^2(\theta_\alpha/2) + \rho_{\alpha\tilde{\downarrow}}\sin^2(\theta_\alpha/2)\right\}\left\{u^2|t_{\alpha1}|^2 + v^2|t_{\alpha2}|^2 + 2uv\,{\rm Re}[e^{i\phi_{KK'}}t_{\alpha1}t_{\alpha2}]\right\}, \tag{C.90a}$$

$$\sum_\sigma \rho_{\alpha\sigma}|t^2_{\alpha\sigma}|^2 = \left\{\rho_{\alpha\tilde{\uparrow}}\sin^2(\theta_\alpha/2) + \rho_{\alpha\tilde{\downarrow}}\cos^2(\theta_\alpha/2)\right\}\left\{u^2|t_{\alpha1}|^2 + v^2|t_{\alpha2}|^2 + 2uv\,{\rm Re}[e^{-i\phi_{KK'}}t^*_{\alpha1}t^*_{\alpha2}]\right\}, \tag{C.90b}$$

$$\sum_\sigma \rho_{\alpha\sigma}|t^3_{\alpha\sigma}|^2 = \left\{\rho_{\alpha\tilde{\uparrow}}\sin^2(\theta_\alpha/2) + \rho_{\alpha\tilde{\downarrow}}\cos^2(\theta_\alpha/2)\right\}\left\{v^2|t_{\alpha1}|^2 + u^2|t_{\alpha2}|^2 - 2uv\,{\rm Re}[e^{-i\phi_{KK'}}t^*_{\alpha1}t^*_{\alpha2}]\right\}, \tag{C.90c}$$

$$\sum_\sigma \rho_{\alpha\sigma}|t^4_{\alpha\sigma}|^2 = \left\{\rho_{\alpha\tilde{\uparrow}}\cos^2(\theta_\alpha/2) + \rho_{\alpha\tilde{\downarrow}}\sin^2(\theta_\alpha/2)\right\}\left\{v^2|t_{\alpha1}|^2 + u^2|t_{\alpha2}|^2 - 2uv\,{\rm Re}[e^{i\phi_{KK'}}t_{\alpha1}t_{\alpha2}]\right\}, \tag{C.90d}$$

$$\sum_\sigma \rho_{\alpha\sigma}(t^1_{\alpha\sigma})^* t^2_{\alpha\sigma} = \left(\rho_{\alpha\tilde{\uparrow}} - \rho_{\alpha\tilde{\downarrow}}\right)\frac{\sin\theta_\alpha}{2}\left\{u^2(t^*_{\alpha1})^2 + v^2e^{i2\phi_{KK'}}t^2_{\alpha2} + uv(e^{i\phi_{KK'}} + e^{i\phi_{KK'}})t^*_{\alpha1}t_{\alpha2}\right\}e^{-i\varphi_\alpha}, \tag{C.90e}$$

$$\sum_\sigma \rho_{\alpha\sigma}(t^1_{\alpha\sigma})^* t^3_{\alpha\sigma} = \left(\rho_{\alpha\tilde{\uparrow}} - \rho_{\alpha\tilde{\downarrow}}\right)\frac{\sin\theta_\alpha}{2}\left\{\left(u^2 - v^2\right)t^*_{\alpha1}t_{\alpha2} + uv\left(t^2_{\alpha2}e^{i\phi_{KK'}} - (t^*_{\alpha1})^2e^{-i\phi_{KK'}}\right)\right\}e^{-i\varphi_\alpha}, \tag{C.90f}$$

$$\sum_\sigma \rho_{\alpha\sigma}(t^1_{\alpha\sigma})^* t^4_{\alpha\sigma} = \left(\rho_{\alpha\tilde{\uparrow}}\cos^2(\theta_\alpha/2) + \rho_{\alpha\tilde{\downarrow}}\sin^2(\theta_\alpha/2)\right)\left\{u^2t^*_{\alpha1}t^*_{\alpha2} - v^2e^{i2\phi_{KK'}}t_{\alpha1}t_{\alpha2} + uve^{i\phi_{KK'}}(|t_{\alpha2}|^2 - |t_{\alpha1}|^2)\right\}, \tag{C.90g}$$

$$\sum_\sigma \rho_{\alpha\sigma}(t^2_{\alpha\sigma})^* t^3_{\alpha\sigma} = \left(\rho_{\alpha\tilde{\uparrow}}\sin^2(\theta_\alpha/2) + \rho_{\alpha\tilde{\downarrow}}\cos^2(\theta_\alpha/2)\right)\left\{u^2t_{\alpha1}t_{\alpha2} - v^2e^{-i2\phi_{KK'}}t^*_{\alpha1}t^*_{\alpha2} + uve^{-i\phi_{KK'}}(|t_{\alpha2}|^2 - |t_{\alpha1}|^2)\right\}, \tag{C.90h}$$

$$\sum_\sigma \rho_{\alpha\sigma}(t^2_{\alpha\sigma})^* t^4_{\alpha\sigma} = \left(\rho_{\alpha\tilde{\uparrow}} - \rho_{\alpha\tilde{\downarrow}}\right)\frac{\sin\theta_\alpha}{2}\left\{\left(u^2 - v^2\right)t_{\alpha1}t^*_{\alpha2} + uv\left((t^*_{\alpha2})^2e^{-i\phi_{KK'}} - t^2_{\alpha1}e^{i\phi_{KK'}}\right)\right\}e^{i\varphi_\alpha}, \tag{C.90i}$$

$$\sum_\sigma \rho_{\alpha\sigma}(t^3_{\alpha\sigma})^* t^4_{\alpha\sigma} = \left(\rho_{\alpha\tilde{\uparrow}} - \rho_{\alpha\tilde{\downarrow}}\right)\frac{\sin\theta_\alpha}{2}\left\{u^2(t^*_{\alpha2})^2 + v^2e^{i2\phi_{KK'}}t^2_{\alpha1} - uv(e^{i\phi_{KK'}} + e^{i\phi_{KK'}})t_{\alpha1}t^*_{\alpha2}\right\}e^{i\varphi_\alpha}. \tag{C.90j}$$

Note that u and v are defined by (C.14). Now we will consider situation when there is no KK'-mixing and spin-orbit coupling. In such a case for parallel collinear and anticollinear lead polarization Hamiltonian $\mathcal{H}_{i,j}$ simplifies into (C.15) form. As was mentioned previously in Section 5.3.1, when there is no spin-orbit coupling it is possible to arbitrarily choose spin-quantization axis in the quantum dot, so the upcoming result for parallel lead polarization is also valid for any angle.

Case 1: $\theta_\alpha = 0$, $\rho_{\alpha\sigma} = \rho_\sigma$, $\Delta_{\mathrm{SO}} = \Delta_{KK'} = B = V = 0$:

Using (C.21) and (C.22) relations and spin sums (C.90) we get:

$$\mathcal{H}_{1,1} - \mathcal{H}_{4,4} = \Delta V_g \kappa^-_\uparrow, \quad \mathcal{H}_{2,2} - \mathcal{H}_{3,3} = \Delta V_g \kappa^-_\downarrow, \tag{C.91a}$$

$$\mathcal{H}_{1,1} + \mathcal{H}_{4,4} = -\Delta V_g \kappa^+_\downarrow, \quad \mathcal{H}_{2,2} + \mathcal{H}_{3,3} = -\Delta V_g \kappa^+_\uparrow, \tag{C.91b}$$

$$\mathcal{H}_{1,4} = \frac{\Delta V_g}{2}(\kappa^o_\uparrow)^*, \quad \mathcal{H}_{2,3} = \frac{\Delta V_g}{2}\kappa^o_\downarrow. \tag{C.91c}$$

where

$$\kappa^\pm_\sigma = \sum_\alpha \frac{\rho_\sigma}{U}(|t_{\alpha 1}|^2 \pm |t_{\alpha 2}|^2), \quad \kappa^o_\sigma = 2\sum_\alpha \frac{\rho_\sigma}{U} t_{\alpha 1} t_{\alpha 2}. \tag{C.92}$$

We can instantly write down the eigenvalues

$$-\frac{\Delta V_g}{2}\left(\kappa^+_\downarrow \pm \sqrt{(\kappa^-_\uparrow)^2 + |\kappa^o_\uparrow|^2}\right), \tag{C.93a}$$

$$-\frac{\Delta V_g}{2}\left(\kappa^+_\uparrow \pm \sqrt{(\kappa^-_\downarrow)^2 + |\kappa^o_\downarrow|^2}\right), \tag{C.93b}$$

and get the following energy differences

$$0\ (\uparrow), \quad \rho_\uparrow \beta \Delta V_g\ (\uparrow), \quad -(\rho_\uparrow - \rho_\downarrow)(\alpha - \beta)\frac{\Delta V_g}{2}\ (\downarrow), \quad \left[-(\rho_\uparrow - \rho_\downarrow)(\alpha - \beta) + 2\rho_\downarrow \beta\right]\frac{\Delta V_g}{2}\ (\downarrow), \tag{C.94}$$

where

$$\alpha = \frac{\kappa^+_\sigma}{\rho_\sigma} = \frac{1}{U}\left(|t_{L1}|^2 + |t_{L2}|^2 + |t_{R1}|^2 + |t_{R2}|^2\right), \tag{C.95a}$$

$$\beta = \frac{\sqrt{(\kappa^-_\sigma)^2 + |\kappa^o_\sigma|^2}}{\rho_\sigma} = \frac{1}{U}\sqrt{\left(|t_{L1}|^2 - |t_{L2}|^2 + |t_{R1}|^2 - |t_{R2}|^2\right)^2 + 4|t_{L1}t_{L2} + t_{R1}t_{R2}|^2}. \tag{C.95b}$$

We see that in the general case there are no degeneracies left, expect in the middle of the diamond $\Delta V_g = 0$, and that is the case even if $t_{L/R,1} = t_{L/R,2} = t_{L/R}$, but then a phase difference between t_L and t_R is required. Note that the above α has nothing to do with lead quantum number, and that relation

$$\alpha > \beta \quad \rightarrow \quad |t_{L1}t^*_{R2} - t^*_{L2}t_{R1}| > 0, \tag{C.96}$$

is always satisfied. If we consider case $\rho_\uparrow > \rho_\downarrow$ and $\Delta V_g < 0$ (left side of the diamond) then the energy differences can always be sorted as

$$-\rho_\uparrow \beta |\Delta V_g|\ (\uparrow), \quad \left\{0\ (\uparrow), \quad \left[(\rho_\uparrow - \rho_\downarrow)(\alpha - \beta) - 2\rho_\downarrow \beta\right]\frac{|\Delta V_g|}{2}\ (\downarrow)\right\}, \quad (\rho_\uparrow - \rho_\downarrow)(\alpha - \beta)\frac{|\Delta V_g|}{2}\ (\downarrow), \tag{C.97}$$

where energy differences inside the curly brackets can have any order, depending on the parameters. We see that in this case the ground state is always a state corresponding to spin up. For the right side of the diamond ($\Delta V_g > 0$) we get the following sorting of energy differences:

$$-(\rho_\uparrow - \rho_\downarrow)(\alpha - \beta)\frac{|\Delta V_g|}{2}\ (\downarrow), \quad \left\{-\left[(\rho_\uparrow - \rho_\downarrow)(\alpha - \beta) - 2\rho_\downarrow \beta\right]\frac{|\Delta V_g|}{2}\ (\downarrow), \quad 0\ (\uparrow)\right\}, \quad \rho_\uparrow \beta |\Delta V_g|\ (\uparrow), \tag{C.98}$$

which corresponds to spin down ground state, for $\rho_\uparrow > \rho_\downarrow$ case.

Case 2: $\theta_L = 0$, $\theta_R = \pi$, $\rho_{\alpha\sigma} = \rho_\sigma$, $\Delta_{\mathrm{SO}} = \Delta_{KK'} = B = V = 0$:

Either using (C.21) and (C.22) relations and setting $\rho_{L\uparrow} = \rho_{R\downarrow}$, $\rho_{L\downarrow} = \rho_{R\uparrow}$, what corresponds to antiparallel leads by keeping the angle $\theta_R = 0$, or using spin sums (C.90) we get:

$$\mathcal{H}_{1,1} - \mathcal{H}_{4,4} = \Delta V_g \kappa^-_\uparrow, \quad \mathcal{H}_{2,2} - \mathcal{H}_{3,3} = \Delta V_g \kappa^-_\downarrow, \tag{C.99a}$$

$$\mathcal{H}_{1,1} + \mathcal{H}_{4,4} = -\Delta V_g \kappa^+_\downarrow, \quad \mathcal{H}_{2,2} + \mathcal{H}_{3,3} = -\Delta V_g \kappa^+_\uparrow, \tag{C.99b}$$

$$\mathcal{H}_{1,4} = \frac{\Delta V_g}{2}(\kappa^o_\uparrow)^*, \quad \mathcal{H}_{2,3} = \frac{\Delta V_g}{2}\kappa^o_\downarrow. \tag{C.99c}$$

where

$$\kappa^\pm_\sigma = \frac{1}{U}\Big[\rho_\sigma(|t_{L1}|^2 \pm |t_{L2}|^2) + \rho_{\bar\sigma}(|t_{R1}|^2 \pm |t_{R2}|^2)\Big], \quad \kappa^o_\sigma = \frac{2}{U}\left[\rho_\sigma t_{L1} t_{L2} + \rho_{\bar\sigma} t_{R1} t_{R2}\right], \tag{C.100}$$
$$\text{with } \sigma = \uparrow, \downarrow \text{ and } \bar\sigma = \downarrow, \uparrow,$$

and eigenvalues are as in the previous case (C.93) with new $\kappa^\pm_\sigma$ and κ^o_σ.

Appendix D

Yosida's wavefunction ansatz

D.1 Single quasiparticle

The possible lowest order approximation for the wavefunctions including single quasiparticle is [74]

$$|S/T^0\rangle = \sum_{\alpha\mathbf{k}} (A_{\alpha\mathbf{k}}|\uparrow_{\alpha\mathbf{k}},\downarrow\rangle + B_{\alpha\mathbf{k}}|\downarrow_{\alpha\mathbf{k}},\uparrow\rangle), \tag{D.1}$$

$$|T^+\rangle = \sum_{\alpha\mathbf{k}} C_{\alpha\mathbf{k}}|\uparrow_{\alpha\mathbf{k}},\uparrow\rangle, \tag{D.2}$$

$$|T^-\rangle = \sum_{\alpha\mathbf{k}} D_{\alpha\mathbf{k}}|\downarrow_{\alpha\mathbf{k}},\downarrow\rangle, \tag{D.3}$$

where the notation (7.30) was used. We require the above states to satisfy the eigenvalue equation $H|\psi\rangle = E|\psi\rangle$, where Hamiltonian is given by (6.23). Then taking the projections $\langle\uparrow_{\alpha'\kappa},\downarrow|H|S/T^0\rangle$, $\langle\downarrow_{\alpha'\kappa},\uparrow|H|S/T^0\rangle$, $\langle\uparrow_{\alpha'\kappa,\uparrow}|H|T^+$, and $\langle\downarrow_{\alpha'\kappa},\downarrow|\rangle H|T^-\rangle$, we obtain equations for expansion coefficients:

$$\begin{aligned} A_{\alpha'\kappa} = \frac{1}{E_\kappa - (E+\tilde{B})} \sum_\alpha \Big[& \frac{1}{2} J_{\alpha'\alpha} \left(u_\kappa S_{\alpha u A} + \mathrm{e}^{\mathrm{i}\phi_{\alpha'\alpha}} v_\kappa S_{\alpha v A} \right) \\ & - J_{\alpha'\alpha} \left(u_\kappa S_{\alpha u B} + \mathrm{e}^{\mathrm{i}\phi_{\alpha'\alpha}} v_\kappa S_{\alpha v B} \right) \\ & - W_{\alpha'\alpha} \left(u_\kappa S_{\alpha u A} - \mathrm{e}^{\mathrm{i}\phi_{\alpha'\alpha}} v_\kappa S_{\alpha v A} \right) \Big], \end{aligned} \tag{D.4a}$$

$$\begin{aligned} B_{\alpha'\kappa} = \frac{1}{E_\kappa - (E-\tilde{B})} \sum_\alpha \Big[& \frac{1}{2} J_{\alpha'\alpha} \left(u_\kappa S_{\alpha u B} + \mathrm{e}^{\mathrm{i}\phi_{\alpha'\alpha}} v_\kappa S_{\alpha v B} \right) \\ & - J_{\alpha'\alpha} \left(u_\kappa S_{\alpha u A} + \mathrm{e}^{\mathrm{i}\phi_{\alpha'\alpha}} v_\kappa S_{\alpha v A} \right) \\ & - W_{\alpha'\alpha} \left(u_\kappa S_{\alpha u B} - \mathrm{e}^{\mathrm{i}\phi_{\alpha'\alpha}} v_\kappa S_{\alpha v B} \right) \Big], \end{aligned} \tag{D.4b}$$

$$\begin{aligned} C_{\alpha'\kappa} = \frac{1}{E_\kappa - (E-\tilde{B})} \sum_\alpha \Big[& -\frac{1}{2} J_{\alpha'\alpha} \left(u_\kappa S_{\alpha u C} + \mathrm{e}^{\mathrm{i}\phi_{\alpha'\alpha}} v_\kappa S_{\alpha v C} \right) \\ & - W_{\alpha'\alpha} \left(u_\kappa S_{\alpha u C} - \mathrm{e}^{\mathrm{i}\phi_{\alpha'\alpha}} v_\kappa S_{\alpha v C} \right) \Big], \end{aligned} \tag{D.4c}$$

$$\begin{aligned} D_{\alpha'\kappa} = \frac{1}{E_\kappa - (E+\tilde{B})} \sum_\alpha \Big[& -\frac{1}{2} J_{\alpha'\alpha} \left(u_\kappa S_{\alpha u D} + \mathrm{e}^{\mathrm{i}\phi_{\alpha'\alpha}} v_\kappa S_{\alpha v D} \right) \\ & - W_{\alpha'\alpha} \left(u_\kappa S_{\alpha u D} - \mathrm{e}^{\mathrm{i}\phi_{\alpha'\alpha}} v_\kappa S_{\alpha v D} \right) \Big], \end{aligned} \tag{D.4d}$$

where the following notation is introduced

$$S_{\alpha aF} = \sum_{\mathbf{q}} a_{\mathbf{q}} F_{\alpha \mathbf{q}}, \quad \phi_{\alpha'\alpha} = \phi_{\alpha'} - \phi_{\alpha}. \tag{D.5}$$

After multiplying Eqs. (D.4) by either u_κ or v_κ and summing over κ we get linear set of equations for sums $S_{\alpha a A}$. The resulting *secular* equation is

$$\begin{vmatrix} \mathbf{1} + \mathcal{M}^j_{LL} & \mathcal{M}^j_{LR} \\ \mathcal{M}^j_{RL} & \mathbf{1} + \mathcal{M}^j_{RR} \end{vmatrix} = 0, \quad j = S/T^0, T^{\pm}, \tag{D.6}$$

where for the state (D.1) [the coefficient matrix is for $\begin{pmatrix} S_{\alpha' u A} & S_{\alpha' v A} & S_{\alpha' u B} & S_{\alpha' v B} \end{pmatrix}$] we have

$$\mathcal{M}^{S/T^0}_{\alpha'\alpha} = \begin{pmatrix} -s^+_{uu}(g_{\alpha'\alpha} - w_{\alpha'\alpha}) & -s^+_{uv}(g_{\alpha'\alpha} + w_{\alpha'\alpha})\mathrm{e}^{\mathrm{i}\phi_{\alpha'\alpha}} & 2s^+_{uu} g_{\alpha'\alpha} & 2s^+_{uv} g_{\alpha'\alpha}\mathrm{e}^{\mathrm{i}\phi_{\alpha'\alpha}} \\ -s^+_{vu}(g_{\alpha'\alpha} - w_{\alpha'\alpha}) & -s^+_{vv}(g_{\alpha'\alpha} + w_{\alpha'\alpha})\mathrm{e}^{\mathrm{i}\phi_{\alpha'\alpha}} & 2s^+_{vu} g_{\alpha'\alpha} & 2s^+_{vv} g_{\alpha'\alpha}\mathrm{e}^{\mathrm{i}\phi_{\alpha'\alpha}} \\ 2s^-_{uu} g_{\alpha'\alpha} & 2s^-_{uv} g_{\alpha'\alpha}\mathrm{e}^{\mathrm{i}\phi_{\alpha'\alpha}} & -s^-_{uu}(g_{\alpha'\alpha} - w_{\alpha'\alpha}) & -s^-_{uv}(g_{\alpha'\alpha} + w_{\alpha'\alpha})\mathrm{e}^{\mathrm{i}\phi_{\alpha'\alpha}} \\ 2s^-_{vu} g_{\alpha'\alpha} & 2s^-_{vv} g_{\alpha'\alpha}\mathrm{e}^{\mathrm{i}\phi_{\alpha'\alpha}} & -s^-_{vu}(g_{\alpha'\alpha} - w_{\alpha'\alpha}) & -s^-_{vv}(g_{\alpha'\alpha} + w_{\alpha'\alpha})\mathrm{e}^{\mathrm{i}\phi_{\alpha'\alpha}} \end{pmatrix}, \tag{D.7}$$

and for the states (D.2) (D.3) we have

$$\mathcal{M}^{\pm}_{\alpha'\alpha} = \begin{pmatrix} \bar{s}^{\mp}_{uu}(g_{\alpha'\alpha} + w_{\alpha'\alpha}) & \bar{s}^{\mp}_{uv}(g_{\alpha'\alpha} - w_{\alpha'\alpha})\mathrm{e}^{\mathrm{i}\phi_{\alpha'\alpha}} \\ \bar{s}^{\mp}_{vu}(g_{\alpha'\alpha} + w_{\alpha'\alpha}) & \bar{s}^{\mp}_{vv}(g_{\alpha'\alpha} - w_{\alpha'\alpha})\mathrm{e}^{\mathrm{i}\phi_{\alpha'\alpha}} \end{pmatrix}. \tag{D.8}$$

Here $\mathbf{1}$ denotes a unit matrix and the following notation was introduced

$$\begin{aligned} s_{ab} &= \frac{1}{\pi \nu_F} \sum_{\kappa} \frac{a_\kappa b_\kappa}{E_\kappa - E}, \\ s^{\pm}_{ab} &= s_{ab}(E \pm \tilde{B}), \quad \bar{s}^{\pm}_{ab} = s_{ab}(E \pm \bar{B}), \\ g_{\alpha'\alpha} &= \frac{1}{2}\pi \nu_F J_{\alpha'\alpha}, \quad w_{\alpha'\alpha} = \pi \nu_F W_{\alpha'\alpha}. \end{aligned} \tag{D.9}$$

After performing κ sums in s_{ab} for symmetric band $\xi_{\mathbf{k}} \in [-D, D]$ we obtain

$$\begin{aligned} s_{uu} = s_{vv} &= \frac{1}{\pi} \ln \left| \frac{D + \sqrt{D^2 + |\Delta|^2}}{|\Delta|} \right| + \frac{E}{|\Delta|} s_{uv}, \\ s_{uv} = s_{vu} &= \frac{1}{\pi} \int_{|\Delta|}^{\sqrt{D^2+|\Delta|^2}} \frac{\mathrm{d}x}{(x - E)\sqrt{x^2 + |\Delta|^2}} = \begin{cases} \dfrac{\frac{1}{2} - \frac{1}{\pi} \arcsin\left(\frac{E\sqrt{D^2+|\Delta|^2}+|\Delta|^2}{|\sqrt{D^2+|\Delta|^2}+E||\Delta|} \right)}{\sqrt{1 - E^2/|\Delta|^2}}, & |E| < |\Delta|, \\ \dfrac{\frac{1}{\pi} \ln \left| \frac{D\sqrt{E^2-|\Delta|^2}+E\sqrt{D^2+|\Delta|^2}+|\Delta|^2}{(\sqrt{D^2+|\Delta|^2}+E)|\Delta|} \right|}{\sqrt{E^2/|\Delta|^2 - 1}}, & |E| > |\Delta|. \end{cases} \end{aligned} \tag{D.10}$$

In the case when there is no magnetic field ($B = 0$, $s^+ = s^- = s$) we can simplify the above equations by choosing (D.1) to be either singlet or triplet state, i.e.,

$$\begin{aligned} B_{\alpha\kappa} &= -A_{\alpha\kappa}, \qquad \text{singlet } |S/T^0\rangle = |S\rangle, \\ B_{\alpha\kappa} &= A_{\alpha\kappa}, \qquad \text{triplet } |S/T^0\rangle = |T^0\rangle. \end{aligned} \tag{D.11}$$

Then for the singlet we get

$$\mathcal{M}^{S}_{\alpha'\alpha} = -\begin{pmatrix} s_{uu}(3g_{\alpha'\alpha} - w_{\alpha'\alpha}) & s_{uv}(3g_{\alpha'\alpha} + w_{\alpha'\alpha})\mathrm{e}^{\mathrm{i}\phi_{\alpha'\alpha}} \\ s_{vu}(3g_{\alpha'\alpha} - w_{\alpha'\alpha}) & s_{vv}(3g_{\alpha'\alpha} + w_{\alpha'\alpha})\mathrm{e}^{\mathrm{i}\phi_{\alpha'\alpha}} \end{pmatrix}, \tag{D.12}$$

and for all the triplets the matrix $\mathcal{M}^{0,\pm}_{\alpha'\alpha}$ has the form (D.8). When there is no potential scattering $w_{\alpha\alpha'}=0$ we can set $S_{\alpha uF}=S_{\alpha vF}$, because $s_{uu}=s_{vv}$, and then we obtain

$$\begin{aligned}
\mathcal{M}^{S/T^0}_{\alpha'\alpha} &\overset{w=0}{=} \begin{pmatrix} -g_{\alpha'\alpha}(s^{+}_{uu}+s^{+}_{uv}e^{i\phi_{\alpha'\alpha}}) & 2g_{\alpha'\alpha}(s^{+}_{uu}+s^{+}_{uv}e^{i\phi_{\alpha'\alpha}}) \\ 2g_{\alpha'\alpha}(s^{-}_{uu}+s^{-}_{uv}e^{i\phi_{\alpha'\alpha}}) & -g_{\alpha'\alpha}(s^{-}_{uu}+s^{-}_{uv}e^{i\phi_{\alpha'\alpha}}) \end{pmatrix}, \\
\mathcal{M}^{\pm}_{\alpha'\alpha} &\overset{w=0}{=} g_{\alpha'\alpha}(\bar{s}^{\mp}_{uu}+\bar{s}^{\mp}_{uv}e^{i\phi_{\alpha'\alpha}}), \\
\mathcal{M}^{S}_{\alpha'\alpha} &\overset{w=0}{=} -3g_{\alpha'\alpha}(s_{uu}+s_{uv}e^{i\phi_{\alpha'\alpha}}).
\end{aligned} \tag{D.13}$$

The perturbative solutions in $g_{\alpha'\alpha}$ of the *secular* equations (D.6) matches the results presented in Section 7.3. Additionally, when there is no magnetic field the inclusion of potential scattering term $w_{\alpha\alpha'}$ yields solution $E=|\Delta|(1-\eta^2)$,

$$|\eta_{0,S}| = \frac{\sqrt{2}}{2}\left(3g \pm \sqrt{9g^2\chi + w^2(1-\chi)}\right), \quad \text{for singlet,} \tag{D.14a}$$

$$|\eta_{0,T}| = -\frac{\sqrt{2}}{2}\left(g \pm \sqrt{g^2\chi + w^2(1-\chi)}\right), \quad \text{for triplet,} \tag{D.14b}$$

where the form (6.26) of the coupling was used and χ is defined in (7.15). For small magnetic field $|\tilde{B}| \ll |\eta_0^2\Delta|$ the above solutions get modified to

$$|\eta_{S,l}| \approx \left(1+\frac{\tilde{B}^2}{8g\eta_0^2|\Delta|^2}\times\frac{2g\sqrt{2}\eta_0-3g^2+(w^2-3g^2)(1-\alpha^2)}{\left[(w^2-12g^2)(1-\alpha^2)+18g^2\right]\sqrt{2}\eta_0+g(w^2-9g^2)(1-\alpha^2)(2+\alpha^2)}\right)\eta_0, \quad \text{singlet like,} \tag{D.15a}$$

$$|\eta_{T^0,l}| \approx \left(1+\frac{\tilde{B}^2}{8g\eta_0^2|\Delta|^2}\times\frac{2g\sqrt{2}\eta_0+3g^2-(w^2+g^2)(1-\alpha^2)}{\left[w^2(1-\alpha^2)+2g^2\right]\sqrt{2}\eta_0-g(w^2-g^2)(1-\alpha^2)(2-\alpha^2)}\right)\eta_0, \quad \text{triplet } T^0 \text{ like,} \tag{D.15b}$$

and for high magnetic field $|\tilde{B}| \gg |g_\delta^2\Delta|$ it becomes $E_h \approx |\Delta|(1-\eta_{0,h}^2)-\tilde{B}$, where $|\eta_{0,h}| = -|\eta_{0,T}|$. Independent of the magnetic field size for the states $|T^{\pm}\rangle$ we get $E_{T^{\pm},l} = |\Delta|(1-\eta_{0,T}^2)\pm\tilde{B}$.

D.2 Three quasiparticles

In this section we will check how does the energy of the state (D.1) is changed when in the ansatz three quasiparticles are included. To make things simple we examine situation with no potential scattering, no magnetic field, and no phase difference. In such a case we have a wavefunction

$$|\psi\rangle = \sum_{\mathbf{q}}\left(A_{\mathbf{q}}|\uparrow_{\mathbf{q}},\downarrow\rangle + B_{\mathbf{q}}|\downarrow_{\mathbf{q}},\uparrow\rangle\right) + \sum_{\mathbf{q}_1\mathbf{q}_2\mathbf{q}_3}\left(a_{\mathbf{q}_1\mathbf{q}_2\mathbf{q}_3}|\uparrow_{\mathbf{q}_1}\uparrow_{\mathbf{q}_2}\downarrow_{\mathbf{q}_3},\downarrow\rangle + b_{\mathbf{q}_1\mathbf{q}_2\mathbf{q}_3}|\downarrow_{\mathbf{q}_1}\downarrow_{\mathbf{q}_2}\uparrow_{\mathbf{q}_3},\uparrow\rangle\right), \tag{D.16}$$

and we get the following equations for the expansion coefficients

$$\begin{aligned}
\langle\uparrow_\kappa,\downarrow|H|\psi_b\rangle &= E_\kappa A_\kappa - \frac{J}{2}\sum_{\mathbf{k}}K_{\kappa\mathbf{k}}A_{\mathbf{k}} + J\sum_{\mathbf{k}}K_{\kappa\mathbf{k}}B_{\mathbf{k}} \\
&\quad - \frac{J}{2}\sum_{\mathbf{k}\mathbf{k}'}(L^*_{\mathbf{k}\mathbf{k}'}-L^*_{\mathbf{k}'\mathbf{k}})(a_{\kappa\mathbf{k}\mathbf{k}'}-a_{\mathbf{k}\kappa\mathbf{k}'}) + J\sum_{\mathbf{k}\mathbf{k}'}L^*_{\mathbf{k}\mathbf{k}'}(b_{\mathbf{k}\mathbf{k}'\kappa}-b_{\mathbf{k}'\mathbf{k}\kappa}) = EA_\kappa,
\end{aligned} \tag{D.17a}$$

$$\begin{aligned}
\langle\downarrow_\kappa,\uparrow|H|\psi_b\rangle &= E_\kappa B_\kappa - \frac{J}{2}\sum_{\mathbf{k}}K_{\kappa\mathbf{k}}B_{\mathbf{k}} + J\sum_{\mathbf{k}}K_{\kappa\mathbf{k}}A_{\mathbf{k}} \\
&\quad - \frac{J}{2}\sum_{\mathbf{k}\mathbf{k}'}(L^*_{\mathbf{k}\mathbf{k}'}-L^*_{\mathbf{k}'\mathbf{k}})(b_{\kappa\mathbf{k}'\mathbf{k}}-b_{\mathbf{k}'\kappa\mathbf{k}}) + J\sum_{\mathbf{k}\mathbf{k}'}L^*_{\mathbf{k}'\mathbf{k}}(a_{\mathbf{k}\mathbf{k}'\kappa}-a_{\mathbf{k}'\mathbf{k}\kappa}) = EB_\kappa,
\end{aligned} \tag{D.17b}$$

$$\begin{aligned}\langle\uparrow_{\kappa_1}\uparrow_{\kappa_2}\downarrow_{\kappa_3},\downarrow|H|\psi_b\rangle &= \underbrace{(E_{\kappa_1}+E_{\kappa_2}+E_{\kappa 3})(a_{\kappa_1\kappa_2\kappa_3}-a_{\kappa_2\kappa_1\kappa_3})}\\ &-\frac{J}{2}\sum_{\mathbf{k}}K_{\kappa_1\mathbf{k}}(a_{\mathbf{k}\kappa_2\kappa_3}-a_{\kappa_2\mathbf{k}\kappa_3})-\frac{J}{2}\sum_{\mathbf{k}}K_{\kappa_2\mathbf{k}}(a_{\kappa_1\mathbf{k}\kappa_3}-a_{\mathbf{k}\kappa_1\kappa_3})+\frac{J}{2}\sum_{\mathbf{k}}K_{\kappa_3\mathbf{k}}(a_{\kappa_1\kappa_2\mathbf{k}}-a_{\kappa_2\kappa_1\mathbf{k}})\\ &+J\sum_{\mathbf{k}}K_{\kappa_1\mathbf{k}}(b_{\kappa_2\kappa_3\mathbf{k}}-b_{\kappa_2\mathbf{k}\kappa_3})+J\sum_{\mathbf{k}}K_{\kappa_2\mathbf{k}}(b_{\kappa_1\mathbf{k}\kappa_3}-b_{\kappa_1\kappa_3\mathbf{k}})\\ &\underbrace{-\frac{J}{2}(L_{\kappa_2\kappa_3}-L_{\kappa_3\kappa_2})A_{\kappa_1}+\frac{J}{2}(L_{\kappa_1\kappa_3}-L_{\kappa_3\kappa_1})A_{\kappa_2}-J(L_{\kappa_1\kappa_2}-L_{\kappa_2\kappa_1})B_{\kappa_3}=E(a_{\kappa_1\kappa_2\kappa_3}-a_{\kappa_2\kappa_1\kappa_3}),}\end{aligned}\tag{D.18a}$$

$$\begin{aligned}\langle\downarrow_{\kappa_1}\downarrow_{\kappa_2}\uparrow_{\kappa_3},\uparrow|H|\psi_b\rangle &= \underbrace{(E_{\kappa_1}+E_{\kappa_2}+E_{\kappa 3})(b_{\kappa_1\kappa_2\kappa_3}-b_{\kappa_2\kappa_1\kappa_3})}\\ &-\frac{J}{2}\sum_{\mathbf{k}}K_{\kappa_1\mathbf{k}}(b_{\mathbf{k}\kappa_2\kappa_3}-b_{\kappa_2\mathbf{k}\kappa_3})-\frac{J}{2}\sum_{\mathbf{k}}K_{\kappa_2\mathbf{k}}(b_{\kappa_1\mathbf{k}\kappa_3}-b_{\mathbf{k}\kappa_1\kappa_3})+\frac{J}{2}\sum_{\mathbf{k}}K_{\kappa_3\mathbf{k}}(b_{\kappa_1\kappa_2\mathbf{k}}-b_{\kappa_2\kappa_1\mathbf{k}})\\ &+J\sum_{\mathbf{k}}K_{\kappa_1\mathbf{k}}(a_{\kappa_3\mathbf{k}\kappa_2}-a_{\mathbf{k}\kappa_3\kappa_2})+J\sum_{\mathbf{k}}K_{\kappa_2\mathbf{k}}(a_{\mathbf{k}\kappa_3\kappa_1}-a_{\kappa_3\mathbf{k}\kappa_1})\\ &\underbrace{-\frac{J}{2}(L_{\kappa_3\kappa_2}-L_{\kappa_2\kappa_3})B_{\kappa_1}+\frac{J}{2}(L_{\kappa_3\kappa_1}-L_{\kappa_1\kappa_3})B_{\kappa_2}-J(L_{\kappa_2\kappa_1}-L_{\kappa_1\kappa_2})A_{\kappa_3}=E(b_{\kappa_1\kappa_2\kappa_3}-b_{\kappa_2\kappa_1\kappa_3}).}\end{aligned}\tag{D.18b}$$

In Eqs. (D.18) we keep only the braced terms, because the other terms correspond to higher order corrections. Then we get the following coefficients

$$a_{\kappa_1\kappa_2\kappa_3}-a_{\kappa_2\kappa_1\kappa_3}\approx\frac{J}{2}\frac{(L_{\kappa_2\kappa_3}-L_{\kappa_3\kappa_2})A_{\kappa_1}-(L_{\kappa_1\kappa_3}-L_{\kappa_3\kappa_1})A_{\kappa_2}+2(L_{\kappa_1\kappa_2}-L_{\kappa_2\kappa_1})B_{\kappa_3}}{E_{\kappa_1}+E_{\kappa_2}+E_{\kappa 3}-E},\tag{D.19a}$$

$$b_{\kappa_1\kappa_2\kappa_3}-b_{\kappa_2\kappa_1\kappa_3}\approx\frac{J}{2}\frac{(L_{\kappa_3\kappa_2}-L_{\kappa_2\kappa_3})B_{\kappa_1}-(L_{\kappa_3\kappa_1}-L_{\kappa_1\kappa_3})B_{\kappa_2}+2(L_{\kappa_2\kappa_1}-L_{\kappa_1\kappa_2})A_{\kappa_3}}{E_{\kappa_1}+E_{\kappa_2}+E_{\kappa 3}-E},\tag{D.19b}$$

which are inserted into (D.17) to give

$$\begin{aligned}&(E_\kappa+\Delta E_\kappa-E)A_\kappa-\frac{3J}{2}\sum_{\mathbf{k}}K_{\kappa\mathbf{k}}A_{\mathbf{k}}-\frac{3J^2}{4}\sum_{\mathbf{k}\mathbf{k}'}\frac{(L_{\kappa\mathbf{k}'}-L_{\mathbf{k}'\kappa})(L_{\mathbf{k}\mathbf{k}'}-L_{\mathbf{k}'\mathbf{k}})}{E_\kappa+E_{\mathbf{k}}+E_{\mathbf{k}'}-E}A_{\mathbf{k}}=0,\quad\text{for singlet } B_\kappa=-A_\kappa,\\ &(E_\kappa+\Delta E_\kappa-E)A_\kappa+\frac{J}{2}\sum_{\mathbf{k}}K_{\kappa\mathbf{k}}A_{\mathbf{k}}+\frac{5J^2}{4}\sum_{\mathbf{k}\mathbf{k}'}\frac{(L_{\kappa\mathbf{k}'}-L_{\mathbf{k}'\kappa})(L_{\mathbf{k}\mathbf{k}'}-L_{\mathbf{k}'\mathbf{k}})}{E_\kappa+E_{\mathbf{k}}+E_{\mathbf{k}'}-E}A_{\mathbf{k}}=0,\quad\text{for triplet } B_\kappa=A_\kappa,\end{aligned}\tag{D.20}$$

where

$$\Delta E_\kappa=-\frac{3J^2}{4}\sum_{\mathbf{k}\mathbf{k}'}\frac{|L_{\mathbf{k}\mathbf{k}'}-L_{\mathbf{k}'\mathbf{k}}|^2}{E_\kappa+E_{\mathbf{k}}+E_{\mathbf{k}'}-E},\tag{D.21}$$

is the quasiparticle energy shift. The integral equation (D.20) is solved iteratively by substituting in the last term

$$\text{for singlet: } A_\kappa\approx\frac{3J}{2}\sum_{\mathbf{k}}\frac{K_{\kappa\mathbf{k}}}{E_\kappa+\Delta E_\kappa-E}A_{\mathbf{k}};\quad\text{for triplet: } A_\kappa\approx-\frac{J}{2}\sum_{\mathbf{k}}\frac{K_{\kappa\mathbf{k}}}{E_\kappa+\Delta E_\kappa-E}A_{\mathbf{k}}.\tag{D.22}$$

Then by having $S_{uA}=S_{vA}$ [see Eq. (D.5)] for symmetric band $\xi\in[-D..D]$, we obtained from Eq. (D.20) with the above approximation (D.22) the following *secular* equations

$$\begin{aligned}&1-\frac{3J}{2}\sum_{\kappa}\frac{u_\kappa^2+u_\kappa v_\kappa}{E_\kappa+\Delta E_\kappa-E}-\frac{9J^3}{8}\sum_{\kappa\mathbf{k}\mathbf{k}'}\frac{(u_\kappa^2+u_\kappa v_\kappa)(u_{\mathbf{k}}^2+u_{\mathbf{k}}v_{\mathbf{k}})(u_{\mathbf{k}'}^2-u_{\mathbf{k}'}v_{\mathbf{k}'})}{(E_\kappa+E_{\mathbf{k}}+E_{\mathbf{k}'}-E)(E_\kappa+\Delta E_\kappa-E)(E_{\mathbf{k}}+\Delta E_{\mathbf{k}}-E)}=0,\ \text{for singlet},\\ &1+\frac{J}{2}\sum_{\kappa}\frac{u_\kappa^2+u_\kappa v_\kappa}{E_\kappa+\Delta E_\kappa-E}-\frac{5J^3}{8}\sum_{\kappa\mathbf{k}\mathbf{k}'}\frac{(u_\kappa^2+u_\kappa v_\kappa)(u_{\mathbf{k}}^2+u_{\mathbf{k}}v_{\mathbf{k}})(u_{\mathbf{k}'}^2-u_{\mathbf{k}'}v_{\mathbf{k}'})}{(E_\kappa+E_{\mathbf{k}}+E_{\mathbf{k}'}-E)(E_\kappa+\Delta E_\kappa-E)(E_{\mathbf{k}}+\Delta E_{\mathbf{k}}-E)}=0,\ \text{for triplet}.\end{aligned}\tag{D.23}$$

Now we want to calculate the bound state energy from equations (D.23). We will write down more detailed calculation for the singlet case, because in the triplet case it is analogous. First thing to note is that ΔE_κ gives ground-state energy shift when we set $E_\kappa - E = 0$ in the expression (D.21). We denote this shift as ΔE_0 and introduce new variables

$$\Delta E_0 = -\frac{3J^2}{4}\sum_{\mathbf{k}\mathbf{k}'}\frac{|L_{\mathbf{k}\mathbf{k}'} - L_{\mathbf{k}'\mathbf{k}}|^2}{E_{\mathbf{k}} + E_{\mathbf{k}'}}, \tag{D.24a}$$

$$E = E' + \Delta E_0, \quad \Delta\tilde{E}_\kappa = \Delta E_\kappa - \Delta E_0. \tag{D.24b}$$

The new variable E' corresponds to energy difference between ground-state doublet and excited singlet/triplet. Using the new variables the equation (D.23) for the singlet becomes

$$\begin{aligned} &1 - \frac{3J}{2}\sum_\kappa \frac{u_\kappa^2 + u_\kappa v_\kappa}{E_\kappa + \Delta\tilde{E}_\kappa - E'} \\ &- \frac{9J^3}{4}\sum_{\kappa\mathbf{k}} \frac{(u_\kappa^2 + u_\kappa v_\kappa)(u_{\mathbf{k}}^2 + u_{\mathbf{k}} v_{\mathbf{k}})}{(E_\kappa + \Delta\tilde{E}_\kappa - E')(E_{\mathbf{k}} + \Delta\tilde{E}_{\mathbf{k}} - E')}\frac{\pi\nu_F}{2} U_-(E' + \Delta E_0 - E_\kappa - E_{\mathbf{k}}) = 0, \end{aligned} \tag{D.25}$$

where we introduced

$$U_\pm(E) = s_{uu} \pm s_{uv}. \tag{D.26}$$

By assuming that $0 < |\Delta| - E' \sim g^2|\Delta| \ll |\Delta|$ the main contribution to the integrals in the last term of (D.25) comes when E_κ and $E_{\mathbf{k}}$ are close to $|\Delta|$. Then we also have

$$\begin{aligned} &\frac{1}{2}\sum_\kappa \frac{u_\kappa^2 + u_\kappa v_\kappa}{E_\kappa + \Delta\tilde{E}_\kappa - E'} \approx \frac{\pi\nu_F}{2} U_+(E')\Big(1 - g^2 c_1\Big), \\ &\Delta\tilde{E}_\kappa \approx (E_\kappa - E')g^2 c_1, \\ &c_1 = \frac{3}{\pi^2\nu_F^2}\sum_{\mathbf{k}\mathbf{k}'}\frac{|L_{\mathbf{k}\mathbf{k}'} - L_{\mathbf{k}'\mathbf{k}}|^2}{(E_{\mathbf{k}} + E_{\mathbf{k}'})^2}, \end{aligned} \tag{D.27}$$

and after leaving the relevant terms which will give contributions to third order in $g = \pi\nu_F J/2$ to E', Eqs. (D.25) become

$$\begin{aligned} &1 - 3gU_+(E') - 9g^3 U_+^2(E')U_-(-|\Delta|) = 0, \quad \text{for singlet,} \\ &1 + gU_+(E') - 5g^3 U_+^2(E')U_-(-|\Delta|) = 0, \quad \text{for triplet.} \end{aligned} \tag{D.28}$$

Once again we write the energy as $E' = |\Delta|(1 - \eta^2)$, which then gives

$$\begin{aligned} U_+(E') &\approx \frac{1}{\pi}\left[\ln\frac{2D}{|\Delta|} + \frac{2}{\eta}\left(\frac{\pi}{\sqrt{2}} - \eta\right)\right], \\ U_-(-|\Delta|) &\approx \frac{1}{\pi}\left(\ln\frac{2D}{|\Delta|} - 2\right), \quad D \gg |\Delta|, \end{aligned} \tag{D.29}$$

and finally from Eqs. (D.28) we obtain

$$\begin{aligned} \eta_S &\approx 3\sqrt{2}g\left[1 + \frac{4g}{\pi}\left(\ln\frac{2D}{|\Delta|} - 2\right)\right], \\ \eta_{T^0} &\approx -\sqrt{2}g\left[1 + \frac{4g}{\pi}\left(\ln\frac{2D}{|\Delta|} - 2\right)\right]. \end{aligned} \tag{D.30}$$

The above result (D.30) is consistent with poor man's scaling for the coupling [70, 149], when $D \gg |\Delta|$, and it differs from the result obtained in [74]. There some small mistakes were made when obtaining the leading-logarithmic contribution $\ln \frac{2D}{|\Delta|}$ for the energy difference. So we resum leading-logarithms $\ln \frac{2D}{|\Delta|}$ in (D.30) using poor man's scaling

$$\eta(g, D) - \eta(g + \delta g, D - \delta D) = 0, \tag{D.31}$$

where η stands for η_{S/T^0}. From Eq. (D.31) we obtain the usual flow equation

$$\frac{dg}{d\lambda} = -\frac{4g^2}{\pi}, \quad d\lambda = d\ln D = \frac{dD}{D}, \tag{D.32}$$

which gives the following running coupling g^* when D is scaled down to D^*

$$g^* = \frac{\pi}{4\ln \frac{D^*}{T_K}}, \quad T_K = D\mathrm{e}^{-\frac{\pi}{4g}}. \tag{D.33}$$

Note that $D^* \gg |\Delta|$ for the usual poor man's scaling equation (D.32) to hold.

Appendix E

Equations for phonon Green's functions

In this Appendix we calculate the following retarded correlation functions

$$G^{ur,R}_{\beta\nu n',tt'} = -\frac{\mathrm{i}}{\hbar}\theta(t-t')[u_{\beta\nu}(t), r_{n'}(t')], \tag{E.1a}$$

$$G^{ru,R}_{n\beta'\nu',tt'} = -\frac{\mathrm{i}}{\hbar}\theta(t-t')[r_{n}(t), u_{\beta'\nu'}(t')], \tag{E.1b}$$

$$D^{R}_{nn',tt'} = -\frac{\mathrm{i}}{\hbar}\theta(t-t')[r_{n}(t), r_{n'}(t')], \tag{E.1c}$$

using the equation of motion technique. Note that the variables are in mass weighted coordinates (9.3) and we use the following shorthand notation $n \equiv i, m$, $\beta \equiv i', \alpha, \mathbf{r}$. Here

$$u_{i\alpha\nu}(\mathbf{r}, t) = \sqrt{\frac{M_\alpha \hbar}{2\rho_\alpha \omega_{\alpha\nu}}}[u^{(\nu)}_{i\alpha}(\mathbf{r})\mathrm{e}^{-\mathrm{i}\omega_{\alpha\nu}t}a_\nu + u^{*(\nu)}_{i\alpha}(\mathbf{r})\mathrm{e}^{\mathrm{i}\omega_{\alpha\nu}t}a^\dagger_\nu] \tag{E.2}$$

is mass weighted displacement vector for particular mode ν. In the calculations we will need such time derivatives [commutators wit Hamiltonian (9.1)] of $r_{n,t}$, $p_{n,t}$, $u_{\beta\nu,t}$ and $\pi_{\beta\nu,t}$:

$$\frac{\partial}{\partial t}r_{n,t} = \frac{\mathrm{i}}{\hbar}[H, r]_t = p_{n,t}, \tag{E.3a}$$

$$\frac{\partial}{\partial t}p_{n,t} = \frac{\mathrm{i}}{\hbar}[H, p]_t = -V_{nn}r_{n,t} - \sum_{n_1 \neq n} V_{nn_1}r_{n_1,t} - \sum_{\beta_1} V_{n\beta_1}u_{\beta_1,t}, \tag{E.3b}$$

$$\frac{\partial}{\partial t}u_{\beta\nu,t} = \frac{\mathrm{i}}{\hbar}[H, u_{\beta\nu}]_t = \frac{M_\beta}{\rho_\beta}\pi_{\beta\nu,t}, \quad \frac{\partial}{\partial t}u_{\beta,t} = \frac{1}{\rho_\alpha}\pi_{\beta,t}, \tag{E.3c}$$

$$\frac{\partial}{\partial t}\pi_{\beta\nu,t} = \frac{\mathrm{i}}{\hbar}[H, \pi_{\beta\nu}]_t = -\frac{\rho_\beta}{M_\beta}\omega^2_{\beta\nu}u_{\beta\nu,t} - \sum_{n_1} r_{n_1,t}V_{n_1\beta_2}c^{(\nu)}_{\beta_2\beta} - \underbrace{\sum_{\beta_1} u_{\beta_1,t}V_{\beta_1}c^{(\nu)}_{\beta_1\beta}}_{\substack{\text{substrate frequency} \\ \text{shift term}}}, \tag{E.3d}$$

where we used the shorthand notation $A_t = A(t)$ for the Heisenberg evolution of an operator, and introduced the function $c^{(\nu)}_{\beta\beta'} \equiv \delta_{\alpha\alpha'}c_{ii',\alpha,\nu,\mathbf{r}\mathbf{r}'} = \delta_{\alpha\alpha'}\mathrm{Re}[u^{(\nu)}_{i\alpha}(\mathbf{r})u^{*(\nu)}_{i'\alpha}(\mathbf{r}')]$ with $u^{(\nu)}_{i\alpha}(\mathbf{r})$ being given by Eq. (10.28). After differentiating Eqs. (E.1a), (E.1c) with respect to time t and Eq. (E.1b) with respect to

time t' we obtain

$$\partial_t G^{ur,R}_{\beta\nu n',tt'} = \frac{M_\beta}{\rho_\beta} G^{\pi r,R}_{\beta\nu n',tt'}, \tag{E.4a}$$

$$\partial_{t'} G^{ru,R}_{n\beta'\nu',tt'} = \frac{M_{\beta'}}{\rho_{\beta'}} G^{r\pi,R}_{n\beta'\nu',tt'}, \tag{E.4b}$$

$$\partial_t D^R_{nn',tt'} = G^{pr,R}_{nn',tt'}, \tag{E.4c}$$

and we see that we need the equations of motion for $G^{\pi r,R}_{\beta\nu n',tt'}$, $G^{r\pi,R}_{n\beta'\nu',tt'}$, and $G^{pr,R}_{nn',tt'}$

$$\partial_t G^{\pi r,R}_{\beta\nu n',tt'} = -\frac{\rho_\beta}{M_\beta}\omega^2_{\beta\nu} G^{ur,R}_{\beta\nu n',tt'} - \sum_{\beta_1 n_2} c^{(\nu)}_{\beta\beta_1} V_{\beta_1 n_2} D^R_{n_2 n',tt'} - \sum_{\beta_1\nu_1} c^{(\nu)}_{\beta\beta_1} V_{\beta_1} G^{ur,R}_{\beta_1\nu_1 n',tt'}, \tag{E.5a}$$

$$\partial_{t'} G^{r\pi,R}_{n\beta'\nu',tt'} = -\frac{\rho_{\beta'}}{M_{\beta'}}\omega^2_{\beta'\nu'} G^{ru,R}_{n\beta'\nu',tt'} - \sum_{n_1\beta_2} D^R_{nn_1,tt'} V_{n_1\beta_2} c^{(\nu')}_{\beta_2\beta'} - \sum_{\nu_1} G^{ru,R}_{n\beta_1\nu_1,tt'} V_{\beta_1} c^{(\nu')}_{\beta_1\beta'}, \tag{E.5b}$$

$$\partial_t G^{pr,R}_{nn',tt'} = -\omega^2_n D^R_{nn',tt'} - \sum_{n_1\neq n} V_{nn_1} D^R_{n_1 n',tt'} - \sum_{\beta_1\nu_1} V_{n\beta_1} G^{ur,R}_{\beta_1\nu_1 n',tt'}, \tag{E.5c}$$

where we denoted $V_{nn} = \omega^2_n$. Combining the equations (E.4) and (E.5) we obtain

$$\partial^2_t G^{ur,R}_{\beta\nu n',tt'} = -\omega^2_{\beta\nu} G^{ur,R}_{\beta\nu n',tt'} - \sum_{\beta_1 n_2} \frac{M_\beta}{\rho_\beta} c^{(\nu)}_{\beta\beta_1} V_{\beta_1 n_2} D^R_{n_2 n',tt'} - \sum_{\beta_1\nu_1} \frac{M_\beta}{\rho_\beta} c^{(\nu)}_{\beta\beta_1} V_{\beta_1} G^{ur,R}_{\beta_1\nu_1 n',tt'}, \tag{E.6a}$$

$$\partial^2_{t'} G^{ru,R}_{n\beta'\nu',tt'} = -\omega^2_{\beta'\nu'} G^{ru,R}_{n\beta'\nu',tt'} - \sum_{n_1\beta_2} D^R_{nn_1,tt'} V_{n_1\beta_2} \frac{M_{\beta'}}{\rho_{\beta'}} c^{(\nu')}_{\beta_2\beta'} - \sum_{\beta_1\nu_1} G^{ru,R}_{n\beta_1\nu_1,tt'} V_{\beta_1} \frac{M_{\beta'}}{\rho_{\beta'}} c^{(\nu')}_{\beta_1\beta'}, \tag{E.6b}$$

$$\partial^2_t D^R_{nn',tt'} = -\omega^2_n D^R_{nn',tt'} - \sum_{n_1\neq n} V_{nn_1} D^R_{n_1 n',tt'} - \sum_{\beta_1\nu_1} V_{n\beta_1} G^{ur,R}_{\beta_1\nu_1 n',tt'}. \tag{E.6c}$$

Now we Fourier transform the above equations with respect to the time difference, i.e., we integrate both sides with $\int_{-\infty}^{+\infty} \mathrm{d}(t-t')\mathrm{e}^{\mathrm{i}(\omega+\mathrm{i}\eta)(t-t')}\ldots$, and then we get

$$-(\omega+\mathrm{i}\eta)^2 G^{ur,R}_{\beta\nu n',\omega} = -\omega^2_{\beta\nu} G^{ur,R}_{\beta\nu n',\omega} - \sum_{\beta_1 n_2} \frac{M_\beta}{\rho_\beta} c^{(\nu)}_{\beta\beta_1} V_{\beta_1 n_2} D^R_{n_2 n',\omega} - \sum_{\beta_1\nu_1} \frac{M_\beta}{\rho_\beta} c^{(\nu)}_{\beta\beta_1} V_{\beta_1} G^{ur,R}_{\beta_1\nu_1 n',\omega}, \tag{E.7a}$$

$$-(\omega+\mathrm{i}\eta)^2 G^{ru,R}_{n\beta'\nu',\omega} = -\omega^2_{\beta'\nu'} G^{ru,R}_{n\beta'\nu',\omega} - \sum_{n_1\beta_2} D^R_{nn_1,\omega} V_{n_1\beta_2} \frac{M_{\beta'}}{\rho_{\beta'}} c^{(\nu')}_{\beta_2\beta'} - \sum_{\beta_1\nu_1} G^{ru,R}_{n\beta_1\nu_1,\omega} V_{\beta_1} \frac{M_{\beta'}}{\rho_{\beta'}} c^{(\nu')}_{\beta_1\beta'}, \tag{E.7b}$$

$$-(\omega+\mathrm{i}\eta)^2 D^R_{nn',\omega} = -\omega^2_n D^R_{nn',\omega} - \sum_{n_1\neq n} V_{nn_1} D^R_{n_1 n',\omega} - \sum_{\beta_1\nu_1} V_{n\beta_1} G^{ur,R}_{\beta_1\nu_1 n',\omega}, \tag{E.7c}$$

which can be rewritten as

$$G^{ur,R}_{\beta\nu n',\omega} = \sum_{\beta_1\nu_1 n_2} S^{0,R}_{\beta\nu,\beta_1\nu_1,\omega} V_{\beta_1 n_2} D^R_{n_2 n',\omega} + \sum_{\beta_1\nu_1} S^{0,R}_{\beta\nu,\beta_1\nu_1,\omega} V_{\beta_1} G^{ur,R}_{\beta_1\nu_1 n',\omega}, \tag{E.8a}$$

$$G^{ru,R}_{n\beta'\nu',\omega} = \sum_{n_1\beta_2\nu_2} D^R_{nn_1,\omega} V_{n_1\beta_2} S^{0,R}_{\beta_2\nu_2,\beta'\nu',\omega} + \sum_{\beta_1\nu_1\nu_2} G^{ru,R}_{n\beta_1\nu_1,\omega} V_{\beta_1} S^{0,R}_{\beta_1\nu_2,\beta'\nu',\omega}, \tag{E.8b}$$

$$D^R_{nn',\omega} = \sum_{n_1\neq n_2} D^{0,R}_{nn_1,\omega} V_{n_1 n_2} D^R_{n_2 n',\omega} + \sum_{n_1\beta_2\nu_2} D^{0,R}_{nn_1,\omega} V_{n_1\beta_2} G^{ur,R}_{\beta_2\nu_2 n',\omega}, \tag{E.8c}$$

where D^0 and S^0 are non-interacting substrate and particle Green's functions which are given in Appendix F by equation (F.1). In the end we will need Green's functions summed over the modes ν

and ν', and by summing the above equations (E.8) over ν and ν' we obtain

$$G^{ur,R}_{\beta n',\omega} = \sum_{\beta_1 n_2} S^{0,R}_{\beta\beta_1,\omega} V_{\beta_1 n_2} D^{R}_{n_2 n',\omega} + \sum_{\beta_1} S^{0,R}_{\beta\beta_1,\omega} V_{\beta_1} G^{ur,R}_{\beta_1 n',\omega}, \tag{E.9a}$$

$$G^{ru,R}_{n\beta',\omega} = \sum_{n_1\beta_2} D^{R}_{nn_1,\omega} V_{n_1\beta_2} S^{0,R}_{\beta_2\beta',\omega} + \sum_{\beta_1} G^{ru,R}_{n\beta_1,\omega} V_{\beta_1} S^{0,R}_{\beta_1\beta',\omega}, \tag{E.9b}$$

$$D^{R}_{nn',\omega} = \sum_{n_1\neq n_2} D^{0,R}_{nn_1,\omega} V_{n_1 n_2} D^{R}_{n_2 n',\omega} + \sum_{n_1\beta_2} D^{0,R}_{nn_1,\omega} V_{n_1\beta_2} G^{ur,R}_{\beta_2 n',\omega}. \tag{E.9c}$$

The equation of motion technique gives exactly the same equations for advanced Green's functions (with $\eta \to -\eta$) and as we can see from Larkin-Ovchinnikov representation (11.9) it also carries to Schwinger-Keldysh space (see Eq. 11.10) [131, 134, 150].

Appendix F

The non-interacting particle D^0 and lead S^0 Green's functions

In this section we present the non-interacting particle Green's function D^0 corresponding to Hamiltonian $H_0 = \sum_{im}(p_{im}^2 + V_{im,im}r_{im}^2)/2$ and lead Green's functions S^0 corresponding to Hamiltonian $H_0 = \sum_{\alpha\nu}\hbar\omega_{\alpha\nu}a_{\alpha\nu}^\dagger a_{\alpha\nu}$. We note that we use mass weighted coordinates (9.3). By using equation of motion we obtain for Fourier transformed retarded Green's functions

$$D^{0,R}_{im,i'm',\omega} = \frac{\delta_{ii'}\delta_{mm'}}{(\omega+\mathrm{i}\eta)^2-\omega_{im}^2}, \quad \omega_{im}^2 = \frac{K_{im}}{M_m}, \tag{F.1a}$$

$$S^{0,R}_{i\alpha\mathbf{r}\nu,i'\alpha'\mathbf{r}'\nu',\omega} = \frac{M_\alpha}{\rho_\alpha}\frac{c_{ii',\alpha,\nu,\mathbf{r}\mathbf{r}'}\delta_{\alpha\alpha'}\delta_{\nu\nu'}}{(\omega+\mathrm{i}\eta)^2-\omega_{\alpha\nu}^2}, \quad \omega_{\alpha\nu} = c_{\alpha t}\sqrt{k_\beta^2+\kappa^2}, \tag{F.1b}$$

where

$$c_{ii',\alpha,\nu,\mathbf{r}\mathbf{r}'} = \mathrm{Re}\left[u_{i\alpha}^{(\nu)}(\mathbf{r})u_{i'\alpha}^{*(\nu)}(\mathbf{r}')\right] = \frac{1}{2}\left[u_{i\alpha}^{(\nu)}(\mathbf{r})u_{i'\alpha}^{*(\nu)}(\mathbf{r}') + u_{i\alpha}^{*(\nu)}(\mathbf{r})u_{i'\alpha}^{(\nu)}(\mathbf{r}')\right], \tag{F.2}$$

and $S^{0,R}_{i\alpha\mathbf{r}\nu,i'\alpha'\mathbf{r}'\nu',\omega}$ corresponds to

$$S^{0,R}_{i\alpha\mathbf{r}\nu,i'\alpha'\mathbf{r}'\nu',tt'} = -\mathrm{i}\theta(t-t')\langle[u_{i\alpha\nu}(\mathbf{r},t),u_{i'\alpha'\nu'}(\mathbf{r}',t')]\rangle_0. \tag{F.3}$$

We are interested in the $\nu\nu'$ summed lead Green's function $S^{0,R}_{i\alpha\mathbf{r},i'\alpha'\mathbf{r}',\omega}$, when molecules are attached only to the surface of the leads $\mathbf{r}_\alpha = (x,y_\alpha,z)$, $\mathbf{r}'_\alpha = (x',y_\alpha,z')$. So we need the coefficient

$$c_{\alpha,ii',\nu,\mathbf{r}_\alpha\mathbf{r}'_\alpha} = \frac{1}{2(2\pi)^2}\left[f_{i\alpha}^{(\nu)}(y_\alpha)f_{i'\alpha}^{*(\nu)}(y_\alpha)\mathrm{e}^{\mathrm{i}k_z(z-z')}\mathrm{e}^{\mathrm{i}k_x(x-x')} + f_{i\alpha}^{*(\nu)}(y_\alpha)f_{i'\alpha}^{(\nu)}(y_\alpha)\mathrm{e}^{-\mathrm{i}k_z(z-z')}\mathrm{e}^{-\mathrm{i}k_x(x-x')}\right], \tag{F.4}$$

and then the required $\nu\nu'$ summed lead Green's function is

$$\begin{aligned} S^{0,R/A}_{i\alpha\mathbf{r}_\alpha,i'\alpha'\mathbf{r}'_\alpha,\omega} = {} & \frac{M_\alpha\delta_{\alpha\alpha'}}{2(2\pi)^2\rho_\alpha}\sum_{m=H,\pm,0,R}\int_0^{\kappa_D}\mathrm{d}\kappa\,\kappa\int_{k_1}^{k_2}\mathrm{d}k_\beta\int_0^{2\pi}\mathrm{d}\theta\,\frac{1}{(\omega\pm\mathrm{i}\eta)^2-c_t^2(k_\beta^2+\kappa^2)} \\ & \times\left[f_{i\alpha}^{(\nu)}(y_\alpha)f_{i'\alpha}^{*(\nu)}(y_\alpha)\mathrm{e}^{\mathrm{i}k_z(z-z')}\mathrm{e}^{\mathrm{i}k_x(x-x')} + f_{i\alpha}^{*(\nu)}(y_\alpha)f_{i'\alpha}^{(\nu)}(y_\alpha)\mathrm{e}^{-\mathrm{i}k_z(z-z')}\mathrm{e}^{-\mathrm{i}k_x(x-x')}\right], \end{aligned} \tag{F.5}$$

where different modes $m = H,\pm,0,R$ and relevant integration intervals k_1, k_2 for these modes are described in Section 10. We have the following expressions for functions $f_{i\alpha,y_\alpha}^{(\kappa,\theta,k_\beta,m)}$, which enter (F.5)

$$
\begin{aligned}
H:\quad & f_z = -\sin\theta\sqrt{\frac{2}{\pi}}, \quad k_1 = 0,\ k_2 = +\infty,\\
& f_x = \cos\theta\sqrt{\frac{2}{\pi}}.\\
\pm:\quad & f_z = \frac{\cos\theta}{\sqrt{4\pi(1+k_\beta^2/\kappa^2)}}\left[\pm\sqrt{\frac{k_\beta}{k_\alpha}}(1-\zeta_\pm) - \mathrm{i}\frac{k_\beta}{\kappa}(1+\zeta_\pm)\right], \quad \zeta_\pm = a \pm \mathrm{i}b, \quad k_\alpha = \frac{c_t}{c_l}\sqrt{k_\beta^2+\kappa^2\left[1-\frac{c_l^2}{c_t^2}\right]},\\
& f_x = \frac{\sin\theta}{\sqrt{4\pi(1+k_\beta^2/\kappa^2)}}\left[\pm\sqrt{\frac{k_\beta}{k_\alpha}}(1-\zeta_\pm) - \mathrm{i}\frac{k_\beta}{\kappa}(1+\zeta_\pm)\right], \quad a = \frac{(k_\beta^2-\kappa^2)^2 - 4\kappa^2 k_\alpha k_\beta}{(k_\beta^2-\kappa^2)^2 + 4\kappa^2 k_\alpha k_\beta}, \quad b = \frac{4\kappa\sqrt{k_\alpha k_\beta}(k_\beta^2-\kappa^2)}{(k_\beta^2-\kappa^2)^2 + 4\kappa^2 k_\alpha k_\beta},\\
& f_y = \frac{1}{\sqrt{4\pi(1+k_\beta^2/\kappa^2)}}\left[\pm\sqrt{\frac{k_\alpha k_\beta}{\kappa^2}}(1+\zeta_\pm) + \mathrm{i}(1-\zeta_\pm)\right], \quad k_1 = \kappa\sqrt{\frac{c_l^2}{c_t^2}-1},\ k_2 = +\infty.\\
0:\quad & f_z = -\mathrm{i}\frac{\cos\theta}{\sqrt{2\pi(1+k_\beta^2/\kappa^2)}}\left[b + \frac{k_\beta}{\kappa}(1+a)\right], \quad k_\gamma = \frac{c_t}{c_l}\sqrt{\kappa^2\left[\frac{c_l^2}{c_t^2}-1\right]-k_\beta^2}, \quad k_\alpha = \mathrm{i}k_\gamma,\\
& f_x = -\mathrm{i}\frac{\sin\theta}{\sqrt{2\pi(1+k_\beta^2/\kappa^2)}}\left[b + \frac{k_\beta}{\kappa}(1+a)\right], \quad a = \frac{(k_\beta^2-\kappa^2)^2 - 4\mathrm{i}\kappa^2 k_\gamma k_\beta}{(k_\beta^2-\kappa^2)^2 + 4\mathrm{i}\kappa^2 k_\gamma k_\beta}, \quad b = \frac{4\kappa k_\beta(k_\beta^2-\kappa^2)}{(k_\beta^2-\kappa^2)^2 + 4\mathrm{i}\kappa^2 k_\gamma k_\beta}.\\
& f_y = \frac{1}{\sqrt{2\pi(1+k_\beta^2/\kappa^2)}}\left[-\frac{k_\gamma}{\kappa}b + \mathrm{i}(1-a)\right], \quad k_1 = 0,\ k_2 = \kappa\sqrt{\frac{c_l^2}{c_t^2}-1}.\\
R:\quad & f_z = \mathrm{i}\cos\theta\sqrt{\frac{\kappa}{K(\sigma)}}\left[1 - \frac{2k_\gamma k_\eta}{\kappa^2+k_\eta^2}\right], \quad k_\beta = \mathrm{i}k_\eta,\\
& f_x = \mathrm{i}\sin\theta\sqrt{\frac{\kappa}{K(\sigma)}}\left[1 - \frac{2k_\gamma k_\eta}{\kappa^2+k_\eta^2}\right], \quad K(\sigma) = \frac{(k_\gamma - k_\eta)(\kappa^2 k_\gamma - \kappa^2 k_\eta + 2k_\gamma k_\eta^2)}{2\kappa k_\gamma k_\eta^2},\\
& f_y = \sqrt{\frac{\kappa}{K(\sigma)}}\left[\frac{k_\gamma}{\kappa} - \frac{2\kappa k_\gamma}{\kappa^2+k_\eta^2}\right], \quad \text{there is no integral over } k_\eta, \text{ because } k_\eta = k_R,
\end{aligned}
\tag{F.6}
$$

where we have suppressed the labels α, y_α, and $(\kappa, \theta, k_\beta, m)$ for simplicity. We can obtain the advanced $S^{0,A}$ and Keldysh $S^{0,K}$ Green's function by noting that in equilibrium for bosonic Green's function G_ω we have the relations $G^A_\omega = [G^R_\omega]^\dagger$ and $G^K_\omega = [2n(\omega)+1](G^R_\omega - G^A_\omega)$.

F.1 Coupling to a single point

If the molecule couples to a single point of the lead $\mathbf{r}_\alpha = (x_\alpha, y_\alpha, z_\alpha)$ then from Eq. (F.5) and Eq. (11.27) we obtain such imaginary part for different modes m of $S^{0,R}_{i\alpha\mathbf{r}_\alpha, i\alpha\mathbf{r}_\alpha,\omega}$:

$$
b_\parallel^H = -\frac{\omega}{4\pi\rho c_t^3}\int_0^1 \frac{x\mathrm{d}x}{\sqrt{1-x^2}} \approx -\frac{\omega}{4\pi\rho c_t^3}, \tag{F.7a}
$$

$$
b_\parallel^\pm = -\frac{\omega}{8\pi\rho c_t^3}\int_0^{1/c_r} \frac{c_r x\sqrt{1-x^2}\mathrm{d}x}{c_r(1-2x^2)^2 + 4x^2\sqrt{1-x^2}\sqrt{1-(c_r x)^2}} \approx -0.042\frac{\omega}{4\pi\rho c_t^3}, \tag{F.7b}
$$

$$
b_\parallel^{(0)} = -\frac{\omega}{4\pi\rho c_t^3}\int_{1/c_r}^1 \frac{c_r^2 x\sqrt{1-x^2}(1-2x^2)^2\mathrm{d}x}{c_r^2\left[1-8x^2(1-x^2)(1-2x^2)\right] - 16x^4(1-x^2)} \approx -0.168\frac{\omega}{4\pi\rho c_t^3}, \tag{F.7c}
$$

$$
b_\parallel^R = -\frac{\omega}{4\pi\rho c_t^3}\frac{\pi\xi\sqrt{(1-\xi)(c_r^2-1+\xi)}[c_r(1+\xi) - 2\sqrt{\xi(c_r^2-1+\xi)}]^2}{c_r(1-\xi^2)^2(\sqrt{c_r^2-1+\xi} - c_r\sqrt{\xi})[(1+2\xi)\sqrt{c_r^2-1+\xi} - c_r\sqrt{\xi}]} \approx -0.151\frac{\omega}{4\pi\rho c_t^3}, \tag{F.7d}
$$

$$b_{\perp}^{\pm} = -\frac{\omega}{4\pi\rho c_t^3}\int_0^{1/c_r}\frac{x\sqrt{1-(c_r x)^2}\mathrm{d}x}{c_r(1-2x^2)^2+4x^2\sqrt{1-x^2}\sqrt{1-(c_r x)^2}} \approx -0.021\frac{\omega}{4\pi\rho c_t^3}, \tag{F.7e}$$

$$b_{\perp}^{(0)} = -\frac{2\omega}{\pi\rho c_t^3}\int_{1/c_r}^1\frac{x^3\sqrt{1-x^2}[(c_r x)^2-1]\mathrm{d}x}{c_r^2\left[1-8x^2(1-x^2)(1-2x^2)\right]-16x^4(1-x^2)} \approx -0.540\frac{\omega}{4\pi\rho c_t^3}, \tag{F.7f}$$

$$b_{\perp}^{R} = -\frac{\omega}{2\pi\rho c_t^3}\frac{\pi\xi(1-\xi)^{5/2}(c_r^2-1+\xi)^{3/2}}{c_r(1-\xi^2)^2(\sqrt{c_r^2-1+\xi}-c_r\sqrt{\xi})[(1+2\xi)\sqrt{c_r^2-1+\xi}-c_r\sqrt{\xi}]} \approx -0.863\frac{\omega}{4\pi\rho c_t^3}. \tag{F.7g}$$

For gold (Au) leads we have

$$c_r = \frac{c_l}{c_t} = \sqrt{\frac{2(1-\sigma)}{1-2\sigma}} \approx 2.693, \quad \text{where } \sigma = 0.42 \text{ is Poisson ratio,} \tag{F.8}$$

and $0<\xi<1$ is determined from Eq. (10.84)

$$\xi^4 + 4\xi^3 + 2\left(3-\frac{8}{c_r^2}\right)\xi^2 - 4\left(3-\frac{4}{c_r^2}\right)\xi + 1 = 0, \quad \xi \approx 0.107. \tag{F.9}$$

Then the total values of imaginary parts are

$$b_{\parallel} \approx -1.404\frac{\omega}{4\pi\rho c_t^3} \equiv -A_{\parallel}\omega, \quad b_{\perp} \approx -1.445\frac{\omega}{4\pi\rho c_t^3} \equiv -A_{\perp}\omega, \tag{F.10}$$

Note that $b_{\parallel}$ corresponds to b_{zz}, b_{xx} components and $b_{\perp}$ corresponds to b_{yy}.

We can calculate the real part using the Kramers-Krönig relations (also known as Hilbert transform). For function $G(\omega)$, which is analytic in the upper complex half-plane (the retarded one), and which decays as ω^{-a} with $a>0$ we have

$$\begin{aligned}\mathrm{Re}\,G(\omega) &= \frac{1}{\pi}\mathcal{P}\int_{-\infty}^{+\infty}\mathrm{d}\omega'\frac{\mathrm{Im}\,G(\omega')}{\omega'-\omega},\\ \mathrm{Im}\,G(\omega) &= -\frac{1}{\pi}\mathcal{P}\int_{-\infty}^{+\infty}\mathrm{d}\omega'\frac{\mathrm{Re}\,G(\omega')}{\omega'-\omega}.\end{aligned} \tag{F.11}$$

In our case the retarded function $S^{0,R}_{i\alpha\mathbf{r}_\alpha, i\alpha\mathbf{r}_\alpha,\omega}$ satisfies all the above mentioned conditions if we cutoff the frequency ω in the imaginary parts of (F.10) by the Debye frequency ω_D. In such a case after applying transformation Eq. (F.11) to Eq. (F.10) we obtain

$$a_{\parallel/\perp} = -\frac{A_{\parallel/\perp}}{\pi}\left(2\omega_D + \omega\ln\left|\frac{\omega_D-\omega}{\omega_D+\omega}\right|\right). \tag{F.12}$$

F.2 Coupling to an area

From Eq. (F.12) we see that the real part $a_{\parallel/\perp}$ depends on the cutoff ω_D even when $\omega_D\to+\infty$, and in such a case the result for the heat current depends on the actual value of ω_D. To see if the assumption of coupling to a single point of the lead is valid we examine coupling to an area as depicted in the inset of Figure F.1. We consider such a function

$$R^0_{ii',\omega} = \frac{1}{a^4}\int_{-\frac{a}{2}}^{\frac{a}{2}}\mathrm{d}z\mathrm{d}x\mathrm{d}z'\mathrm{d}x' S^0_{ii',\mathbf{r}_\alpha\mathbf{r}'_\alpha,\omega}, \tag{F.13}$$

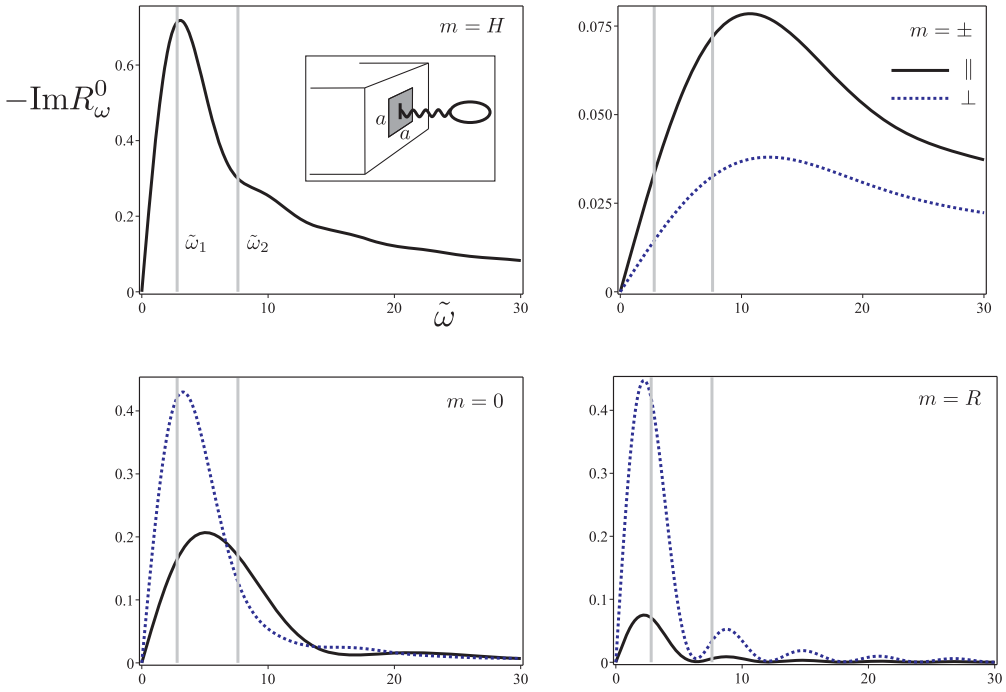

Figure F.1: The imaginary part of function $R^{0,R}_{ii',\omega}$ (F.15) for different modes m. Solid black curves correspond to $R^{0,R}_{zz,\omega}$, $R^{0,R}_{xx,\omega}$ and dotted blue curves correspond to $R^{0,R}_{yy,\omega}$. Solid vertical gray lines denote the values of dimensionless Debye frequencies $\tilde{\omega}_1 \approx 2.80$ corresponding to radius of a gold atom $a_1 = 1.5$ Å, and $\tilde{\omega}_2 \approx 7.61$ corresponding to a lattice constant $a_2 = 4.08$ Å.

where we integrate the lead Green's function over area a^2 for every of the variables $\mathbf{r}_\alpha = (x, y_\alpha, z)$ and $\mathbf{r}'_\alpha = (x', y_\alpha, z')$. Note that we have neglected the label α for convenience. If the coupling area is of the size of the lead atom the Debye ω_D frequency should cutoff the imaginary part of the function (F.13) before it starts decaying do to coupling to a finite area. Using the following integrals

$$\begin{aligned} I_{zz} = I_{xx} &= \int_0^{2\pi} \frac{\mathrm{d}\theta}{\cos^2\theta} \sin^2\!\left(\frac{\kappa a}{2}\cos\theta\right)\sin^2\!\left(\frac{\kappa a}{2}\sin\theta\right), \\ I_{yy} &= \int_0^{2\pi} \frac{\mathrm{d}\theta}{\cos^2\theta\sin^2\theta} \sin^2\!\left(\frac{\kappa a}{2}\cos\theta\right)\sin^2\!\left(\frac{\kappa a}{2}\sin\theta\right), \end{aligned} \tag{F.14}$$

we can rewrite the retarded function of (F.13) as

$$\begin{aligned} R^{0,R}_{ii',\omega} &= \frac{1}{2(2\pi)^2\rho} \sum_{m=H,\pm,0,R} \int_0^{\kappa_D} \mathrm{d}\kappa\kappa \int_{k_1}^{k_2} \mathrm{d}k_\beta \frac{\bar{f}^{(\nu)}_i \bar{f}^{*(\nu)}_{i'} + \bar{f}^{*(\nu)}_i \bar{f}^{(\nu)}_{i'}}{(\omega \pm \mathrm{i}\eta)^2 - c_t^2(k_\beta^2 + \kappa^2)} \times \boxed{\frac{16}{a^4\kappa^4} I_{ii'}\!\left(\frac{\kappa a}{2}\right)} \\ &= \frac{16}{2(2\pi)^2\rho c_t^2 a} \sum_{m=H,\pm,0,R} \int_0^{\kappa_D a} \frac{\mathrm{d}u}{u^3} \int_{k_1 a}^{k_2 a} \mathrm{d}v \frac{\bar{f}^{(\nu)}_i \bar{f}^{*(\nu)}_{i'} + \bar{f}^{*(\nu)}_i \bar{f}^{(\nu)}_{i'}}{(\tilde{\omega} \pm \mathrm{i}\eta)^2 - (v^2 + u^2)} \times I_{ii'}\!\left(\frac{u}{2}\right), \end{aligned} \tag{F.15}$$

where $\bar{f}$ represents functions in (F.6) without trigonometric factors dependent on the angle θ. Also the new variables and the dimensionless frequency are

$$\tilde{\omega} = \omega a / c_t, \quad u = \kappa a, \quad v = k_\beta a. \tag{F.16}$$

Now in expression (F.15) we separate the real and imaginary part in the denominator, i.e.,

$$\frac{1}{(\tilde{\omega}\pm \mathrm{i}\eta)^2-(v^2+u^2)} = -\mathcal{P}\frac{1}{v^2+u^2-\tilde{\omega}^2} \mp \frac{\mathrm{i}\pi}{2}\frac{\mathrm{sgn}(\tilde{\omega})}{\sqrt{\tilde{\omega}^2-u^2}}\delta(v-\sqrt{\tilde{\omega}^2-u^2}), \tag{F.17}$$

where we used

$$\delta(\sqrt{v^2+u^2}\mp\tilde{\omega}) = \frac{|\tilde{\omega}|}{\sqrt{\tilde{\omega}^2-u^2}}\delta(v-\sqrt{\tilde{\omega}^2-u^2}). \tag{F.18}$$

Note that for Rayleigh mode R we have fixed value of $v^2 = -u^2\xi$, where ξ satisfies Eq. (10.84), and then we use the following form of the relation (F.17)

$$\frac{1}{(\tilde{\omega}\pm \mathrm{i}\eta)^2-u^2(1-\xi)} = -\mathcal{P}\frac{1}{u^2(1-\xi)-\tilde{\omega}^2} \mp \frac{\mathrm{i}\pi}{2(\tilde{\omega}\pm\mathrm{i}\eta)\sqrt{1-\xi}}\delta\left(u-\frac{|\tilde{\omega}|}{\sqrt{1-\xi}}\right). \tag{F.19}$$

Using Eqs. (F.17) and (F.19) we find the imaginary part of function $R^{0,R}_{ii',\omega}$ (F.15), which is plotted in Figure F.1 for different modes m. Solid vertical gray lines denote Debye frequency $\omega_D = 22.2$ THz for $a_1 = 1.5$ Å corresponding to radius of a gold atom, which gives dimensionless frequency $\tilde{\omega}_1 \approx 2.80$, and $a_2 = 4.08$ Å corresponding to a lattice constant, which gives dimensionless frequency $\tilde{\omega}_2 \approx 7.61$. We see when the coupling area is shrunk to size of gold atom the Debye frequency cutoff is consistent with cutoff, which appears due to coupling to a finite area.

Appendix G

Normal modes of the two masses model

We want to rewrite Hamiltonian (9.1) with the coupling (9.2) for two masses model in the normal mode basis, which is useful when calculating the transmission (11.30). For simplicity, we suppress the coordinate label i and then we need to diagonalize the following Hamiltonian

$$H_{\mathrm{M}} = \frac{p_1^2}{2} + \frac{p_2^2}{2} + \frac{K+K_L}{2M_1} r_1^2 + \frac{K+K_R}{2M_2} r_2^2 - \frac{K}{\sqrt{M_1 M_2}} r_1 r_2, \tag{G.1a}$$

$$V = -\frac{K_L}{\sqrt{M_L M_1}} r_1 u_L - \frac{K_R}{\sqrt{M_R M_2}} r_2 u_R. \tag{G.1b}$$

In order to find the normal modes of (G.1a) we need to diagonalize the following Hessian matrix

$$\mathcal{H} = \begin{pmatrix} \frac{K_1}{M_1} & -\frac{K}{\sqrt{M_1 M_2}} \\ -\frac{K}{\sqrt{M_1 M_2}} & \frac{K_2}{M_2} \end{pmatrix} = \begin{pmatrix} \omega_1^2 & V_{12} \\ V_{12} & \omega_2^2 \end{pmatrix} = \mathcal{P}\mathcal{D}\mathcal{P}^{-1}, \tag{G.2}$$

where

$$K_1 = K + K_L, \quad K_2 = K + K_R. \tag{G.3}$$

The matrices $\mathcal{D}$, $\mathcal{P}$, $\mathcal{P}^{-1}$ are

$$\mathcal{D} = \begin{pmatrix} \omega_+^2 & 0 \\ 0 & \omega_-^2 \end{pmatrix}, \quad \mathcal{P} = \begin{pmatrix} u & v \\ -v & u \end{pmatrix}, \quad \mathcal{P}^{-1} = \begin{pmatrix} u & -v \\ v & u \end{pmatrix}, \quad \mathcal{P}\mathcal{P}^{-1} = \mathbf{1}, \tag{G.4}$$

with

$$\omega_\pm^2 = \frac{\omega_1^2 + \omega_2^2}{2} \pm \Delta, \quad \Delta = \sqrt{\delta^2 + V_{12}^2} \quad \delta = \frac{\omega_1^2 - \omega_2^2}{2}, \tag{G.5}$$

$$u = \sqrt{\frac{1}{2}\left(1 + \frac{\delta}{\Delta}\right)}, \quad v = \sqrt{\frac{1}{2}\left(1 - \frac{\delta}{\Delta}\right)}. \tag{G.6}$$

Then the normal mode coordinates are expressed as

$$\begin{pmatrix} r_+ \\ r_- \end{pmatrix} = \mathcal{P}^{-1} \begin{pmatrix} r_1 \\ r_2 \end{pmatrix} = \begin{pmatrix} u & -v \\ v & u \end{pmatrix} \begin{pmatrix} r_1 \\ r_2 \end{pmatrix} = \begin{pmatrix} u r_1 - v r_2 \\ u r_2 + v r_1 \end{pmatrix} \tag{G.7}$$

and the inverse transformation is

$$\begin{pmatrix} r_1 \\ r_2 \end{pmatrix} = \mathcal{P} \begin{pmatrix} r_+ \\ r_- \end{pmatrix} = \begin{pmatrix} u & v \\ -v & u \end{pmatrix} \begin{pmatrix} r_+ \\ r_- \end{pmatrix} = \begin{pmatrix} u r_+ + v r_- \\ u r_- - v r_+ \end{pmatrix}. \tag{G.8}$$

In the normal mode basis the Hamiltonian (G.1) is expressed as

$$H_{\mathrm{M}} = \frac{p_+^2}{2} + \frac{p_-^2}{2} + \frac{1}{2}\omega_+^2 r_+^2 + \frac{1}{2}\omega_-^2 r_-^2, \tag{G.9a}$$

$$V = r_+ \left(V_{+L} u_L + V_{+R} u_R\right) + r_- \left(V_{-L} u_L + V_{-R} u_R\right), \tag{G.9b}$$

where

$$\begin{aligned} V_{+L} &= -\frac{K_L u}{\sqrt{M_L M_1}}, \quad V_{+R} = +\frac{K_R v}{\sqrt{M_R M_2}}, \\ V_{-L} &= -\frac{K_L v}{\sqrt{M_L M_1}}, \quad V_{-R} = -\frac{K_R u}{\sqrt{M_R M_2}}, \end{aligned} \tag{G.10}$$

Note that u_α corresponds to the displacement vector of the leads and u is just given by (G.6).

Bibliography

[1] L. P. Kouwenhoven, C. M. Marcus, P. L. Mceuen, S. Tarucha, R. M. Westervelt, and N. S. Wingreen, *Electron Transport in Quantum Dots*, edited by L. L. Sohn, L. P. Kouwenhoven, and G. Schön (Kluwer Academic Publishers, 1997).

[2] L. P. Kouwenhoven, T. H. Oosterkamp, M. W. S. Danoesastro, M. Eto, D. G. Austing, T. Honda, and S. Tarucha, "Excitation Spectra of Circular, Few-Electron Quantum Dots", Science **278**, 1788–1792 (1997) 10.1126/science.278.5344.1788.

[3] T. Chakraborty, *Quantum Dots: A Survey of the Properties of Artificial Atoms* (Elsevier Science, Amsterdam, 1999).

[4] H. Grabert and M. H. Devoret, *Single charge tunneling: Coulomb blockade phenomena in nanostructures* (Plenum Press and NATO Scientific Affairs Division, New York, 1992).

[5] P. Lafarge, H. Pothier, E. R. Williams, D. Esteve, C. Urbina, and M. H. Devoret, "Direct observation of macroscopic charge quantization", Z. Phys. B Con. Mat. **85**, 327–332 (1991) 10.1007/BF01307627.

[6] A. A. M. Staring, L. W. Molenkamp, B. W. Alphenaar, H. van Houten, O. J. A. Buyk, M. A. A. Mabesoone, C. W. J. Beenakker, and C. T. Foxon, "Coulomb-Blockade Oscillations in the Thermopower of a Quantum Dot", EPL-Europhys. Lett. **22**, 57–62 (1993) 10.1209/0295-5075/22/1/011.

[7] G. D. Mahan and J. O. Sofo, "The best thermoelectric.", P. Natl. Acad. Sci. USA **93**, 7436–9 (1996).

[8] W. J. de Haas, J. de Boer, and G. J. van dën Berg, "The electrical resistance of gold, copper and lead at low temperatures", Physica **1**, 1115–1124 (1934) 10.1016/S0031-8914(34)80310-2.

[9] J. Kondo, "Resistance Minimum in Dilute Magnetic Alloys", Prog. Theor. Phys. **32**, 37–49 (1964) 10.1143/PTP.32.37.

[10] D. Goldhaber-Gordon, H. Shtrikman, D. Mahalu, D. Abusch-Magder, U. Meirav, and M. A. Kastner, "Kondo effect in a single-electron transistor", Nature **391**, 156 (1998) 10.1038/34373.

[11] S. M. Cronenwett, T. H. Oosterkamp, and L. P. Kouwenhoven, "A Tunable Kondo Effect in Quantum Dots", Science **281**, 540–544 (1998) 10.1126/science.281.5376.540.

[12] A. A. Abrikosov, "Electron scattering on magnetic impurities in metals and anomalous resistivity effects", Physics **2**, 5–20 (1965).

[13] H. Suhl, "Dispersion Theory of the Kondo Effect", Phys. Rev. **138**, A515–A523 (1965) 10.1103/PhysRev.138.A515.

[14] S. De Franceschi, L. P. Kouwenhoven, C. Schönenberger, and W. Wernsdorfer, "Hybrid superconductor-quantum dot devices.", Nat. Nanotechnol. **5**, 703–11 (2010) 10.1038/nnano.2010.173.

[15] R. Hanson, J. R. Petta, S. Tarucha, and L. M. K. Vandersypen, "Spins in few-electron quantum dots", Rev. Mod. Phys. **79**, 1217–1265 (2007) 10.1103/RevModPhys.79.1217.

[16]S. J. Tans, M. H. Devoret, H. Dai, A. Thess, R. E. Smalley, L. J. Geerligs, and C. Dekker, "Individual single-wall carbon nanotubes as quantum wires", Nature **386**, 474–477 (1997) 10.1038/386474a0.

[17]M. Bockrath, D. H. Cobden, P. L. McEuen, N. G. Chopra, A. Zettl, A. Thess, and R. E. Smalley, "Single-Electron Transport in Ropes of Carbon Nanotubes", Science **275**, 1922–1925 (1997) 10.1126/science.275.5308.1922.

[18]D. Cobden and J. Nygård, "Shell Filling in Closed Single-Wall Carbon Nanotube Quantum Dots", Phys. Rev. Lett. **89**, 046803 (2002) 10.1103/PhysRevLett.89.046803.

[19]F. D. M. Haldane, "Scaling Theory of the Asymmetric Anderson Model", Phys. Rev. Lett. **40**, 416–419 (1978) 10.1103/PhysRevLett.40.416.

[20]E. L. Wolf and D. L. Losee, "G-shifts in the "s-d" exchange theory of zero-bias tunneling anomalies", Phys. Lett. A **29**, 334–335 (1969) 10.1016/0375-9601(69)90156-X.

[21]J. Holm, H. Jørgensen, K. Grove-Rasmussen, J. Paaske, K. Flensberg, and P. Lindelof, "Gate-dependent tunneling-induced level shifts observed in carbon nanotube quantum dots", Phys. Rev. B **77**, 161406 (2008) 10.1103/PhysRevB.77.161406.

[22]M. M. Deshmukh and D. C. Ralph, "Using Single Quantum States as Spin Filters to Study Spin Polarization in Ferromagnets", Phys. Rev. Lett. **89**, 266803 (2002) 10.1103/PhysRevLett.89.266803.

[23]R. Potok, J. Folk, C. M. Marcus, V. Umansky, M. Hanson, and A. Gossard, "Spin and Polarized Current from Coulomb Blockaded Quantum Dots", Phys. Rev. Lett. **91**, 016802 (2003) 10.1103/PhysRevLett.91.016802.

[24]A. N. Pasupathy, R. C. Bialczak, J. Martinek, J. E. Grose, L. A. K. Donev, P. L. McEuen, and D. C. Ralph, "The Kondo effect in the presence of ferromagnetism.", Science **306**, 86–9 (2004) 10.1126/science.1102068.

[25]K. Hamaya, M. Kitabatake, K. Shibata, M. Jung, M. Kawamura, K. Hirakawa, T. Machida, T. Taniyama, S. Ishida, and Y. Arakawa, "Kondo effect in a semiconductor quantum dot coupled to ferromagnetic electrodes", Appl. Phys. Lett. **91**, 232105 (2007) 10.1063/1.2820445.

[26]J. R. Hauptmann, J. Paaske, and P. E. Lindelof, "Electric-field-controlled spin reversal in a quantum dot with ferromagnetic contacts", Nat. Phys. **4**, 373–376 (2008) 10.1038/nphys931.

[27]L. Hofstetter, A. Geresdi, M. Aagesen, J. Nygård, C. Schönenberger, and S. Csonka, "Ferromagnetic Proximity Effect in a Ferromagnet-Quantum-Dot-Superconductor Device", Phys. Rev. Lett. **104**, 246804 (2010) 10.1103/PhysRevLett.104.246804.

[28]M. Gaass, A. K. Hüttel, K. Kang, I. Weymann, J. von Delft, and C. Strunk, "Universality of the Kondo Effect in Quantum Dots with Ferromagnetic Leads", Phys. Rev. Lett. **107**, 176808 (2011) 10.1103/PhysRevLett.107.176808.

[29]J. Martinek, J. Barnaś, S. Maekawa, H. Schoeller, and G. Schön, "Spin accumulation in ferromagnetic single-electron transistors in the cotunneling regime", Phys. Rev. B **66**, 014402 (2002) 10.1103/PhysRevB.66.014402.

[30]N. Sergueev, Q.-f. Sun, H. Guo, B. Wang, and J. Wang, "Spin-polarized transport through a quantum dot: Anderson model with on-site Coulomb repulsion", Phys. Rev. B **65**, 165303 (2002) 10.1103/PhysRevB.65.165303.

[31]J. Fransson, O. Eriksson, and I. Sandalov, "Many-Body Approach to Spin-Dependent Transport in Quantum Dot Systems", Phys. Rev. Lett. **88**, 226601 (2002) 10.1103/PhysRevLett.88.226601.

[32]J. Martinek, Y. Utsumi, H. Imamura, J. Barnaś, S. Maekawa, J. König, and G. Schön, "Kondo Effect in Quantum Dots Coupled to Ferromagnetic Leads", Phys. Rev. Lett. **91**, 127203 (2003) 10.1103/PhysRevLett.91.127203.

[33]J. Martinek, M. Sindel, L. Borda, J. Barnaś, J. König, G. Schön, and J. von Delft, "Kondo Effect in the Presence of Itinerant-Electron Ferromagnetism Studied with the Numerical Renormalization Group Method", Phys. Rev. Lett. **91**, 247202 (2003) 10.1103/PhysRevLett.91.247202.

[34]J. König and J. Martinek, "Interaction-Driven Spin Precession in Quantum-Dot Spin Valves", Phys. Rev. Lett. **90**, 166602 (2003) 10.1103/PhysRevLett.90.166602.

[35]M. Braun, J. König, and J. Martinek, "Theory of transport through quantum-dot spin valves in the weak-coupling regime", Phys. Rev. B **70**, 195345 (2004) 10.1103/PhysRevB.70.195345.

[36]J. Ma and X. L. Lei, "Kondo correlation and spin-flip scattering in spin-dependent transport through a quantum dot coupled to ferromagnetic leads", EPL-Europhys. Lett. **67**, 432–438 (2004) 10.1209/epl/i2004-10079-7.

[37]M.-S. Choi, D. Sánchez, and R. López, "Kondo Effect in a Quantum Dot Coupled to Ferromagnetic Leads: A Numerical Renormalization Group Analysis", Phys. Rev. Lett. **92**, 056601 (2004) 10.1103/PhysRevLett.92.056601.

[38]S. Braig and P. Brouwer, "Rate equations for Coulomb blockade with ferromagnetic leads", Phys. Rev. B **71**, 195324 (2005) 10.1103/PhysRevB.71.195324.

[39]J. Martinek, M. Sindel, L. Borda, J. Barnaś, R. Bulla, J. König, G. Schön, S. Maekawa, and J. von Delft, "Gate-controlled spin splitting in quantum dots with ferromagnetic leads in the Kondo regime", Phys. Rev. B **72**, 121302 (2005) 10.1103/PhysRevB.72.121302.

[40]J. Pedersen, J. Thomassen, and K. Flensberg, "Noncollinear magnetoconductance of a quantum dot", Phys. Rev. B **72**, 045341 (2005) 10.1103/PhysRevB.72.045341.

[41]I. Weymann, J. König, J. Martinek, J. Barnaś, and G. Schön, "Tunnel magnetoresistance of quantum dots coupled to ferromagnetic leads in the sequential and cotunneling regimes", Phys. Rev. B **72**, 115334 (2005) 10.1103/PhysRevB.72.115334.

[42]M. Sindel, L. Borda, J. Martinek, R. Bulla, J. König, G. Schön, S. Maekawa, and J. von Delft, "Kondo quantum dot coupled to ferromagnetic leads: Numerical renormalization group study", Phys. Rev. B **76**, 045321 (2007) 10.1103/PhysRevB.76.045321.

[43]L. Li, Y.-Y. Ni, T.-F. Fang, and H.-G. Luo, "Compensation effect in carbon nanotube quantum dots coupled to polarized electrodes in the presence of spin-orbit coupling", Phys. Rev. B **84**, 235405 (2011) 10.1103/PhysRevB.84.235405.

[44]S. Koller, M. Grifoni, and J. Paaske, "Sources of negative tunneling magnetoresistance in multilevel quantum dots with ferromagnetic contacts", Phys. Rev. B **85**, 045313 (2012) 10.1103/PhysRevB.85.045313.

[45]K. Grove-Rasmussen, S. Grap, J. Paaske, K. Flensberg, S. Andergassen, V. Meden, H. I. Jørgensen, K. Muraki, and T. Fujisawa, "Magnetic-Field Dependence of Tunnel Couplings in Carbon Nanotube Quantum Dots", Phys. Rev. Lett. **108**, 176802 (2012) 10.1103/PhysRevLett.108.176802.

[46]P.-O. Löwdin, "A Note on the Quantum-Mechanical Perturbation Theory", J. Chem. Phys. **19**, 1396 (1951) 10.1063/1.1748067.

[47]R. Winkler, *Spin-Orbit Coupling Effects in Two-Dimensional Electron and Hole systems* (Springer-Verlag, 2003).

[48]K. Yosida, *Theory of Magnetism* (Springer, 1996).

[49]T. Ando, "Theory of Electronic States and Transport in Carbon Nanotubes", J. Phys. Soc. Jpn. **74**, 777–817 (2005) 10.1143/JPSJ.74.777.

[50]S. Weiss, E. I. Rashba, F. Kuemmeth, H. O. H. Churchill, and K. Flensberg, "Spin-orbit effects in carbon-nanotube double quantum dots", Phys. Rev. B **82**, 165427 (2010) 10.1103/PhysRevB.82.165427.

[51]D. Bulaev, B. Trauzettel, and D. Loss, "Spin-orbit interaction and anomalous spin relaxation in carbon nanotube quantum dots", Phys. Rev. B **77**, 235301 (2008) 10.1103/PhysRevB.77.235301.

[52]R. Saito, G. Dresselhaus, and M. S. Dresselhaus, *Physical Properties of Carbon Nanotubes* (Imperial College Press, 1998).

[53]W. Izumida, K. Sato, and R. Saito, "Spin-Orbit Interaction in Single Wall Carbon Nanotubes: Symmetry Adapted Tight-Binding Calculation and Effective Model Analysis", J. Phys. Soc. Jpn. **78**, 074707 (2009) 10.1143/JPSJ.78.074707.

[54]C. Kittel, *Introduction to Solid State Physics* (John Wiley & Sons, Inc., New York, 2004).

[55]T. S. Jespersen, K. Grove-Rasmussen, J. Paaske, K. Muraki, T. Fujisawa, J. Nygård, and K. Flensberg, "Gate-dependent spin-orbit coupling in multielectron carbon nanotubes", Nat. Phys. **7**, 348–353 (2011) 10.1038/nphys1880.

[56]W. Liang, M. Bockrath, and H. Park, "Shell Filling and Exchange Coupling in Metallic Single-Walled Carbon Nanotubes", Phys. Rev. Lett. **88**, 126801 (2002) 10.1103/PhysRevLett.88.126801.

[57]H. A. Bethe, "The Electromagnetic Shift of Energy Levels", Phys. Rev. **72**, 339–341 (1947) 10.1103/PhysRev.72.339.

[58]W. Lamb and R. Retherford, "Fine Structure of the Hydrogen Atom by a Microwave Method", Phys. Rev. **72**, 241–243 (1947) 10.1103/PhysRev.72.241.

[59]W. D. Knight, "Nuclear Magnetic Resonance Shift in Metals", Phys. Rev. **76**, 1259–1260 (1949) 10.1103/PhysRev.76.1259.2.

[60]J. Bardeen, L. N. Cooper, and J. R. Schrieffer, "Theory of Superconductivity", Phys. Rev. **108**, 1175–1204 (1957) 10.1103/PhysRev.108.1175.

[61]R. Žitko, J. S. Lim, R. López, and R. Aguado, "Shiba states and zero-bias anomalies in the hybrid normal-superconductor Anderson model", (2014), arXiv:1405.6084.

[62]W. Chang, V. E. Manucharyan, T. S. Jespersen, J. Nygård, and C. M. Marcus, "Tunneling Spectroscopy of Quasiparticle Bound States in a Spinful Josephson Junction", Phys. Rev. Lett. **110**, 217005 (2013) 10.1103/PhysRevLett.110.217005.

[63]W. Chang, "Superconducting Proximity Effect in InAs Nanowires", PhD thesis (Harvard University, 2014).

[64]R. S. Deacon, Y. Tanaka, A. Oiwa, R. Sakano, K. Yoshida, K. Shibata, K. Hirakawa, and S. Tarucha, "Kondo-enhanced Andreev transport in single self-assembled InAs quantum dots contacted with normal and superconducting leads", Phys. Rev. B **81**, 121308 (2010) 10.1103/PhysRevB.81.121308.

[65]R. S. Deacon, Y. Tanaka, A. Oiwa, R. Sakano, K. Yoshida, K. Shibata, K. Hirakawa, and S. Tarucha, "Tunneling Spectroscopy of Andreev Energy Levels in a Quantum Dot Coupled to a Superconductor", Phys. Rev. Lett. **104**, 076805 (2010) 10.1103/PhysRevLett.104.076805.

[66]E. J. H. Lee, X. Jiang, R. Aguado, G. Katsaros, C. M. Lieber, and S. De Franceschi, "Zero-Bias Anomaly in a Nanowire Quantum Dot Coupled to Superconductors", Phys. Rev. Lett. **109**, 186802 (2012) 10.1103/PhysRevLett.109.186802.

[67]E. J. H. Lee, X. Jiang, M. Houzet, R. Aguado, C. M. Lieber, and S. De Franceschi, "Spin-resolved Andreev levels and parity crossings in hybrid superconductor-semiconductor nanostructures.", Nat. Nanotechnol. **9**, 79–84 (2014) 10.1038/nnano.2013.267.

[68]J. Schrieffer and P. Wolff, "Relation between the Anderson and Kondo Hamiltonians", Phys. Rev. **149**, 491–492 (1966) 10.1103/PhysRev.149.491.

[69]M. M. Salomaa, "Schrieffer-Wolff transformation for the Anderson Hamiltonian in a superconductor", Phys. Rev. B **37**, 9312–9317 (1988) 10.1103/PhysRevB.37.9312.

[70]A. C. Hewson, *The Kondo Problem to Heavy Fermions* (Cambridge University Press, 1993).

[71]L. Yu, "Bound state in superconductors with paramagnetic impurities", Acta Phys. Sin. **21**, 75–91 (1965).

[72]H. Shiba, "Classical Spins in Superconductors", Prog. Theor. Phys. **40**, 435–451 (1968) 10.1143/PTP.40.435.

[73]A. I. Rusinov, "Superconductivity near a paramagnetic impurity", JETP Lett.-USSR **9**, 85–87 (1969).

[74]T. Soda, T. Matsuura, and Y. Nagaoka, "s - d Exchange Interaction in a Superconductor", Prog. Theor. Phys. **38**, 551–567 (1967) 10.1143/PTP.38.551.

[75]Y. Nagaoka and T. Matsuura, "Bound States Due to a Magnetic Impurity in a Superconductor. I", Prog. Theor. Phys. **46**, 364–386 (1971) 10.1143/PTP.46.364.

[76]E. Müller-Hartmann and J. Zittartz, "Theory of magnetic impurities in superconductors. II", Z. Phys. **234**, 58–69 (1970) 10.1007/BF01392497.

[77]J. Zittartz, "Theory of magnetic impurities in superconductors. III Structure of the bound states", Z. Phys. **237**, 419–426 (1970) 10.1007/BF01407639.

[78]E. Müller-Hartmann and J. Zittartz, "Theory of magnetic impurities in superconductors", Z. Phys. **256**, 366–379 (1972) 10.1007/BF01391983.

[79]T. Meng, S. Florens, and P. Simon, "Self-consistent description of Andreev bound states in Josephson quantum dot devices", Phys. Rev. B **79**, 224521 (2009) 10.1103/PhysRevB.79.224521.

[80]K. Satori, H. Shiba, O. Sakai, and Y. Shimizu, "Numerical Renormalization Group Study of Magnetic Impurities in Superconductors", J. Phys. Soc. Jpn. **61**, 3239–3254 (1992) 10.1143/JPSJ.61.3239.

[81]J. Bauer, A. Oguri, and A. C. Hewson, "Spectral properties of locally correlated electrons in a Bardeen-Cooper-Schrieffer superconductor", J. Phys.-Condens. Matter **19**, 486211 (2007) 10.1088/0953-8984/19/48/486211.

[82]A. Martín-Rodero and A. Levy Yeyati, "The Andreev states of a superconducting quantum dot: mean field versus exact numerical results.", J. Phys.-Condens. Matter **24**, 385303 (2012) 10.1088/0953-8984/24/38/385303.

[83]D. Futterer, J. Swiebodzinski, M. Governale, and J. König, "Renormalization effects in interacting quantum dots coupled to superconducting leads", Phys. Rev. B **87**, 014509 (2013) 10.1103/PhysRevB.87.014509.

[84]K. J. Franke, G. Schulze, and J. I. Pascual, "Competition of superconducting phenomena and Kondo screening at the nanoscale.", Science **332**, 940–4 (2011) 10.1126/science.1202204.

[85]J.-D. Pillet, C. H. L. Quay, P. Morfin, C. Bena, a. L. Yeyati, and P. Joyez, "Andreev bound states in supercurrent-carrying carbon nanotubes revealed", Nat. Phys. **6**, 965–969 (2010) 10.1038/nphys1811.

[86]D. Averin and A. Bardas, "AC Josephson Effect in a Single Quantum Channel", Phys. Rev. Lett. **75**, 1831–1834 (1995) 10.1103/PhysRevLett.75.1831.

[87]E. Bratus', V. Shumeiko, and G. Wendin, "Theory of Subharmonic Gap Structure in Superconducting Mesoscopic Tunnel Contacts", Phys. Rev. Lett. **74**, 2110–2113 (1995) 10.1103/PhysRevLett.74.2110.

[88]J. Cuevas, A. Martín-Rodero, and A. Yeyati, "Hamiltonian approach to the transport properties of superconducting quantum point contacts", Phys. Rev. B **54**, 7366–7379 (1996) 10.1103/PhysRevB.54.7366.

[89]A. Eichler, M. Weiss, S. Oberholzer, C. Schönenberger, A. Levy Yeyati, J. Cuevas, and A. Martín-Rodero, "Even-Odd Effect in Andreev Transport through a Carbon Nanotube Quantum Dot", Phys. Rev. Lett. **99**, 126602 (2007) 10.1103/PhysRevLett.99.126602.

[90]T. Sand-Jespersen, J. Paaske, B. Andersen, K. Grove-Rasmussen, H. Jørgensen, M. Aagesen, C. Sørensen, P. Lindelof, K. Flensberg, and J. Nygård, "Kondo-Enhanced Andreev Tunneling in InAs Nanowire Quantum Dots", Phys. Rev. Lett. **99**, 126603 (2007) 10.1103/PhysRevLett.99.126603.

[91]K. Grove-Rasmussen, H. I. Jørgensen, B. Andersen, J. Paaske, T. S. Jespersen, J. Nygård, K. Flensberg, and P. E. Lindelof, "Superconductivity-enhanced bias spectroscopy in carbon nanotube quantum dots", Phys. Rev. B **79**, 134518 (2009) 10.1103/PhysRevB.79.134518.

[92]B. M. Andersen, K. Flensberg, V. Koerting, and J. Paaske, "Nonequilibrium Transport through a Spinful Quantum Dot with Superconducting Leads", Phys. Rev. Lett. **107**, 256802 (2011) 10.1103/PhysRevLett.107.256802.

[93]V. Koerting, B. M. Andersen, K. Flensberg, and J. Paaske, "Nonequilibrium transport via spin-induced subgap states in superconductor/quantum dot/normal metal cotunnel junctions", Phys. Rev. B **82**, 245108 (2010) 10.1103/PhysRevB.82.245108.

[94]W. Haberkorn, H. Knauer, and J. Richter, "A theoretical study of the current-phase relation in Josephson contacts", Phys. Status Solidi A **47**, K161–K164 (1978) 10.1002/pssa.2210470266.

[95]A. V. Zaitsev, "Quasiclassical equations of the theory of superconductivity for contiguous metals and the properties of constricted microcontacts", Sov. Phys. JETP-USSR **59**, 1015–1024 (1984).

[96]G. B. Arnold, "Superconducting tunneling without the tunneling Hamiltonian", J. Low Temp. Phys. **59**, 143–183 (1985) 10.1007/BF00681510.

[97]A. Furusaki and M. Tsukada, "A unified theory of clean Josephson junctions", Physica B **165-166**, 967–968 (1990) 10.1016/S0921-4526(09)80069-0.

[98]C. W. J. Beenakker, "Universal limit of critical-current fluctuations in mesoscopic Josephson junctions", Phys. Rev. Lett. **67**, 3836–3839 (1991) 10.1103/PhysRevLett.67.3836.

[99]K. Yosida, "Bound State Due to the s-d Exchange Interaction", Phys. Rev. **147**, 223–227 (1966) 10.1103/PhysRev.147.223.

[100]K. Yosida, "Ground State Energy of Conduction Electrons Interacting with a Localized Spin", Prog. Theor. Phys. **36**, 875–886 (1966) 10.1143/PTP.36.875.

[101]B. Josephson, "Possible new effects in superconductive tunnelling", Phys. Lett. **1**, 251–253 (1962) 10.1016/0031-9163(62)91369-0.

[102]J.-P. Cleuziou, W. Wernsdorfer, V. Bouchiat, T. Ondarçuhu, and M. Monthioux, "Carbon nanotube superconducting quantum interference device.", Nat. Nanotechnol. **1**, 53–9 (2006) 10.1038/nnano.2006.54.

[103]J. A. van Dam, Y. V. Nazarov, E. P. A. M. Bakkers, S. De Franceschi, and L. P. Kouwenhoven, "Supercurrent reversal in quantum dots.", Nature **442**, 667–70 (2006) 10.1038/nature05018.

[104]H. I. Jørgensen, T. Novotný, K. Grove-Rasmussen, K. Flensberg, and P. E. Lindelof, "Critical current 0-pi transition in designed Josephson Quantum Dot junctions.", Nano Lett. **7**, 2441–5 (2007) 10.1021/nl071152w.

[105]A. Eichler, R. Deblock, M. Weiss, C. Karrasch, V. Meden, C. Schönenberger, and H. Bouchiat, "Tuning the Josephson current in carbon nanotubes with the Kondo effect", Phys. Rev. B **79**, 161407 (2009) 10.1103/PhysRevB.79.161407.

[106]I. O. Kulik, "Magnitude of the critical Josephson tunnel current", Sov. Phys. JETP-USSR **22**, 841–843 (1966).

[107]L. N. Bulaevskii, V. V. Kuzii, and A. A. Sobyanin, "Superconducting system with weak coupling to the current in the ground state", JETP Lett.-USSR **25**, 290–294 (1977).

[108]L. N. Bulaevskii, V. V. Kuzii, and A. A. Sobyanin, "On possibility of the spontaneous magnetic flux in a Josephson junction containing magnetic impurities", Solid State Commun. **25**, 1053–1057 (1978) 10.1016/0038-1098(78)90906-7.

[109]L. I. Glazman and K. A. Matveev, "Resonant Josephson current through Kondo impurities in a tunnel barrier", JETP Lett.-USSR **49**, 659–662 (1989).

[110]B. Spivak and S. Kivelson, "Negative local superfluid densities: The difference between dirty superconductors and dirty Bose liquids", Phys. Rev. B **43**, 3740–3743 (1991) 10.1103/PhysRevB.43.3740.

[111]A. Rozhkov and D. Arovas, "Josephson Coupling through a Magnetic Impurity", Phys. Rev. Lett. **82**, 2788–2791 (1999) 10.1103/PhysRevLett.82.2788.

[112]A. Rozhkov and D. Arovas, "Interacting-impurity Josephson junction: Variational wave functions and slave-boson mean-field theory", Phys. Rev. B **62**, 6687–6691 (2000) 10.1103/PhysRevB.62.6687.

[113]F. Siano and R. Egger, "Josephson Current through a Nanoscale Magnetic Quantum Dot", Phys. Rev. Lett. **93**, 047002 (2004) 10.1103/PhysRevLett.93.047002.

[114]M.-S. Choi, M. Lee, K. Kang, and W. Belzig, "Kondo effect and Josephson current through a quantum dot between two superconductors", Phys. Rev. B **70**, 020502 (2004) 10.1103/PhysRevB.70.020502.

[115]C. Karrasch, A. Oguri, and V. Meden, "Josephson current through a single Anderson impurity coupled to BCS leads", Phys. Rev. B **77**, 024517 (2008) 10.1103/PhysRevB.77.024517.

[116]P. W. Anderson, *Lectures on the Many-body Problem, Vol. 2*, edited by E. R. Caianiello (Academic Press, 1964).

[117]P. Murphy, S. Mukerjee, and J. Moore, "Optimal thermoelectric figure of merit of a molecular junction", Phys. Rev. B **78**, 161406 (2008) 10.1103/PhysRevB.78.161406.

[118]C. Finch, V. Garcia-Suarez, and C. Lambert, "Giant thermopower and figure of merit in single-molecule devices", Phys. Rev. B **79**, 033405 (2009) 10.1103/PhysRevB.79.033405.

[119]G. C. Solomon, D. Q. Andrews, T. Hansen, R. H. Goldsmith, M. R. Wasielewski, R. P. Van Duyne, and M. A. Ratner, "Understanding quantum interference in coherent molecular conduction.", J. Chem. Phys. **129**, 054701 (2008) 10.1063/1.2958275.

[120]O. Karlström, H. Linke, G. Karlström, and A. Wacker, "Increasing thermoelectric performance using coherent transport", Phys. Rev. B **84**, 113415 (2011) 10.1103/PhysRevB.84.113415.

[121]J. S. Seldenthuis, H. S. J. van der Zant, M. A. Ratner, and J. M. Thijssen, "Vibrational excitations in weakly coupled single-molecule junctions: a computational analysis.", ACS Nano **2**, 1445–51 (2008) 10.1021/nn800170h.

[122]http://en.wikipedia.org/wiki/Stacking_(chemistry) (visited on 06/15/2014).

[123]H. Ezawa, "Phonons in a half space", Ann. Phys. **67**, 438–460 (1971) 10.1016/0003-4916(71)90149-7.

[124]K. Patton and M. Geller, "Thermal transport through a mesoscopic weak link", Phys. Rev. B **64**, 155320 (2001) 10.1103/PhysRevB.64.155320.

[125]K. Patton and M. Geller, "Phonons in a nanoparticle mechanically coupled to a substrate", Phys. Rev. B **67**, 155418 (2003) 10.1103/PhysRevB.67.155418.

[126]M. Geller, "Local phonon density of states in an elastic substrate", Phys. Rev. B **70**, 205421 (2004) 10.1103/PhysRevB.70.205421.

[127]L. D. Landau, E. M. Lifshitz, A. M. Kosevich, and L. P. Pitaevskii, *Theory of Elasticity* (Pergamon Press, Oxford, 1986).

[128]D. Segal, A. Nitzan, and P. Hänggi, "Thermal conductance through molecular wires", J. Chem. Phys. **119**, 6840 (2003) 10.1063/1.1603211.

[129]N. Mingo, "Anharmonic phonon flow through molecular-sized junctions", Phys. Rev. B **74**, 125402 (2006) 10.1103/PhysRevB.74.125402.

[130]T. Yamamoto and K. Watanabe, "Nonequilibrium Green's Function Approach to Phonon Transport in Defective Carbon Nanotubes", Phys. Rev. Lett. **96**, 255503 (2006) 10.1103/PhysRevLett.96.255503.

[131]J.-S. Wang, N. Zeng, J. Wang, and C. K. Gan, "Nonequilibrium Green's function method for thermal transport in junctions", Phys. Rev. E **75**, 061128 (2007) 10.1103/PhysRevE.75.061128.

[132]L. V. Keldysh, "Diagram technique for nonequilibrium processes", Sov. Phys. JETP-USSR **20**, 1018–1026 (1965).

[133]A. I. Larkin and Y. N. Ovchinnikov, "Nonlinear conductivity of superconductors in the mixed state", Sov. Phys. JETP-USSR **41**, 960–965 (1975).

[134]J. Rammer and H. Smith, "Quantum field-theoretical methods in transport theory of metals", Rev. Mod. Phys. **58**, 323–359 (1986) 10.1103/RevModPhys.58.323.

[135]R. Landauer, "Spatial Variation of Currents and Fields Due to Localized Scatterers in Metallic Conduction", IBM J. Res. Dev. **1**, 223–231 (1957) 10.1147/rd.13.0223.

[136]R. Landauer, "Electrical resistance of disordered one-dimensional lattices", Philos. Mag. **21**, 863–867 (1970) 10.1080/14786437008238472.

[137]M. Büttiker, Y. Imry, R. Landauer, and S. Pinhas, "Generalized many-channel conductance formula with application to small rings", Phys. Rev. B **31**, 6207–6215 (1985) 10.1103/PhysRevB.31.6207.

[138]C. Caroli, R. Combescot, P. Nozieres, and D. Saint-James, "Direct calculation of the tunneling current", J. Phys. C Solid State Phys. **4**, 916–929 (1971) 10.1088/0022-3719/4/8/018.

[139]http://en.wikipedia.org/wiki/Gold (visited on 06/15/2014).

[140]G. V. Samsonov, *Handbook of the Physicochemical Properties of the Elements* (IFI/Plenum, New York-Washington, 1968).

[141]H. J. Goldsmid, *Thermoelectric Refrigeration* (Plenum Press, New York, 1964).

[142]U. Sivan and Y. Imry, "Multichannel Landauer formula for thermoelectric transport with application to thermopower near the mobility edge", Phys. Rev. B **33**, 551–558 (1986) 10.1103/PhysRevB.33.551.

[143]A. M. Lunde and K. Flensberg, "On the Mott formula for the thermopower of non-interacting electrons in quantum point contacts.", J. Phys.-Condens. Matter **17**, 3879–84 (2005) 10.1088/0953-8984/17/25/014.

[144]K. Esfarjani, M. Zebarjadi, and Y. Kawazoe, "Thermoelectric properties of a nanocontact made of two-capped single-wall carbon nanotubes calculated within the tight-binding approximation", Phys. Rev. B **73**, 085406 (2006) 10.1103/PhysRevB.73.085406.

[145]G. Kiršanskas, L. Qian, K. Flesnberg, G. C. Solomon, and M. Leijnse, "Designing π-stacked molecular structures to be phonon insulators but electric conductors", (To be published).

[146]T. Humphrey and H. Linke, "Reversible Thermoelectric Nanomaterials", Phys. Rev. Lett. **94**, 096601 (2005) 10.1103/PhysRevLett.94.096601.

[147]M. Esposito, K. Lindenberg, and C. Van den Broeck, "Thermoelectric efficiency at maximum power in a quantum dot", EPL-Europhys. Lett. **85**, 60010 (2009) 10.1209/0295-5075/85/60010.

[148]M. Leijnse, M. R. Wegewijs, and K. Flensberg, "Nonlinear thermoelectric properties of molecular junctions with vibrational coupling", Phys. Rev. B **82**, 045412 (2010) 10.1103/PhysRevB.82.045412.

[149]P. W. Anderson, "A poor man's derivation of scaling laws for the Kondo problem", J. Phys. C Solid State Phys. **3**, 2436–2441 (1970) 10.1088/0022-3719/3/12/008.

[150]H. Haug and A.-P. Jauho, *Quantum Kinetics in Transport and Optics of Semiconductors*, Springer Series in Solid-State Sciences (Springer, 2007).